CRANFIELD UNIVERSITY

AMINU JA'AFAR ABUBAKAR KOGUNA

A STUDY OF FLOW BEHAVIOUR OF DENSE PHASE AT LOW CONCENTRATIONS IN PIPES

SCHOOL OF WATER, ENERY AND ENVIRONMENT
OIL AND GAS ENGINEERING CENTRE

PHD Thesis
Academic Year: 2015 - 2016

Supervisor: Professor Hoi Yeung
September 2016

CRANFIELD UNIVERSITY

SCHOOL OF WATER, ENERY AND ENVIRONMENT
OIL AND GAS ENGINEERING CENTRE

PHD Thesis

Academic Year 2015 - 2016

AMINU JA'AFAR ABUBAKAR KOGUNA

A STUDY OF FLOW BEHAVIOUR OF DENSE PHASE AT LOW CONCENTRATIONS IN PIPES

Supervisor: Professor Hoi Yeung
September 2016

This thesis is submitted in partial fulfilment of the requirements for the degree of PhD in Energy

ABSTRACT

Offshore production fluids from the reservoir are often transported in pipelines from the wellheads to the platform and from the platform to process facilities. At low flow velocity water, sand or liquids like condensate could settle at the bottom of pipelines that may lead to grave implications for flow assurance. During shutdown the settled heavy liquid (e.g. water), could result in corrosion in pipelines, while following restart stages the settled water could form water plugs that could damage equipment, while settled sand could also form a blockage that needs to be purged. Furthermore, there is a requirement to know the quantity of water and base sediment for fiscal metering and custody transfer purposes.

A series of experiments were carried out to observe low water cut in oil and water flows in four inch diameter pipeline. Similarly low sand concentrations in water and sand, water, air and sand flows were observed in two inch diameter pipelines. Conductive film thickness sensors were used to ascertain structural velocities, height and dense phase fractions. Comparisons are made between two cases in order to gain better understanding of the behaviours and dispersal process of low loading denser phase in multiphase flows.

The arrangement enabled production of flow regime maps for low water cut oil and water flow, as well as water sand and water, air and sand flows, structural velocities and denser phase removal velocities were also acertained. Actual in-situ liquid velocities were obtained experimentally. A novel detection of sand in water and water and sand flows was produced. The experimentally obtained film thickness was in agreement with two fluid model predictions. Thus, confirming use of conductive sensors for dense phase classification, film thickness, velocity and holdup measurements in pipelines.

Keywords:

Water/oil flow, Solid/liquid flow, Low water cut, Interface height, Low sand loading, Velocity

ACKNOWLEDGEMENTS

I would like first to acknowledge my gratitude to my creator most merciful Allah, then my parents and family for moral and financial support.

I would like to express my deep appreciation to the continued support that I had received from my supervisor Professor Hoi Yeung and pay special tribute to Professor Gioia Falcone for support with the thesis corrections, Dr Paul Fairhurst from Brtish Petroleum for intial project guidance, other staff at Cranfield University in the form of Dr Liyun Lao who has given guidance and directions, Sam Skears for her constant support, David Whittington, Kelvin white, Ian Hutchins and Stan Collins for support with my experiments. Similarly, John Knop, Shaun Collins have contributed immensely to my progress at Cranfield University. I would also like to acknowledge contributions from my fellow students that are too numerous to mention.

Last but not the least the Nigerian Petroleum Technology Development Fund who provided my initial scholarship.

PUBLICATIONS AND SEMINARS

Aminu J.A . Koguna (2011). “Water Drop Out in Transfer Pipelines”, Researcher Programme Meetings Seminar 31 May, 2011.

Aminu J.A . Koguna (2012). “Removal of Settled Heavier Phase in Undulating Oil and Gas Transfer Pipeline”, Researcher Programme Meetings Seminar 7 February, 2012.

Aminu J.A . Koguna (2014). “Removal of Settled Heavier Phase in Undulating Oil and Gas Transfer Pipeline”, poster presentation DTC Poster Conference School of Engineering, 2014.

Aminu J.A . Koguna (2015). “Removal of Settled Heavier Phase in Undulating Oil and Gas Transfer Pipeline”, Researcher Programme Meetings Seminar 3 February, 2015.

Aminu J.A . Koguna (2015). “Removal of Settled Heavier Phase in Undulating Oil and Gas Transfer Pipeline”, poster presentation DTC Poster Conference School of Engineering, 2015.

Aminu J. A. Koguna, Aliyu M. Aliyu, Olawale T. Fajemidupe, Yahaya D. Baba (2015). “Study of Low Loading Heavier Phase in Oil and Water Liquid-Liquid Pipe Flow” Waset 2015 Paris, World Academy of Science Engineering and Technology, International Journal of Mechanical, Aerospace, Industrial, Machatronic and Manufacturing Engineering Vol:9, No:11, 2015.

O.T. Fajemidupe, A.J.Koguna, H. Yeung, L. Lao (2015). “Experimental Investigation of Sand Movements Using Conductivity Film Thickness Probe” ISMTMF, 23th-25th, September, 2015, Sapporo, Hokkaido, Japan.

Aminu J.A . Koguna, Dr Liyun Lao, Professor Hoi Yeung (2015). “Study on the Behaviours of Low Loading Heavier phase in Two Phase Flows in Pipelines” SPE-SPE-175117-MS-MS SPE Annual Technical Conference and Exhibition held in Houston, Texas, USA, 28–30 September 2015.

Aminu J.A . Koguna, Liyun Lao and Hoi Yeung (2016). “Study on the removal of low loading heavier phase by lighter phase in multiphase pipe” ICMF 2016 International Conference of Multiphase Flow Firenze, Italy 22-24 May, 2016

TABLE OF CONTENTS

LIST OF FIGURES

LIST OF TABLES

LIST OF EQUATIONS

NOMENCLATURE

A_o	[m^2]	area oil
A_w	[m^2]	area water
a	[-]	constant
b	[-]	constant
c	[-]	water cut
c_{bot}	[-]	bottom concentration
c_{avg}	[-]	average in-situ water concentration
D_{EQ}	[m]	equivalent diameter of flow region above water phase
d_{max}	[m]	maximum droplet diameter
D_P	[m]	internal pipe diameter
E	[eV]	specific power dissipation
F	[-]	densimetric Froude number
g	[m/s2]	acceleration due to gravity
g_c g_L	[m/s2] [m/s2]	gravitational constant gravitational acceleration
H_L	[-]	no slip holdup
S_i	[m]	wetted perimeter interface
S_o	[m]	wetted perimeter oil
S_w	[m]	wetted perimeter water
U	[m/s]	velocity
U_c	[m/s]	continuous phase velocity
U_{so}	[m/s]	superficial oil velocity
U_{omH}	[m/s]	oil continuous layer mixture transition velocity Hinze
U_{omH}	[m/s]	oil continuous layer mixture transition velocity Hinze
U_{omH}	[m/s]	oil continuous layer mixture transition velocity Hinze
U_{wwL}	[m/s]	water continuous layer transition velocity Levich
U_{ws}	[m/s]	water superficial velocity
U_{sw}	[m/s]	superficial water velocity
V	[m/s]	terminal velocity due to gravity
V_s	[-]	bottom concentration of the droplets
τ	[Pa]	shear stress

τ_o	[Pa] shear stress oil
τ_w	[Pa] shear stress water
τ_i	[Pa] shear stress interface
$\Delta\rho$	[kg/m^3] oil-water density difference
σ	[N/m] surface tension
r	[-] polar coordinate
Π	[-] dimensionless parameter
α	[-] turbulent damping coefficient
n	[-] exponent for hindered settling
ρ_o	[kg/m^3] oil density
ρ_m	[kg/m^3] mixture density
ρ_w	[kg/m^3] water density
ε_w	[-] in-situ water cut
f	[-] friction factor
G^*	[-] non dimensional
$\mathrm{l_c}$	[m] characteristic length
ϕ_0	[-] view angle from centre of pipe
ϕ^*	[-] interphase plane angle
μ	[kg/s-m] viscosity
f_i	[-] interfacial friction factor
ρ_i	[kg/m^3] interfacial density
ξ	[-] phase angle
γ	[s/m] specific conductivity of the liquid in Siemens per metre
β	[-] inclination angle
Fr_o	[-] Froude number
s	[-] dimensionless parameter
η_o	[Pa-s] oil phase viscosity
e	= rate of energy dissipation
υ	[m^2/s] kinematic viscosity
$\rho_{m,hom}$	[kg/m^3] mixture density homogenous
$\rho_w \varepsilon_{w,hom}$	[kg/m^3] water density water cut homogenous

1 INTRODUCTION

Study of multiphase flow is very vital to oil industry especially in transporting crude oil from underground oil and gas reservoirs to the wellhead or platform and subsequently to the refineries. Mostly pipelines that are constructed of steel do this transportation. Oil and gas production involve drilling and pumping production fluid from reservoirs to end users. Transfer pipelines transport produced fluids from the wellhead and manifold to the platform/FPSO. Then from the platform/FPSO to shore where, there are storage facilities, process plants and refineries. Within the process facilities and storage depots, pipelines distribute the products.

Pipelines are far cheaper than other forms of transport and are made of steel to various standards. However, they are expensive to construct and maintain and at low flow velocities, free water, solids and other heavier phases can separate from the oil/gas and deposit at the bottom of the pipeline. This leads to severe corrosion and erosion with eventual leakages leading to environmental pollution. Furthermore, with the depletion of easier crude oil reserves, oil production has moved towards deeper offshore fields and consideration of heavier crude oil types that require recovery techniques that involve increased use of water, gas and sand to transport. In addition, as reservoir production declines from peak production more water is present in the flows until it becomes uneconomical to continue production by the larger multinational oil companies.

For custody transfer, the pipelines are used to transfer the fluids from the producer to the user or in other words from seller to buyer. Study of phase distribution to know whether the flow is segregated or dispersed is important due to regulation by (DECC, 2012) for allowing 1% water content for transfer pipelines carrying crude oil to export terminals and from oil tankers. Refineries and process facilities are not designed to handle water plugs when pigging pipelines. Similarly, sensors, equipment, densitometer and sampling are also sensitive to the water content. In addition, sand and other settled solid particles can cause damage further downstream to equipment. Furthermore, with the fluctuating price of produced fluids it is imperative to have this knowledge for fiscal

metering purposes. This knowledge would also be required to predict and optimise the pumping costs for transfer of production fluids.

Though there has been extensive research in multiphase liquid-liquid flows these have generally been on the flow phenomena and few have touched on a particular aspect of low water cut, some have delved into the effect of corrosion inhibitors, some on slug flow and others on phase inversion. However, there have not been specific discussions on water settlement in transfer pipelines, especially at low water cut. Some literature such as (Cai et al., 2005) (Pots, Hollenberg and Hendriksen, 2006) (Tang et al., 2007) have concluded that corrosion occurs even at a low water cut and is absent only when oil wetting occurs solely in pipelines,. Practically water content is detected by taking samples and tested in-situ or at laboratory as discussed in (Coordination, 1995) (Pharris and Kolpa, 2007) (Bubar, 2011).

Similarly, there are few studies that engage the behaviour of low loading dense phase such as sand and liquids in pipelines. It is important to know the crude oil sediment and water content in custody transfer as discussed by (Anon, n.d.)

1.1 Background

Oil and gas production and transport systems encounter multiphase flows, i.e. oil, water, gas, solids (sand). Because of density differences different flow regimes exists. Much of the current work had been for horizontal and vertical flow lines but unfortunately, pipelines are often undulating. For gas liquid flows, the effects of gravity mean that in downward inclined pipes, stratified flow is more prominent, whilst slug flow is favoured in upward orientation. It is also fair to say that much of the research work has been on relatively high concentration of the heavier phases this is because in flow lines there is a high percentage of dense phase such as water and sand in the production of oil and gas. This percentage is altered when the produced fluid is separated on the platform or in subsea separators. Thus for transfer pipelines the dense phase is usually less than the lighter phase.

The observations made from available literature show that there has been extensive research on flows in pipelines involving liquid-gas flow and relatively few on liquid–liquid and liquid-solid flows and a summary of these papers and conditions of their experiments are included in Appendix A.1. These deal with flow patterns called flow regimes such as stratified or dispersed flow, churn flow, bubbly flow and slug flow. Based on the Reynolds number, the flow in the pipe can also be described as laminar or turbulent flow. The fluids could also have Newtonian or Non-Newtonian flow characteristics.

These flows are studied to know certain characteristics such as pressure drop, hold up, slip, drop size, drop entrainment, water deposition, wall wetting, and phase inversion to mention a few for the different physical fluid physical properties and parameters such as viscosity, surface tension, velocity, and friction factors. Knowledge of these factors and characteristics enable accurate prediction of flow in pipeline systems so as to minimize costs and problems from the design stage to operational stage in pipeline systems.

The basic production methods used in the oil and gas industry involves drilling and pumping production fluids from the reservoir to processing and end user facilities. The medium for transporting the fluid is transfer pipelines. Transfer pipelines transport produced fluids from;

- The well head and manifold to the platform/FPSO
- The platform/FPSO to shore (storage/refineries)
- Process/Storage to distribution

They are made of steel to various standards according to the design requirements of the fluid flow systems in terms of operating temperatures and pressures. They are a far cheaper than other forms of transport such as rail, marine and truck transport of fluids. Pipelines especially in the United Kingdom and United States as stated by (Anon2011) now transport a large percentage of produced fluids. Because they are expensive to construct and maintain it is vital to understand flow phenomena in transfer pipelines for specification at the design stage and operation.

1.1.1 Composition of produced fluid in transfer pipelines

Fluid produced in transfer pipelines generally contains the product of an oil and gas production process:

For a crude oil field, the composition will likely be crude oil and small amounts of water that has not been separated by the separator. It could also contain a higher percentage of water if it is heavy crude oil, as water is injected to aid production and transportation. Small particles of sand, condensed gas, paraffin, wax and hydrates could be present; these are mostly dependent on the reservoirs' fluid characteristics.

For a gas field the fluid composition will mostly consist of gas and small amounts of water, condensate and sometimes this result in formation of hydrates. Produced sand, corrosion products, iron carbonate, iron oxides, black powder and iron sulphide, metallic iron, weld splatter, salt, asphaltenes and scale are also present in gas pipelines.

1.1.2 Topography of pipelines

The path or route in which pipelines are laid is determined by many factors. These could include buildings, roads, mountains, oceans, seas, lakes, rivers, forests and farms. Passing through built up areas increases the compensation and land rights cost. The geography of the route has a role in cost reduction, as avoiding hill terrain would reduce the number of pumping stations required. The angles of inclination and number of bends have critical effects on fluid flows. Thus, pipeline topography is a critical factor to consider for the design of transfer pipelines.

1.1.3 Conditions for heavier phase settled – normal operation, shut down

Under normal operating conditions, the heavier phase would continue to be dispersed within the lighter phase especially at high flow rates. The heavier phase has the tendency to settle increased by a reduction in flow velocity. Intermittent

flows also decrease the tendency for heavier phase settlement. Other factors that affect this tendency are the type of water and wax content of the oil.

At shut down especially at low sections or with an unplanned shut down after pumping of heavier oil and followed by passage of low viscosity oil will result in settlement and create unwanted mixing resulting in lower quality oil. Unplanned shut down in gas pipelines also results in formation of gas hydrates as reported by (Xu et al., 2011).

According to (Wicks and Fraser, 1975) after shut down water that was entrained in the oil would settle at the bottom of the transfer line. This accumulates at the low spots causing corrosion until flushed out by high velocity flow. With a sufficient velocity Kelvin-Helmholtz wave's form on the water surface and with further increase in velocity, the waves tend to break up and form water droplets in the oil flow. These have different sizes, but smaller droplets tend to be formed with increasing flow velocity. The size for the droplets concurs with Hinze's prediction of the critical Weber number in equation (1-1) below,

$$\frac{d_{max}\rho_o U^2}{\sigma g_c} = 22 \qquad \textbf{(1-1)}$$

The droplets that break up from the water surface form an axial vortex that is of several pipe diameters in length, exhibiting circular motion before sliding back coalesces and re-join the water mass. The series diagram in Figure 1-1 below highlights the process.

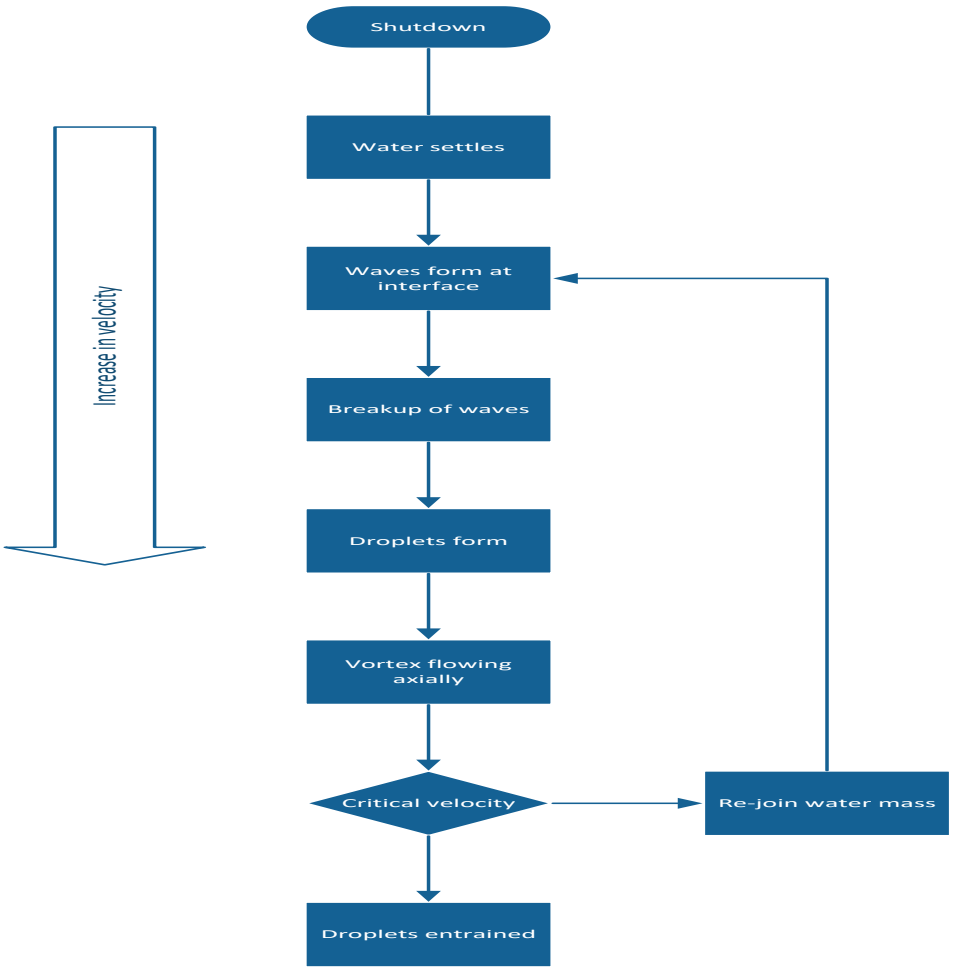

Figure 1-1 series diagram of the droplet formation process

At a higher flow rate, the droplets are all removed from the inclined section. A model for predicting critical velocity for sweeping out settled water was established with two assumptions;

1. Once entrained the water particles tend to behave like solid particles

2. The lower limit of velocity for net axial transport of solid particles (or water) is equal to the upper limit of velocity for existence of a stationary layer of solid particles.

This also analysed the bed height of a dilute solid/liquid system to predict zero bed height or the minimum velocity for net or total axial transport of solid or liquid particles. A correlation between two dimensionless parameters ψ and S in equations (1-2) and (1-3) was derived from experiments.

$$\psi = \frac{\rho_o^3}{\rho_w - \rho_o} \frac{d_{max}}{g_L \mu^2} \quad \textbf{(1-2)}$$

$$s = \frac{D_{EQ} U \rho_o}{\mu} \left(\frac{d_{max}}{D_P}\right)^{2/3} \quad \textbf{(1-3)}$$

Calculations for the water droplets are made using the largest stable drop size only. There is a relation between specific gravity and viscosity. Water entrainment tended to be more obtainable with lower interfacial tension. The critical flow velocity increases with pipe diameter. Factors that affect formation of droplets and their size include;

1. Specific gravities of oil and water,
2. interfacial tension between the oil and water,
3. viscosity of oil,
4. pipe diameter,
5. Velocity.

Figure 1-2 highlights the distribution of droplet sizes for various water and oil emulsions indicating that looser emulsions tend to have higher droplet diameters.

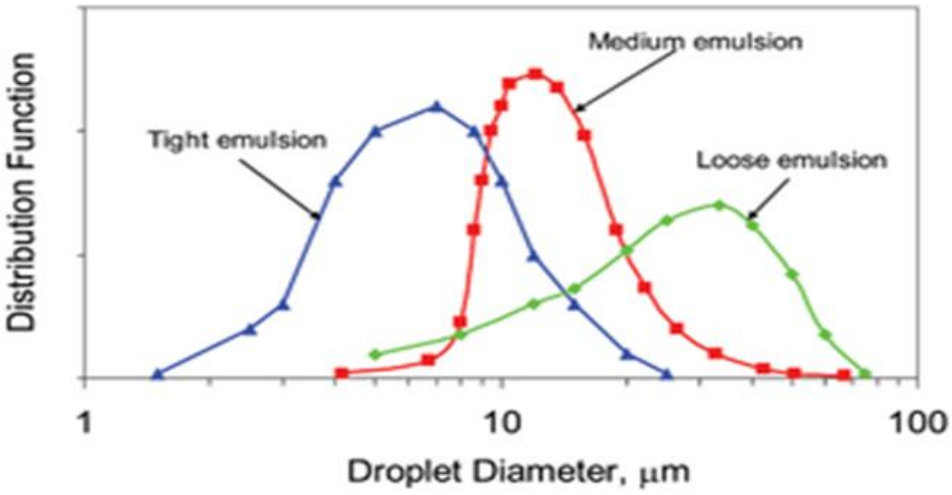

Figure 1-2 droplet size distribution of petroleum emulsions (Anon, n.d.**)**

A study by (Wu, 1995) provided an improvement on the Wicks and Fraser model by explaining that water is entrained on fully dispersed (mist flow) and stratified dispersed flows but not in purely stratified flows. With a lower water volume ratio, interaction is negligible following the Wicks and Frasers' first assumption and for the second assumption it suggests that the patterns of the two systems are so different that the correlation is difficult, most prominently at transition stages. This new method uses the distinctive flow patterns and appropriate physical properties such as phase height and maximum droplet size. While the Hinze models describe isotropic homogenous turbulence solely so that the kinetic energy drop diameter could be calculated.

There have not been previous specific discussions on; water settlement in transfer pipelines, especially at low water cut, though some literature such as (Cai et al., 2005; Pots et al., 2006; Tang et al., 2006) have concluded that corrosion occurs even at a low water cut and is absent only when oil wetting occurs solely in pipelines.

Xu (2011) developed a prediction model for water displacement by oil flow based on formation of a water plug in the lowest elbow of the test section. Water displacement is enhanced by increasing density and oil viscosity. The maximum water layer height has to surpass a stable height for entrainment while it has to surpass a critical height for plug formation this is indicated in Figure 1-3. The water plug formation is enhanced by increasing the oil superficial velocity. While the critical water holdup increases with increased pipe diameter thus requiring increased oil superficial velocity to form the water plug. The velocity for entrainment is given in equation (1-4).

$$V_e = \int_{h_s}^{h_{cr}} \frac{A_w}{dh/dx}(h)\ dh + AL_2 \qquad \textbf{(1-4)}$$

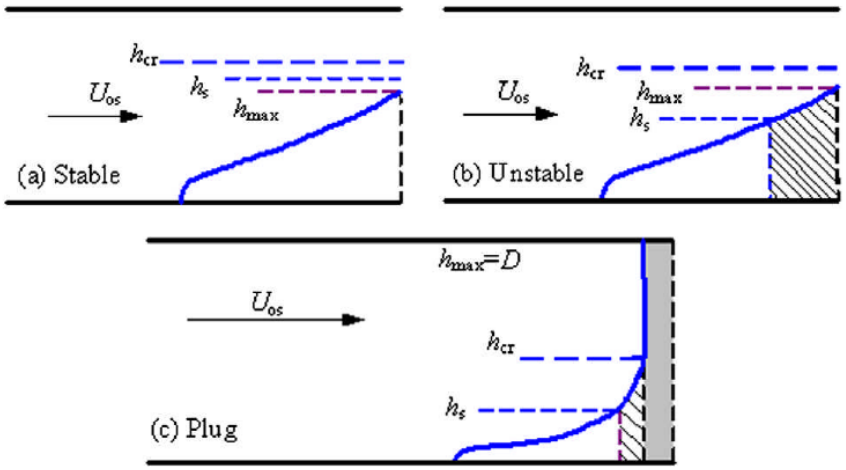

Figure 1-3 water displacement by oil diagram Xu et. al. (2011)

Furthermore (Bowden and Hassan, 2011) discuss the onset of gas/liquid entrainment and the critical height based on Froude number for dual discharging branches and superficial velocities for the inlet to study flow regime transition from stratified smooth to stratified wavy and slug flow. Similarly (Brauner, 2001) discuss flow boundaries for liquid/liquid and gas/liquid flows producing a prediction model for transitions to dispersed flows using Eotvos/Reynolds, Kolmogorov/Hinze, prediction models for maximum drop size.

(Weber and et al., 1974) and (Weber, 1986; Weber M, 1978) observed that the solid particles in a slurry flow were affected by pressure and drag forces, (King, Fairhurst and Hill, 2001) experimented with sand transport from a dipped low section, While (Smart, 2009) calculated the minimum velocity that is required to move solid particles in an oil and gas flow pipeline based on a hydrodynamic model that relate to the drag and lift forces on the particles. The velocities reported for sand transport are similar to those encountered in the water and sand flow experiments in this project.

(Zeinali et al., 2012) used particle image velocimetry and sampling to study the effect of burst sweep activity (near-wall turbulence) as the mechanism of segregated entrainment of sand particles in the water flow with coarser particles removed first from the lenticular deposit. However (Matoušek, 2009)

characterised the sand flow transported as suspended or contact load in the water and that the throughput of sand depends on shear stress. (Davies, 1987) provided a better relation then the Durand relation for calculating the critical velocities for solids suspension in horizontal pipes. Similarly Oudeman (1993, 1994) studied sand transport in horizontal wells.

A study by (McLaury et al., 2011) discussed particle effects on pipe wall erosion; the velocities reported are also similar to this experiment. (Salama, 2000) characterised erosion and flow rate limits for sand particle impact using empirical and CFD to produce a prediction model. Furthermore sand transport settling and removal was identified for multiphase flows in relation to flow velocities and sand flow patterns

The literature has highlighted the need to observe interfaces height for liquid-liquid and gas-liquid flow transitions and entrainment for solid liquid flows.

1.1.4 Implication of settled phase

The settled phase forms sand dunes or water pools that cause erosion and corrosion. It could contain some impurities in the form of hydrogen sulphide and carbon dioxide dissolved in free water that would further enhance the advent of corrosion. For settled solids on the pipeline they cause erosion, fouling at low flow velocity and damage filters. Solid particles will continue flowing in a pipe until the flow rate is reduced or upon reaching compressor station.

1.2 Objectives

In further reiterating the above mentioned reasons for knowing the behaviour of the heavier phases in pipelines, those listed below are most critical;

1. In the transportation of oil, there is a legal maximum water content (for fiscal metering the producers want to have more water in the transfer pipeline whilst the refinery/processor wants to have more oil in pipeline to avoid paying for water rather than oil) thus a regulation of not more than 3% water in the United States as reported by (Pharris and Kolpa, 2007) is required in pipelines. The traditional

way of determining how much water is in the oil is by stirring up the water and take samples across the pipe. Thus, the understanding of the behaviour of the heavier phase could help to design these type of mixing and sampling system.

2. Settlement of water, with and without sand could accelerate the chance of corrosion. The presence of water at the bends/dips in the pipeline would lead to water or dense phase such as sand settlement at low flow rates or during shut downs. Furthermore on restart of production the settled water would form water plugs that would have consequences for refiners/ process facilities as the equipment are not designed to handle high water contents. The objective of the research is to carry out some careful experiments to observe the settled phase concentration profile under different flow condition and pipeline orientation so as to determine the required velocity to move or flush it out. The result will be used to further validate a prediction model. However the water drop out behaviour or phase settlement is not limited to water as it could apply to the heavier phase in multiphase oil and gas transfer pipelines, as water behaves as a solid particle in such a flow configuration; (Wicks and Fraser, 1975), this will be adapted to investigate air-water, water-oil air-oil and water-sand flows.

This could lead to developing an inspection process or tool to monitor or detect and remove heavier phase settlement and know the oil-water, water-sand, and air-oil and air-water flow phenomena characteristics at low heavier phase percentage or water cut. This procedure would improve on current methods that detect and remove phase settlement. The methodology would involve use of prediction methods, correlations, first principles and computational fluid dynamics. It would also involve use of monitoring devices that could use infrared rays and develop experiments with surface mounted electrodes.

The main objectives of this work are;

- To observe the behaviour of small amount of water in oil, small amount of sand in water in a horizontal pipe
- To observe the behaviour of small amount sand, air and water as well as small amount of water in air in a horizontal pipe.

- To establish the conditions and mechanism that dense phase can flow within the lighter phase experimentally.
- To develop models to predict the dense phase behaviour
- Observe the behaviour of settled sand, sand in water and sand in air water in a dip pipeline.

1.3 Structure

Chapter one highlights an introduction to the topic and the project objectives. Chapter two present a literature review describing fluid and solid flows, multiphase flow and instrumentation. Chapter three present details experiments for low water cut in oil in a four inch pipe, Chapter four gives details of experiments sand in water and sand in air water in a two inch horizontal pipeline, Chapter five present details of investigative experiments that were conducted with air, water and sand in a two inch pipe dip section. Chapter six gives a conclusion and outline of future work required in this project.

2 LITERATURE REVIEW

2.1 General Description of Oil and Gas Transfer Pipelines

Oil and gas transfer pipelines are an economic means of transporting fluids; being cheaper per unit than rail, road and sea transport whilst delivering greater volumes. Transfer pipelines could be grouped into;

1. Gathering pipe lines that are connected within a production field transporting oil and gas to processing and pumping stations in short distances.
2. Transportation pipelines that transport the oil and gas to long distances to refineries, jetties or even other countries and continents.
3. Distribution pipe lines that are for transporting oil and gas within storage depots and distribution networks for example gas supplied directly to homes.

Transfer pipelines are made with steel, plastics and carbon steel. They may be coated internally and externally or internally or externally only according to the type of fluid being transported. The pipe's diameter varies extensively based on the topography, required system pressure, temperature, flow rate and costs.

Pipelines transferring gas require compressor stations along the route while oil transfer pipelines need pumping stations along the route to maintain flow. Various techniques have been developed to monitor conditions in transfer pipelines using real-time data links that relay information from remote sensors to the manned control centre. These sensors could detect corrosion rates, leaks, and pressure and temperature changes in the pipelines. Regulatory authorities constantly enact legislations for pipelines so as to mitigate spills that would damage the environment.

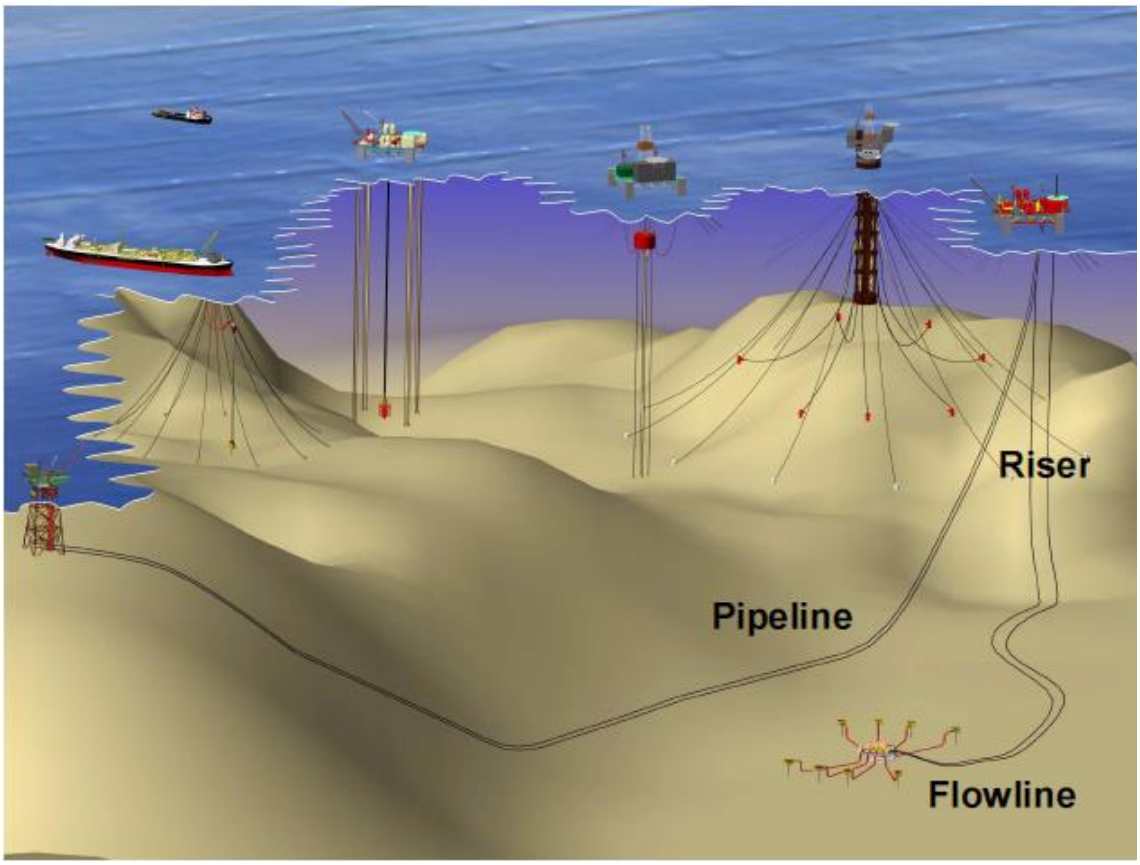

Figure 2-1 subsea pipelines and flow lines

2.2 Flow Classification

Flows can be classified into single phase or multiphase flow. Single phase flow consists of one phase flowing while multiphase flows consist of more than one phase.

2.3 Multiphase flow

Fluid flow can be single phase in which one component is flowing at a time liquid, gas or solid. A flow becomes multiphase when it has more than one component in its composition. It could be a two-phase liquid-liquid, gas-solid, liquid-solid, and liquid-gas flow, or even three-phase liquid-gas-solid flow.

Multiphase flows are common in oil and gas and chemicals industry and even within the human body in form blood circulation.

Holdup in multiphase flow indicates the area occupied by liquid in the pipe cross section compared with the total area of pipe. Void fraction indicates the area occupied by gas in pipe cross section by the total area of the pipe cross section.

Superficial liquid velocity refers to the velocity of the liquid in a pipe assuming it is flowing alone without any other phase in the pipe. While superficial gas velocity refers to the velocity of gas flowing in the pipe assuming that only the gas is flowing in the pipe. Mixture velocity refers to the velocity of all the phases or components flowing in a pipe as if only one phase or component is flowing in the pipe. The slip is the difference between velocities of fluids flowing in a pipeline.

2.4 Flow Regimes

Flows of two liquids occur in industrial processes and in petroleum production. This two phase flow in a pipe has “deformable contacting interfaces of the two fluids which have a range of distinctive distributions that are known as flow regimes or flow patterns. From (Angeli and Hewitt, 2000b) the flow patterns in each flow regime, the flow has apparent hydrodynamic characteristics”, an example of this could be observed in Figure 2-2. Observation of flow patterns could lead to development of more accurate models for two-phase flows.

Flow patterns in gas-liquid flows were observed through literature on flow pattern boundaries with different fluid properties by (Angeli and Hewitt, 2000b) and (Angeli and Hewitt 1998) and proposed models that envisage or estimate the transition between flow patterns, though for liquid-liquid flows there was not much available data on flow patterns. Flow regimes that were established in horizontal fluid flows could be stated as:

“Stratified flow: the two fluids comprise separate layers each being distinct from the other due to their different densities that is each is flowing in the pipe as an immiscible component with a distinct boundary between them with heavier fluid at the bottom of the pipe with the lighter fluid at the top of the pipe.

Annular flow: in this type one fluid impinges the pipe wall as an annular film while the other flows surrounded by the other fluid in the pipe centre. This mostly occurs when fluids have nearly equal densities or when one fluid is highly viscous.

Dispersed flow: one fluid flows continuously while the other does not flow continuously but rather flows as dispersed drops in it. That is the other fluid consists of droplets within the other fluid."

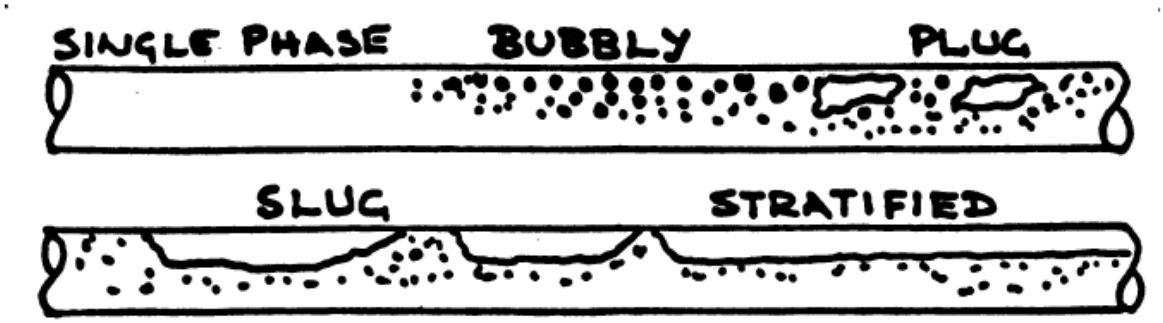

Figure 2-2 Flow Patterns Cranfield (University Lecture Notes)

2.5 Oil and Water Flows

Oil and water flows are encountered mainly in flows of production fluids from the reservoirs. For oil and water flows, the flow pattern identification and characteristics are described in the following sections.

2.5.1 Methods of flow pattern identification

Flow pattern identification is made by observing the flow using a visible conduit or a transparent part on the pipe wall. Other visual observation techniques like, photography or video are used; and for very fast moving phenomena, high speed video or photography is used. Though, this may still not give a clear demarcation of the flow pattern, due to interface reflections, refractions and also the fact that the cameras and visual observation obtain view from the pipe wall where there might be an inaccurate view close to the flow pattern boundaries, where the optical differences between two flow patterns can be very minute. Thus for gas-liquid flows, other methods have been used to supplement the visual observations (Hewitt, 1978).

However, for liquid-liquid flows, the technique mostly used was visual observation and photography (Russell and Charles, 1959); Charles et al., (1961); (Hasson,

Mann and Nir, 1970); (Arirachakaran et al., 1989). On the other hand, it is worth noting that(Nädler and Mewes, 1995) used a conductivity probe for identification of the continuous phase in the dispersed region. (Lovick and Angeli, 2004) used an impedance probe to acquire the phase distribution in an inclined pipeline oil-water flow.

Local probes can be used to obtain the volume fraction distribution over a pipe cross section and thus specify the different flow patterns supplementing visual observation. (Angeli and Hewitt, 2000a) further described use of high speed video camera for visual phase pattern identification, high frequency impedance probe to measure phase distribution and conductivity probe to measure the continuous phase. Similarly (Soleimani, Lawrence and Hewitt, 1999) used capacitance tomography for liquid-liquid flow regime identification. Flow pattern maps were subsequently produced from these studies; nevertheless, these had significant variations.

A study by (Trallero.L, 1995) observed oil-water flow patterns transitions in horizontal pipes and classified them into two, dispersed flow and segregated flow which have sub categories stratified and stratified with some mixing at the interface. Then dispersed water dominated or oil dominated flow, dispersion of oil in water over a water layer with water as dominant phase and an emulsion of water in oil and a dispersion of water in oil or a dispersion of oil in water both being oil dominated. A summary of the oil-water flow pattern in horizontal pipelines derived as follows:

1) Segregated Flow: this flow is one in which each fluid is flowing continuously but separated by an interface.

a) Stratified (ST), in this flow as shown in Figure 2-3 the oil flows on top of the water with a distinct layer between separating each fluid.

b) Stratified flow with mixing at the interface (ST& MI), in this flow there is a distinctive layer between each fluid but oil mixes with the water as droplets within each fluid at the interface as seen in Figure 2-3.

2) Dispersed Flow: In this type of flow, one of the fluids is not flowing in a continuous stream but rather consist as droplets within the other continuous fluid.

a) Water Dominated

I) Dispersion of oil in water and water (D o/w & w), as seen in Figure 2-3 at the pipe bottom water is continuous while on top there is a mixture of droplets of water and droplets of oil.

II) Oil in water emulsion (o/w), as indicated in Figure 2-3 droplets of oil are in the water so mixed that there is not distinct boundary between the droplets and continuous water flow at the top of the pipe.

b) Oil Dominated

I) Dispersions of water in oil and oil in water (D w/o & D w/o), as in Figure 2-3 water droplets are mixed with oil droplet towards the pipe bottom with an oil continuous layer on top.

II) Water in oil emulsion (w/o), as in Figure 2-3 here the droplets of water in the oil are being so mixed that there is not distinct boundary between the droplets and continuous oil flow at the bottom of the pipe

(Trallero.L, 1995) also gave a criterion for transitions between flow patterns as indicated in table 1.

Stratified Flow (ST)

1, a)

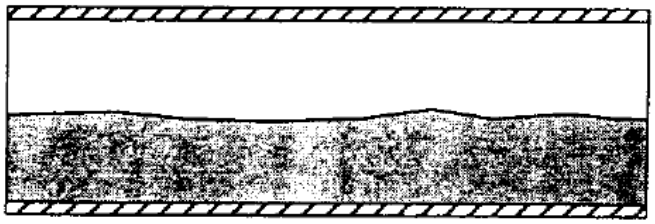

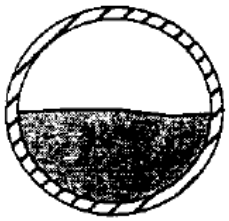

Stratified Flow with mixing at the interface (ST & MI)

1, b)

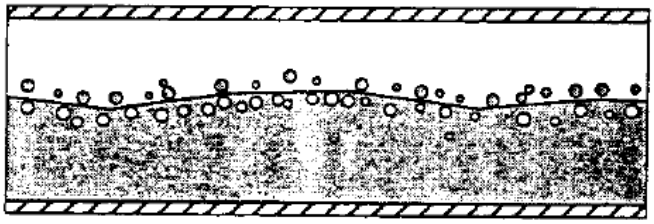

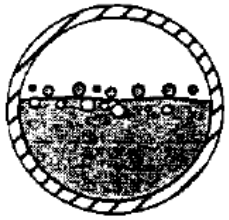

Dispersion of oil in water and water (Do/w & w)

2, a, l)

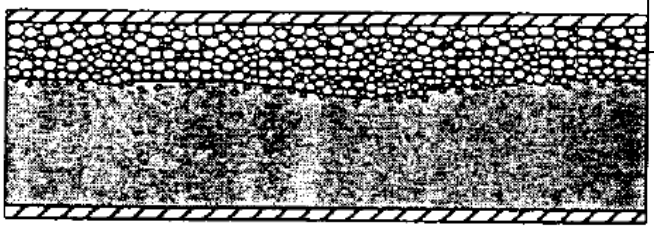

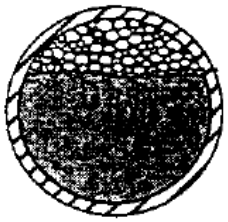

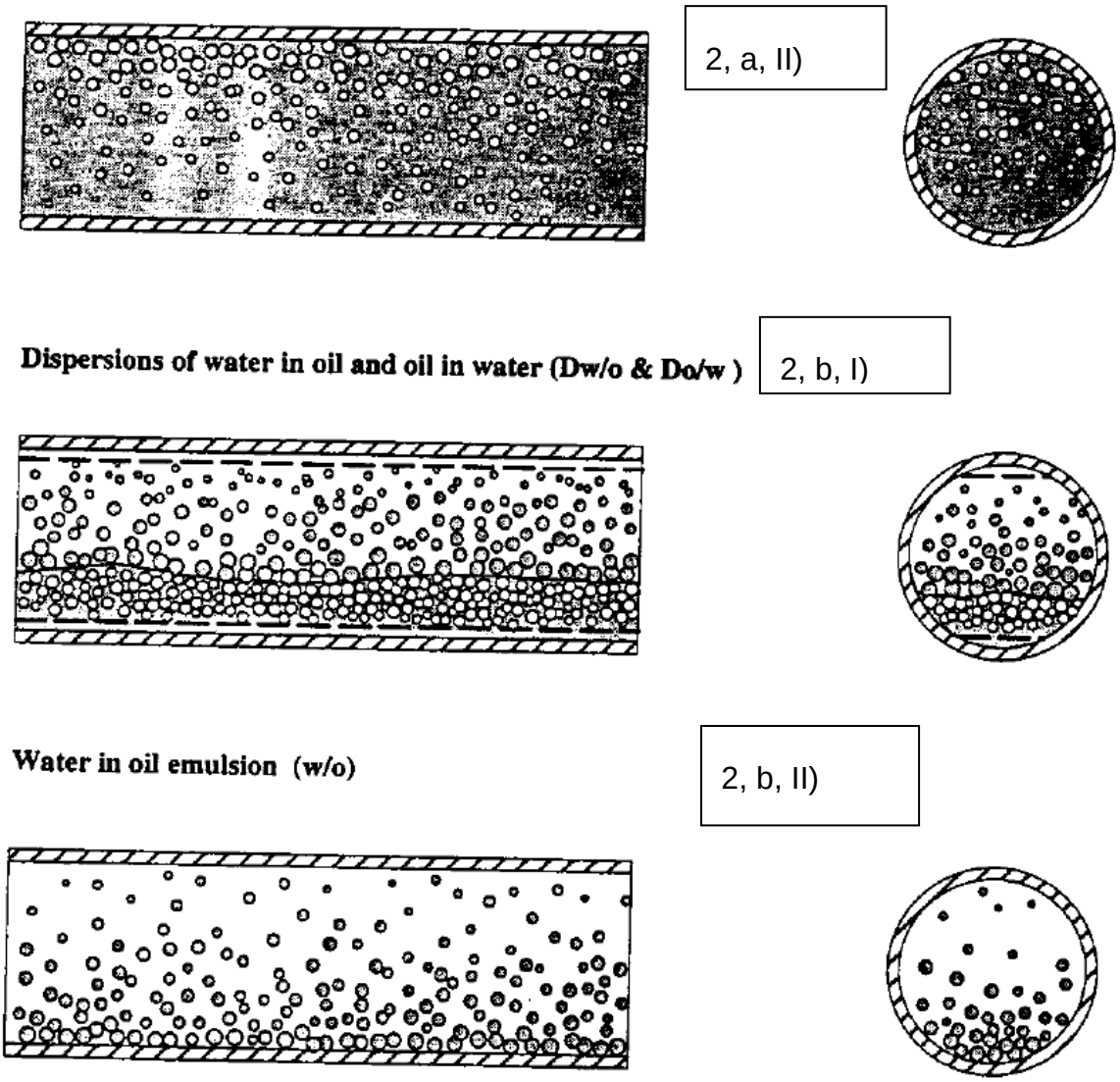

Figure 2-3 Oil and Water Flow Classifications; (Trallero.L, 1995)

Table 2-1 Flow transitions (Trallero.L, 1995)

Segregated flow Patterns			
Flow Pattern		Transition Criteria	
Stratified		Viscous Kelvin Helmholtz	
Stratified with mixing at interface		Inviscid Kelvin Helmholtz $U_w < U_{wwL}$ & $U_w > U_O$	
Dispersed flow patterns			
Water Dominated Region		Oil Dominated Region	
Flow Pattern	Transition criteria	Flow pattern	Transition criteria
Dispersed oil in water and water	$U_w < U_{wmH}$ & $U_w > U_o$ Outside IKH	Dispersed water in oil and water Dispersed oil in water	$U_o \geq U_{ooH}$ & $U_w \geq U_{wwH}$
Oil in Water	$U_w \geq U_{wmH}$ & $U_w > U_o$ Outside IKH	Water in oil	$U_o \geq U_{omH}$ & $U_w < U_o$ Outside IKH $U_o \geq U_{omH}$ Inside IKH

2.5.2 Orientation

Orientation of a pipe has major contribution to water drop out or settling in oil-water pipeline transportation. This is as a result of gravitation forces acting on the flow affecting the flow velocity at inclined position and pipe bends. These could aggravate formation of water slugs.

A study by (Beggs and Brill, 1973) observed that most correlations on two-phase gas-liquid flows deal with either horizontal or vertical flows for hold up and pressure drop. However this does not fit with two-phase flows as the downhill flow mixture density is lower thus affecting pressure recovery. In reality most pipelines are undulating and with advent of directional drilling, there was a need to drill wells from one platform due to harsh environment. To avoid the pressure gradients for slightly inclined pipelines having the elevation pressure gradient being much higher than the frictional pressure gradient. It is imperative to have an accurate prediction of liquid hold-up so as to the predict pressure drop. Correlations used for liquid hold-up and friction factor were developed to predict pressure gradients for two-phase flow in pipes at all angles for various flow conditions. This further reiterates the need to conduct this study measuring the holdup of the desnser phase as given in the following chapters 3,4 and 5 repectively.

Similarly (Rodriguez and Oliemans, 2006) also studied the effect of inclination angle on holdup and pressure drop for oil–water flow patterns with the same properties of oil and water used by near-horizontal production wells with inclination angles varying from -5 to +5 degrees from the horizontal. Data was obtained from an adequately instrumented large-scale experimental facility to validate and extend flow-pattern-dependent holdup and pressure gradient models. Hold up measurement was obtained by two gamma densitometers and for visual observations; a high-speed video was used. To develop new models the data had to be substantial and qualitative. The six inclination angles and horizontal flow data was collected on two-phase pressure gradient, in situ volumetric fraction of the liquid phases or holdup and video images of the flow. These were presented as a function of the inclinations, flow patterns and

superficial velocities, for the whole range of flow rates. The predictions of oil-water pressure gradient and hold up were presented as a function of pipe inclination. The prediction model utilised was area averaged steady-state two-fluid models for stratified flow while the homogenous model was for dispersed flow. The equations are given below;

For homogenous water holdup

$$\varepsilon'_{w,hom} = \frac{\rho_m - \rho_o}{\rho_w - \rho_o} \quad \textbf{(2-1)}$$

For stratified water holdup

$$\varepsilon'_{w,strat} = \frac{1}{\pi}\left\{\cos^{-1}\left(1 - 2\varepsilon'_{w,hom}\right) - \left(1 - 2\varepsilon'_{w,hom}\right)\sin\left[\cos^{-1}(1 - 2\varepsilon'_{w,hom})\right]\right\} \quad \textbf{(2-2)}$$

Homogenous mixture density is given by

$$\rho_{m,hom} = \rho_w \varepsilon_{w,hom} + \left(1 - \varepsilon_{w,hom}\right)\rho_o \quad \textbf{(2-3)}$$

Where

$$\varepsilon_{w,hom} = \frac{U_{ws}}{U_{ws} + U_{os}} \quad \textbf{(2-4)}$$

Holdup is given by

$$-\frac{\tau_w S_w}{A_w} + \frac{\tau_o S_o}{A_o} \pm \tau_i S_i \left(\frac{1}{A_w} + \frac{1}{A_o}\right) - (\rho_w - \rho_o) g \sin\theta = 0 \quad \textbf{(2-5)}$$

Pressure drop is given by

$$\frac{d_p}{d_x} = -\frac{f_{m,hom}\rho_{m,hom}U_m^2}{2D} - \rho_{m.hom}g\sin\theta \quad \textbf{(2-6)}$$

2.5.3 Water Cut

The percentage composition of water in the flow has some effect on formation of water drop out. With a certain percentage the water no longer undergoes phase inversion with the oil and at some point with a reduced flow velocity it has the tendency to drop out especially if the water is flowing as a thin annular around the oil. Observations made using carousel found out that the carousel produces results that allows ranking of field oils in terms of water dropout tendency, absolute quantification has not been possible so far, even using Computational Fluid Dynamics (CFD) simulation to "correct" for mismatches between lab and field. Main drawbacks of the carousel are that, Secondary helical flow influences the motion of water droplets. The transition Reynolds number from laminar flow to turbulent flow is considerably higher than in a pipeline (~11,000 versus 2100)".the graph for the critical flow velocity against water cut is given in Figure 2-6 while figure 2-5 shows the carousel used in the experiments.

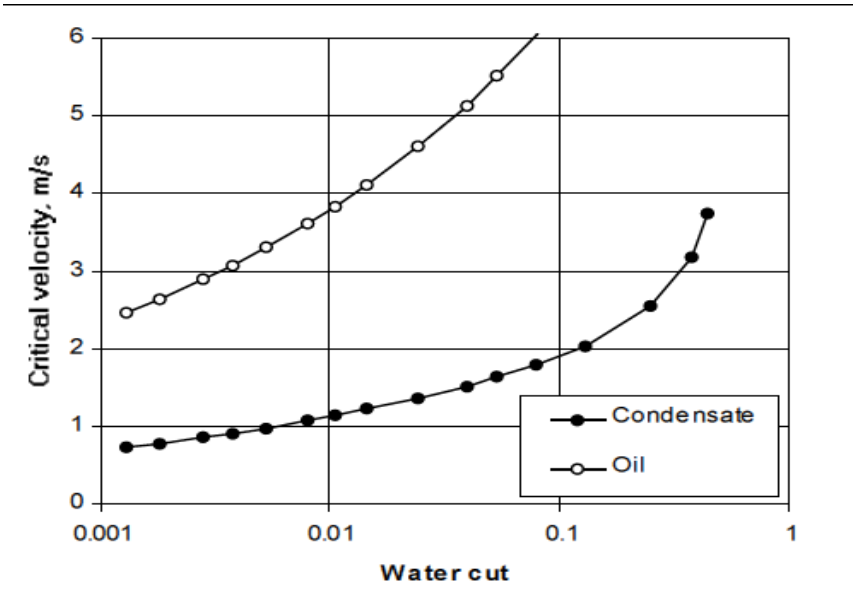

Figure 2-4 Critical flow velocities for maintaining water dispersion in condensate and oil in 20-inch pipeline using K/S modelling (Pots, Hollenberg and Hendriksen, 2006)

Figure 2-5.Carousel (Pots, Hollenberg and Hendriksen, 2006)

2.5.4 Effect of Fluid Properties

From the available literature fluid physical properties has significant impact on oil-water flows. These include density, viscosity, temperature, friction factor.

Angeli and Hewitt (1998, 2000), concluded that apart from the apparent influence of phase superficial velocities and channel diameter, other variables that also influence flow patterns were:

Density difference: previous experiments that were carried out had significant density deference between the phases consequently for the horizontal pipes; this led to observation of asymmetries within the flow having the heavier phase inclining to flow adjoining the bottom of the tube. Conversely, Charles et al., (1961) utilised oils with an equivalent density as that of water; in this case symmetrical flow patterns and the occurrence of annular flow were observed.

Oil viscosity: for a dispersed flow pattern and having water as the continuous phase, there was little effect of oil viscosity on flow behaviour (Arirachakaran et al., 1989). The viscosity has a strong influence on the incidence of annular flows when there is density difference between the phases; for annular flow, having water forming the annulus adjoining the tube wall occurs only with oils having

higher viscosities. Apparently annular flow having the oil phase flowing adjoining the tube wall occur only with oils having transitional viscosities, whereas for lower viscosity oils this flow pattern is consumed by the oil continuous dispersed flow patterns Guzhov et al., (1973);(Arirachakaran et al., 1989).

Wall wetting properties: The main phenomenon explored was the influence of the material used for the wall on the flow behaviour. The wall wetting effects was identified by Charles et al. (1961) as the cause of the different behaviour between the low and high viscosity oils used in experiments. (Hasson, Mann and Nir, 1970) , studied water and oil mixtures having equal densities, proposed that wall wetting effects were imperative in the annular core break-up mechanism and in the transition from annular flow to other flow regimes. However (Angeli and Hewitt, 2000b) were the first to investigate such effects in the normal range of flow patterns and fluid densities.

Similarly, Hewitt and Angeli (1998) discussed the effect of pipe physical properties on the flow characteristics like pressure drop due to differences in pipeline material. Laboratory tests are usually conducted using acrylic pipes but in the industry, steel pipes are used.

Experimental results obtained showed 100% difference in pressure gradient between steel pipe and acrylic resin pipes. This is consequence of tube roughness and wettability characteristics of the materials. Apparently the flow patterns for a given pipe orientation and diameter are expected to be determined by the volume fractions, and the velocities physical properties (viscosity and density) of the respective phases. An additional expected important parameter is the wetting characteristics of the tube wall. These effects can be significant in gas-liquid flows, for example when the channel wall is hydrophobic in air-water flow, although they are not generally considered. By comparing the pressure gradients in stainless steel and acrylic tubes for the same conditions (Angeli, 1996; Angeli and Hewitt, 1998) identified significant differences in values obtained for the different wall materials.

Conclusions were made that the material of the pipe wall can have a strong effect on the pressure gradient for two phase liquid-liquid flow. The pressure gradients

were higher at the steel than in the acrylic pipes for similar mixture velocities and flow volume fractions for all conditions, the difference being more than what is expected from that in wall roughness. For oil continuous flows a significant drag reduction was identified in both pipes which were consistent with a reduction in Von Kármán (a constant that is a dimensionless logarithmic velocity profile of turbulent flow), by up to 35%. After this data was compared to experimental and phenomenological models, they were mostly in poor concurrence possibly as a result of wetting phenomena and drag reduction effects mentioned earlier. There is a need to develop models in future that would consider these effects. From the results it would be ideal to have additional study of the effects of material on wetting properties and drag reduction on two phase liquid-liquid flows.

(Pots and Kapusta, 2005) describes that flow can influence corrosion in many ways and grouped the effects as a distribution of fluid phases, including the water phase distribution and the pipe wall wetting by free water.

“For stratified or separated multi-phase flow, dewing corrosion in the top of the line can become an issue especially because inhibitors generally cannot reach the top of the line. For the same flow pattern, a corrosion inhibitor has to be selected for the bottom of the line that partitions well in the water phase, to ensure that the inhibitor gets to the wall where the corrosion is. The presence of settled solids may lead to bacterial corrosion problems, aggravate oxygen corrosion, prevent corrosion inhibitors to do their job, destabilize natural or intentional protective iron carbonate or iron sulphide scales, etc. A further summary is given below;

Effect of Flow Pattern on Corrosion

“To identify the corrosion rate in pipelines, vital knowledge of the process of mass transport of material, and the number of corrosion mechanisms and mass transport of corrosive material to the wall across the diffusion boundary layer is required. This applies to corrosion by protons, organic acids, and oxygen. While where a corrosion product scale forms, the transport of corrosion products away from the wall can be the rate-determining step. The high mass transfer of corrosion products can prevent protective corrosion product scales to form. The

distribution of corrosion inhibitor over the steel wall is another example. This includes the mixing of corrosion inhibitor with the relevant liquid phase after injection and the distribution of the inhibitor along a pipeline.

Mechanical forces, these are liquid shear stresses caused by high flow velocity, forces induced by cavitating gas/vapour bubbles, impact forces by liquid droplets, etc.

Corrosion inhibitor failure caused by high flow, often related to high shear stress, breakdown of corrosion product layers leading to erosion/corrosion and as a result of scouring of corrosion inhibitor films or corrosion product layers that are intentionally deposited when pH stabilization is used to control corrosion.

From field experience internal corrosion may not be an issue, even though potentially corrosive water is produced. There are also examples of pipeline systems that experience internal corrosion, even though the water cut is very low and water dropout seems unlikely. This remains a recurring issue in the industry.

An all-encompassing theory or model that describes water or oil wetting will probably remain a challenge forever, as there are too many parameters and effects that would have to be accounted for. Attempts to capture flow effects in a single parameter, like flow velocity, shear stress, a flow pattern transition, etc., ignore the complexities of flow effects on corrosion. Use of such parameters as a correlating parameter should be discouraged when a direct mechanistic relationship is questionable. An example is the use of shear stress in a corrosion rate calculation when the prevailing mechanisms are a mixture of mass transfer, charge transfer kinetics, and chemical reaction.

The following oil protection categories can be distinguished: Presence of “natural” constituents in the oil or condensate that may behave like corrosion inhibitors such as oil or water surface wetting due to contact angle effects. For instance, a clean carbon-steel surface may be oil surface wetted, while a corroded surface is water surface wetted. Another category is the physical contact of the wall as a result of the forces of the flow of oil or water phase. This includes water dropout, water entrainment, and water droplet impingement in

annular dispersed flow and water being forced to the wall by centrifugal forces due to changes in flow direction, at the bottom of a riser. The above distinction is a somewhat simplified representation as effects may fall in more than one category. The cause of any corrosion reduction seen is not explained by field experiments or laboratory tests."

(Pots, Hollenberg and Hendriksen, 2006) provided a translation to multi-phase flow by stating that "the interpretation of the diameter and liquid mixture velocity in the model equations is a complication of three-phase flow. Without experimental data, a practical approach is to use the hydraulic diameter of the liquid phase for the diameter and the liquid phase velocity for the velocity. The hydraulic diameter equals 4 times the cross-sectional area covered by the liquid phase divided by the wetted perimeter. A second consideration is how to interpret the above for the various flow patterns:

For stratified flow, application of the above rule is straightforward.

For slug flow, the conservative assumption may be taken to only consider the lower flow velocities in the film part of the slug. Actually, the flow in the slug may lead to full entrainment, which is maintained in the film.

For annular dispersed flow, the water phase may be forced to the wall. This is a very conservative and perhaps questionable assumption, but it is supported by subjective field findings in wells. Dispersed bubble flow can be interpreted as single-phase flow."

2.5.5 Flow Models

There have been a few models developed for flow such as the two fluid model and homogenous model. The two fluid model treats the flow as if each fluid is flowing separately in the pipe while the homogenous model treats the flow as if only one fluid is flowing in the pipe.

A study by (Trallero, Sarica and Brill, 1997) observed pressure drop decreases when the flow transitions to a dispersed flow. Furthermore use of conductance probe data and high speed photographs are adequate for flow pattern

identification while wall pressure fluctuations are not. Slippage between the two fluid velocities is only relevant for segregated flow patterns.

The two-fluid model and a balance between turbulent and gravity fluctuations normal to the axial flow direction was used to predict the oil-water flow pattern transitions for light oils. Linear and non-linear analyses indicate that the stratified or non-stratified transition must be considered with the complete two-fluid model. For Stratified flow, it is predicted by viscous Kelvin-Helmholtz analysis while the ST & MI flow pattern is predicted by the inviscid Kelvin-Helmholtz theory.

The viscous Kelvin-Helmholtz analysis and structural stability criterion are both satisfied simultaneously. For the dispersed flow pattern, the predicted drop sizes from the Hinze and Levich models are modified in so as to consider the effect of the dispersed phase concentration. The controlling parameter for the coalescence phenomena is the water fraction. The performance of the model was exceptional and compared well with published data. Moreover, the model gave reasonable predictions for inclined flow. The model flow regime map is given in Figure 2-6 below.

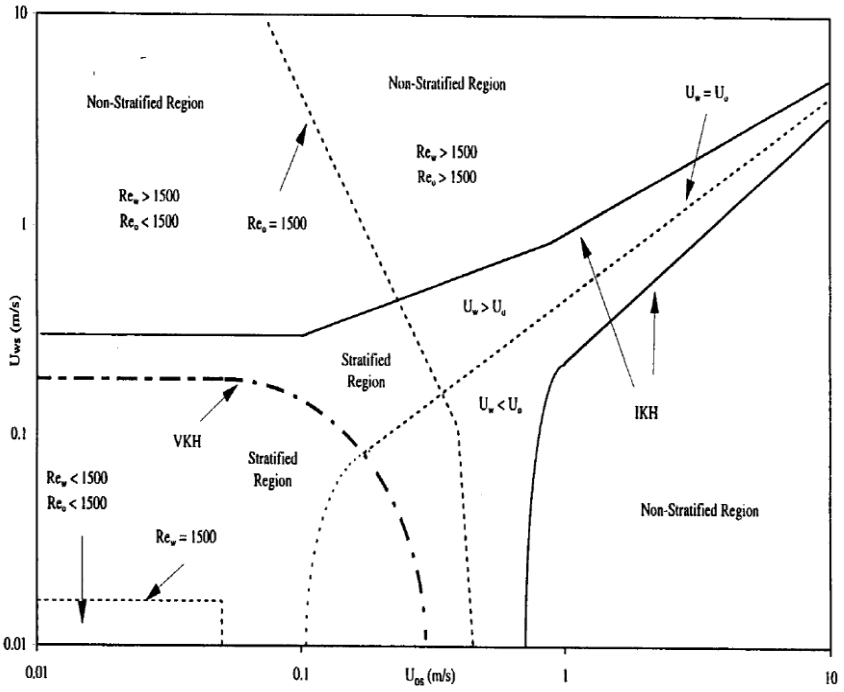

Figure 2-6 Two-fluid model prediction, VKH and IKH analysis Trallero (1995)

There are forces at play between formation of stratified to dispersed flow regimes. These are the Kelvin Helmholtz Instability and droplet formation and breakup. The Kelvin Helmholtz Instability treats the process of interfacial contact between a lighter-phase that flows over a heavier phase resulting in the formation of waves on increase of flow velocity. This wave start as smooth ripple waves transitioning to pebble, pebble and finally roll waves. Upon formation of roll waves, a velocity increase result in formation of eddies on the crest of the waves where droplets are formed by shearing force overcoming the attracting viscous forces. The drop is then dispersed in the lighter phase

(Angeli, 2001) noted that the(Hinze, 1955) model under predicts the experimental maximum drop size while the Rosin-Rammler distribution concurs with the experimental maximum drop sizes. Similarly (Kostoglou and Karabelas, 1998) argued that experimentally obtained particle size distributions did not agree with theoretical steady state predictions as a result of the need for an extended period of time needed to reach steady state in a pipe flow. Concluded that most experimental data on the maximum droplet diameter as transients.

The maximum drop size that is formed and the dispersed phase have effects on heat/mass transfer rates, separation equipment and pressure drop. The drop size is affected by the drops breaking up and coalescing. The breakup maximum diameter is the maximum size diameter of a drop that could resist breakup in a turbulent pipe flow. This is also associated with the Sauter Mean diameter that gives the available interfacial area in dispersions. While the Weber number is a function of drop stabilization and drop breakup forces and being a ratio of external to interfacial tension. The Kolmogoroff scale on the other hand gives the inertial sub range of turbulence.

Drop coalescence occur as drops come into contact and during the contact interval the continuous layer then reaches the critical thickness for rupture. There is a minimum drop size for coalescence.

Work by (Hutchinson, Hewitt and Dukler, 1971) derived a model for particle and droplet deposition in turbulent gas flow indicting a difference between eddy and

particles motions. The tube diameter of the particle, density ratio, covered distance and Reynolds number determine the deposition rate of the particles.

(Pots, Hollenberg and Hendriksen, 2006) “Models for Prediction of Water Drop-Out in Oil Pipelines; this identified a number of rules or models that describe the “likelihood” of water wetting. Though these simple models have their limitations, more complex models are not necessarily better. The main disadvantage of all models is that they are based on physics only instead of a combination of physics and chemistry. However, models may still help to build an understanding of the “likelihood” of water dropout.

The (Wicks and Fraser, 1975) model refers to the pick-up or sweep out of accumulations of water by flowing oil from low points. It is often used as a rule of thumb to predict water wetting in oil pipelines. This model is based on a combination of two correlations: one for the minimum velocity for the net axial transport of sand particles and one for water droplet size. It was assumed that the correlation for the sand particles could be equally applied to rigid droplets of the same size. The sand transport correlation was derived from experimental data for transport of sand in various liquids. The droplet size was taken from Hinze. The size refers to the maximum water drop size (d 95) in a turbulent flow field. The Wicks and Fraser model was validated for a kerosene/water mixture in a 1-inch flow loop. Rule of critical flow velocity of 1 m/s and maximum water cut based on the work by Wicks and Fraser, a guideline that called for a minimal mixture flow velocity of 1 m/s and maximum water cut of 20%. For a long time, this rule was associated with the safe and corrosion-free operation of oil pipelines. Later work by Lotz (1990) suggested a much greater maximum water cut of 40%. However these studies have a much higher water cut than those considered in this study do.

Similarly(Tsahalis, 1977); modelled the sweeping of settled water based on instability of a water layer and pick up or entrainment of water into the oil phase. This model gives typical critical flow velocities below 0.5 m/s. The value is low compared with Wicks rule due to the pipe diameter used in the experiments.

Furthermore,(Snuverink, Lansink and Duijvestijn, 1987)**;** studied the sweeping of water from a foot of an inclined section in lab experiments using various pipe diameters, inclinations, and model fluids. They correlated the critical velocity, for pushing water batches over the “hill”, with the densimetric Froude number in equation (2-7):

$$F = \sqrt{\frac{\rho_o}{\Delta\rho g D}} \tag{2-7}$$

Where, ρ_o is the density of oil, $\Delta\rho$ is the oil-water density difference, g the acceleration due to gravity, and D the pipe diameter. The Froude number is the ratio of shear to gravity forces. The critical Froude number is a function of pipe inclination but for inclinations larger than 5 degrees, the value was found to be F=0.67. The rule is conservative for inclinations less than 5 degrees. The rule only applies when the flow is turbulent.

On the other hand (Hollenberg and Oliemans, 1992); Based on work by Davies, describe a model that establishes the critical velocity at which sufficient turbulence is created to break up large water droplets and to maintain them in dispersion against sedimentation. Turbulent damping and hindered settling are considered. A model requirement is that the flow is turbulent. The following assumptions apply: homogeneous dispersion, single droplet size, drops act as solid particles, smooth pipe wall (Blasius friction factor), and horizontal line. The final expression for the critical velocity can be rearranged in dimensionless groups. The critical velocity is expressed as a Froude number:

$$F = f(c)\Pi^{\frac{1}{22}} \tag{2-8}$$

$$f(c) = 1.5(1 + \alpha c)^{\frac{10}{11}}(1 - c)^{\frac{5n}{11}} \tag{2-9}$$

$$\Pi = \frac{\sigma^2}{\upsilon^2 \rho_o \Delta\rho g D} \tag{2-10}$$

Where, c is the water cut, v the oil viscosity, and σ the oil/water interfacial tension. The exponent for hindered settling is taken as n=3, the turbulent damping coefficient as α=3.64. The function f reaches a maximum at a water cut of 24%. For all practical field and lab cases, the calculated critical Froude number is within 20% of the value F=2.

Furthermore Karabelas and later Segev; developed models to calculate the distribution of particles or water droplets in oil pipelines called the Karabelas/Segev (K/S) model as demonstrated in Figure 2-7 and given by equations (2-11) to(2-19). Starting point is a diffusion-convection equation for the flux of droplets in a gravitational and turbulent flow field:

$$j = -D\nabla c + cV_s \tag{2-11}$$

Droplet flux

$$c(r,\theta) = c_o exp\left(-\alpha\, cos\theta \frac{r}{R}\right) \tag{2-12}$$

Droplet distribution is obtained by use of 2-11

$$\alpha = \frac{V_s R}{D} \tag{2-13}$$

Ratio

$$c_{bot} = c_{avg}(1 + a\alpha)^b \tag{2-14}$$

Bottom concentration of the droplets is

$$V_s = \frac{g\rho\Delta d^2}{18\mu} \quad \textbf{(2-15)}$$

Terminal velocity for the droplets is given by

$$d = a\left(\frac{\sigma}{\rho_o}\right)^{0.6} E^{-0.4} \quad \textbf{(2-16)}$$

Hinze droplet size

$$E = \frac{1}{\rho_O}\frac{dz}{dp}V = \frac{2fV^3}{D} \quad \textbf{(2-17)}$$

Specific power dissipation

$$D = 0.255RV^* \quad \textbf{(2-18)}$$

$$V^* = \left(\frac{f}{2}\right)^{0.5} V \quad \textbf{(2-19)}$$

$$V^* = \left(\frac{f}{2}\right)^{0.5} V \quad \textbf{(2-20)}$$

Droplet Eddy diffusivity

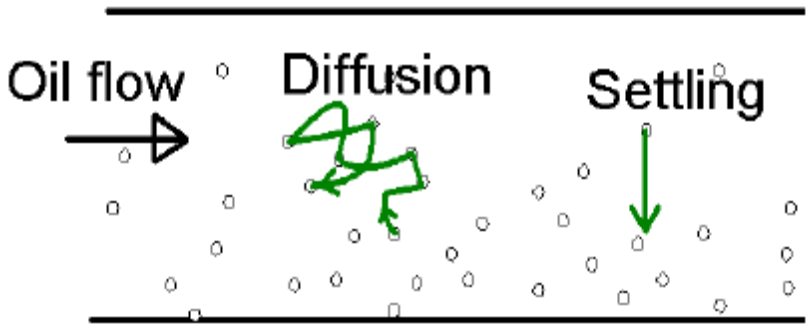

Figure 2-7 Karabalas/Segev modelling: turbulent diffusion versus gravity settling (Pots, Hollenberg and Hendriksen, 2006)

However (Brauner, Moalem Maron and Rovinsky, 1998) developed a practical methodology for predicting the interface shape for stratified flow of a general two-fluid system with consideration of a curved interface. The two-fluid model was adapted to solve momentum equations for available interface curvature. The complete solution was obtained from an "operational monogram" as well as the interface shape, pressure drop and in situ holdup. This was established for turbulent or mixed, laminar flow regimes in the two phases. The Brauner interface diagram could be seen in Figure 2-8 while the previous cross sectional view in seen in Figure 2-9

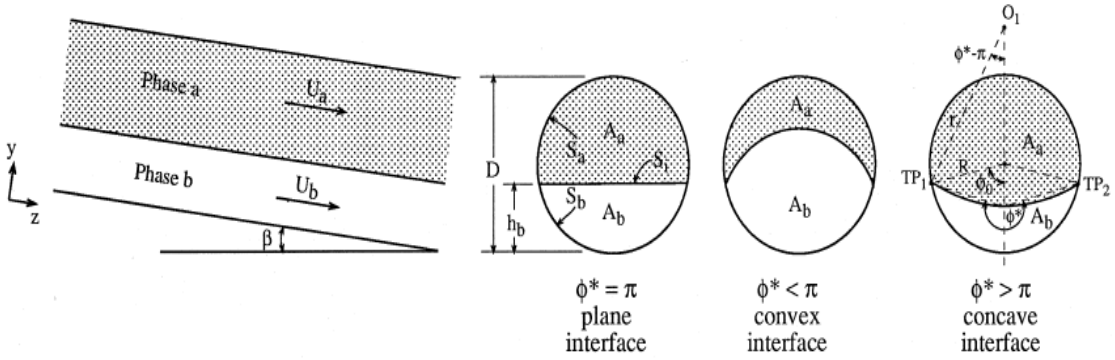

Figure 2-8 Model for curved interface (Brauner, Moalem Maron and Rovinsky, 1998)

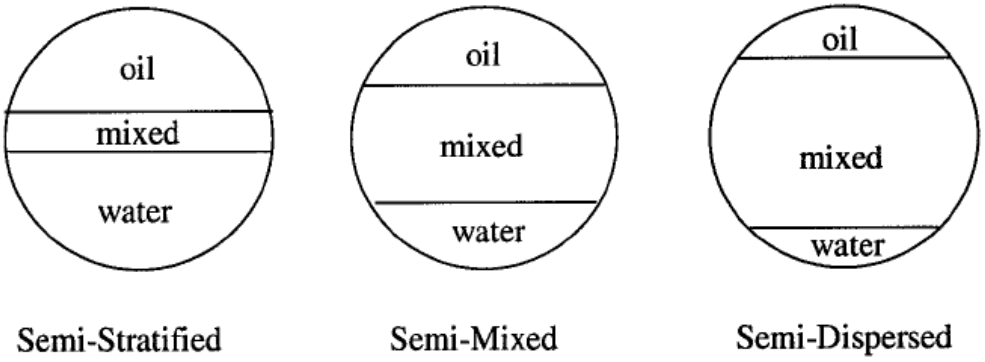

Figure 2-9 Cross sectional view for three-phase flow patterns; Vedapuri (1997)

Work by (Shi et al., 2002) developed a mathematical segregated flow model; subsequently a four-layer/phase was developed for intermediate oil-water flow patterns of mixed, semi-segregated and semi-mixed three-phase model with experimental data. A further classification into oil in water (water continuous) and water in oil (oil continuous) layers of the mixed layer in the three-phase model was the phase inversion point. This model predicts the thickness and in situ velocity of each layer given the properties of oil and water and pipe diameter. It was concluded that velocity and in situ water holdup are affected by superficial mixture velocity and input water cut. Four phase segregated flow model was practical method for corrosion behaviour prediction in oil and water flows due to the use of the total water film thickness. Three and four phase/layer models cannot predict settling or water drop out from oil and water dispersions and emulsions. Essentially the model works only within the 10-90% water cut range. A mechanistic multilayer model developed with commercial CFD, CFX was then developed that could significantly predict water drop out.

(Cai et al., 2005) modelled water wetting in oil-water pipe flows given from equation (2-21) to (2-44). The approach follows (Brauner, 2001) and (Barnea 1987) to predict water in oil, fully dispersed flow. A criterion to calculate the critical velocity for water entrainment into the flowing oil was developed, a comparison of maximum droplet size that relate to breakup. For maximum droplet size he used the (Hinze, 1955) which use dimensional analysis in examining forces that control droplet breakup of a liquid-liquid flow to know the maximum droplet size

that could be sustained by the flow prior to break up. For drop splitting in turbulent flow the Weber Number is

$$We_{crit} = \frac{\tau\, d_{max}}{\sigma} \tag{2-21}$$

This shows the ratio between external hydrodynamic stresses(τ) that deform drops and the counter acting surface tension σ

For dilute water in oil dispersion from (Brauner, 2001)

$$\left(\frac{d_{max}}{D}\right) = 0.55\left(\frac{\rho_c U_c^2 D}{\sigma}\right)^{-0.6}\left[\frac{\rho_m}{\rho_o(1-\varepsilon_w)}f\right]^{-0.4} \tag{2-22}$$

$$\varepsilon_w = \frac{U_{sw}}{U_{sw}+U_{so}} \tag{2-23}$$

$$U_c = U_{sw} + U_{so} \tag{2-24}$$

$$U_c = U_{sw} + U_{so} \tag{2-25}$$

$$\left(\frac{d_{max}}{D}\right)_{dilute} = 1.88\left[\frac{\rho_o(1-\varepsilon_w)}{\rho_m}\right]^{-0.4} We_o^{-0.6} Re_o^{0.08} \tag{2-26}$$

Where:

$$Re = \frac{\rho_o D U_c^2}{\eta_o} \tag{2-27}$$

$$We = \frac{\rho_c U_c^2 D}{\sigma} \quad \textbf{(2-28)}$$

$$f = 0.046/Re_o^{0.2} \quad \textbf{(2-29)}$$

The above equation could only be used if;

$$(1 - \varepsilon_w)\frac{\rho_o}{\rho_m} \cong 1 \quad \textbf{(2-30)}$$

Dense water in oil dispersions

$$\frac{\rho_o U'^2}{2} Q_o = C_H \frac{4\sigma}{d_{max}} Q_w \quad \textbf{(2-31)}$$

Where:

$$Q_o = \frac{\pi}{4} D^2 U_{so} \quad \textbf{(2-32)}$$

$$\mathrm{Q_w} = \frac{\pi}{4} D^2 U_{sw} \quad \textbf{(2-33)}$$

$$U'^2 = 2\mathrm{ed_{max}}^{2/3} \quad \textbf{(2-34)}$$

For isotropic homogenous turbulence, the kinetic energy would be related to the rate of turbulent energy dissipation, e:

$$e = \frac{4\tau U_o}{D\rho_{o(1-\varepsilon_w)}} = \frac{2U_c^3 f}{D} \frac{\rho_m}{\rho_o(1 - \varepsilon_w)} \quad \textbf{(2-35)}$$

*e*Substituting equations

$$\left(\frac{d_{max}}{D}\right)_{dense} = 2.22C_H^{0.6}\left(\frac{\rho_O U_c^2 C}{\sigma}\right)^{-0.6}\left(\frac{\varepsilon_w}{1-\varepsilon_w}\right)^{0.6}\left[\frac{\rho_m}{\rho_o(1-\varepsilon_w)}f\right]^{-0.4} \quad \textbf{(2-36)}$$

Maximum droplet size is given by

$$\frac{d_{max}}{D} = Max\left\{\left(\frac{d_{max}}{D}\right)_{dilute}, \left(\frac{d_{max}}{D}\right)_{dense}\right\} \quad \textbf{(2-37)}$$

Critical droplet size is one beyond which the drop separates from the two-phase dispersion as a result of gravity forces, usually in horizontal flow or creaming from deformation in vertical flow.

Gravity effect

$$\left(\frac{d_{cb}}{D}\right) = \frac{3}{8}\frac{\rho_o}{|\Delta\rho|}\frac{fU_c^2}{Dgcos(\theta)} = \frac{3}{8}f\frac{\rho_o}{\Delta\rho}Fr_o \quad \textbf{(2-38)}$$

Where Froude Number is:

$$Fr_o = \frac{U_c^2}{Dgcos(\theta)} \quad \textbf{(2-39)}$$

And

$$\Delta\rho = |\rho_o - \rho_o| \quad \textbf{(2-40)}$$

Creaming

$$\left(\frac{d_{c\sigma}}{D}\right) = \left[\frac{0.4\sigma}{||\rho_o - \rho_w|gD^2cos(\beta)|}\right]^{0.5} \quad \textbf{(2-41)}$$

$$\beta = \begin{cases} |\theta| & |\theta| < 45 \\ 90 - |\theta| & |\theta| > 45 \end{cases} \quad \textbf{(2-42)}$$

Where,

θ is the pipe inclination angle.

The critical diameter can be estimated from;

$$\frac{d_{crit}}{D} = Min\left\{\left(\frac{d_{cb}}{D}\right), \left(\frac{d_{c\sigma}}{D}\right)\right\} \quad \textbf{(2-43)}$$

The criterion for stable water in oil dispersion

$$d_{max} \leq d_{crit} \quad \textbf{(2-44)}$$

(Xu et al., 2011) discussed water displacement by oil flow in pipelines and observed certain oil flow velocities and volume fractions at different pipeline orientations. The water displacement by oil in the pipe is necessary so as to prevent water plug formation which causes blockages when pigging of oil product pipelines. Trapping valves units were placed along the test pipeline so as to know the quantity of water drawn from the horizontal section into the upward inclined section. Based on formation of a water plug in the lowest elbow of the test section, a model for predicting water displacement by the oil flow was presented this is shown in Figure 1-3 above. Prediction of the quantity of water withdrawn from the outlet valves compared positively with results from experiments using two different pipe diameters. This model predicts that the water displacement is enhanced by increasing density and oil viscosity. For gas pipelines a much higher critical superficial velocity of the gas medium is required to displace the water by gas flow. Onset of entrainment is given by equation 2-45

$$V_e = \int_{h_s}^{h_{cr}} \frac{A_w}{dh/dx}(h)\ dh + AL_2 \quad \textbf{(2-45)}$$

2.6 Gas Liquid Flows

Gas-liquid flows are having different characteristics than liquid-liquid flows in terms of flow patterns which are; slug, bubbly, annular, plug, stratified and churn flow. The flow pattern determines slip ratio difference in gas-liquid flows.

Hewitt and Taylor-Hall (1970) gave the interfacial characteristics for stratified gas-liquid flow; start as a smooth interface at low gas and liquid flow rates, upon increase in gas velocity ripple waves start forming two-dimensional waves, further increase in velocity results pebbled waves develop forming three-dimensional waves, though pebble wave form a stable interface and further velocity increase results in formation of roll waves and finally upon further velocity increase entrainment takes place with droplets detaching from the eddies formed on the waves due to the shearing force being greater than the surface tension of the liquid. The droplets are then transported in the gas as droplets.

Fairhurst and Barrett (1997) studied the liquid accumulation in gas/condensate pipelines. The presence of water made it difficult to predict flow stream operation by using standard two-phase flow models. This hindered normal flow operations in terms of flow capacity, hydrate formation and function of corrosion inhibitors. Two-phase and three-phase experiments were conducted and compared with transient, mechanistic and computer models. The figure 2-10 give a description of undulating flow while Figures 2-11 and 2-12 give the prediction model comparison and flow regime map respectively.

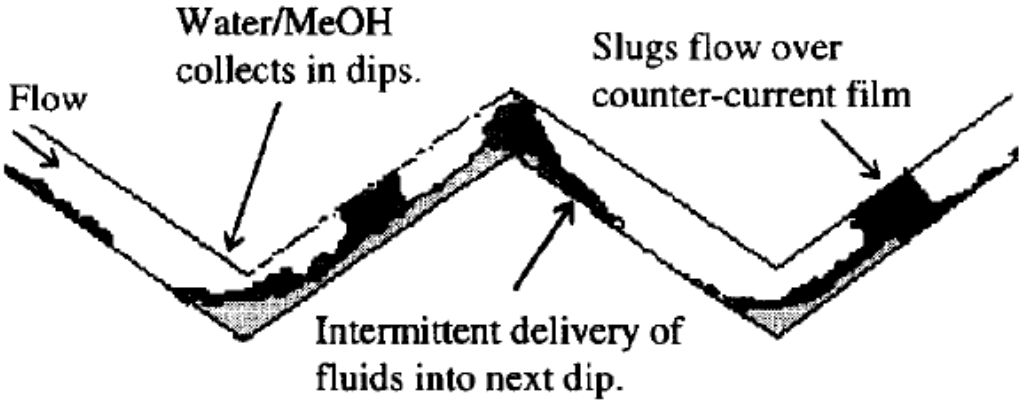

Figure 2-10 undulating flow Fairhurst and Barret (1997)

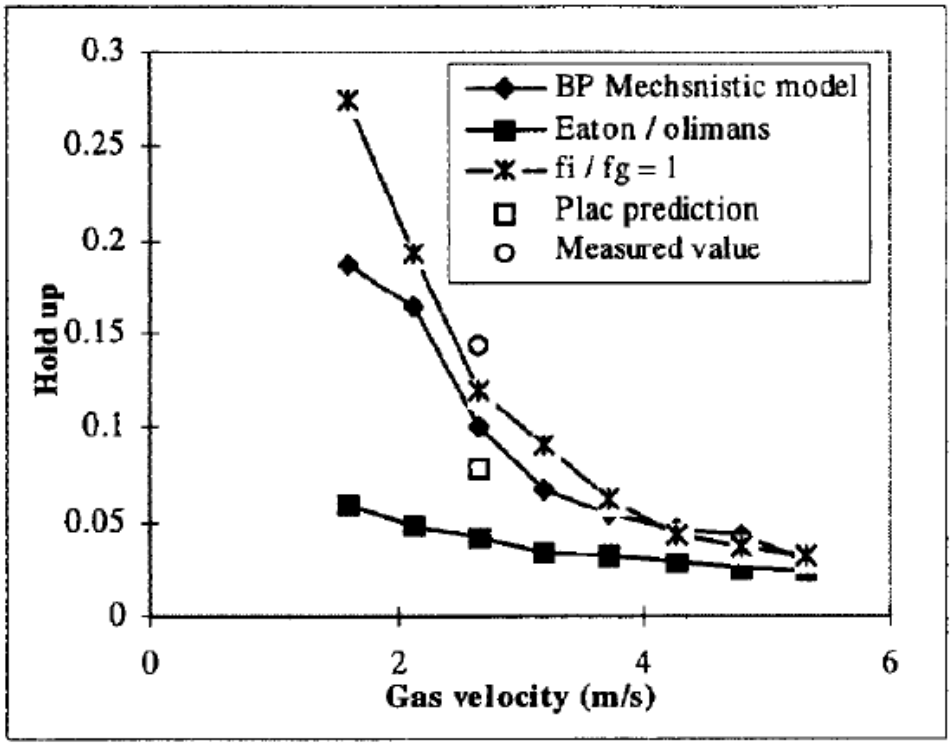

Figure 2-11 Fairhurst and Barret model comparison

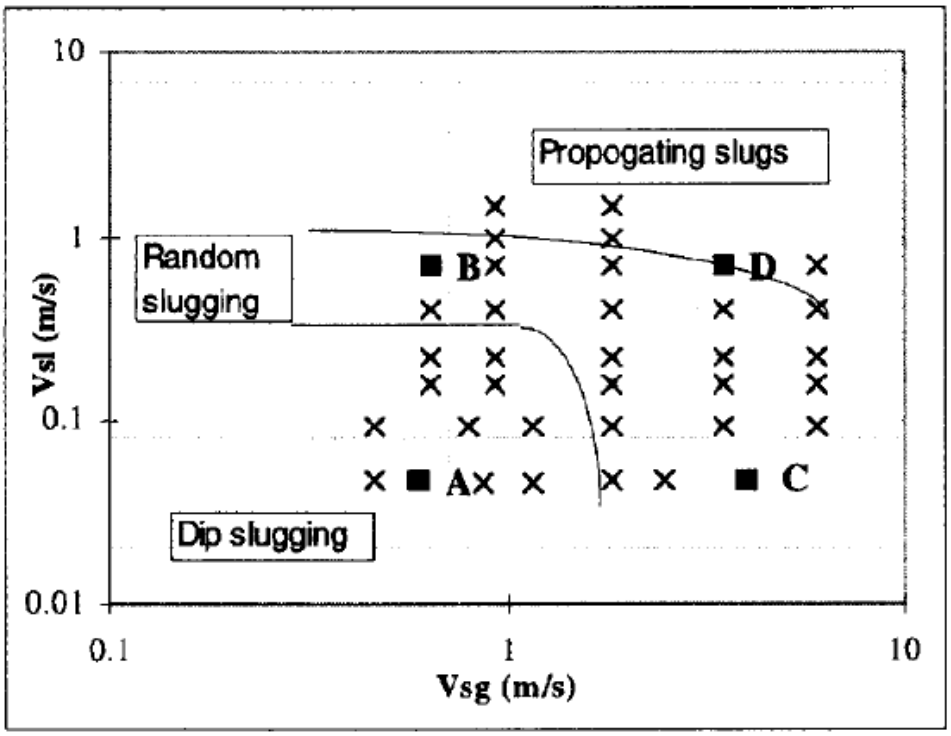

Figure 2-12 Fairhurst and Barret flow regime map

Similarly (Zhang and Sarica, 2011a) studied low liquid content or loading in gas pipelines and proposed models for flow pattern pressure gradient and liquid holdup predictions, suggesting use of accurate closure relationships like wetted perimeter, interfacial friction factor and liquid entrainment fraction determined accuracy of the mechanistic models. The Figure 2-13 explains the liquid entrainment by the flowing gas flow.

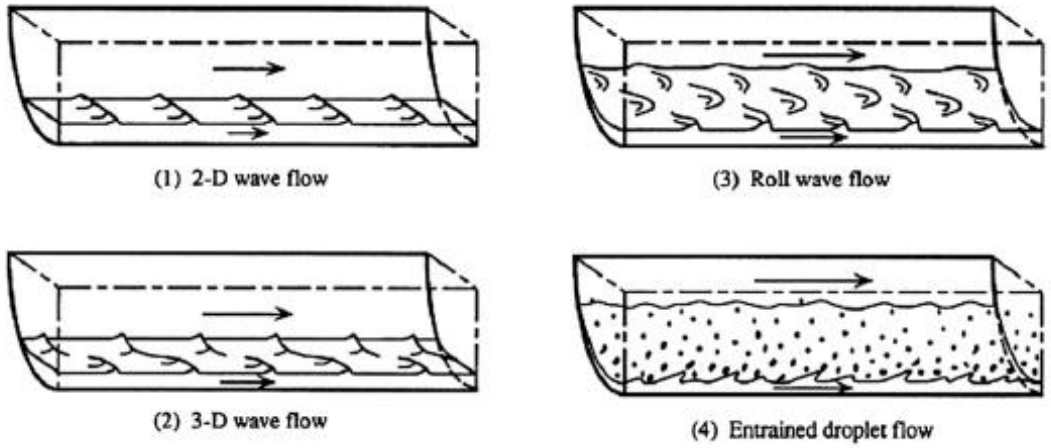

Figure 2-13 water drop entrainment Chen et al 1997

2.7 Liquid Solid Flows

Horizontal liquid solid flows are described in the Figure 2-13 below. They are encountered in oil and gas production and transportation. The presence of sand leads to erosion especially around valves and chokes as well as piping fittings such as elbows and tees. Previous studies have produced erosion models such as the API 14E, which use density of the mixture and (Salama, 2000) which considers sand flowrate, sand particle shape and pipe diameter. The sand flow could be classified as;

Stationary bed: It occurs when the velocity of the liquid is very low and the sand is deposited at the bottom of the pipe. This leads to local sand build-up as more sand is produced. The reduction in the cross-sectional area increases the liquid

velocity; this makes the upper particles to move further as separate layers increasing the bed length to the point when a stable bed height is reached.

Moving Bed and Saltation: When above a certain critical velocity, the sand particles start to move, either rolling or Saltating, and when increasing the velocity as a continuous sand bed along the pipe bottom. This critical velocity is a function of the pipe diameter, particle size and liquid/solid physical properties.

Suspension: At high liquid flowrates more particles are suspended in the fluid above the bed until all particles the bed disappears and no particles move at the bottom of the pipe.

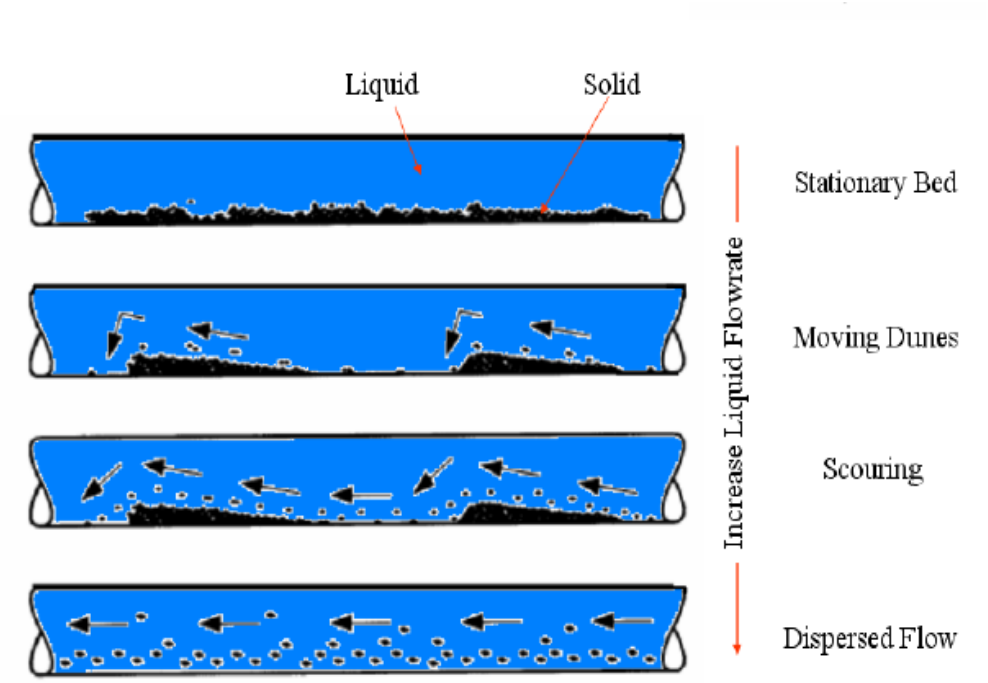

Figure 2-14 Horizontal sand and water flow regimes

The Liquid-solid flows are also different in their flow patterns than gas-liquid flows. Liquid-solid or slurry flows involve flow of solid particles in a continuous flow of a liquid.(Weber and et al., 1974), (Weber, 1978) (Weber, 1986), Weber (1978, 1986) observed that the solid particles in a slurry flow were affected by pressure

and drag forces. There are two characterisations one is the total mixture or homogenous flow with consideration of pipe Reynolds number and the other is relative flow which considers particle Reynolds number. The solids would be suspended, segregated or dispersed in the fluid based on the particle shape, size, density, physical properties of the fluid like density and viscosity and flow parameters like pipe diameter and velocity. Fine solids particles are suspended in Brownian motion without incidence of turbulence in a homogenous flow while larger particles have more segregation in flow and have a higher velocity for settling. This settling or critical deposition velocity is the minimum velocity in which solids need to flow in a fluid to prevent settlement or deposition on the bottom. It occurs at the minimum pressure drop and transportation of solids is possible only when the flow velocity is greater than the critical deposition velocity Wasp (1977).

When the fluid moves at high velocities transporting sand, the solids are continuously conveyed without accumulation or deposition, however as the velocity decreases, particles may begin to settle creating a sliding bed at this point the system will have reached the sand minimum transport condition (MTC).

Visual observations were used to arrive at the MTC by researchers. At Cranfield University researchers have focused their investigations using the definition by (Thomas 1962) which says that the minimum transport condition is the ***"the mean stream velocity required to prevent the accumulation of a layer of sliding particles at the bottom of horizontal pipe"***.

2.8 Liquid gas solid flows

(III, 2009) calculated the minimum velocity that is required to move solid particles in an oil and gas flow pipeline based on a hydrodynamic model. This was achieved by observing that the velocity was a function of particle shape, density, size and diameter. Low flow velocity in a pipeline results in particle settlement and on subsequent increase in flow velocity, the solid particles move and cause damage or blockage downstream. For solid particles that have been wetted by

glycol, wax, paraffin, corrosion inhibitors and compressor oil a much higher velocity is required to move the particles. Lift, drag, gravity and buoyancy are the forces affect solid particles thus for motion to occur, the buoyant, drag and lift forces must be greater than gravity force. The Wicks and Fraser correlation was also employed to predict the required flow velocity for water in oil, iron components like iron carbonate and iron sulphate in water and black power in gas.

However (King, Fairhurst and Hill, 2001) experimented with sand transport from a dipped low section in a pipeline by using different fluids so as to observe the viscosity effect. The fluids were water, oil and solutions that have viscosity of 150 and 300 centipoises. Water and low viscosity oil could transport the deposited solids during slug flow whilst higher viscosity oils were not able to transport the solids. Pre-wetting the sand and using oil flow also did not transport the sand until the advent of water flow. Increasing the velocity for air and water flow results in settled solids transport. Oils with medium range viscosity were also not able to transport the sand while highly viscous oils could transport solids due to shear. The developed model highlighted the minimum pressure gradient for solids transport, and it is related to particle diameter being smaller or greater than the viscous sub layer.

The velocity threshold for solids transport is significantly higher for viscous crude oil than that for light crude oil. It could be predicted by using a model that accounts for both boundary layer and viscous drag effects; three-phase transport of solids did not occur at low water cuts and could be as a result of surface tension effects.

Figure 2-15 give a illustrate liquid gas and solid flows

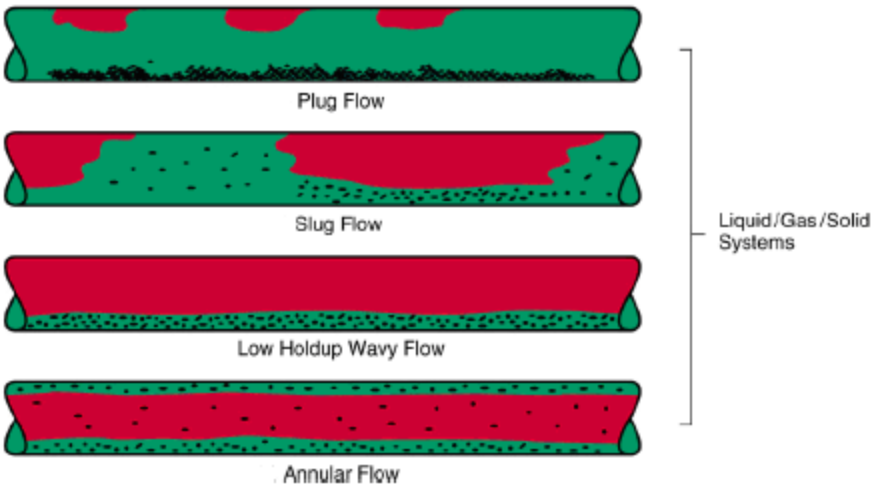

Figure 2-15 Horizontal sand water and air flow regimes

2.9 Instrumentation

The various instruments used form the available literature indicates use appropriate instruments according to need, physical constraints and available budget. Such instrumentation include; optical cameras, gamma-rays, x-rays, densitometers, wall conductance electrodes, laser induced fluorescence, wire mesh sensors, pitot probes, surface mounted electrodes, multiphase flow meters, conductivity rings, laser Doppler anemometry and film thickness probes

2.10 Measurement Techniques

Various flow measurement methods have been devised from previous and ongoing studies. There is a need to view all the methods and subsequently identify the most suitable for water drop out prediction/identification.

Hall and Hewitt (1992) analysed application of analytical and numerical studies to study stratified oil-water flows using exact solution methods for two-dimensional and numerical solution for three-dimensional flow for laminar flow of both fluids. A model based on Taitel and Duckler (1976) analysis for hold up flows in circular pipe and flows between flat plates was derived for liquid-liquid and liquid-gas flows.

However (Shirley, Chakrabarti and Das, 2012) Used Artificial Neural Networks as a custom made design for prediction of flow pattern and transition phases, by

using phase superficial velocities as the input parameters in liquid-liquid two-phase flow through a horizontal pipe. Viscosity, surface tension, pipe inclination, fluid densities were kept constant. Use of a design architecture that has five layers with neurons in the final output layer producing a binary output was a flow classifier to restrict error to within 4%.oil density was not a major influence unlike wetting characteristics of the pipe, viscosity, fluid–fluid interfacial tension and design of pipe entry mixer. Thus Artificial Neural Networks could be used for two-phase flow regime identification. This could be a useful tool in modelling water drop out behaviour.

However(Liu, Matar and Hewitt, 2006) used a dye tracing non-invasive technique Laser Induced Florescence to study simultaneous flow of two immiscible organic-aqueous liquid flows in pipelines at a high dispersed fraction. This enhanced visual observation of the dispersion in greater detail and by using one dimensional technique produced agreement with experimental values of the predicted values of volume fractions of the relevant phases. This methodology is suited for dynamic observation of water drop out phenomena.

While Soleimani et al. (2000) experimented with a high frequency impedance probe and densitometer for measurement of volume fraction distribution across the tube to obtain topographic results for phase distribution. It was observed that gamma densitometer gave more reliable method of measuring volume fraction than the impedance probe. Water hold up was higher around the sides of the tube at lower mixture velocities and is affected by input volume fraction. For the dispersed high mixture velocity flow, the oil droplets tended to concentrate at the tube centre. There was oil encapsulation by the water at low mixture velocity.

Similarly(Lovick and Angeli, 2004) considered dual continuous flow patterns of two immiscible liquid phases with phase identification obtained by use of conductivity and impedance probes. A 38 mm diameter, stainless steel, horizontal test section was set up for the experiment, dual continuous flow pattern boundaries were identified through the use of impedance and a conductivity probe. Mixture velocities measurements ranged from 0.8 to 3 m/s and input oil volume fractions ranged from 10% to 90%. Observation of dual continuous flow

was at intermediate mixture velocities between dispersed and stratified flow this made the pressure gradients lower than those for single phase oil flow; with increasing input oil fraction, the velocity ratio increased being higher than 1 at high oil fractions excluding the highest mixture velocities where the values where less than 1. This phenomenon was explained by the shape of the oil–water interface and the in situ phase distribution data. Using the standard two-fluid model could not predict hold-up and the pressure gradient during dual continuous flow. Figures 2-16 and 2-17, gives dual continuous flow and results.

Figure 2-16 Schematic diagram of dual continuous flow; (Lovick and Angeli 2010)

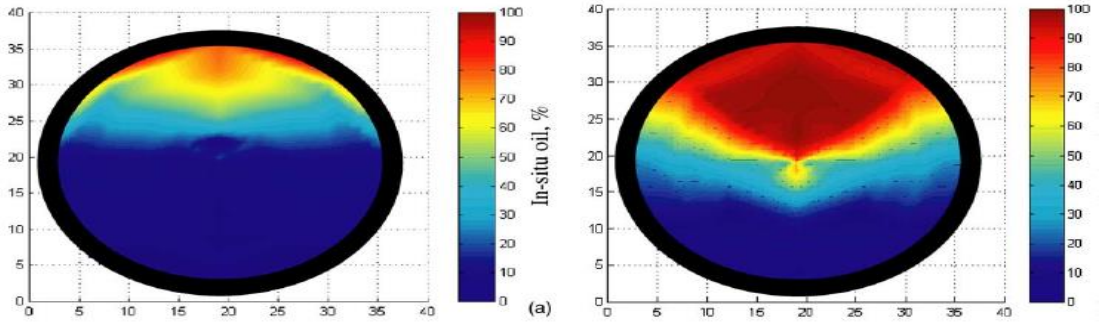

Figure 2-17 oil volume fraction at a fixed velocity and different input oil fraction Lovick and Angeli (2004

However Hu et al (2000) described use of a two beam X-ray computed tomography system for multiphase flow measurement. CT or computer assisted tomography reconstructs the interior image of an object by collecting the projected data from different angles at its exterior, a system diagram is shown in Figure 2-18. This scanner was invented by Cormack and Hounsfield. This accurate reconstruction depends on the penetration ability of the subject medium. The system that was developed made use of algorithms used to convert the projected data into tomography images. This system produced accurate results of concentrations of oil (or water) in a mixed layer or in stratified layers. This method could be used as a template for further study into the water drop out.

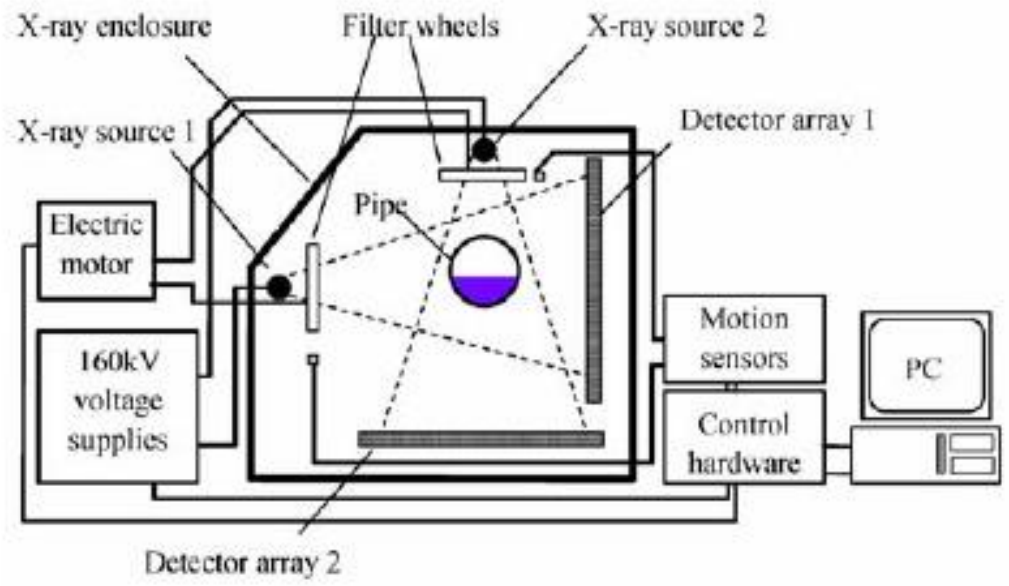

Figure 2-18 (Hu et al., 2000) X-ray System

(Al-Wahaibi and Angeli, 2009) used empirical methods to predict drop entrainment or pick up of one phase into another in dual continuous horizontal water-oil flows, depending on the balance between drop deposition rate and drop entrainment. As earlier indicated this literature also describes some aspects of water drop out expressed as drop deposition. It concludes that oil-water flow entrainment occurs from water to oil and from oil to water in both directions and transpires as the retracting drag force of the waves of the stratified wavy flow become greater than the attaching surface tension force figure 2-19 highlights this phenomena. From data on entrained fraction oil-water flows, a deposition rate constant was developed. This could predict the available experimental data from literature on the entrained fraction in diverse water-oil flow systems.

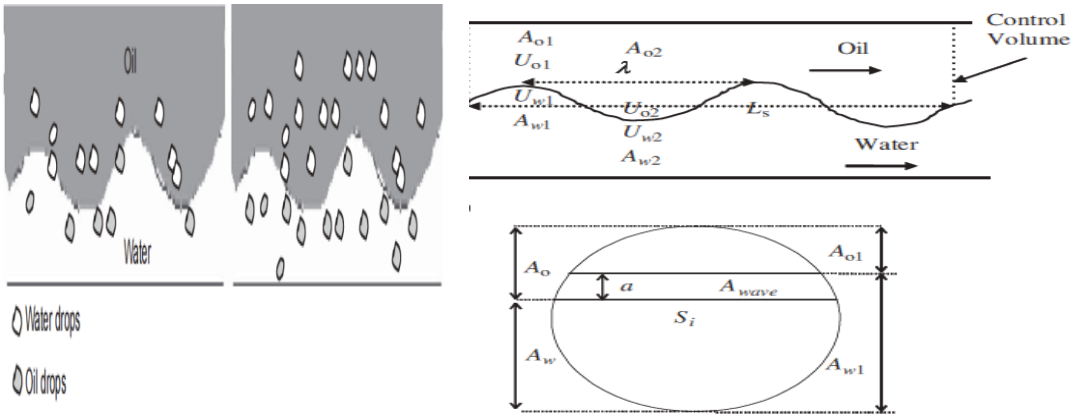

Figure 2-19 Drop deposition and drop entrainment rate Al Wahabi and Angeli (2009)

(Li et al., 2006) studied water wetting in two-phase oil-water flows and used four main methods of flow pattern visualization, wall sampling, iron concentration monitoring and wall conductance probes to detect phase wetting at different superficial water and oil velocities in large diameter horizontal pipes. The conclusions were that a phase wetting map was produced based on the methods. Four flow patterns were identified; stratified flow with mixed layer, stratified flow, dispersed and semi-dispersed flow. The three types of phase wetting were identified; intermittent wetting, oil wetting, and water wetting. By using the iron concentration monitoring, it was determined that lack of corrosion is certain only when wetting by oil occur, whereas intermittent and water wetting could result in presence of corrosion. The developed model agreed with experimental results

2.11 Conclusion

From the literature it could be concluded that various models and experiments have been proposed and conducted on removal of heavier phase in pipes. The conditions for phase settlement are affected by fluid and solid physical properties and flow regimes. Though this area of research is vital for oil and gas industry, there is a need for further study and experimentation and it is possible to produce a contribution to knowledge of flow assurance with this project.

3 LOW CONCENTRATION WATER IN OIL BEHAVIOUR IN HORIZONTAL PIPE

3.1 Introduction

Transportation of petroleum products is essential in meeting global energy demand. As already mentioned in chapter 1, water post separation is present in oil and gas transfer lines. It is thus imperative to know what amount is present so that the buyer will not to pay for water. At low velocity flow this could also tend to settle with the consequence of corrosion as earlier explained in chapter 2. Experiments were conducted on the four-inch horizontal test section on the three-phase facility in PSE laboratory at Cranfield University to determine the behaviour of the low water concentration in oil flow. Two film thickness sensors were mounted in test spool on a 26.54 m long horizontal section to detect the presence water in low concentration so as to measure the water film velocity and water film thickness.

Such flow conditions are frequently encountered in the petroleum transfer pipelines. The formed water layer is formed as a result of decrease in oil and water flow velocity flowed by the gradual aggregation of the dispersed water drops in the oil and water emulsion. While the removal of the settled layer starts with the formation of an unstable interface layer. The drag force overcomes the gravitational force resulting in deformation and detachment of the water droplets derived from Kelvin Helmholtz instabilities.

This chapter is divided into five sections, introduction, and design of oil and water experiment test spool, description of the three-phase facility, calibration of sensors experiments, results and model development.

3.2 Design of Oil and Water Experiment Test Spool

The experiments required a means of detecting the presence water in oil in a four-inch pipe with a water cut varying from 0.5% to 5% in 0.5% steps with flow mixture velocity varied from 0.1 to 1 m/s in steps of 0.1 m/s.

To investigate a water film in oil or air flow in a horizontal pipeline, flush mounted surface mounted electrodes in the form of parallel strip steel film thickness sensors were selected. These sensors were highlighted in Collier and Hewitt (1964) , (Coney, 1973), (Hewitt, 1982), (Kang and Kim, 1992),(Koskie, Mudawar and Tiederman, 1989) as well as in (Fossa, 1998a).

The sensors that are two strips of stainless steel are configured so that the gap between the two conductive strips gives the maximum resolution in vertical film thickness. For instance a sensor with a 4mm width, it would have a maximum resolution of 4mm vertical water film thickness/height. There is a change in the conductivity between the two strips, with a change in water film thickness t. From (Hewitt, 1982) the response could be given by a non-dimensional form;

$$G^* = \frac{C}{\gamma l_c} \quad \textbf{(3-1)}$$

With, C as conductance across the sensors in Siemens, γ as the specific conductivity of the liquid in Siemens per metre and l_c as the characteristic length that depends on the sensor design. For this design h as the non-dimensional film thickness and a as the gap between the two conductive plates are related by;

$$h = \frac{t}{(a/2)} \quad \textbf{(3-2)}$$

The relation gives the relationship between the non-dimensional conductivity and non-dimensional film thickness,

$$G^* = 0.5h \quad \textbf{(3-3)}$$

3.2.1 Data Acquisition

A LabVIEW data acquisition system was used to collect the data from the sensors. The system consisted of,

- Signal Conditioning Box; this connects between the sensors and the data acquisition this is illustrated in Figure 3-1 below.
- Data Acquisition Box for LabVIEW computer software; this box converts all the electrical signals generated by the probe switch box for input into the software.
- A Computer with a monitor, keyboard and hard drive.

Figure 3-1 signal conditioning box

The conditioning circuit converts the conductivity of the sensors into voltage with output being a function of film thickness. It consists of,

- AC driving circuit
- AC signal amplifier
- The rectifier
- DC signal amplifier

The configuration of the conditioning circuit as explained in (Fossa, 1998a) for converting conductivity into voltage. This has the frequency obtained through the

external sine wave oscillator and applied to a Wheatstone bridge in the form of an operational amplifier, thus decoupling the input impedance from the load impedance. The classic circuit scheme has the resistivity sensor occupying one branch of a Wheatstone bridge. While the instrumentation amplifier was arranged to give high dynamic response and a good decoupling of the electronic circuit from the measuring bridge. The instrumentation amplifier output is applied to a sensitivity variable gain amplifier and then to an electronic rectifier. With the final output to the data acquisition system at the sampling rate of 200 Hz. The circuit diagram is given in Figure 3-2 below;

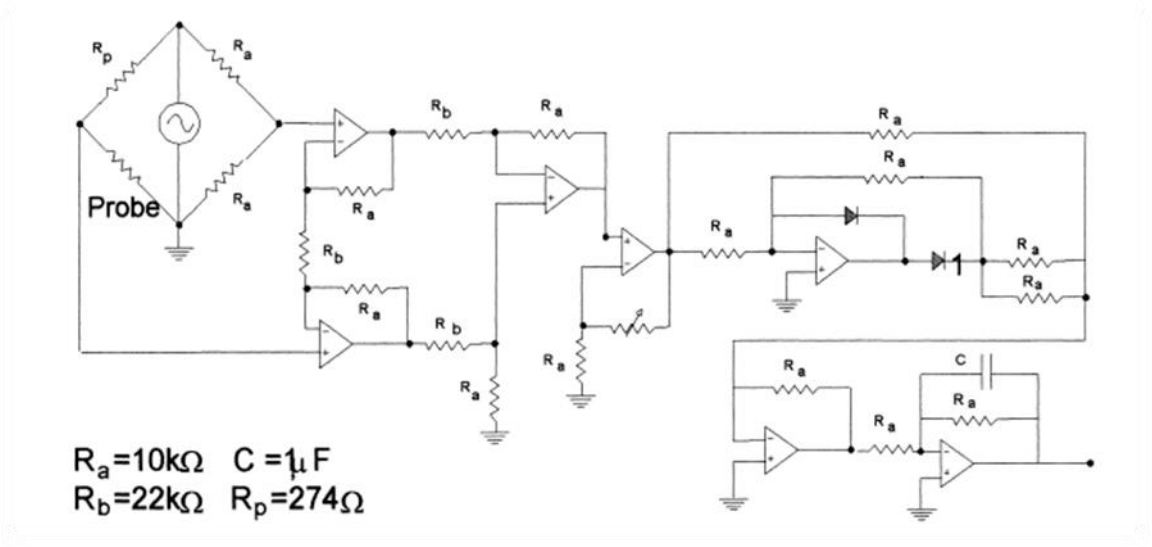

Figure 3-2 electronics circuit diagram of the film thickness sensor (Fossa 1998).

Parallel plate conductive film thickness sensors were selected and a test spool was designed with specification;

It is made from a 300mm long rectangular solid Perspex block, machined to give a 108.2 mm ID pipe section attached to the 4" steel pipeline through stainless steel end plates that are compatible with ANSI 150 flanges. It has two parallel plate film thickness sensors each separated by a 4-mm gap. The first sensor 1 is 100mm from the test spool inlet and the second sensor 2 is 100mm downstream of the first probe in the same axial direction. Key test spool features include;

- Transparent Perspex for visual observations.

- An inlet at the top 50mm before the sensor 1 water insertion at the top.
- An inlet at the top to mount a conductive needle probe located 50mm downstream of the 4mm film thickness probes, used for calibration.
- The film thickness sensors are mounted in the Perspex to enable viewing from the bottom and sides of the test spool.
- The water injection points are 10D, 30D and 50D upstream from the first sensor
- The test spool is movable in the test section so as to move it further away from the water injection points.
- The film thickness sensors are mounted flush with pipe internal diameter.
- There is no step between the flange joints to prevent accumulation

The pipe is a steel pipe with Schedule 10 and has a nominal diameter of 4". This test section use 4" ANSI 150 flanges to bolt the pipe sections to each other. The sketch of the film thickness sensor test spool and sketch of the film thickness sensors are given in Figures 3-3 and Figure 3-4, while a picture of the test spool is given in Figure 3-5. While the dimensions for the conductors are rectangular 12mm long, 3mm wide and 2 mm thick flush mounted with inner wall of the Perspex pipe section perpendicular to the flow direction with no gaps in between the Perspex and conductors.

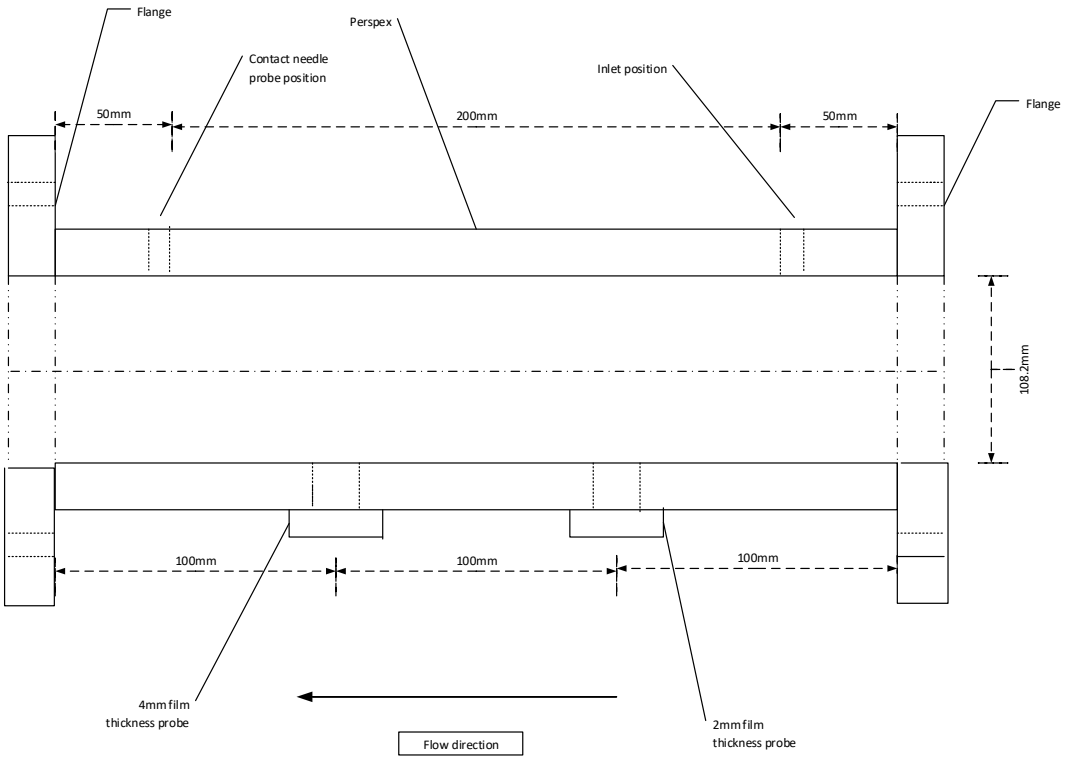

Figure 3-3 sketch of the film thickness sensor test spool

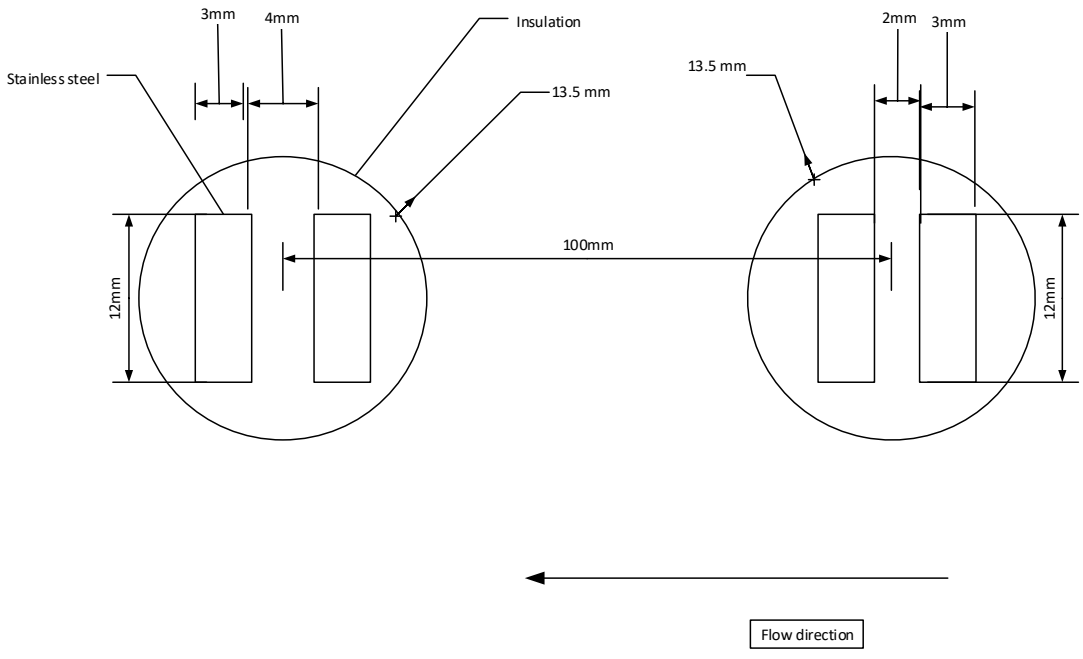

Figure 3-4 Diagram of the film thickness sensors

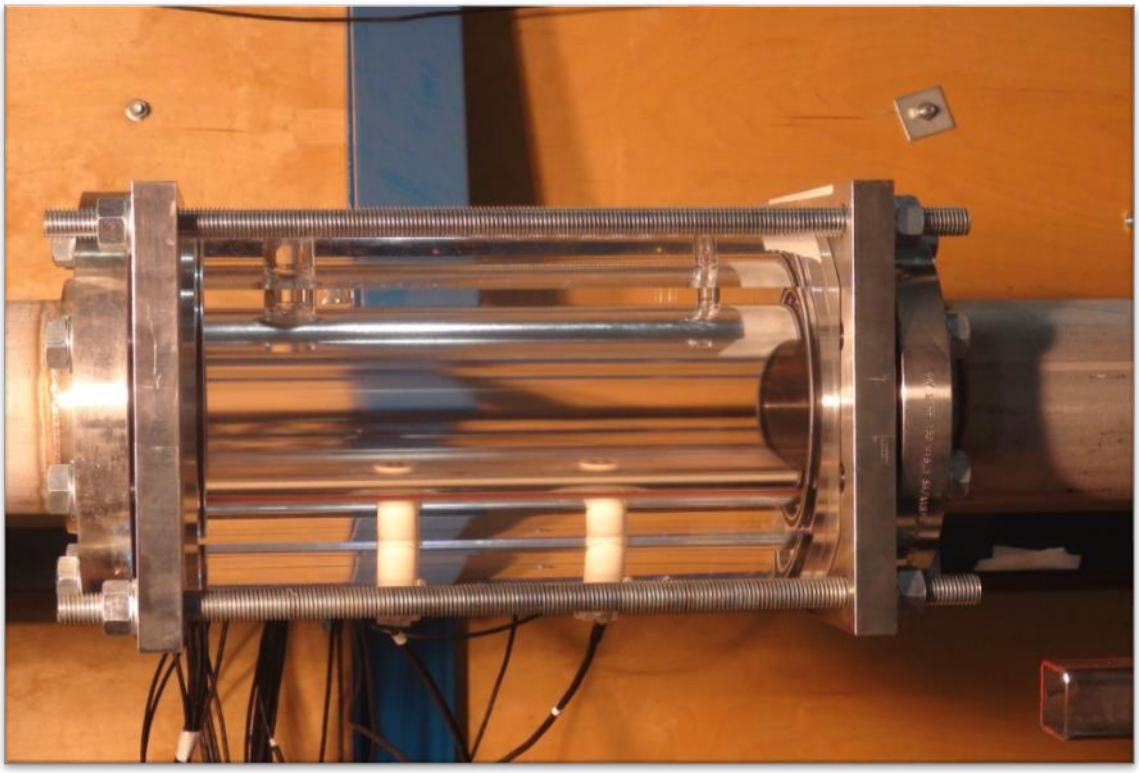

Figure 3-5 test spool with the film thickness sensors mounted on the four-inch pipeline

3.3 Description of the Three-Phase Facility

The Three-Phase Test Facility is a fully automated high pressure test facility designed to supply a measured and controlled rate of water, oil and air mixture through a flow metering area to the test area and finally into the phase separation area where the water, oil and air are separated. After separation in a horizontal three-phase gravity separator, the water and oil are cleaned in their respective coalescers before returning to their storage tanks while the air is exhausted into the atmosphere. Figure 3-6 shows a schematic of the Three-Phase Test Facility.

All pipes and equipment in the test facility are made from stainless steel. The test facility is rated to 20 bar but the capability is currently limited by the maximum pressure of air from the compressors at 7 bar. The test facility is controlled by Delta V; a Fieldbus based supervisory, control and data acquisition (SCADA) software supplied by Emerson Process Management.

The test facility can be divided into four areas – the fluid supply and metering area, the valve manifold area, the test area and the separation area.

3.3.1 Fluid Supply and Flow Metering Area

3.3.1.1 Air supply

Air is supplied from a bank of two compressors connected in parallel. When both compressors are run in parallel, a maximum air flow rate of 1410 $m3/hr$ FAD @ 7 bar g can be supplied. The air from the two compressors is accumulated in a large air receiver to reduce the pressure fluctuation from the compressor. Air from the receiver passes through a bank of three filters (coarse, medium and fine) and then through a cooler where debris and condensates (present in the air) are stripped from the air before passing through the flow meters. Both compressors have to be started and stopped manually at the compressor. However, in an emergency, it can be stopped remotely from the Control Cabin using the emergency button.

3.3.1.2 Water and oil supply

Water is supplied from a 12,500 litres capacity water tank, and oil is supplied from a bunded oil tank of similar capacity. The water tank is situated inside the laboratory while the oil tank is located outdoors and has a bund with 110% (by volume) of the tank capacity. The water and oil are supplied into the flow loop by two multistage Grundfos CR90-5 pumps. Both water and oil pumps are identical and have a duty of 100 $m3/hr$ at 10 bar. Speed control is achieved using inverters. The pumps are operated remotely using Delta V.

3.3.1.3 Flow metering

The flow rates of the air, water and oil are regulated by their respective control valves. The water flow rate is metered by a 1” Rosemount 8742 Magnetic flow meter (up to 1 kg/s) and 3” Foxboro CFT50 Coriolis meter (up to 10 kg/s) while the oil flow rate is metered by a 1” Micro Motion Mass flow meter (up to 1 kg/s) and 3” Foxboro CFT50 Coriolis meter (up to 10 kg/s). The air is metered by a bank of two Rosemount Mass Probar flow meters of ½” and 1” diameter respectively. The smaller air flow meter measures the lower air flow rate (up to

120 m3/hr) while the larger one meters the higher air flow rate up to 4250 sm3/hr (subject to compressor capacity).

The pressure and liquid level in the two-phase separator can be controlled to a desired pressure by a pressure controller and radar gauge level controller using the Delta V control system. The separated air and oil/water mixture then flow through separate air and liquid lines back to the three-phase gravity separator.

The air from the vertical two-phase separator is metered by a 1" Rosemount Vortex flow meter while the water/oil mixture is metered by a 2" Micro Motion Mass flow meter. The 2" meter currently induces a bottleneck to the liquid going through into the 3-Phase Flow Test Facility three-phase separator (max 7 kg/s). A by-pass line with a manual valve is installed across the 2" flow meter to facilitate experiments which require large liquid flow rates.

When the total liquid flow rate (water plus oil) is less than 7 kg/s, the by-pass valve should be closed so that the flow meter can register the flow rate returning to the three phase separator. The by-pass valve should be opened only when the rig operates at total liquid flow rate higher than 7kg/s.

3.3.1.3.1 Test Area

The test area comprises the 4" and 2" flow loops. Their connections are explained respectively as follows.

3.3.1.3.1.1 The 4" flow loop

The air, water and oil are mixed in a mixing section before entering the flow loop, comprising a 55 m long and 2° downward inclined pipeline leading to a 10.5 m high catenary riser. The end of the riser is connected to a 1.2m high and 0.5m of diameter vertical two-phase separator. There is a 4" control valve installed at the inlet of the two-phase separator.

In order to extend the range of available flow regimes of the test, a horizontal 4" line which is diverted from the middle point of the above 4" inclined line has also constructed. The length of the horizontal test section is 26.3 m and this is where

the test spool is mounted 12.0m from the inlet. This horizontal line exits directly into the 3-phase separator on the ground floor.

3.3.1.3.1.2 The 2” flow loop

The water enters into a 40 m long horizontal 2” flow loop, which connects to a 10.5 m high vertical riser. Oil supply is directly connected to the base of the riser. Air supply can be configured either mixing with water to enter into the horizontal loop or directly connecting to the riser base. At the end of the riser, there are two E+H 2” Coriolis meters, vertically and horizontally before the two-phase separator. A 2” control valve is installed between the riser and the two-phase separator to regulate the riser outlet flow rate. For these experiments air is injected into the riser base so that the system would maintain 1 bar separator pressure.

3.3.2 Phase Separation Area

Air, water and oil are gravity separated in the horizontal three-phase separator. The pressure, oil/water interface level and gas/liquid interface level are controlled by the use of pressure controller and two level-displacer type level controllers, maintained by the Delta V control system.

After separation and cleaning in the three-phase separator air is exhausted into the atmosphere. Water and oil from the three-phase separator enter their respective coalescers, where the liquids are further cleaned before returning to their respective storage tanks. There are two flow control valves of different sizes (i.e. 1” and 3” valves) for each of the water and oil return lines. This is employed in a split range flow control scheme to keep the oil/water and gas/liquid interfaces stable in the three phase separator, e.g. the smaller valve will operate when a small amount of water or oil exits the separator and vice versa.

3.3.3 Specifications and Operating Conditions

The current specifications and operating conditions of the test facility and riser test loop are summarised as follows:

Table 3-1 flow loop specifications

	4” Flow Loop	2” Flow Loop
Diameter of flow loop & riser	4” NB Schedule 10	2” NB Schedule 10
Internal diameter of flow loop	108.2 mm	54 mm
Inclination of flow loop	0°	0°
Shape of riser	Catenary	Vertical
Pressure rating of flow loops	20 bar	20 bar
Temperature rating test facility	0 - 80°C	
Duty of water pump	100 m3/hr at10 bar	
Duty of oil pump	100 m3/hr at 10 bar	
Duty of air compressor-1#	570 m3/hr FAD at 7 bar	
Duty of air compressor-2#	840 m3/hr FAD at 7 bar	
Range of water flow meter	– 7.36 kg/s and 0-30kg/s	
Range of oil flow meter	0 – 9.47 kg/s and 0-30kg/s	
Range of air flow meter	0 – 120 sm3/hr and 100 – 4250 sm3/hr	

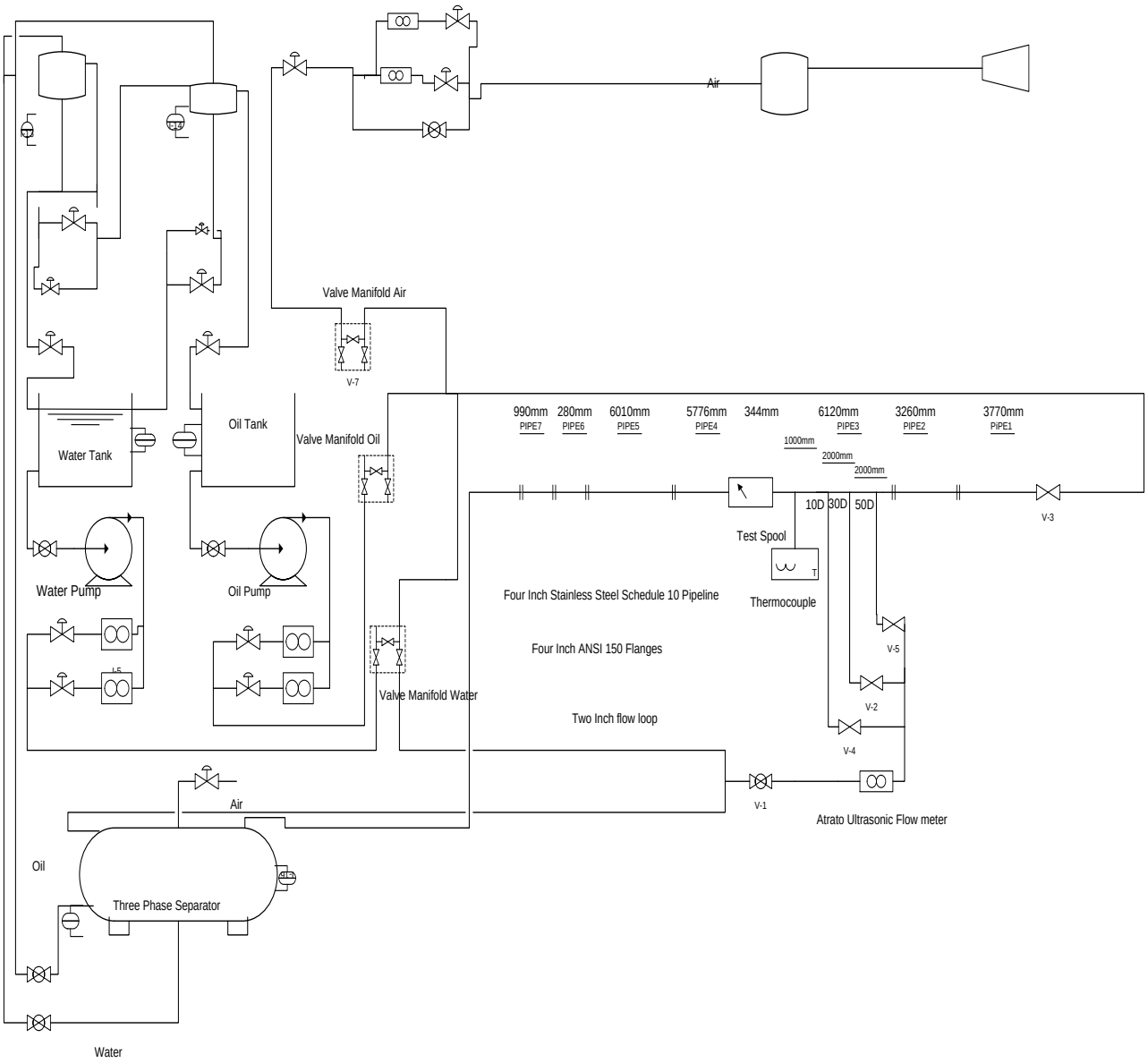

Figure 3-6 test section on the three phase rig

3.4 Procedure

The standard procedure was observed for turning on the three phase rig. The Delta V SCADA system is then turned on and the system is pressurised to 1 bar. The flow rate is varied for oil and water according to the experimental program. The oil flow is from the four-inch pipeline while the water flow is injected from the

two-inch pipeline. Air is injected through the riser base to maintain system pressure at 1 barg.

The film thickness sensors were mounted on a test spool on the four-inch pipeline. There are three injection points 10D, 30D and 500D from the test spool through which water was injected from the two inch pipeline.

After inserting the value of the test matrix oil flow rate in the Delta V computer, the water flow rate was then set by varying the valve on the two-inch line injection point. The LabVIEW data acquisition system is then turned on and the flow condition variables set. The cameras are also turned on at this stage. These are located beside the test section on the three-phase facility with one giving a side view while the other gives the bottom view. This is given in Figure below 3-7.

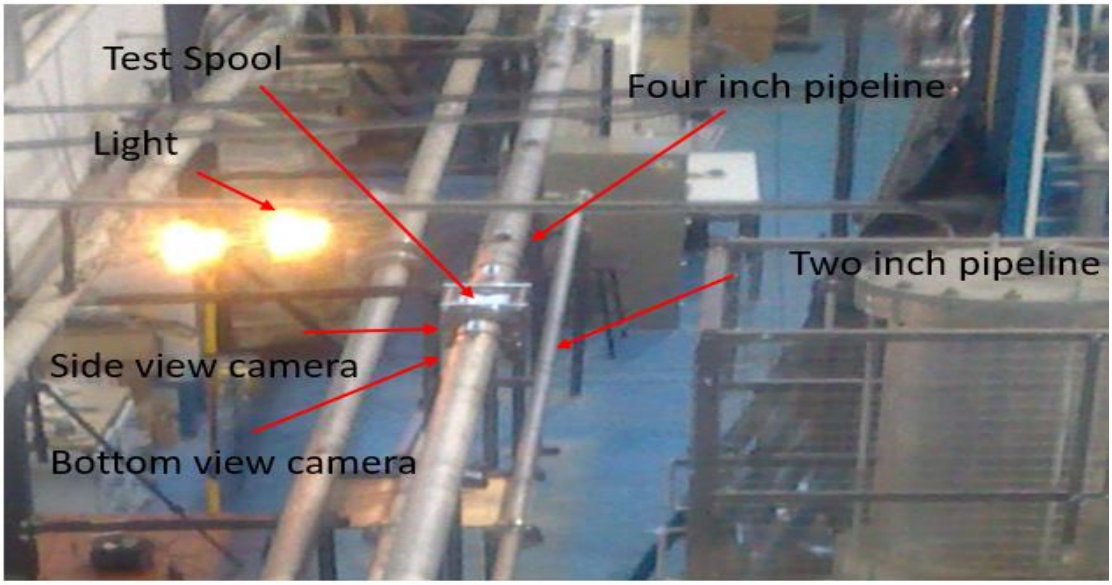

Figure 3-7 test section on the three phase rig

3.5 Results

The test involved start-up of the oil flow with no water. Then the oil flow is set so as to remove settled water from the test spool before increasing or decreasing the flow rate for the test run. Then water is inserted at required flow rate for the test run. Then the water injection point is changed from 10D upstream of the test spool to 30D and 50D denoted as injection a, b and c respectively. The process

is then repeated for next data point. The results for 0.1 to 1/s for injection point a (10D) from tht test spool, are given in the Appendix A.2 while some selected results are given below;

3.5.1 Structural Velocity

According to (Al-yarubi, 2012) structural velocity is a measure of disturbance passing through an upstream and downstream identical sensors over a known distance. This disturbance is conveyed from the upstream sensor to the downstream sensor with minor difference to give a near identical output signal. The time delay between the repeated signal of the upstream and downstream sensors, represent the time taken for the disturbance to travel between them and this is inversely proportional to the flow velocity. The structural velocity for was obtained by using a cross correlation function on the signals from the film thickness sensors to determine the time delay. Table 3-3 gives a summary of structural velocities for mixture velocities 0.1 to 0.5 m/s at 1%, 3% and 5% water cut respectively.

Table 3-2 structural velocities

Vm	1%	3%	5%
0.1m/s	0.2198	0.1600	0.2083
0.2m/s	0.2353	0.1316	0.1087
0.3m/s	0.2532	0.1802	0.1667
0.4m/s	0.2703	0.2222	0.3125
0.5m/s	0.2817	0.3077	0.3636

3.5.1.1 The effect of mixture velocity on the structural velocity

The structural velocity, in general, increases with an increase in mixture velocity as in Figure 3-8 below and table above. However, there is a decrease in the structural velocity with increasing water cut for an increase in mixture velocity.

This decrease in the structural velocity could be attributed to the increase in the oil and water interface height. Which would tends to reduce disturbances.

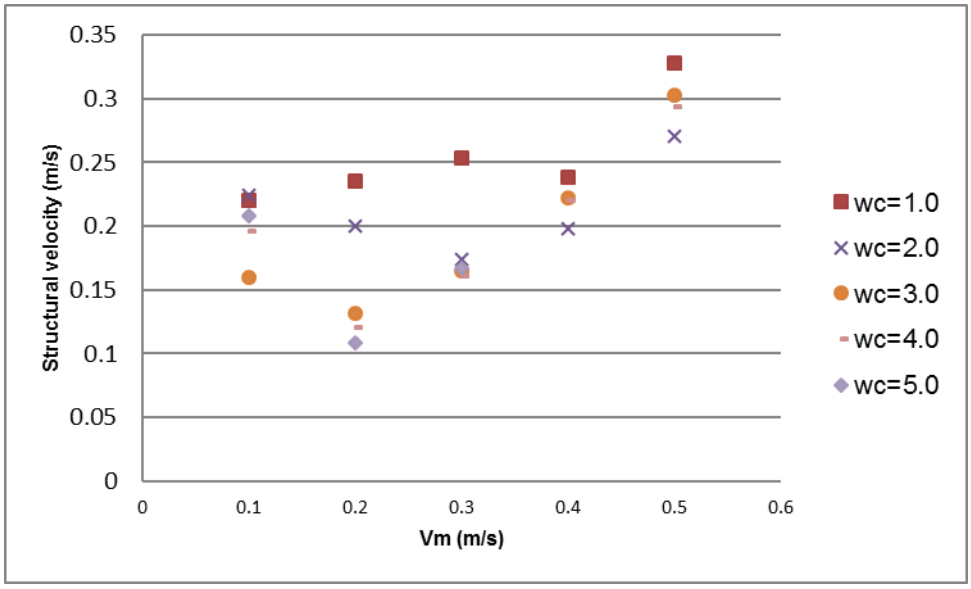

Figure 3-8 structural against mixture velocity for 1% to 5% water cut

3.5.1.2 Effect of water cut on the structural velocity

There is a decreasing structural velocity for an increasing water cut as depicted in Figure 3-9 below, though the structural velocity increases for higher mixture velocities. For mixture velocities 0.2 , 0.3 and 0.5 m/s the structural velocity decreases with increasing water cut as depicted in Figures3-10, 3-11 and 3-12 below. It could be concluded from the results that this velocity declines from 0.5 to 3% water cut before stabilising between 3.5 to 5% water cut. This turning point could be due to the increase in the interface height at a specific mixture velocity or due to turbulent transition.

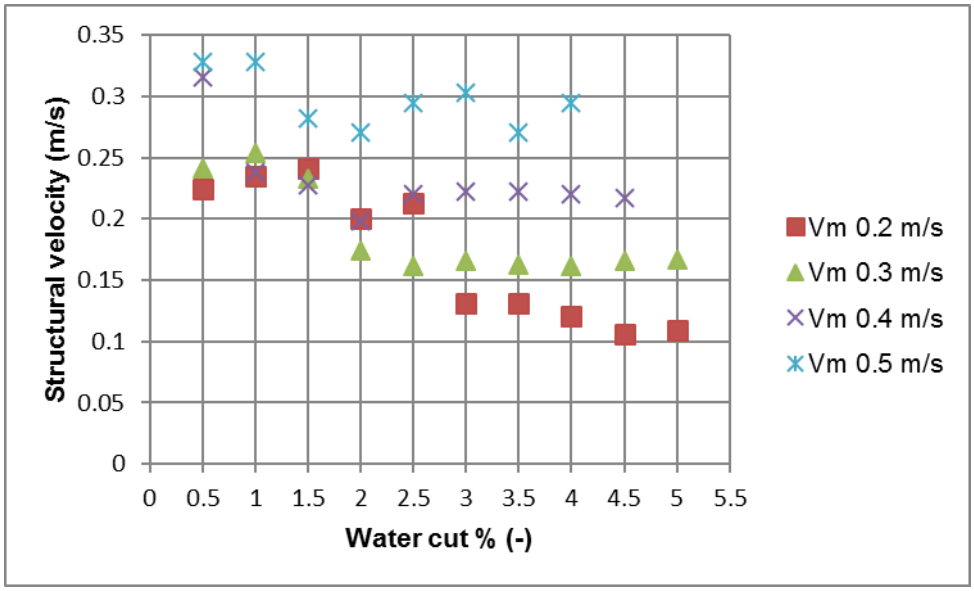

Figure 3-9 structural velocity against water cut

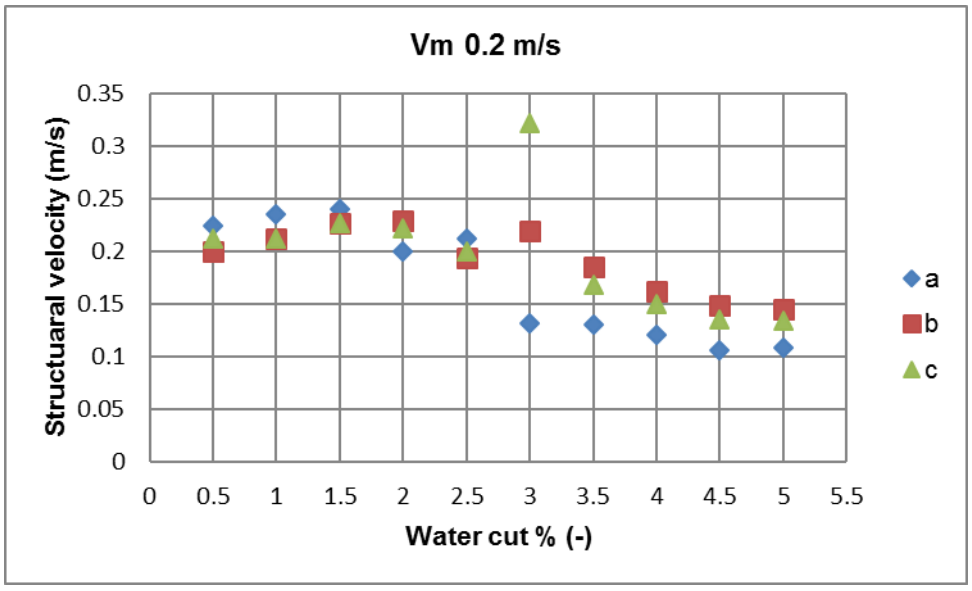

Figure 3-10 water film velocity against water cut for Vm 0.2 m/s for injection points a, b and c 10D, 30D and 50D from test spool respectively

3.5.1.3 Effect of water flow development length on the structural velocity

For the same mixture velocity there is no defined effect of the injection points for 0.2 and 0.3ms/ mixture velocities as given in in Figure 3-10 and 3-11 respectively.

However there is a distinct decrease in the structural velocities with increasing distance of the water injection points for the same mixture velocity, this is depicted in Figure 3-12. This could be as a result stability of the oil and water interface.

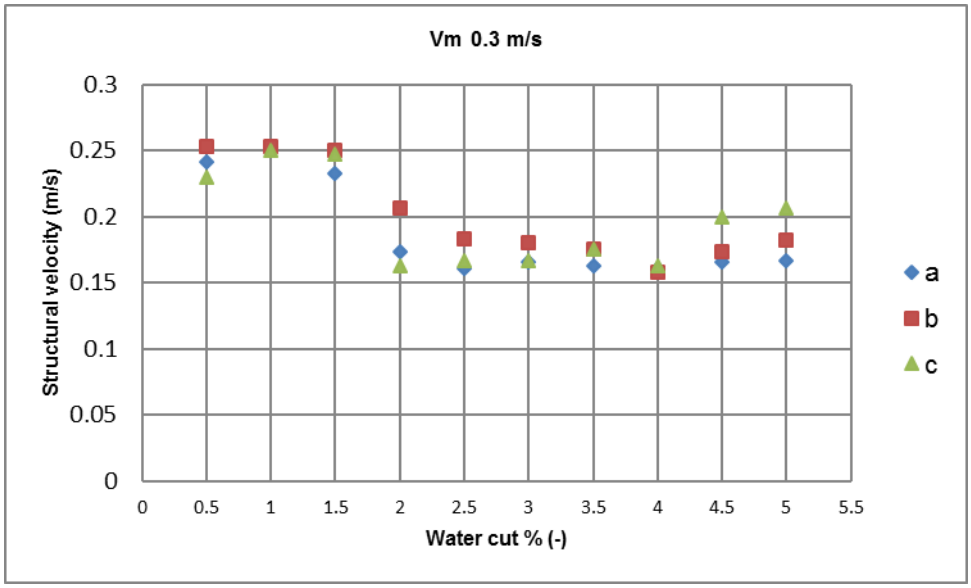

Figure 3-11 Structural velocity against water cut at Vm 0.3 m/s for injection points a, b and c 10D, 30D and 50D from test spool respectively

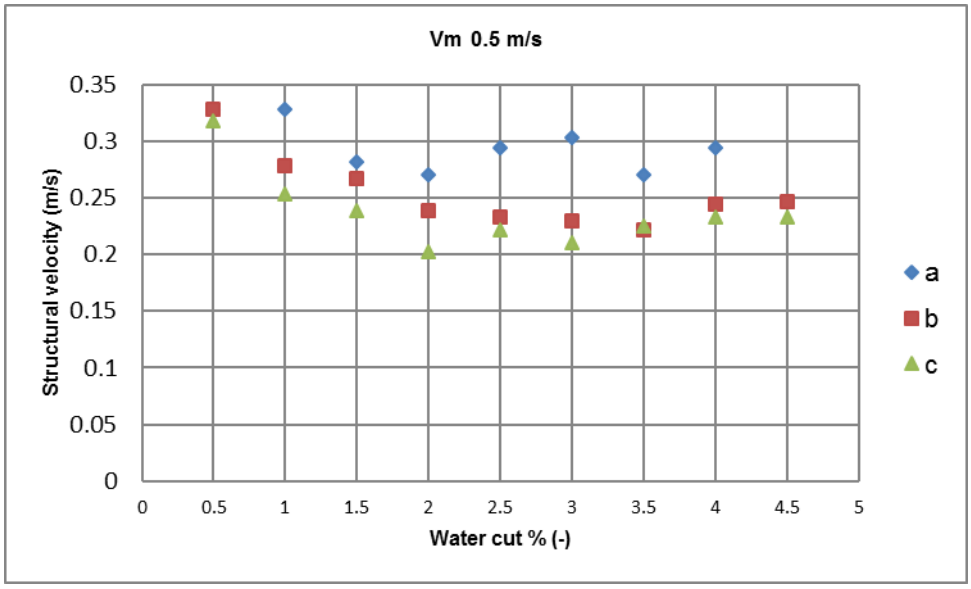

Figure 3-12 structural velocity against water cut at Vm 0.5 m/s for injection points a, b and c 10D, 30D and 50D from test spool respectively

Average structural velocity

The flow mixture velocity was plotted against the structural velocity this is illustrated in Figure 3-13 below based on the average structural velocity and average input mixture velocity. The average structural velocity was obtained from the structural velocity average from the experimental runs. A distinct change was observed with increase in the flow mixture velocity. The structural velocity increased up to 0.7 m/s beyond which the structural velocity massively decayed. This could be explained by the fact that at higher mixture velocities the denser phase in this case water is entrained by the flowing lighter phase oil. Thus, the wave at the interface will not be available for detection as a disturbance. It means that the water droplets or film at the pipe bottom is no longer in continuous contact with the pipe surface, thus do not make contact with the sensors.

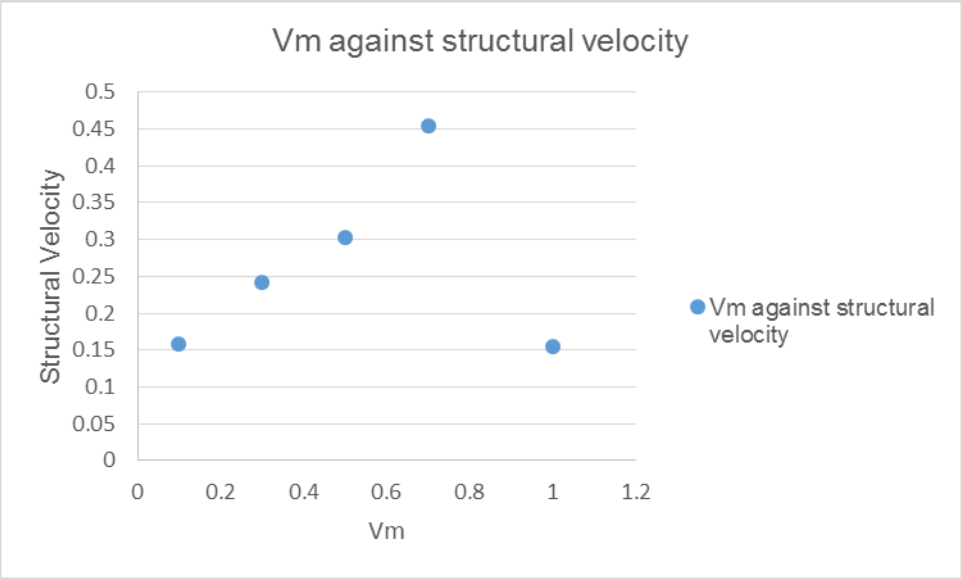

Figure 3-13 average structural velocity change with mixture velocity

3.5.2 Flow Visualization and Flow Regime Map

Visual observation as well as High speed videos and photography were also used for flow regime identification. The flow regime map for the oil and water flow for this study is given in Figure 3-20; this indicates stratified smooth and a stratified with globules flow regime that correspond with (Cai et al., 2012) classification.

Transition occurs at 0.3 m/s with mixture velocities 0.1 and 0.2 m/s falling in the stratified smooth flow regime and 0.4 and 0.5 m/s falling within the stratified with globules flow regime. As shown in Figures 3-14 to 3-20, are the bottom views of the pipe during experiments showing the oil-water interface at each condition 0.1, 0.2, 0.3, 0.5, 0.7, 0.8, 0.9 and 1 m/s mixture velocity respectively, it can be seen that occasional oil globules entrained in the water phase are clearly visible. These help to classify the respective flow regimes as shown in Figure 3-21 into stratified, transition, and stratified with intermittent globules. The flow regime map was identified using the visual observations and high speed photographs. The bottom view photographs of water layer with the oil – water interface clearly visible for mixture velocities of 0.1 m/s Figure 2-14, 0.2 Figure 3-15, and 0.5 m/s Figure 3-16 all at 3% water cut. However for higher mixture velocities from 0.9 and 1m/s the flow regimes is dispersed flow regime with the water being entrained in the lighter oil phase. This is seen in Figures 3-19 and 3-20 below.

Based on visual observation, video analysis and sensor response the results also show that the flow regime derived for oil and water flow lies within the oil wetted region for flow mixture velocities of 0 to 0.5m/s as defined by the (Cai et al., 2012) model predictor this is given in Figure 3-22.

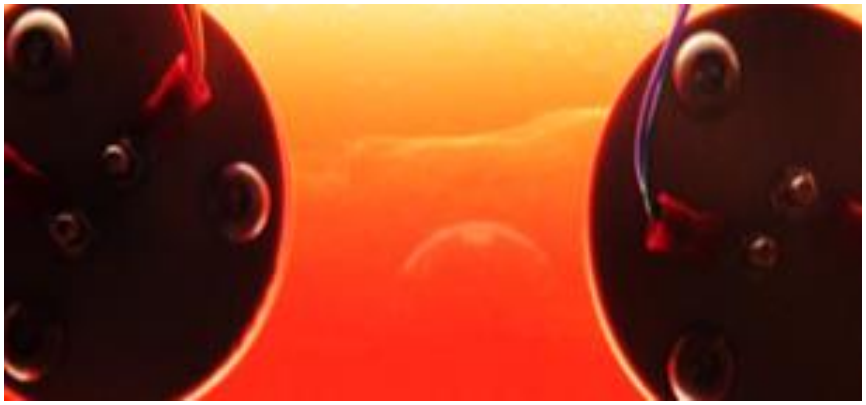

Figure 3-14 mixture velocity 0.1 m/s

Figure 3-15 oil and water mixture velocity 0.2 m/s

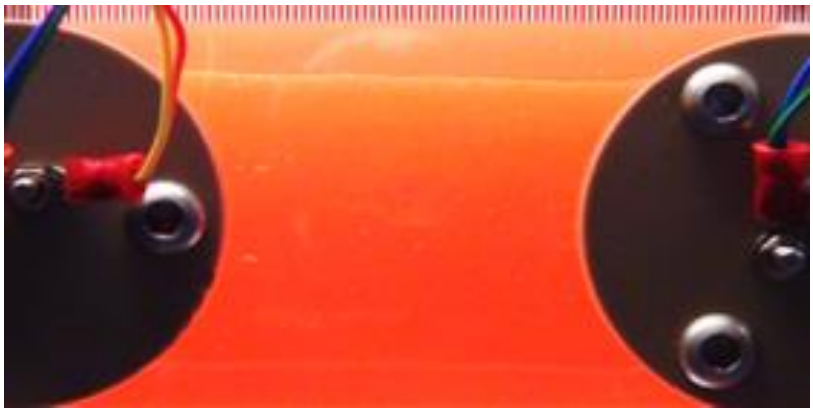

Figure 3-16 oil and water mixture velocity 0.5 m/s

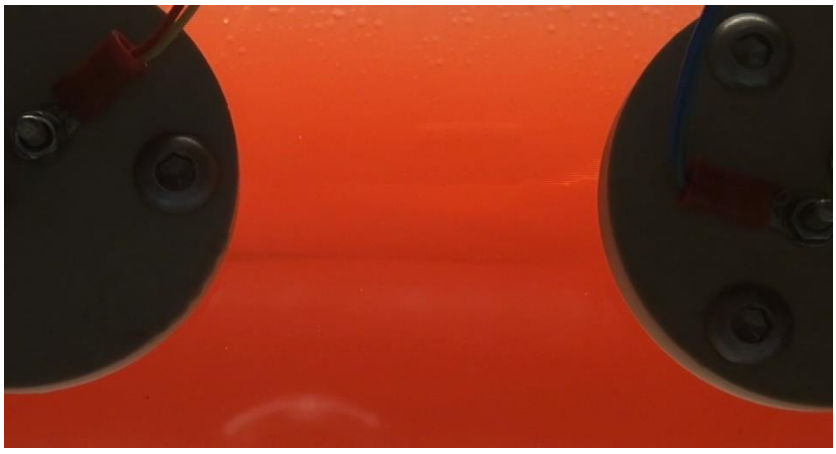

Figure 3-17 oil and water mixture velocity 0.7 m/s

Figure 3-18 oil and water mixture velocity 0.8m/s

Figure 3-19 oil and water mixture velocity 0.9m/s

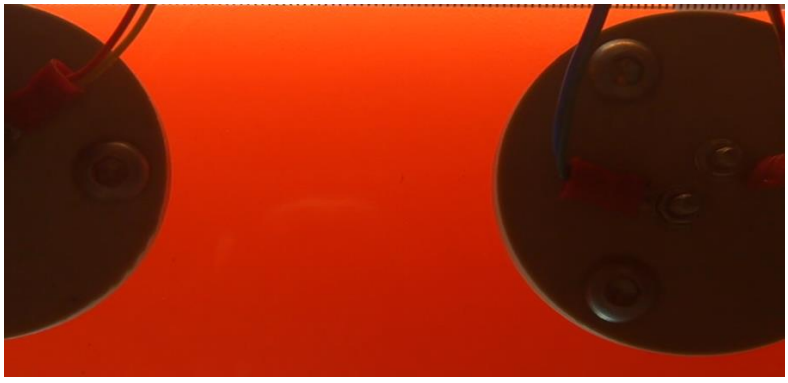

Figure 3-20 oil and water mixture velocity 1m/s

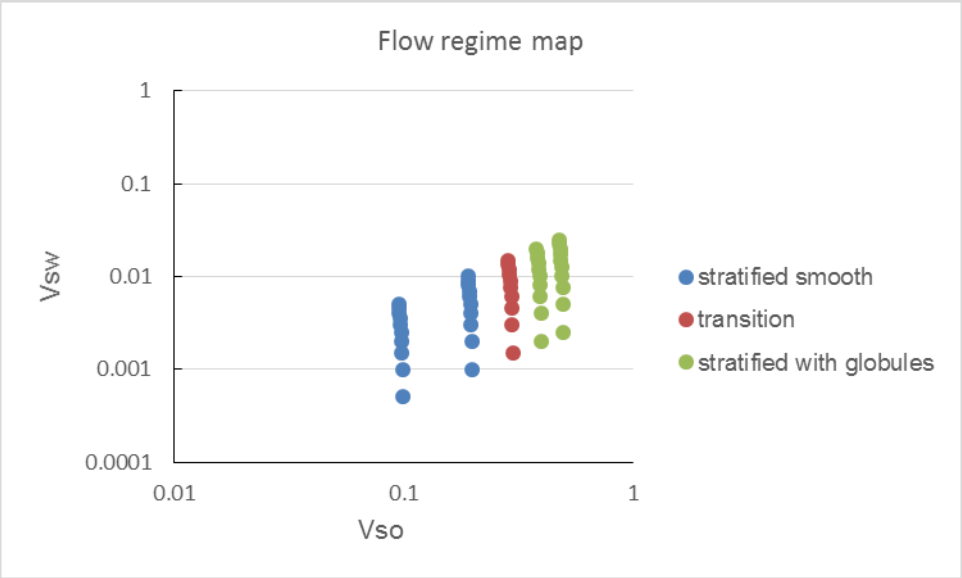

Figure 3-21 the flow regime map depicting stratified smooth for 0.1 and 0.2 m/s and stratified wavy with globules for 0.4 and 0.5 m/s respectively with transition at 0.3 m/s

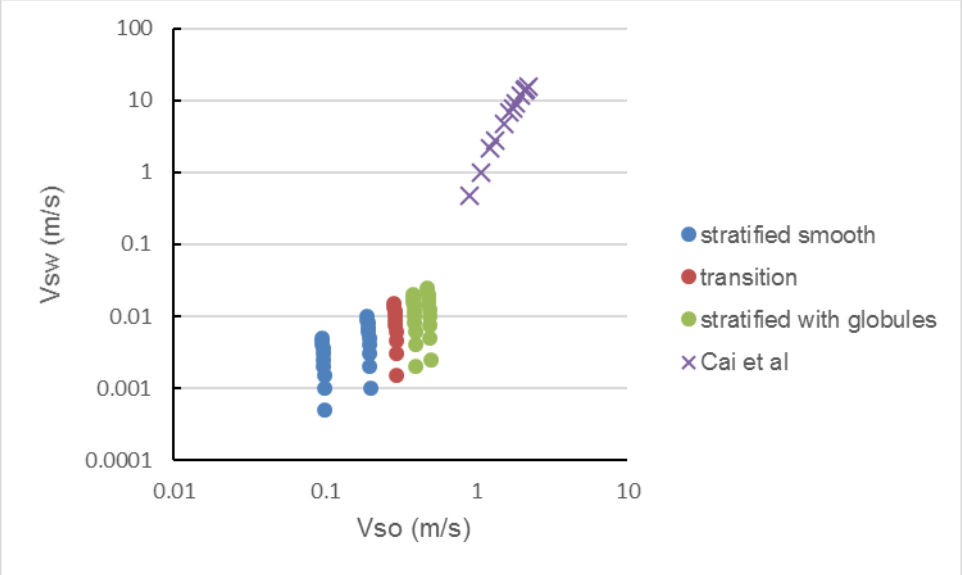

Figure 3-22 current work compared with Cai et. al. (2012) prediction model

3.6 Model Development and Validation

3.6.1 Introduction

Oil and water and or liquid-liquid flows are encountered in oil and gas and other industries. Modelling these flows is vital in understanding their behaviour under a set of conditions. This section looks at modifying the two fluid model to provide a prediction of the interface height or hold up of water in oil flow for low water cut oil and water flow. This is necessary because the results of the adapted two low model predictions would be used to compare with experimental results.

3.6.2 Water film measurements compared with the Two-fluid model

From (Rodriguez and Oliemans, 2006) as applied to liquid –liquid flow, the two fluid model flow parameters such as velocities, pressure gradient and settled phase (water) holdup are calculated for both phases from the combined momentum equation for steady-state flow. This is a modified form of the two fluid model. The pressure drop terms are eliminated from the equations of each phase. Thus the two fluid model presented by (Sunder Raj, Chakrabarti and Das, 2005) was used to predict the oil and water hold up as the water film height through considering the curvature of the oil and water interface by reformulating (Brauner, Moalem Maron and Rovinsky, 1998) from phase velocities. However, for this study, since our experiments are in the low mixture velocity region, a no slip assumption is used though in the water layer would have a higher proportional resistance due to wall friction. Also, low water cuts of 5% and less used in the experiments ensures that the geometrical description using a flat interface for our two-fluid model (as shown in Figure 3-23) is a good representation. Thus, treating effect of surface tension and surface wetting as negligible. The no-slip holdup is given by;

$$H_L = \frac{V_{L2}}{V_{L1} + V_{L2}} \quad \textbf{(3-4)}$$

where V_{L1} and V_{L2} are volumes occupied by the phases with subscript 1 representing the lighter phase which is oil and subscript 2 representing the heavier phase which is water in this work. Given that $\tau, f,\ \rho\ , S\ , \upsilon$ and D represent the shear stress, friction factor, density, wetted perimeter, kinematic viscosity and hydraulic diameter of the respective phase. While the constants C and n depend on the value of the corresponding Reynolds number of each phase. The values are C=16 and n=1 for Reynolds number <2100 and C=0.046 and n=0.2 for Reynolds number > 2100.

$$\frac{\tau_1 S_1}{1-H_L} - \frac{\tau_2 S_2}{H_L} \pm \tau_i S_i \left(\frac{1}{1-H_L} + \frac{1}{H_L}\right) + (\rho_1 - \rho_2) Ag.\sin\xi = 0 \quad \textbf{(3-5)}$$

Where τ_1 and τ_2 the wall shear stresses with the respective fluids while τ_i is the interfacial shear stress between the fluids. These are given by:

$$\tau_1 = f_1 \rho_1 \frac{U_1^2}{2}\ and\ f_1 = C_1 \left(\frac{D_1 U_1}{\nu_1}\right)^{-n_1} \quad \textbf{(3-6)}$$

$$\tau_2 = f_2 \rho_2 \frac{U_2^2}{2}\ and f_2 = C_2 \left(\frac{D_1 U_2}{\nu_2}\right)^{-n_2} \quad \textbf{(3-7)}$$

$$\tau_i = f_i \rho_i \frac{(U_1 - U_2)}{2} |U_1 - U_2| \quad \textbf{(3-8)}$$

$and\ f_i = f_1, \rho_i = \rho_1\ for\ U_1 > U_2$

$f_i = f_2, \rho_i = \rho_2\ for\ U_2 > U_1$

The frictional factors $f_i = f_1, \rho_i = \rho_1\ for\ U_1 > U_2$ and $f_i = f_2,\ \rho_i = \rho_2\ for\ U_2 > U_1$, while D_1 and D_2 are the hydraulic diameters calculated as follows:

$$D_1 = \frac{4A_1}{S_1+S_i} \qquad D_2 = \frac{4A_2}{S_2} \qquad U_1 > U_2 \tag{3-9}$$

$$D_1 = \frac{4A_1}{S_1} \qquad D_2 = \frac{4A_2}{S_2+S_i} \qquad U_1 < U_2 \tag{3-10}$$

$$D_1 = \frac{4A_1}{S_1} \qquad D_2 = \frac{4A_2}{S_2} \qquad U_1 \approx U_2 \tag{3-11}$$

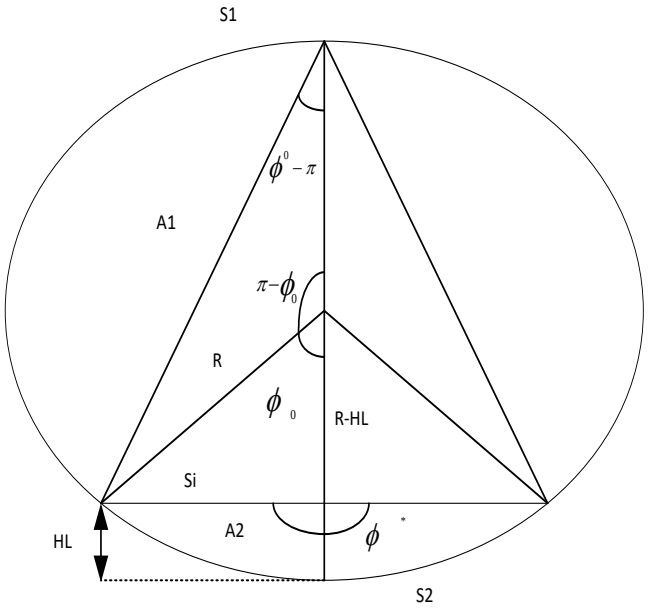

Figure 3-23 modified cross-sectional view of stratified layer

The pipe radius is R and A_1 and A_2denote the area of the lighter and heavier phase respectively. Geometrically, these are given as:

$$A_1 = R^2 \left\{\left[\pi - \phi_0 + \frac{1}{2}\sin(2\phi_0) + \frac{sin^2\phi_0}{sin^2\phi^*}\left[\phi^* - \pi - \frac{1}{2}\sin(2\phi^*)\right]\right]\right\} \tag{3-12}$$

$$A_2 = R^2 \left\{ \left[\phi_0 - \frac{1}{2} sin(2\phi_0) - \frac{sin^2\phi_0}{sin^2\phi^*} \left[\phi^* - \pi - \frac{1}{2} sin(2\phi^*) \right] \right] \right\} \quad \textbf{(3-13)}$$

$$S_1 = 2R(\pi - \phi_0) \ , S_2 = 2R\phi_0, S_i = 2R(\pi - \phi^*) \frac{\sin(\phi_0)}{\sin(\phi^*)} \quad \textbf{(3-14)}$$

Due to the assumption of a flat interface ϕ^*= 180 degrees, thus equation 3-5 becomes equation 3-15, while equations 3-12 and 3-13 become equations 3-16 and 3-17. Substituting from the geometry equations 3-14 becomes equation 3-18.

$$\frac{\tau_1 S_1}{1-H_L} - \frac{\tau_2 S_2}{H_L} \pm \tau_i S_i \left(\frac{1}{1-H_L} + \frac{1}{H_L} \right) = 0 \quad \textbf{(3-15)}$$

$$A_1 = R^2 \ \left\{ \left[\pi - \phi_0 + \frac{1}{2} sin(2\phi_0) \right] \right\} \quad \textbf{(3-16)}$$

$$A_2 = R^2 \left\{ \left[\phi_0 - \frac{1}{2} \ sin(2\phi_0) \right] \right\} \quad \textbf{(3-17)}$$

$$S_1 = 2R \left(\pi - sin^{-1} \frac{S_i}{R} \right), \ S_2 = 2R \ sin^{-1} \frac{S_i}{R}, S_i = 2R(\pi - \phi^*) \frac{sin(\phi_0)}{sin(\phi^*)} \quad \textbf{(3-18)}$$

The values were substituted in equation 3-15 and solved iteratively for H_L in a code written in MATLAB, the value of the holdup as water film height was obtained at various water cuts and mixture velocities. A comparison of these two-fluid model predictions with the experimentally measured water film height is shown in Figures 3-24 to 3-26. The calibration curve for the film thickness sensor is given in the Appendix A.2. There is an increase in water film thickness with an increase in water cut.

As can be seen, the two fluid model predictions at 0.1 m/s mixture velocity Figure 3-24 well matches the experimentally observed values except at higher water cuts where the model under predicts. This can be explained by the fact that as the water cut increases, the curvature of the interface increases thereby deviating from the flat interface assumption of the two fluid model, these changes could be from effect of surface tension and water wetting characteristics. For the higher mixture velocities of 0.2 and 0.5 m/s in Figures 3-25 and 3-26, more discrepancies occur most of which are over-predictions of the experimental values. This could be attributed to increase in phase slip with an increase in mixture velocity that is caused by an increase of water only flowrate as well as the aforementioned proportional frictional increase due to wall. Therefore, the premise of no-slip used in the model is slightly weakened. Nevertheless, the differences between the model predictions and experimental values are no more than ±15%.

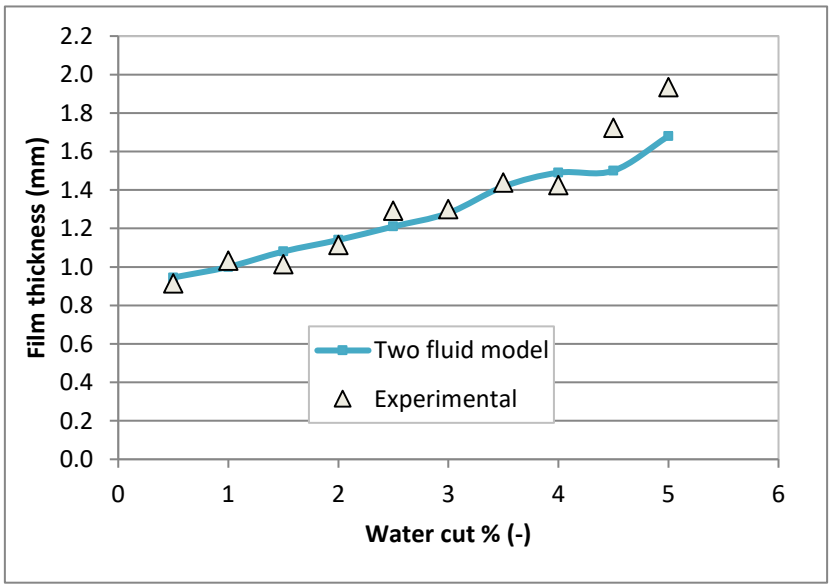

Figure 3-24 Variation of experimental and predicted film thicknesses against water cut at 0.1 m/s mixture velocity

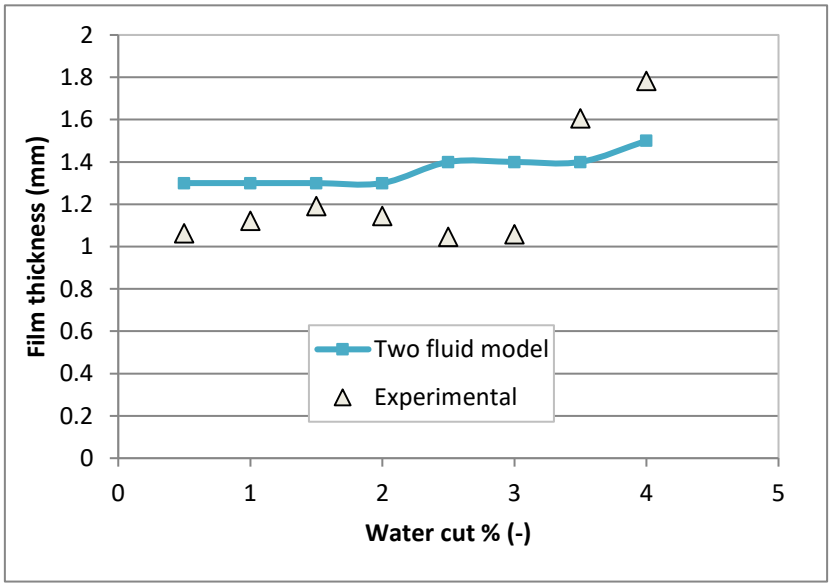

Figure 3-25 Variation of experimental and predicted film thicknesses against water cut at 0.2 m/s mixture velocity

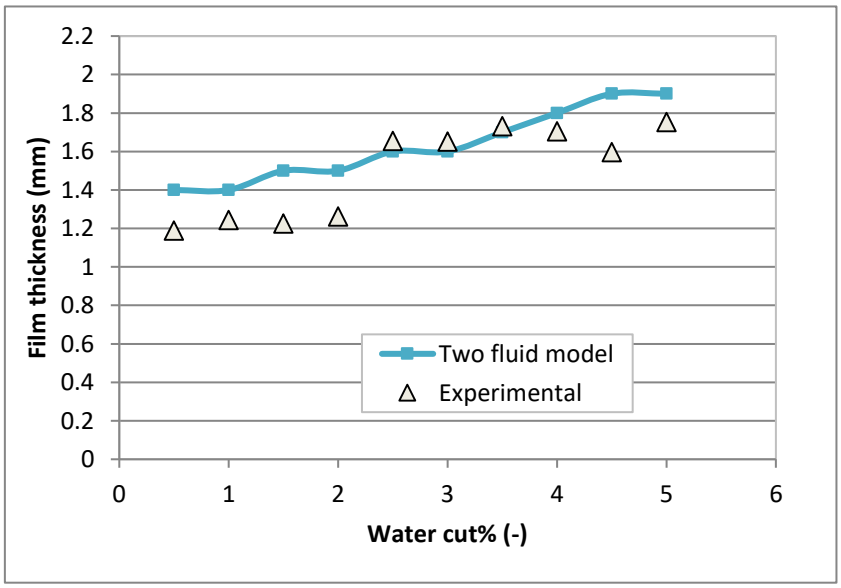

Figure 3-26 Variation of experimental and predicted film thicknesses against water cut at 0.5 m/s mixture velocity

This means that in order to improve predictions, more complicated geometrical relationships for curved interfaces may be applied. Furthermore, the no-slip assumption may be abandoned, but this may not result in more accurate solutions of the two fluid model at very low mixture velocities.

The average film thickness obtained from the experiments was compared with the two fluid model prediction as highlighted in Figure 3-27 below. The two fluid model generally under predicts the film thickness especially at the transition to dispersed flow and higher mixture velocities of 0.6 to 0.8m/s. From the two fluid model given in Figure 3-28 it can be said that the film thickness slightly increases with flow velocity and and slightly dercrease with increasing water cut.

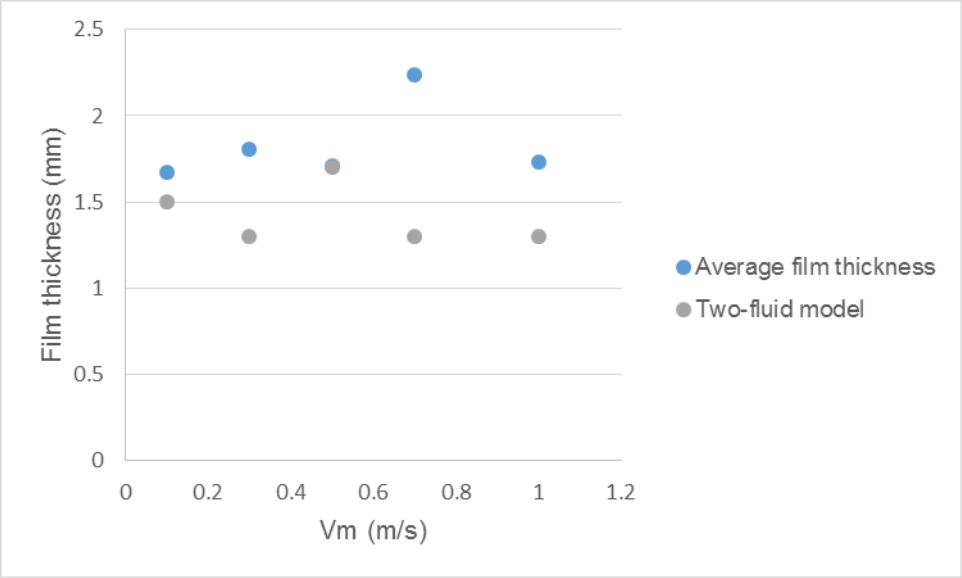

Figure 3-27 Average film thickness againts mixture flow velocities for experimental and two fluid model predictions.

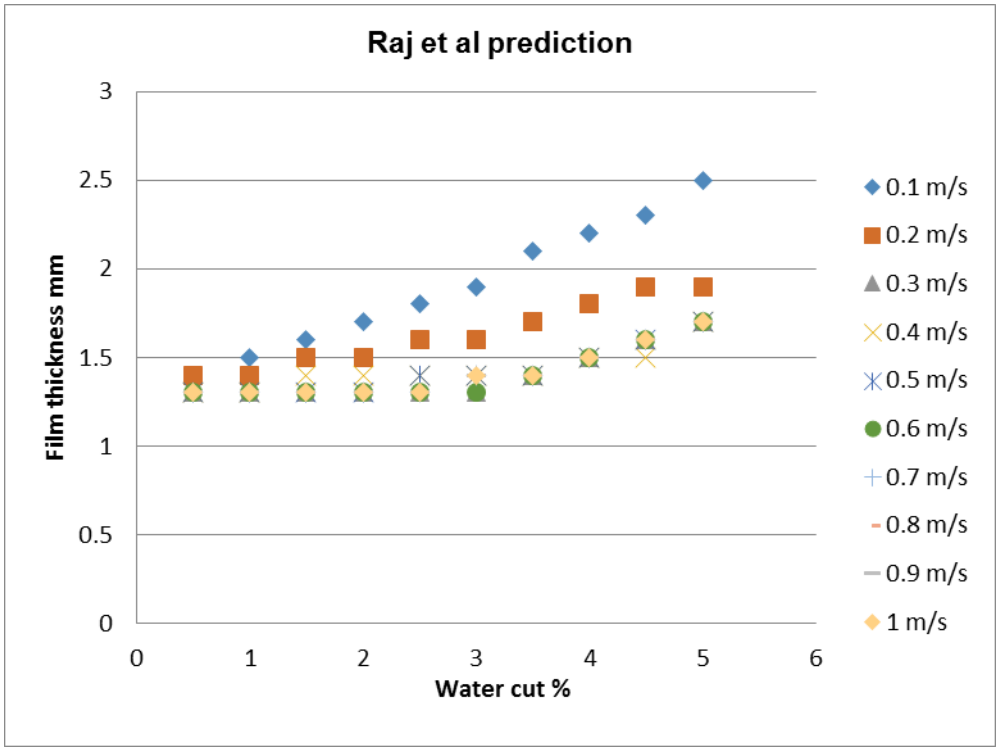

Figure 3-28 Raj et al film thickness prediction at experimental flow velocities for different water cuts.

3.6.3 Image analysis of oil and water flow

The images for oil and water flow were analysed using MATLAB image viewer app so as to measure the film thickness and compare the water fim thickness obtained from the experimental and two fluid model predictions. For oil and water mixture velocity 0.1 m/s and 1% water cut, the images are given in Figures 3-29 and 3-30 below. The measured length for 1cm (10 mm) is 39.50 pixels thus 1mm is 3.95 pixels, thus the water film thickness measured are 11.03, 11.57 and 13.58 pixels giving 2.79,2.92 and 3.47 mm respectively. This results are much higher than the results for the experimental and the two fluid model predictions.

Figure 3-29 oil and water mixture velocity 0.1 m/s at 1% water cut

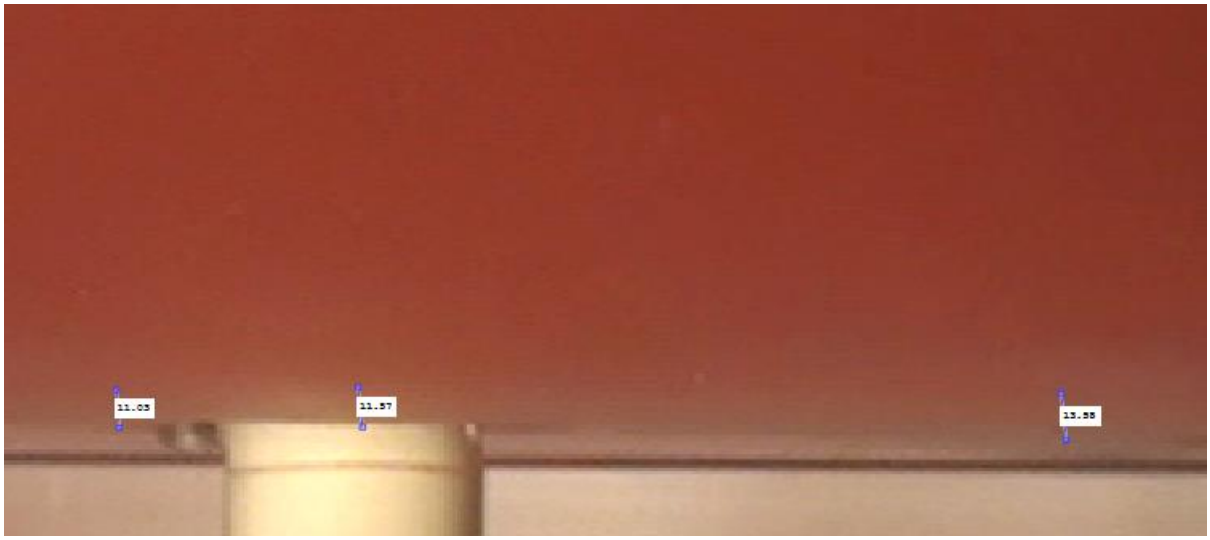

Figure 3-30 measured water film thickness for mixture velocity 0.1 m/s at 1% water cut

For oil and water mixture velocity 0.2 m/s and 1% water cut the images are given in Figures 3-31 and 3-32 below. For this higher flow rate the measured length of 1cm (10 mm) gives 147.54 pixels thus, 1mm is equivalent to 14.754 pixels as given in Figure 3-31 below. While in Figure 3-32 it can be seen that the measured height will be 3.01 and 3.02 mm respectively. These results also show that the measured film thickness are much higher than the results for the experimental

and the two fluid model predictions. Though the values for both mixture velocities are almost double the the experimental and predicted film thickness, this could be because of issues with the test spool construction. There is an issue of parallax error as a result of slight chamfer on the Perspex surface at the bottom and top sides to accomdate the bolting of the stainless steel flanges as mention in section 3.2 above and illustrated in Figure 3-5 above. This limits the use of image processesing for water film thickness measured for this study.

Figure 3-31 oil and water mixture velocity 0.1 m/s at 1% water cut

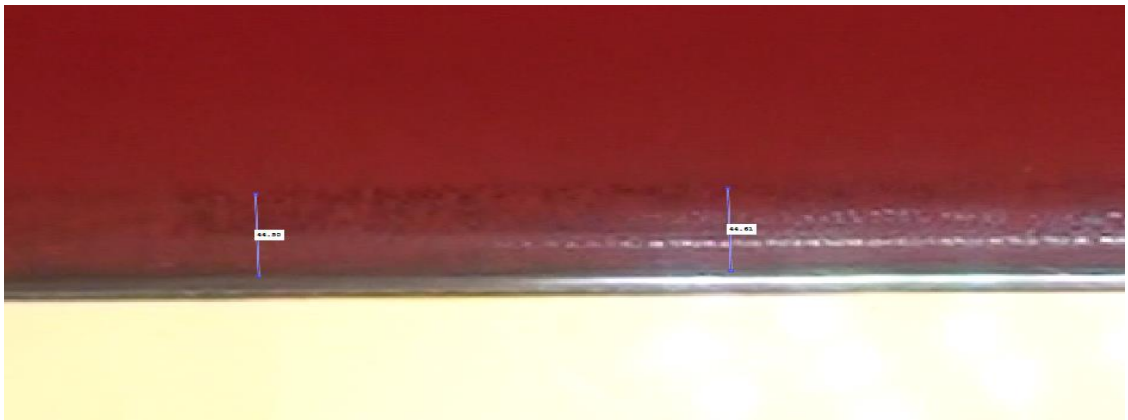

Figure 3-32 measured water film thickness for mixture velocity 0.2 m/s at 1% water cut

3.7 Conclusion

This experimental study provided behaviour of oil and water flow at low water cuts of less than 5% which are rare in the reported literature.

The structural velocity obtained by the cross correlation function increase with increasing mixture velocity and higher water cut.

The film thickness sensor could be used to detect the presence and subsequent absence of conductive low loading heavier phase in pipe such as water in oil and gas pipeline. The signals gave the height of a water layer in oil and water flow in four inch horizontal pipe and the results show that water height measured, is proportional to both the inlet water cut and mixture velocity. The water film thickness increase with increasing water cut and mixture velocity.

The flow regime formed was initially stratified smooth at low flow rate of 0.1m/s transitioning to stratified wavy flow with bubbles or goblets at the interface for the higher flow rates of 0.3, 0.4 and 0.5m/s. this transitions stratified wavy between 0.6 to 0.8 m/s before being fully dispersed at 0.9 and 1m/s.

Model predictions using a modified two-fluid model were in agreement with the experimental heavier phase heights. Thus this shows that the adapted two fluid model could be used for holdup prediction for low water cut liquid-liquid stratified flows. Although, it can be concluded that the two fluid prediction model slightly over predicts the experimental water film height at lower mixture velocities for the sensors while it predicts the experimental film thickness at higher mixture velocities.

The prediction model as expected provides an increase in the water film height with increasing water cut. Thus this shows that the adapted two fluid model could be used for holdup prediction for liquid-liquid stratified flows.

There is a need to deduce flow parameters such as Reynolds, wave amplitude and interfacial tension for further analysis so as to compare with similar work such as (Hart, J,Hamersma, P.J, Fortuin, 1989) , (Paras, Vlachos and Karabelas, 1994), (Zhang and Sarica, 2011b) .

4 SAND BEHAVIOUR IN SINGLE AND TWO PHASE HORIZONTAL PIPE

4.1 Experimental Studies

Previous researchers at Cranfield University have conducted a number of experimental tests in order to understand the sand transport behaviour in single-phase and multiphase flow systems. However, most have used visual observation for the water/sand and water/air/sand experiments. The experiments for this study were conducted on two-inch rig used concentric film thickness sensors for water/sand, water/air, sand/air and water/air/sand flows. This provided sensors for in-situ velocity measurements of the water and sand flows. The two-inch rig is described in the following sections below;

4.2 Experimental test rig, instrumentation and procedure

A two-inch internal diameter rig was utilised to perform the multiphase flow water-sand experiments. The test rig has a 2 inch (50.24 mm) inner diameter Perspex pipeline that is 10.5 m long and 0.6 m high from the floor. At the midpoint, there is a horizontal inlet line, of which 2.1 m is PVC pipe and 2 m is Perspex pipe while the water supply is through a 2 inch PVC pipe that is 10.5 meters long. Figures 4-1and 4-2 show the sand hopper and diagram of the 2 inch rig. The test section is located on the above-mentioned transparent Perspex pipe comprising two conductivity ring pairs with a sand sensor flush mounted in the middle. An additional sand sensor is mounted 210mm downstream. Installed are two differential pressure transducers that separated by a distance of 2m.

The water storage tank contains a baffle internally to prevent sand particle mixing with water. The pump is centrifugal capable of pumping up to 40 m3/hr hour into the loop. An electromagnetic flow meter, ABB model K280/0 AS with a flow range of 0 to 20 m3/hr is used to measure the water flow rate.

Air supply was through a screw compressor that has maximum flow rate of 400 $m3/hr$ having a maximum discharge pressure of 10 bar. A single pressure transducer, (PMP1400 that has 6 bar absolute pressure transducer, a range gas

flow meter, a thermal couple) are installed in the gas line that has half an inch internal diameter.

The air is injected through a horizontal inlet pipeline of 4 m total length. A single pressure transducer (PMP 1400 that has 6 bar absolute range) and second thermal couple are also installed at the end of the horizontal pipeline. The resuts calibration of the pressure transducer is given in the Appendix A.3.

Sand injection was done through use of a 400 litre capacity sand hopper that has a lower and upper impeller to stir the water sand mixture. The sand hopper is highlighted in Figure 4-1 below. The hopper has a positive displacement pump at the bottom with a maximum mixture flow velocity of 0.6m/s. The connection to the loop is through a flexible hose and valve at the beginning of the Perspex section. The methodology for determining the in-situ sand concentration is described by (Wei, 2010).

Flow meters	Type	Range
ABB K280/0 AS model	electromagnetic	0 to 20m3/hr
Endress + Hauser	Proline t-mass flanged	0 to 70m3/hr
65 F 15PMP 1400		6 barg
Krohne 1-inch	magnetic flow meter	$0.16x10^{-3}$ m^3/s
OPTIFLUX 23000C		

Video camera were mounted on a tripod stand by the side and under the Perspex viewing section to record the flow behaviour at this section.

Figure 4-1 Sand Hopper

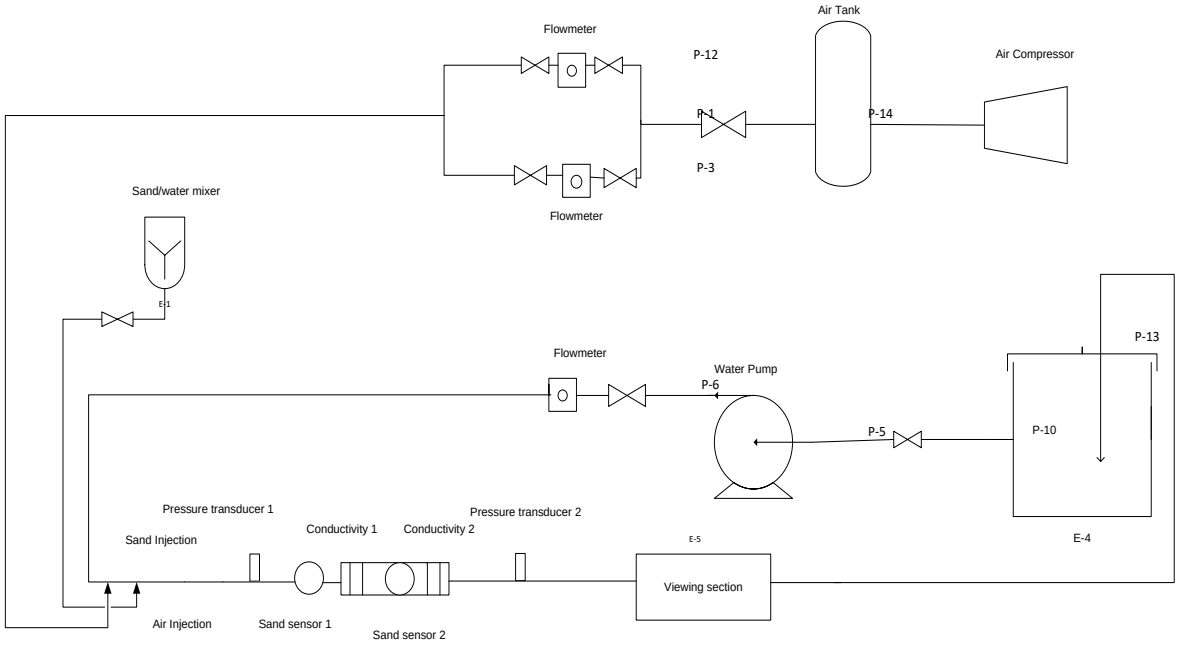

Figure 4-2 diagram of the two inch horizontal rig

4.2.1 Concentric film thickness probe sand calibration

To observe the sand behaviour in water flow, concentric film thickness sensors were used on both the 2” horizontal and 2” dip rigs for sand particle detection, this is a ground breaking approach and a major contribution to knowledge. These sensors have the same working principle as the parallel plate film thickness sensors described above chapter 3. The sensor was connected through a conductivity box to LabVIEW data acquisition system. The scan rate was 1000Hz and the data-sampling rate was 200 Hz.

Sand has always been present in sand oil production (Wei, 2010) especially at the decline stage for reservoirs. Thus, there is a need to have an understanding of the characteristics of sand movement and velocity in a pipeline. It is in this regard that tests were conducted to find out if a circular film thickness sensor could detect a presence of sand at the bottom of a pipe.

Conductive film thickness sensors have been used by (Hewitt and Bouré, 1973) (Collier and Hewitt 1964), (Coney, 1973), (Hewitt, 1982),(Kang and Kim, 1992) , (Koskie, Mudawar and Tiederman, 1989) and (Lao and Yeung 2008). The methodology for calibration was by use of inserted concentric blocks that gave a specific gap between the walls of pipe so as to get a voltage reading that corresponds with the gap, this has been used in (Chu and Dukler, 1974) and (Lao and Yeung 2008).

However, these sensors were used for water film thickness only in air or oil flow, this study provided the first time the sensors are used for sand concentration. For sand measurement, the sensors give a voltage difference for the same water volume. That is if a specific water volume gives a particular voltage, presence of sand give a slight variation in voltage. This could be because of the sand particles covering the sensor’s surface limiting the measured conductivity of water.

4.2.2 Concentric Film thickness sensor design

The concentric sensors consist of two electrodes, a central circular pin electrode and the channel wall or an outer circular pin as the other. A circular insulator separates them. There is a change in the conductivity between the two circular electrodes with a change in water film thickness t. The sensor are similar to the parallel plate ones described in chapter 3. The concentric sensors had been utilised by Butterworth (1968), Brown (1978) and Leskovar et al. (1979). The only difference is by presuming d_1 = diameter of the central electrode and d_2 is the diameter of the insulted zone then;

$$\mathrm{l_c} = \mathrm{l_1} = \mathrm{l_2} = \mathrm{d_2} - \mathrm{d_1} \qquad \textbf{(4-1)}$$

The relation gives the relationship between the non-dimensional conductivity and non-dimensional film thickness;

$$\mathrm{G^*} = \frac{2\pi \mathrm{h}}{\ln\left(\mathrm{d_2}/\mathrm{d_1}\right)} \qquad \textbf{(4-2)}$$

From the theory as reported by (Hewitt, 1982) and analysis conducted by (Coney, 1973) the sensors are a means of continuous film thickness measurements for a conducting fluid.

The probe is operated with a high oscillatory frequency of 200 Hz to reduce double layer effects. The current supplied is constant and thus the output reading is taken as voltage. This has been reported by (Kang and Kim, 1992) that with a sensor high spatial resolution, the output voltage only depends on film height and with a non-folding wave the voltage output changes monotonically with film height. The suitability of using impedance method for multiphase flow has been highlighted by (Falcone, 2009) considering the high sensitivity for conductance and capacitance systems.

4.2.3 Procedure

The film thickness sensor was mounted on the bottom of a Perspex cylinder with an open top, the surface of this sensor is flushed with the bottom of this 100mm long of 26mm radius cylinder. The sensor is bolted as depicted in the sketch given in Figure 4-3 below;

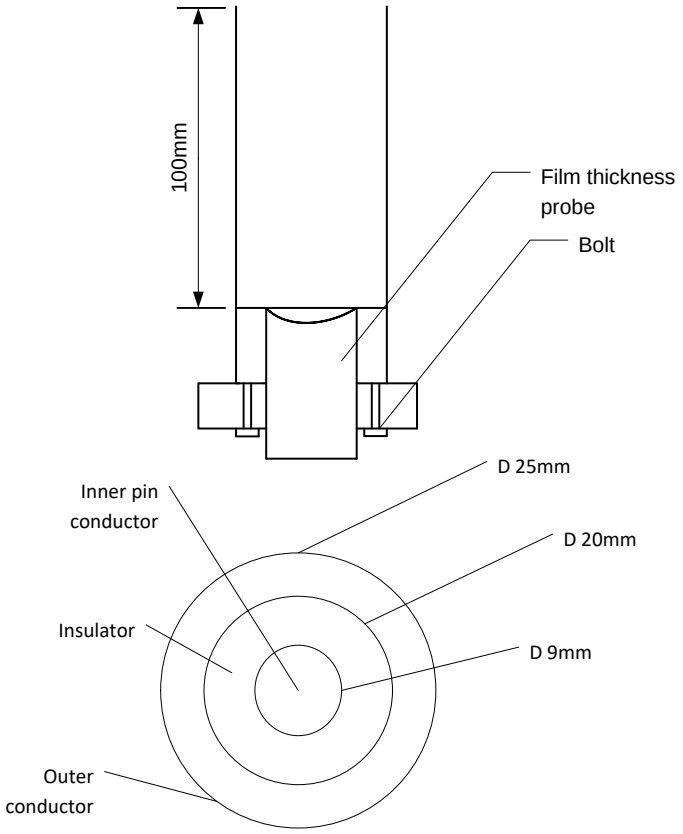

Figure 4-3 sketch of concentric film thickness sensor calibration setup

The voltage is then recorded for the film thickness sensor with no water giving zero water, zero sand reading. Subsequently the water is inserted into the calibration tube (50ml) corresponding to a 50mm liquid height and the output voltage reading was recorded as the zero sand, water reading. Then sand was weighted on a scale measured to 2 grams and this was subsequently inserted into the calibration tube and the film thickness sensor voltage output reading was recorded, this was added stepwise to the water in contact with sand sensor. The output voltage continued to decrease as sand particles are added to the water in contact with the sensor. The maximum sand inserted was 22 grams, which

corresponded with the 10% of the sand fraction in the cylinder when filled with sand and the voltage, became saturated. The calibration curve based on sand fraction is given in Figure 4-4 below, while that for equivalent sand thickness is also given in Figure 4-5 below;

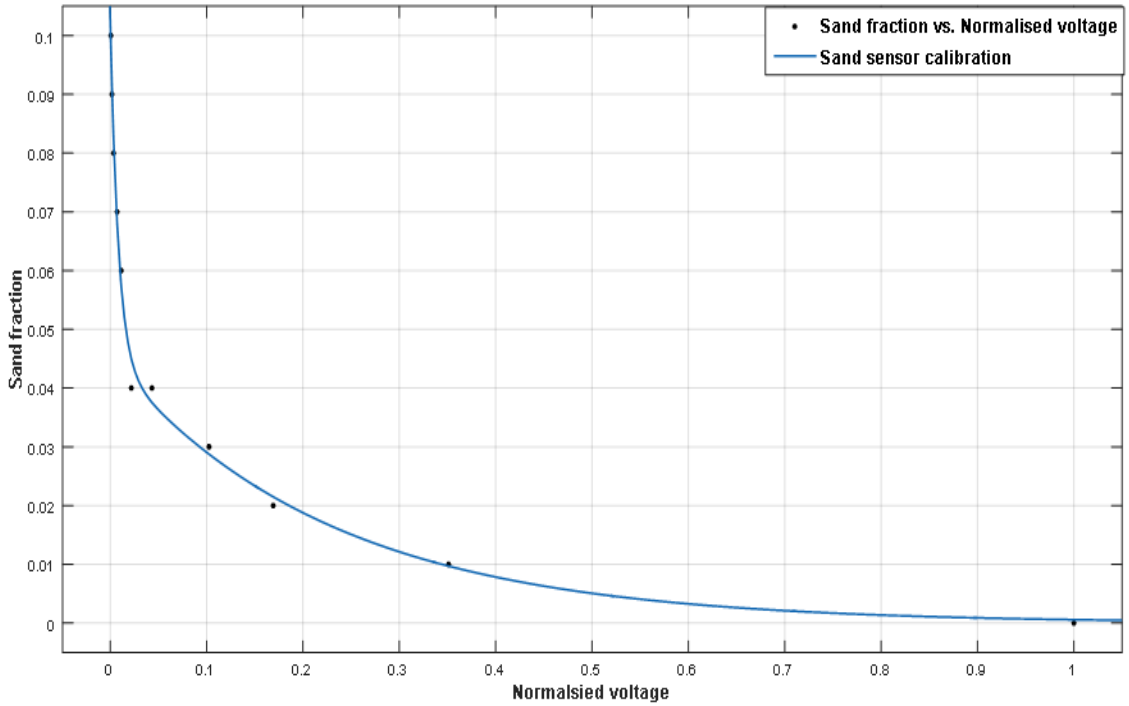

Figure 4-4 sand and water calibration for concentric film thickness sensor (sand fraction against normalised voltage)

The curve fit and corresponding coefficient of determination is given in Equation 4-3 below;

$$y = 3.667^{-10}\exp(-36.35x) + 0.0228\exp(-1.31x) \quad \textbf{(4-3)}$$

$R^2 = 0.9948$

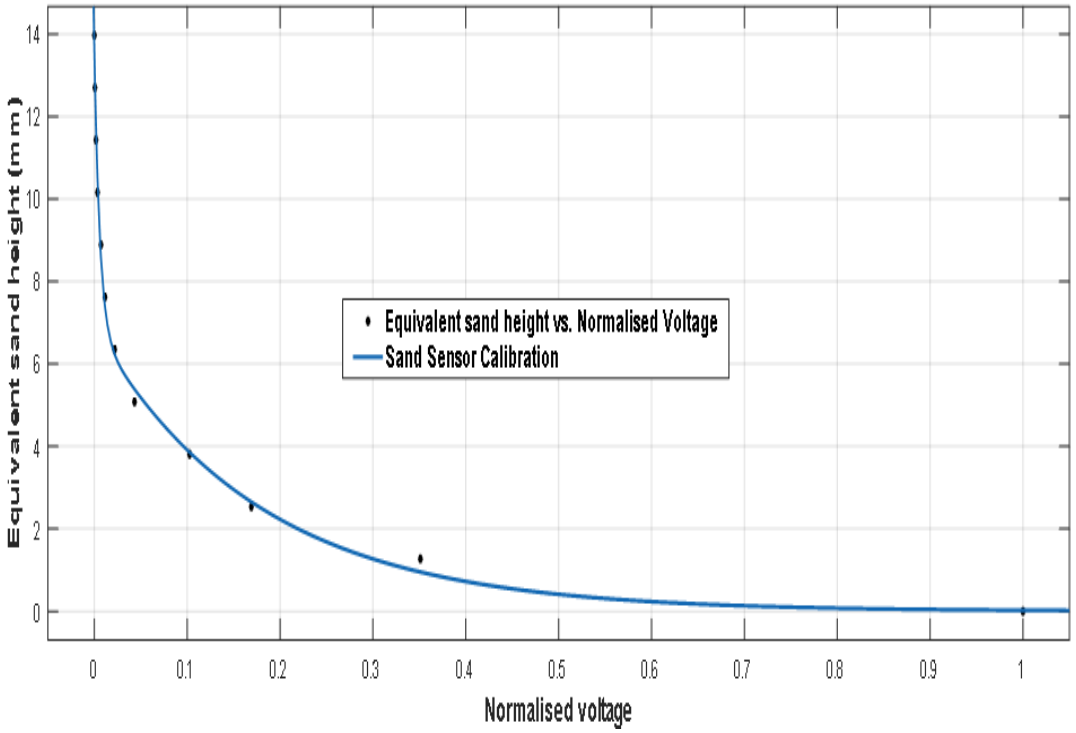

Figure 4-5 sand and water calibration for concentric film thickness sensor (sand equivalent height against normalised voltage)

The calibration curve will be used to obtain sand fraction or equivalent sand height from experiments conducted on the 2” rig. The calibration cylinder set up is highlighted in Figure 4-6.

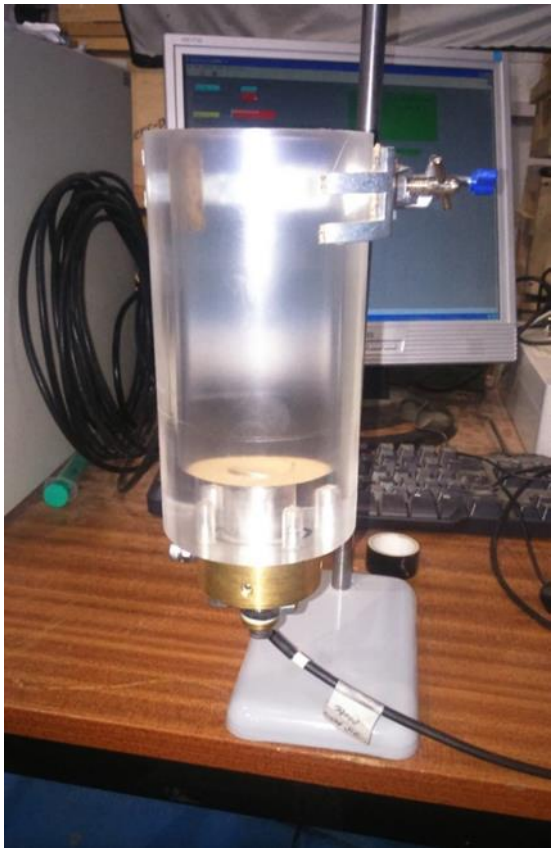

Figure 4-6 sand and water calibration cylinder setup for concentric film thickness sensor

4.2.4 Water calibration of conductivity rings

A test piece that consist of conductivity ring pair with the two rings separated by a distance of 68mm was used in a blanked 2” pipe. One end of the blank has a bolted inlet through which water is inserted. This was positioned horizontally during the calibration process. The conductivity ring pair was connected through a conductivity signal-conditioning box to LabVIEW data acquisition system. The scan rate was 1000Hz and the data-sampling rate was 200 Hz.

4.2.4.1 Procedure

The procedure is similar to methods used by (Fossa, 1998a) and (Andreussi, Di Donfrancesco and Messia, 1988). This involved taking the conductivity ring voltage output readings with air only or zero water reading. Water was then inserted through the inlet filling 10% of the cylinder volume and the voltage reading taken. This was repeated inserting 10% water volume at a time till

reaching 100% water volume and voltage output readings taken respectively. The results of the resulting calibration curves for conductivity ring 1 and 2 depicting the normalised water fraction and resultant voltages are given in Figure 4-7 below;

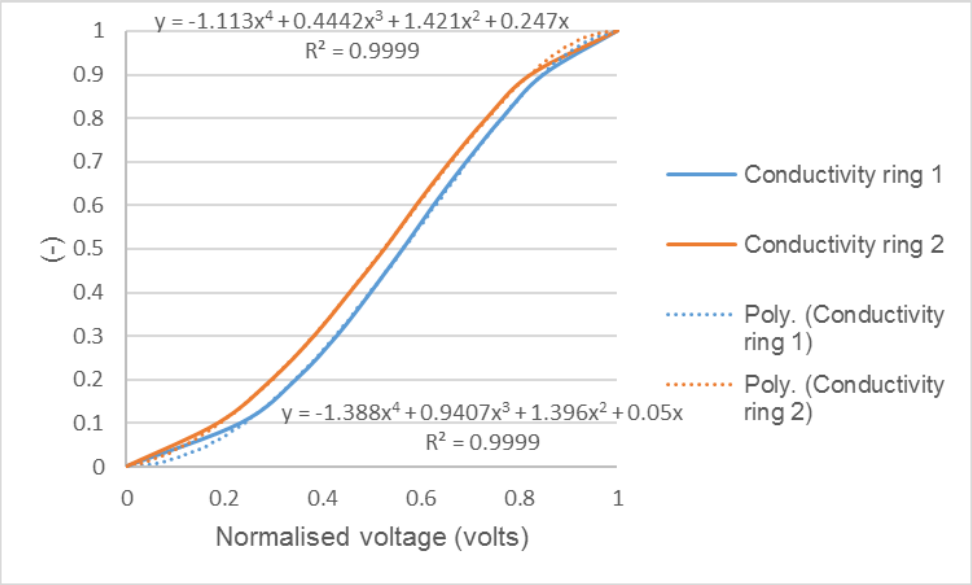

Figure 4-7 water calibration for conductivity ring

Conductivity ring 1 water calibration curve fit and corresponding coefficient of determination is given in Equation 4-4 below;

$$y = -1.113x^4 + 0.442x^3 - 1.421x^2 + 0.0247x \quad \textbf{(4-4)}$$

$$R^2 = 0.9999$$

Conductivity ring 2 water calibration and corresponding coefficient of determination is given in Equation 4-5 below;

$$y = -1.388x^4 + 0.9407x^3 - 1.396^2 + 0.05x \quad \textbf{(4-5)}$$

$$R^2 = 0.9999$$

4.3 Results and discussion

Experiments were conducted on the two inch rig horizontal rig. These consists of one conducted with single phase water and low concentration sand as given in section 4.3.1 and the other having two-phase water/air flow and low concentration sand as given in section 4.3.2 below. This was conducted to quantify concentration of sand particle in stratified wavy flow on 2-inch rig using film thickness sensor (high gas flow rate and low liquid volumetric flow rate, which can be termed as low liquid loading)

- To identify velocity of flow of sand particles or sand bed or moving sand dune (in conjunction with conductivity ring for water) and sand fraction or equivalent sand height.
- Identify factors affecting sand velocity and height in terms of sand particle size and concentration.

4.3.1 Sand in water pipe flow

Experiments were conducted on the horizontal two-inch rig described above. The sands porosity for 150 microns is 30% while that for 355 microns is 28.71%. The methodology for the sand properties measurement is given in the Appedix A.3. Table 4-1 below gives a summary of the particle and concentration used in this study,

Table-4-1 summary of particle concentrations used for the sand and water experiment

Particle	Nominal diameter (microns)	Density (Kg/m3)	Shape	Sand volume Fraction (v/v)	Superficial liquid velocity range (m/s)	Vsl at mtc (m/s)

sand	150	2650	irregular	0.00005 0.0001 0.0003	0.099 to 0.320	0.270 0.270 0.270
sand	355	2650	irregular	0.00005 0.0001 0.0003	0.099 to 0.320	0.300 0.320 0.320

Sand sensor behaviour was observed for different flow regimes some of which have been observed by (Ibarra et al., 2014), (Al-lababidi, Yan and Yeung, 2012) (Yan et al., 2011). This observed behaviour had been characterised as follows,

4.3.1.1 Sand bed

At Vsl of 0.099m /s, a sand bed was observed as depicted in Figure 4-11 below. The response of the sand sensor indicates a high voltage output as well as a higher sand fraction due to the height of the sliding sand bed. The normalised voltage output given in Figure 4-8 is much closer to unity because of the sand particles covering the flush mounted sensor and there little or no undulations due the fact that is a sand bed. The pdf of the sand fraction obtained by the sand sensor as in Figure 4-9 highlights the presence of a sand bed that have perturbations as a result of water flow velocity, similarly the equivalent sand height is also consistent with a little perturbations as in this figure. The frequency

domain provides a peak signal at about 0.1Hz as can be observed in Figure 4-10 below, this implies little amount of energy is used thus the sand settling as a bed.

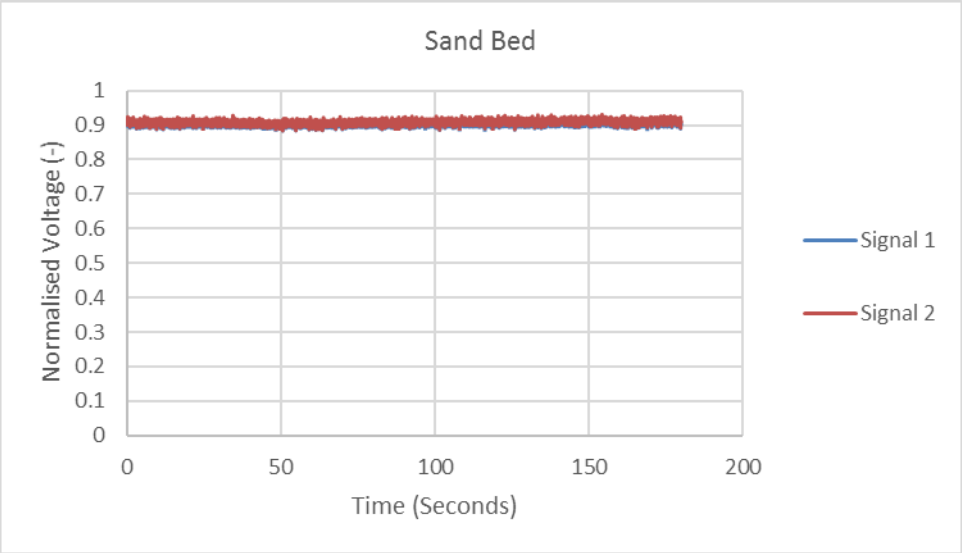

Figure 4-8 normalised voltage Vsl 0.099m/s 0.00005 v/v 150 microns

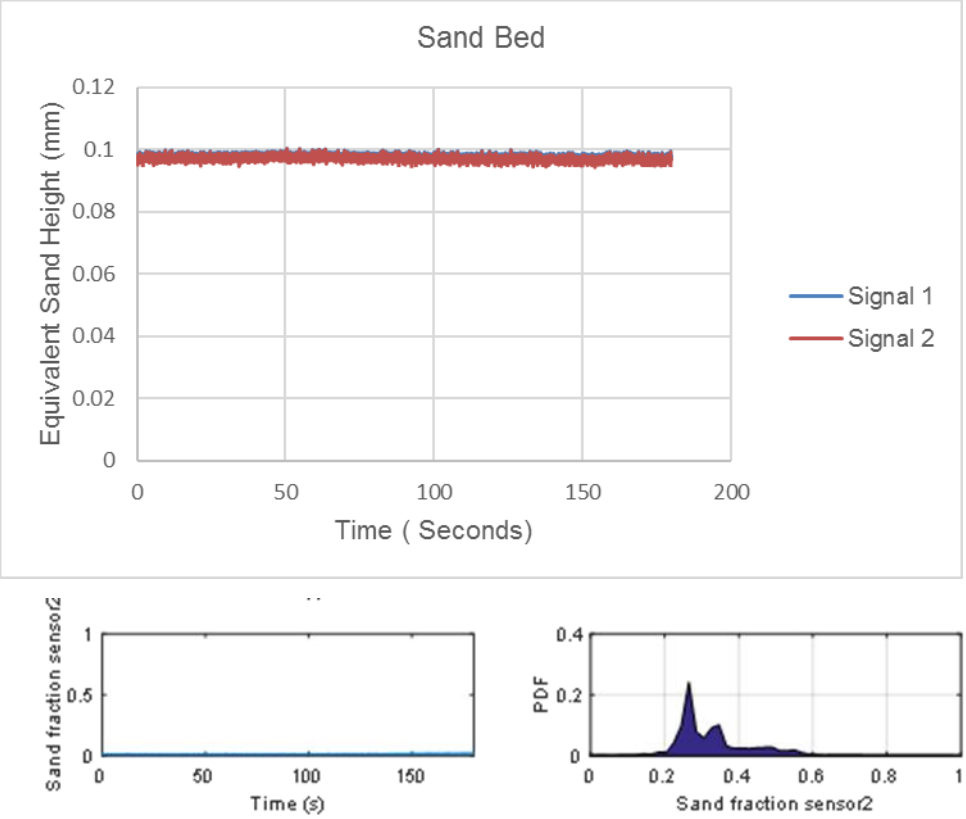

Figure 4-9 sand sensor equivalent sand height, sand fraction and pdf Vsl 0.099m/s 0.00005 v/v 150 microns

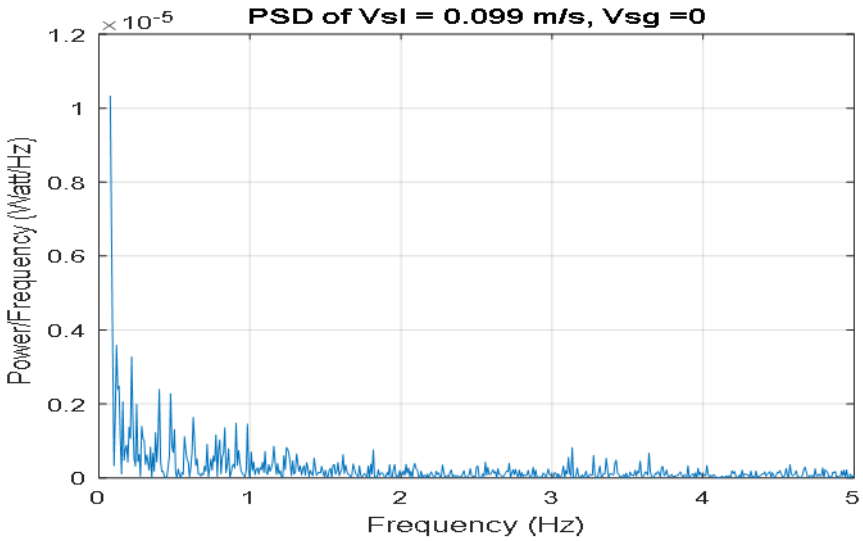

Figure 4-10 PSD for Vsl 0.099m/s 0.00005 v/v

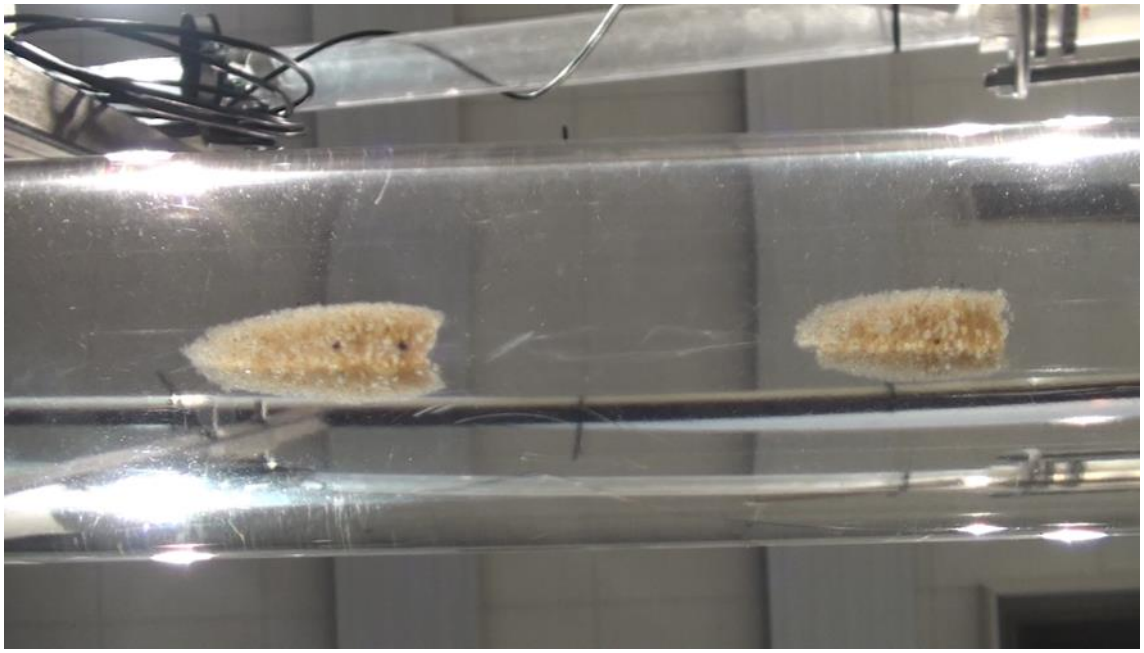

Figure 4-11 sand bed Vsl 0.099m/s concentration of 0.00005 v/v

4.3.1.2 Sand dune

For a moving sand bed flow regime, identification can be achieved by using the sand sensor as demonstrated in Figure 4-12 below. From observing the time series and normalised voltage output the sensors can detect the passage of a dune. The voltage decreases substantially because of the sand particles covering

the sensor resulting higher resistivity of the circuit. This dip in the voltage is recovered as soon as the sand dunes are conveyed further downstream. Water then replaces the sand particles and the voltage returns to that for water. Thus having two sand sensors enable the cross-correlation of the signals to obtain the sand structural velocity though there are high uncertainties due to the incoherent signal generated by the dune passage. As can be seen in Figure 4-13 the frequency have a single peeks at 0.08Hz indicating the passage of a sand dune. The side view of the dune passage is highlighted in Figure 4-14. The sand sensor sand fraction given in Figure 4-15 indicate the average holdup peaking at the passage of the sand dune, while the equivalent sand height increases at the passage of the sand dune over the sensors.

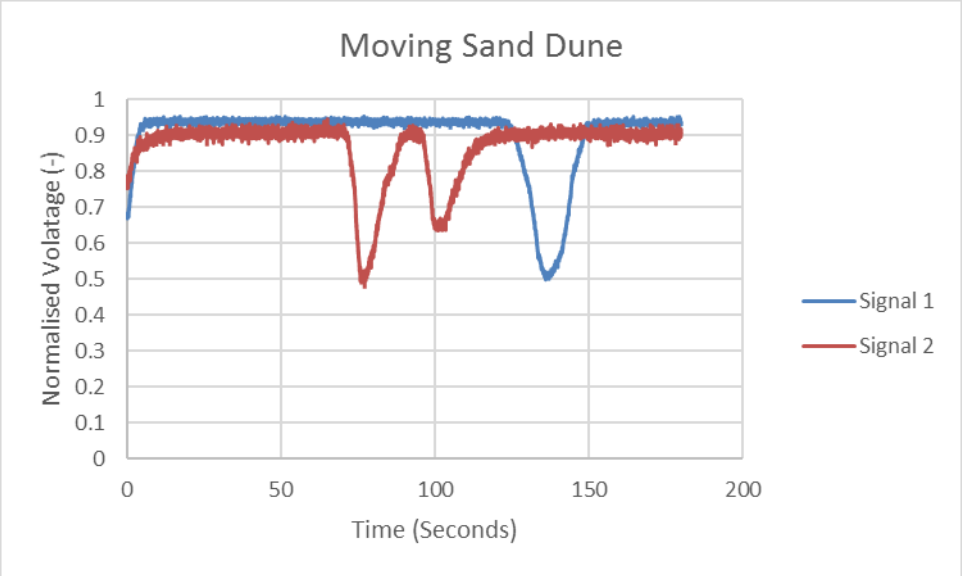

Figure 4-12 sand sensor normalised voltage for dune passage 355 microns Vsl 0.140 m/s 0.0003 v/v

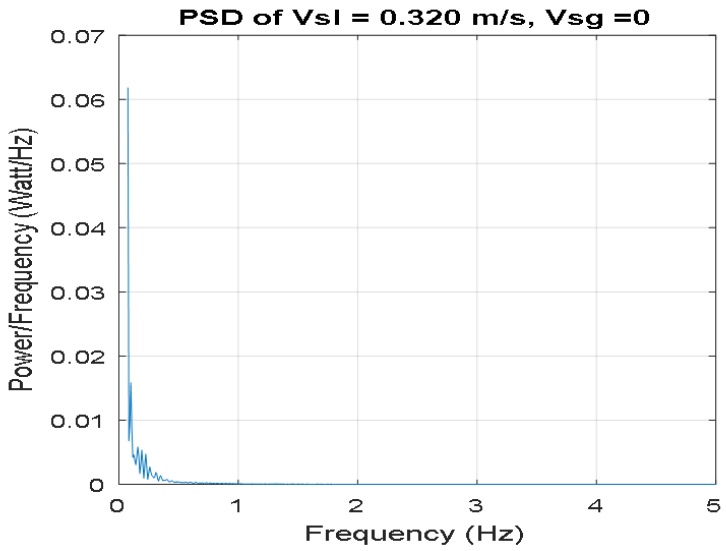

Figure 4-13 PSD for dune passage 355 microns at Vsl 0.14m/s 0.0003 v/v

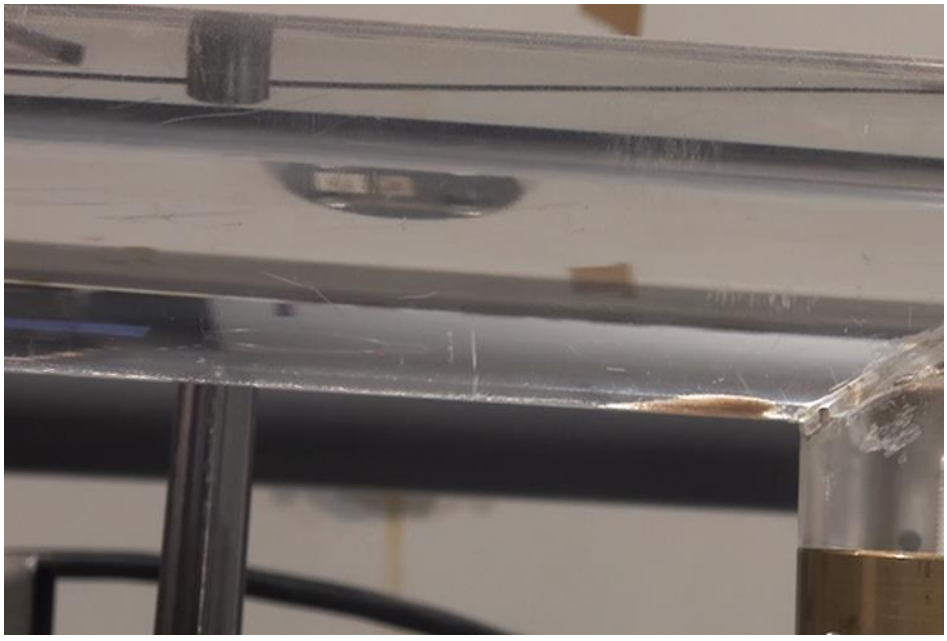

Figure 4-14 side view of sand dune passage for 355 microns at Vsl 0.14m/s and concentration of 0.0003 v/v

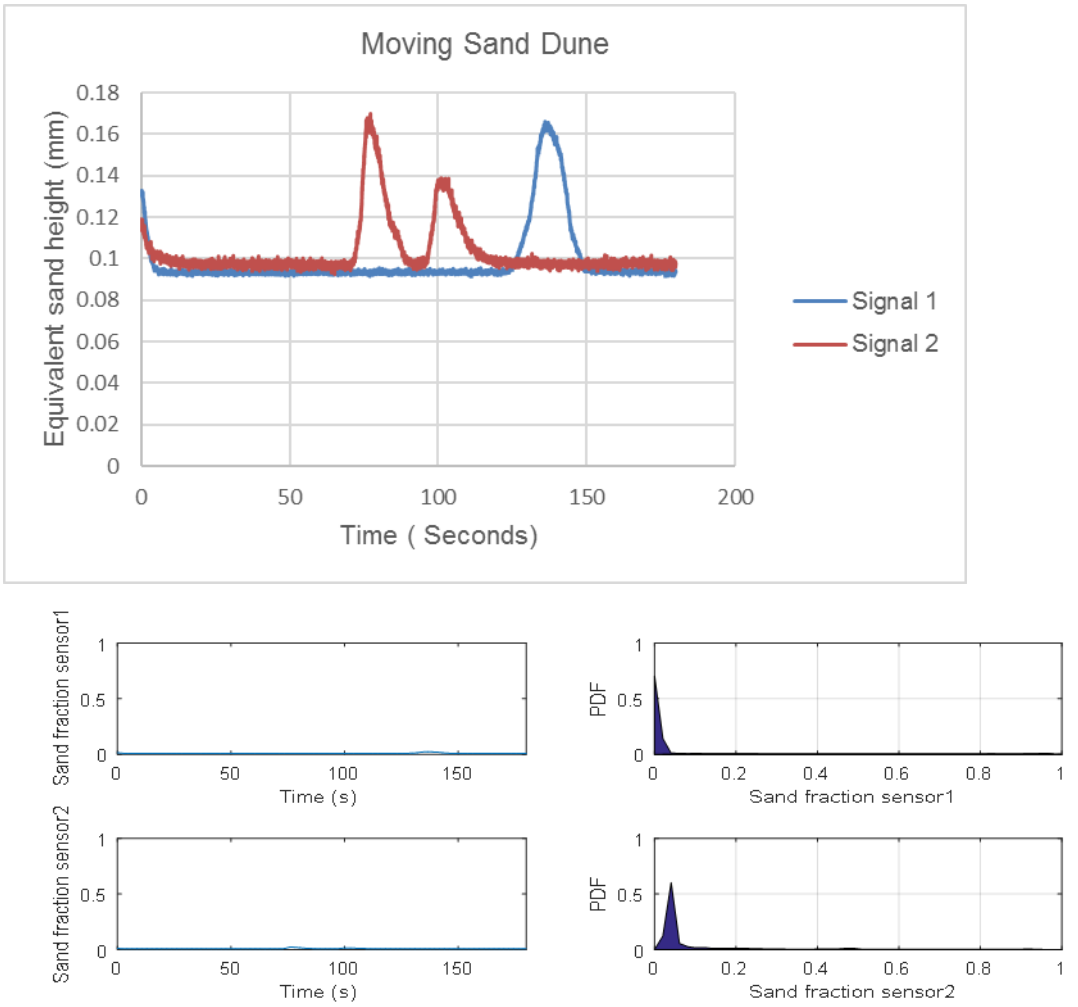

Figure 4-15 sand sensor equivalent sand height, sand fraction and sand fraction pdf for dune passage 355 microns at Vsl 0.14m/s and 0.0003 v/v

4.3.1.3 Saltation

The sand sensor response under the saltation flow regime are given in Figures 4-16 and 4-17 below in the form of normalised voltage and sand fraction and their respective pdf. The voltage signal has multiple peaks that could be explained by the moving sand particles covering the sensor and uncovering the sensor as they saltate. Similarly, from Figure 4-18 the frequency have multiple peaks from 0.1 to 0.8Hz indicating the intermittent coverage of the sand sensor by the sand particles, and implying the slight energy increase in moving the sand particles. The equivalent sand height varies slightly due to the change caused by the Saltating sand particles as depicted in Figure 4-17. The saltation flow is illustrated in Figure 4-19 below.

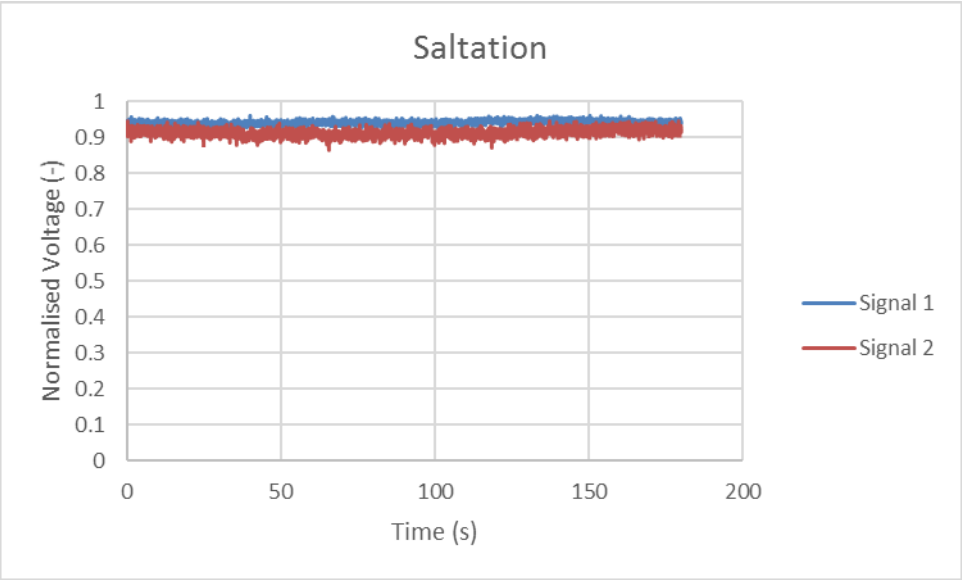

Figure 4-16 normalised voltage for saltation at Vsl 0.180m/s 0.00005 v/v

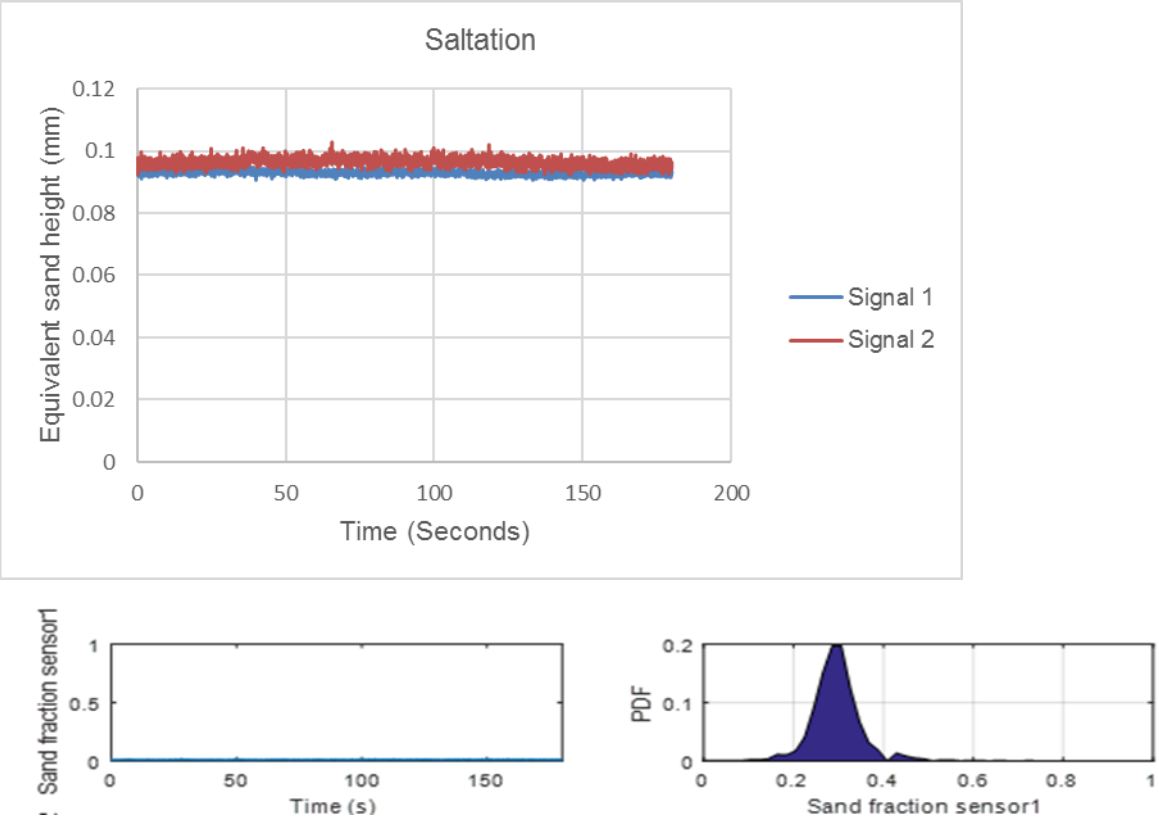

Figure 4-17 Sand sensor equivalent sand height, sand fraction for saltation at Vsl 0.180m/s 0.00005 v/v

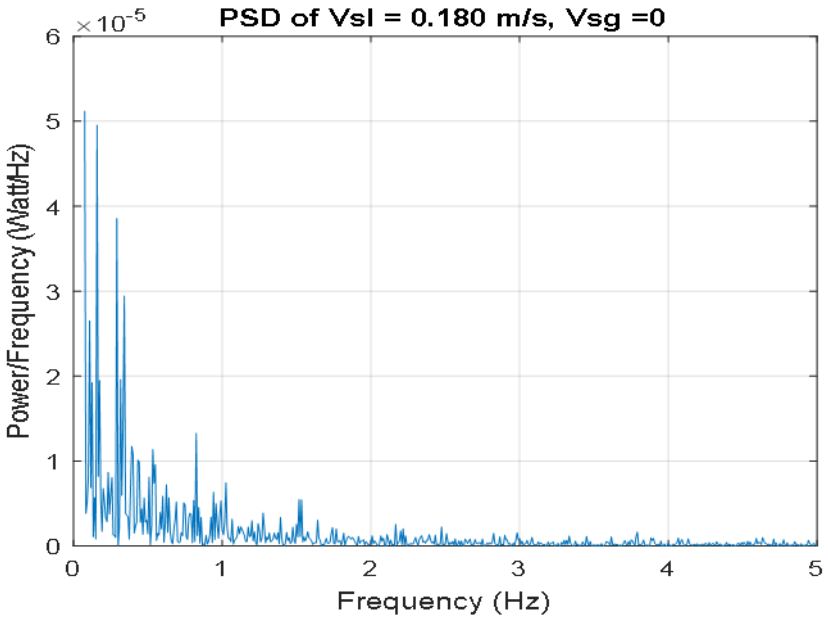

Figure 4-18 PSD for saltation at Vsl 0.180m/s 0.00005 v/v

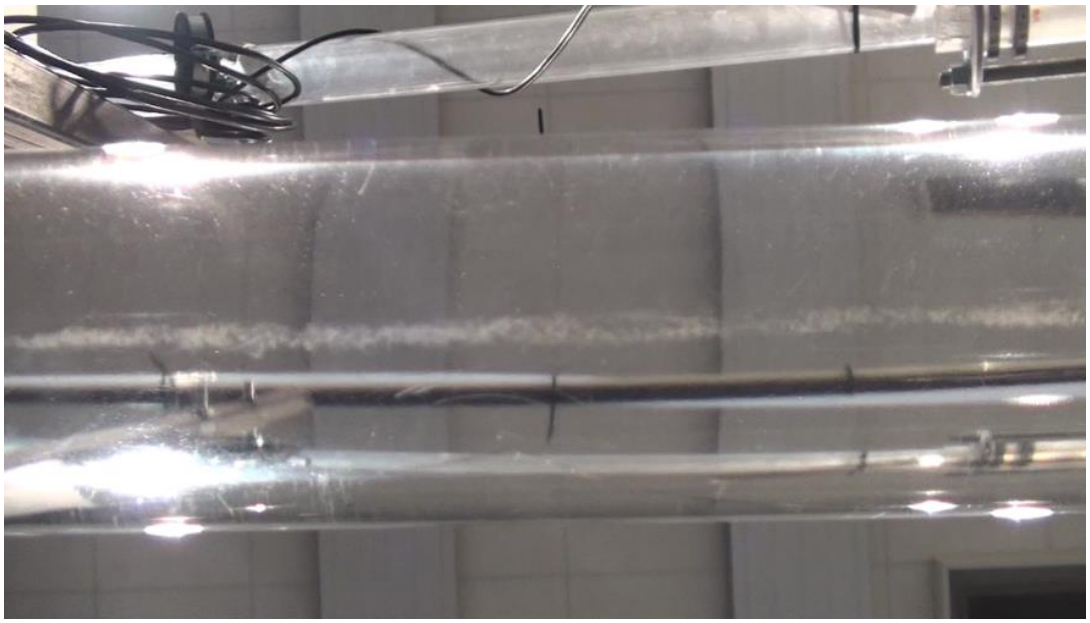

Figure 4-19 bottom view of saltation at Vsl 0.180 m/s concentration 0.00005 v/v

4.3.1.4 Streak

The sand sensor response to streak flow regime is given in in Figures 4-20 and 4-21 for normalised voltage output and sand fraction with their respective pdf. The normalised voltage output is much close to unity. Both the voltage and sand sensor pdf highlight multiple spike peaks that indicate sudden intermittent

covering of the sand sensor by the sand particles. Similarly the frequency as seen in Figure 4-22 below indicate disturbances peaking between 0.1Hz and 4.6Hz caused by the moving sand streaks, implying greater energy used in moving the sand particles. There is a noticeable drop in the equivalent sand height and sand fraction as given in Figure 4-21. Figure 4-23 illustrates the streak flow regime.

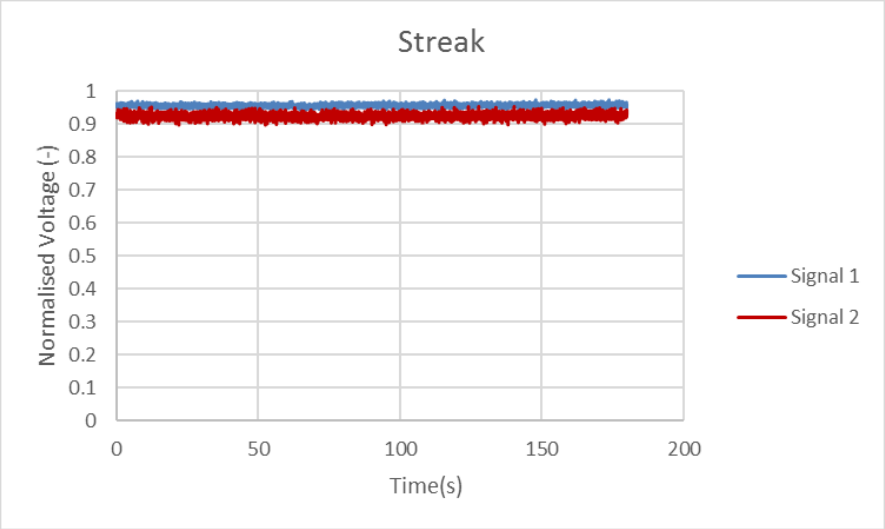

Figure 4-20 normalised voltage for streak at Vsl 0.200m/s 0.0003 v/v

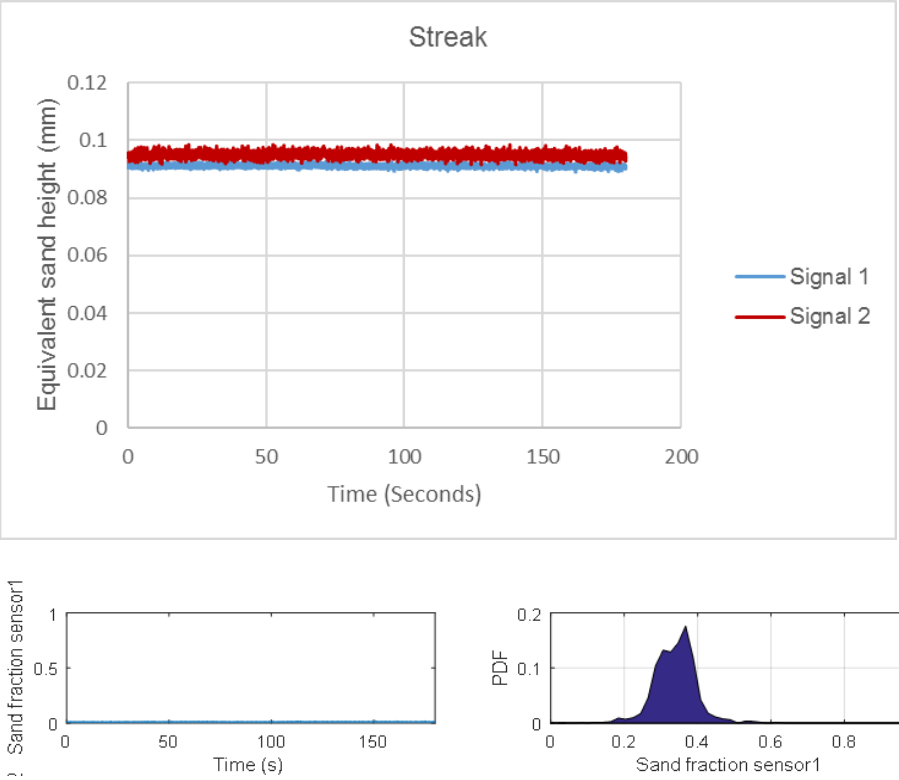

Figure 4-21 Sand sensor equivalent sand height, sand fraction for streak at Vsl 0.200m/s 0.0003 v/v

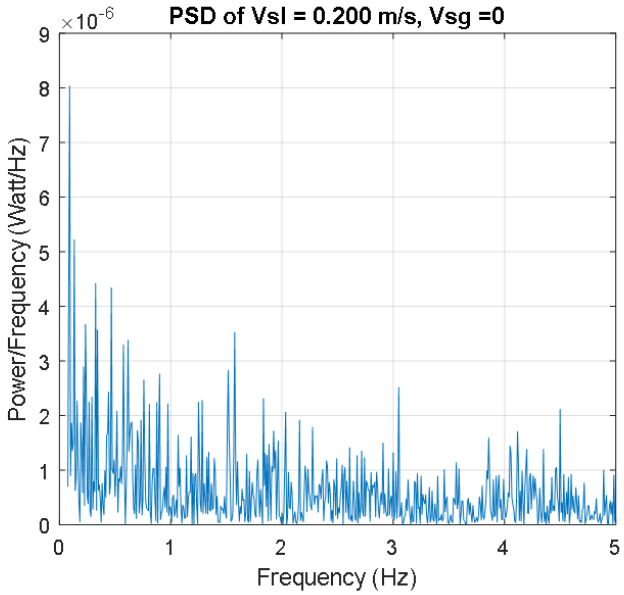

Figure 4-22 PSD and amplitude for streak at Vsl 0.200m/s 0.0003 v/v

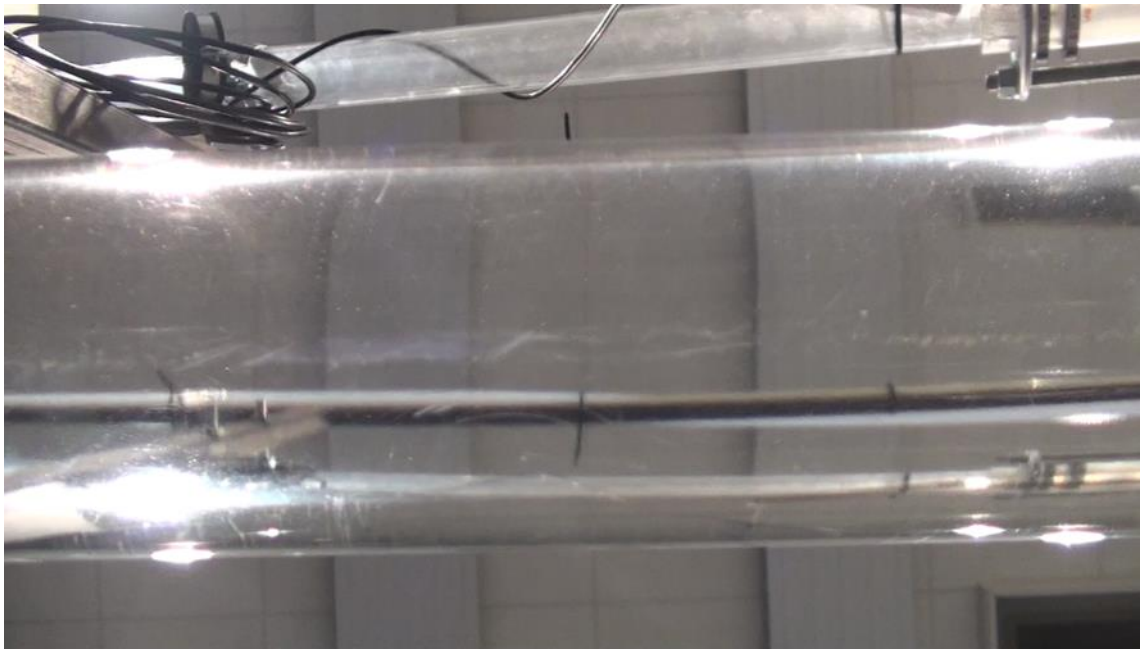

Figure 4-23 bottom view of streak at Vsl 0.200m/s concentration 0.0003 v/v

4.3.1.5 Suspension

This flow regime was identified by the sensor response as highlighted in Figures 4-24 and 4-25 for normalised voltage and sand sensor with their respective pdf. The normalised voltage output is almost at unity as the sand particles are suspended in the water flow without impinging on the sensor. The sand sensor pdf indicate a single peak that indicate to denote a constant voltage will little or occasional covering of the sand sensor by the sand particles, while the equivalent sand height reduces further indicating little or no sand layer as given in Figure 4.25 below. Similarly, the frequency as seen in Figure 4-26 below indicate several a peaks between at 0.1Hz and 4.9Hz implying higher energy required to maintain the particles in the flow. Figure 4-27 illustrates the suspension flow regime.

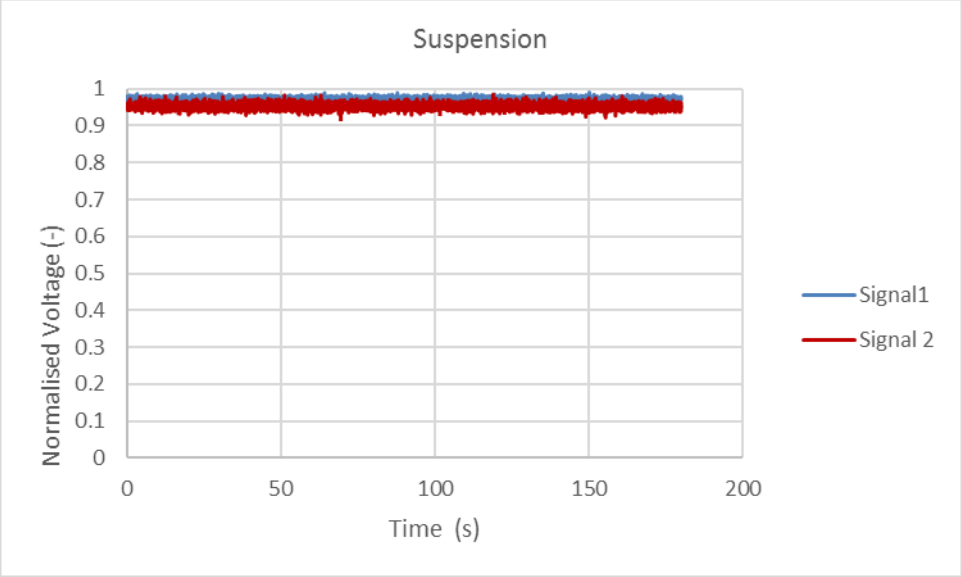

Figure 4-24 normalised voltage and pdf for suspension at Vsl 0.27m/s concentration 0.0003 v/v

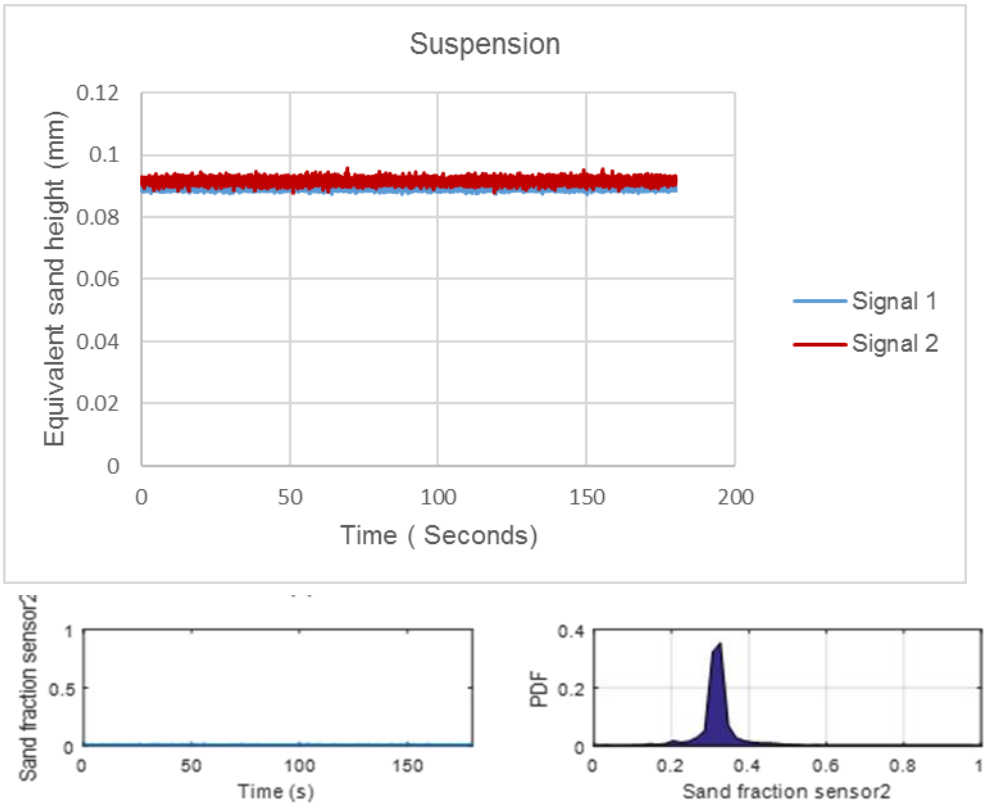

Figure 4-25 Sand sensor equivalent sand height, sand fraction for suspension at Vsl 0.27m/s concentration 0.0003v/v

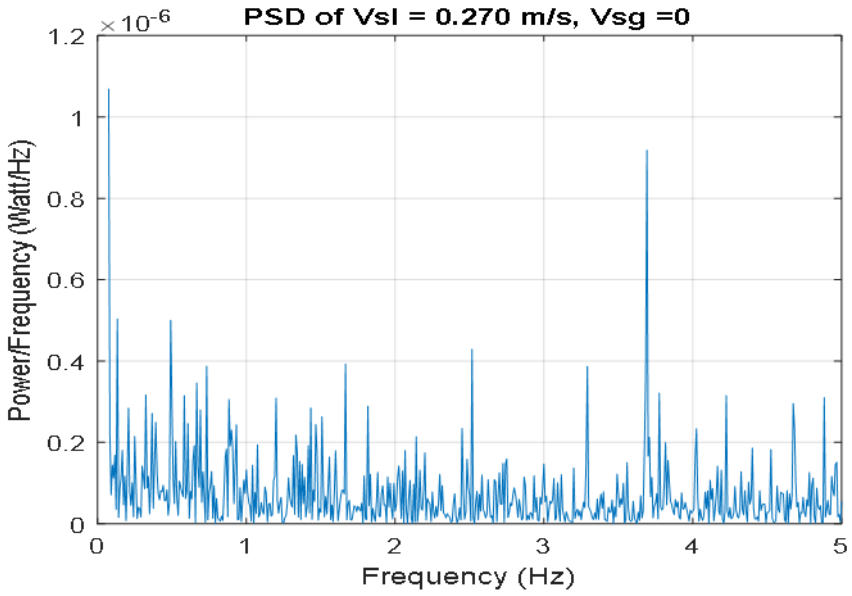

Figure 4-26 PSD and amplitude of suspension at Vsl 0.27m/s concentration 0.0003 v/v

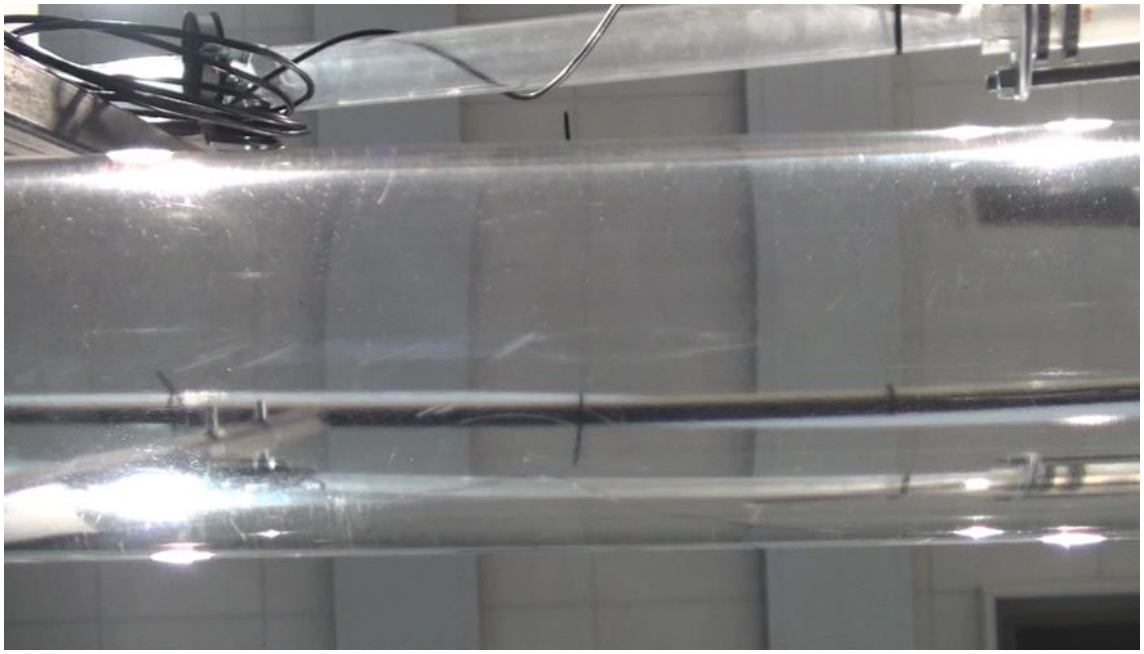

Figure 4-27 bottom view of suspension at Vsl 0.27m/s concentration 0.0003v/v

The Table 4-2 below gives the coefficient of variation for the normalised voltage output and the equivalent sand height obtained from the sand sensor. While table 4-3 give a summary of the identified flow regimes for the horizontal two-inch pipe flow.

Table 4-2 coefficient of variation for the normalised Voltage and equivalent sand height for 150 microns 0.00005 v/v

Flow Regime	Vsl (m/s)	Mean Normalised Voltage	Standard Deviation of Normalised Voltage	Coefficient of variation	Equivalent sand height (mm)
Moving Bed	0.099	0.9065	0.0009	0.0970	0.1250
Moving Bed	0.128	0.9188	0.0045	0.4847	0.0958
Moving Bed	0.14	0.8824	0.0070	0.7945	0.1005
Saltation	0.18	0.8983	0.0021	0.2341	0.0984

Streak	0.2	0.9412	0.0025	0.2603	0.0931
Suspension	0.235	0.9958	0.0015	0.1515	0.0870
Suspension	0.27	0.0019	0.9653	0.1916	0.0906
Suspension	0.3	0.9586	0.0024	0.2535	0.0910
Suspension	0.32	0.9704	0.0021	0.2143	0.0895

Table 4-3 flow pattern for 150 microns 0.00005 v/v

Side view	Vsl m/s	Pattern	Sand sensor normalised voltage and sand fraction
	0.099	Moving bed	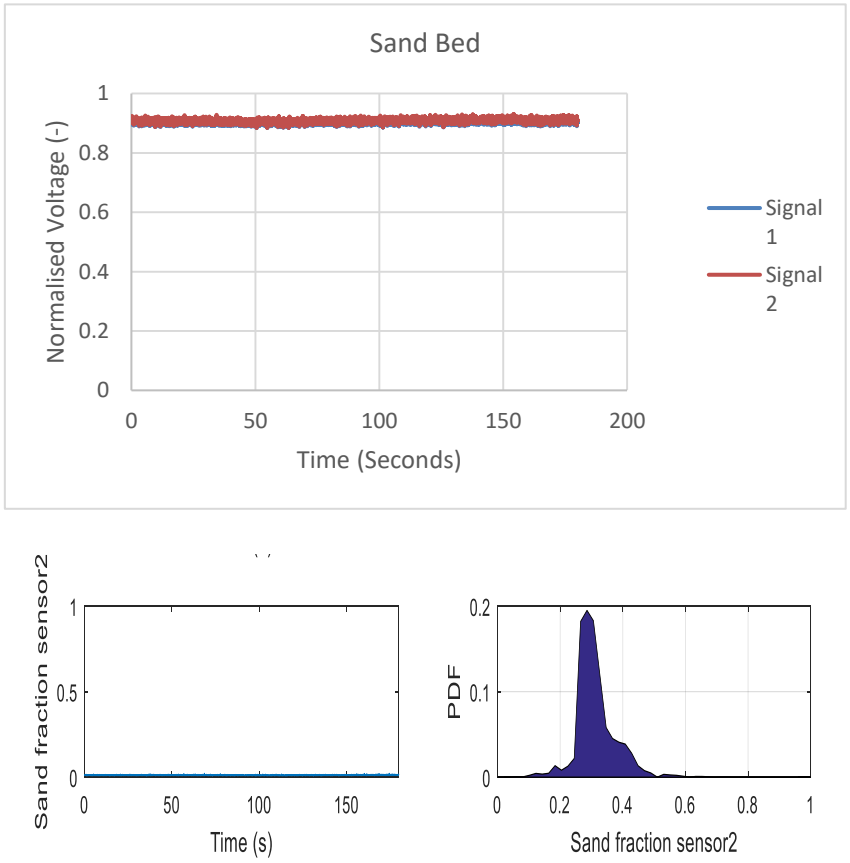

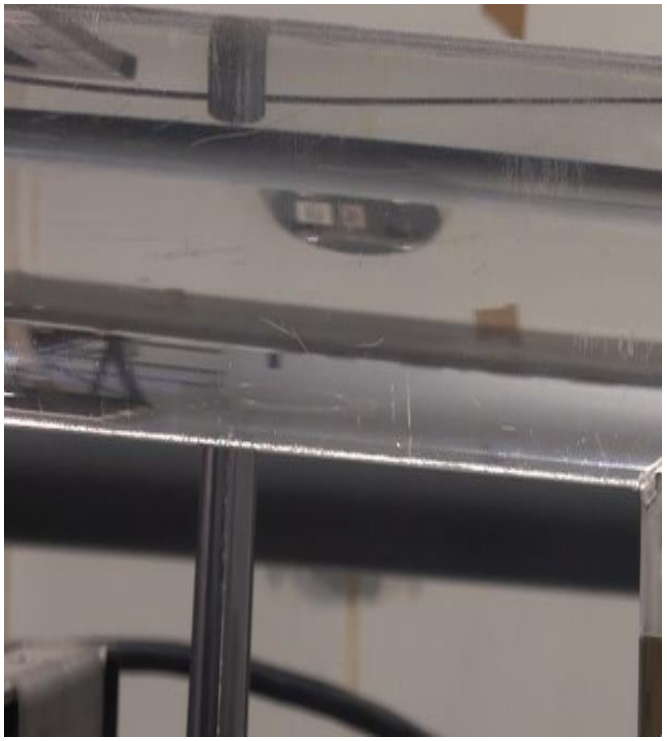

0.128 Moving bed

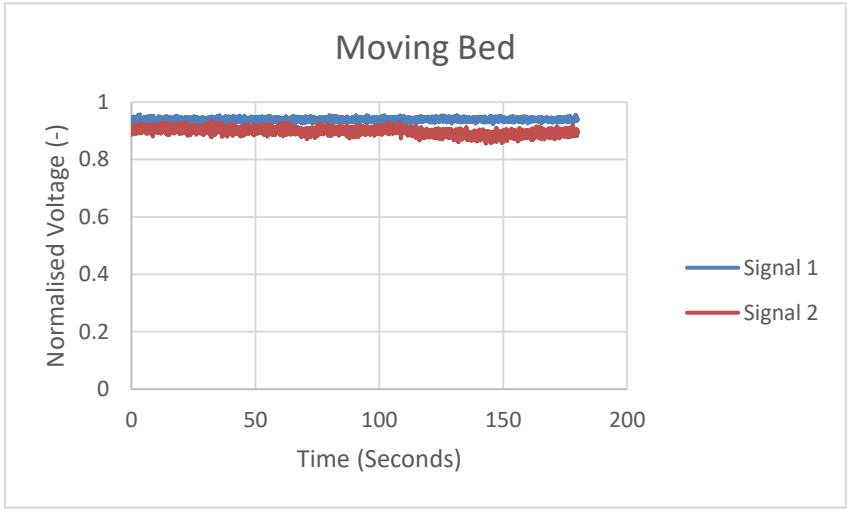

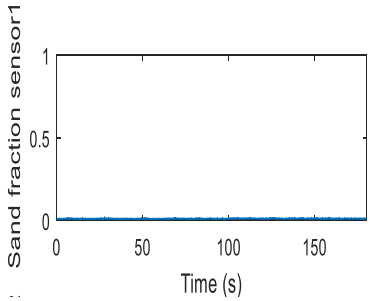

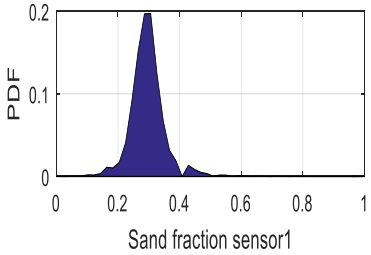

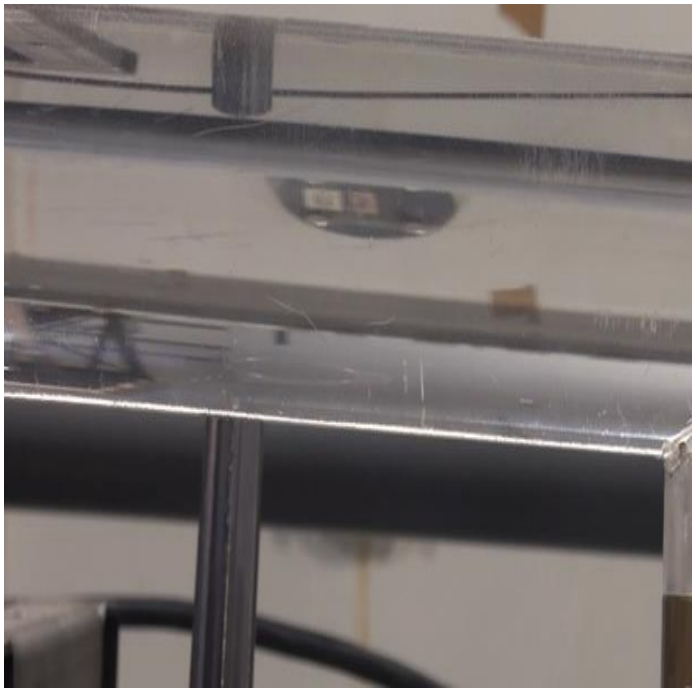

0.140 Moving bed

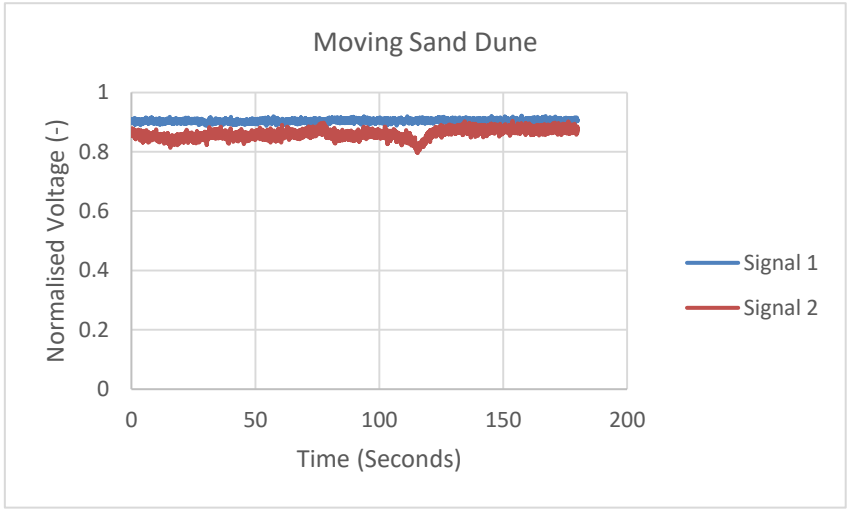

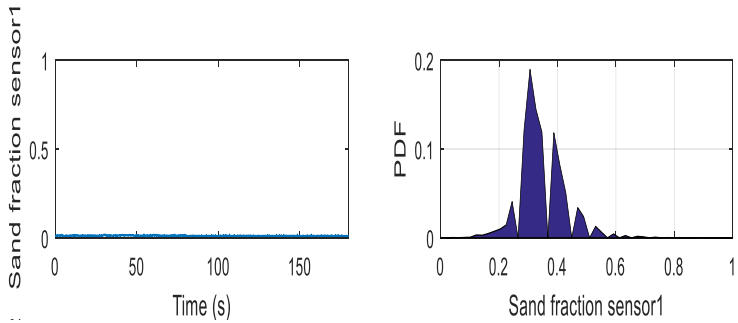

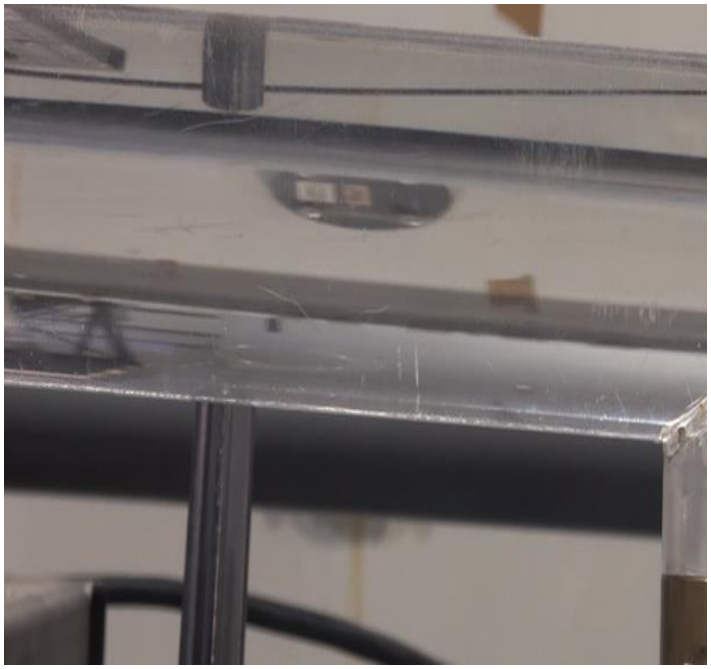

0.180

Saltation

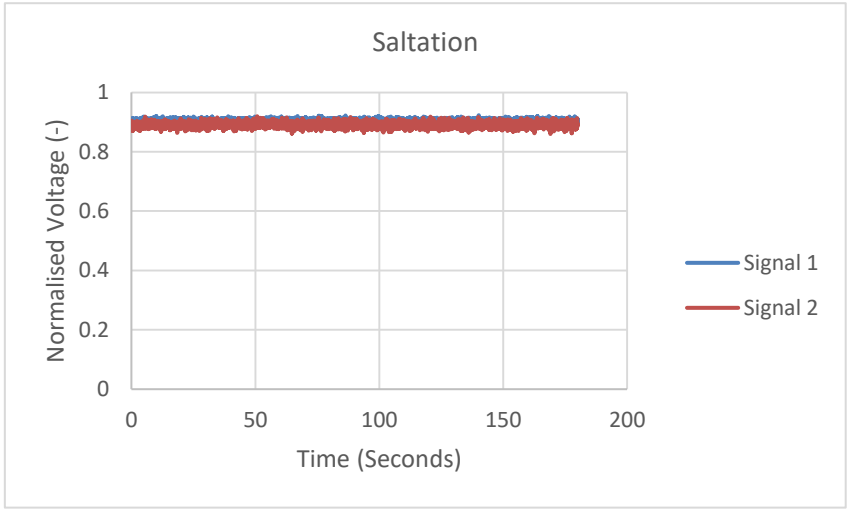

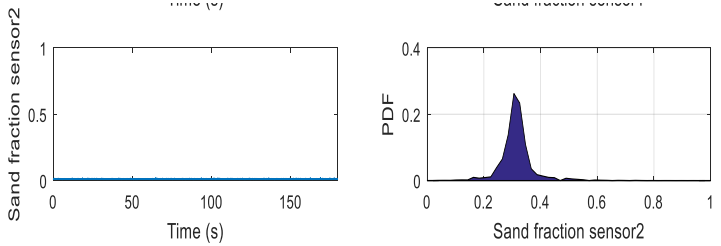

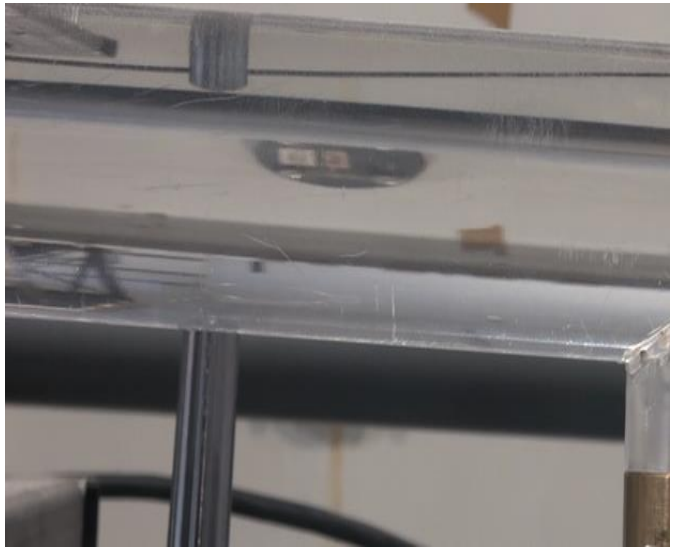

0.235 Suspension

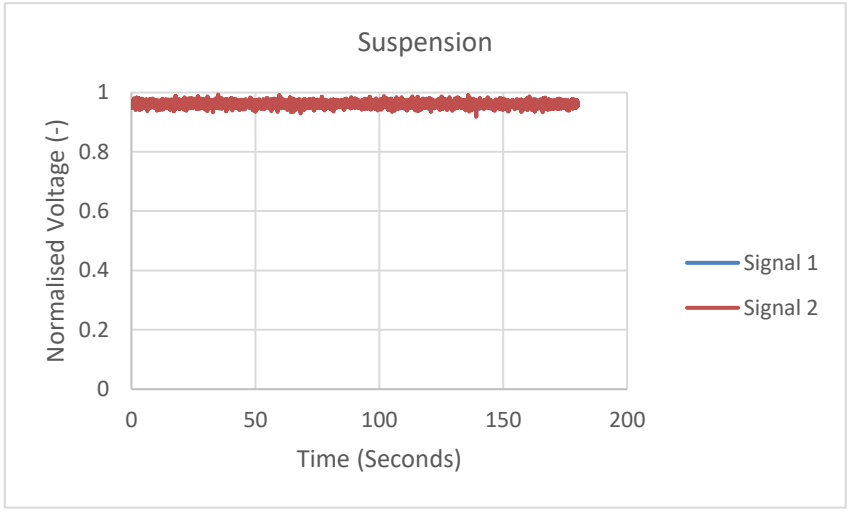

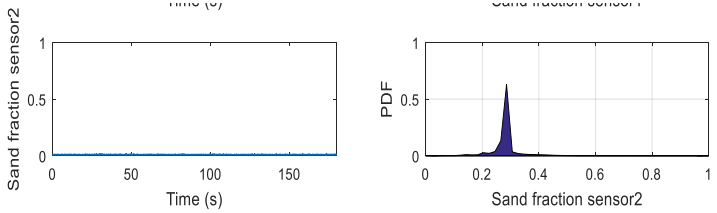

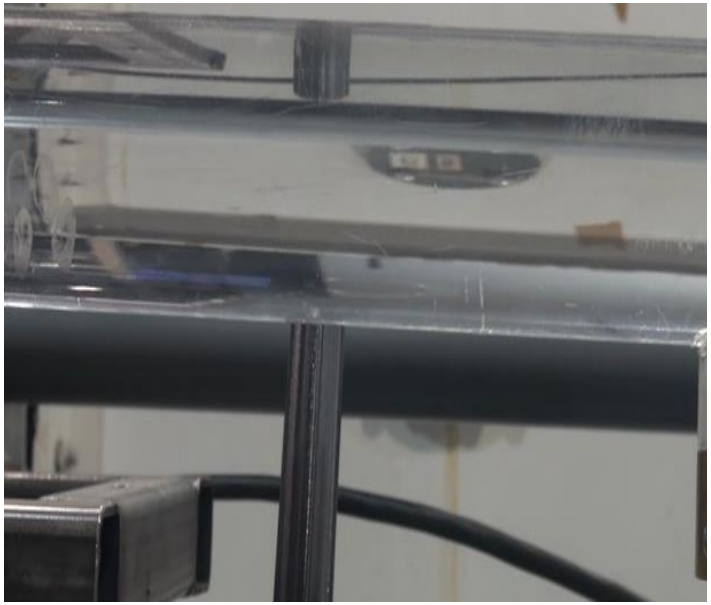

0.270

Suspension

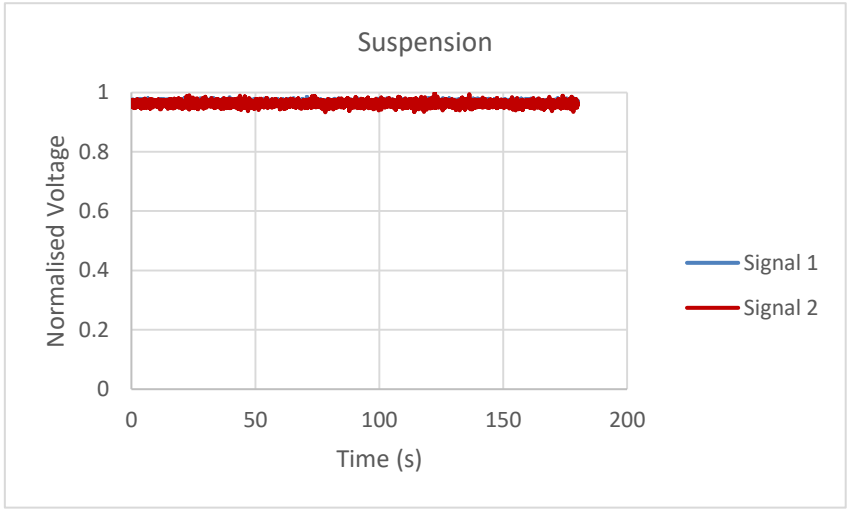

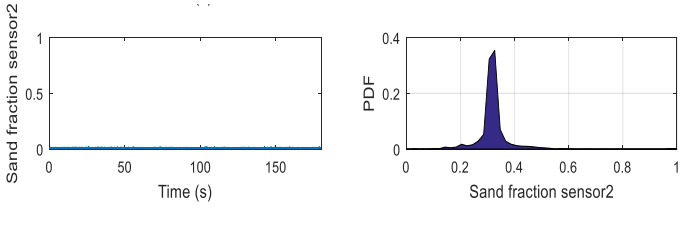

0.3 Suspension

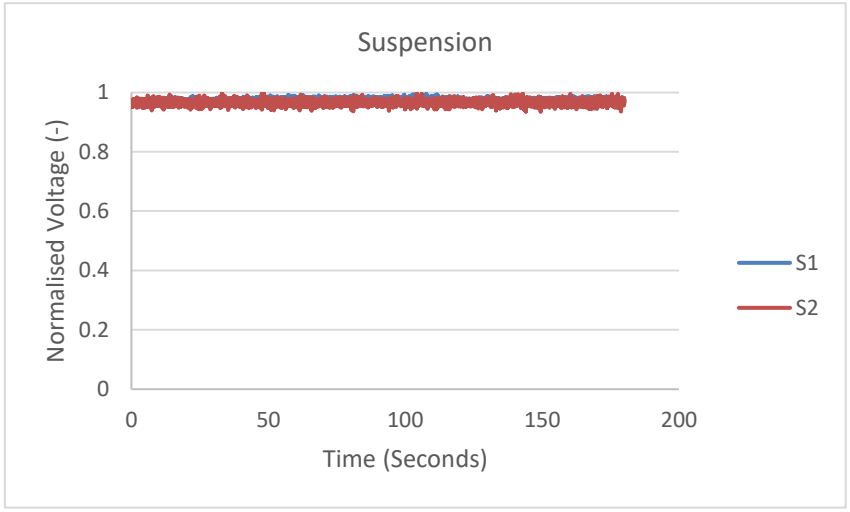

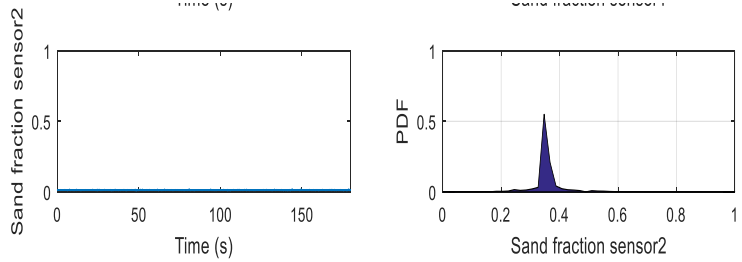

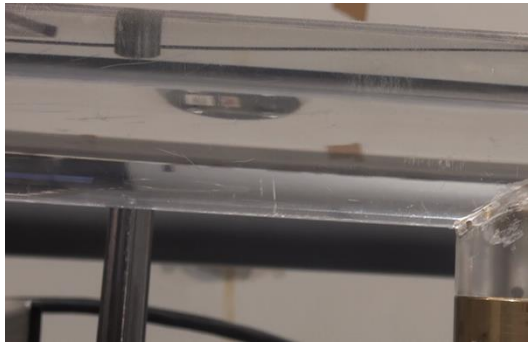

0.32 Suspension

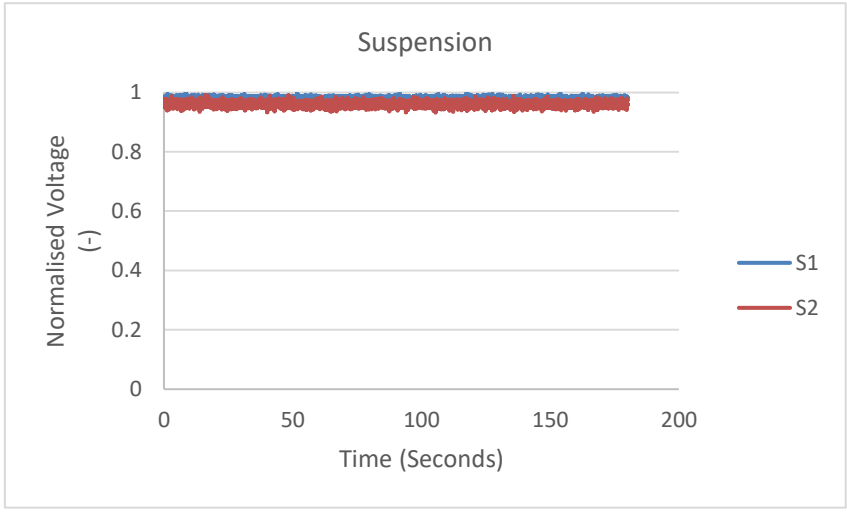

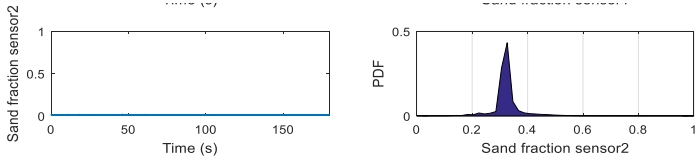

4.3.1.6 Effect of liquid superficial velocity

The effect of liquid superficial velocity on the sand fraction obtained from the sand sensor is described in Figures 4-28 below. The average sand fraction tends to decrease as the liquid superficial velocity is increased. This phenomenon suggests that the higher the water flow velocity, the less amount of sand settling or touching the pipe bottom. This trend for the same concentration, have a higher concentration of smaller sized particle than bigger sized particles at lower superficial velocity. While having a lower concentration of smaller sized particles than larger sized particles at higher water superficial velocity.

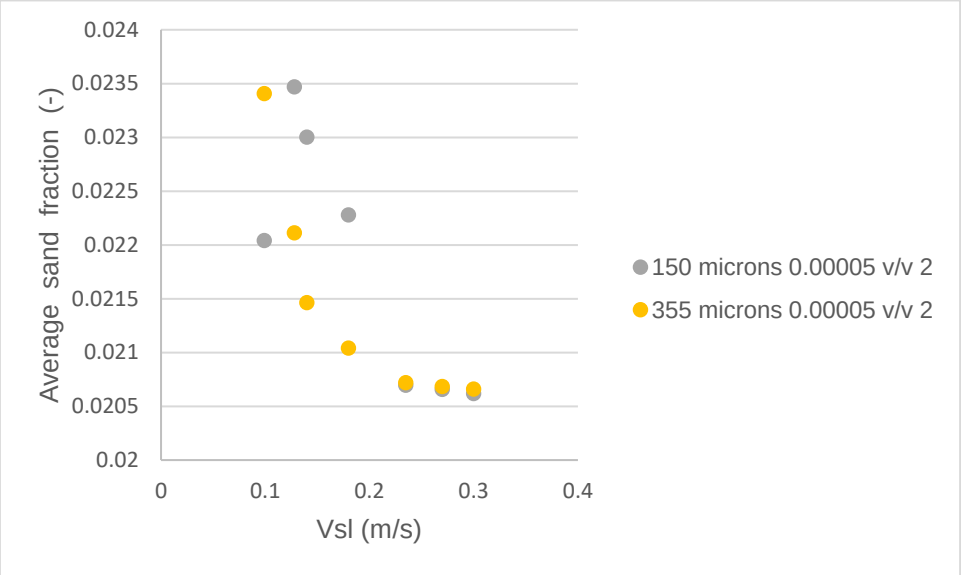

Figure 4-28 average sand fraction against Vsl for sensor

The average voltage tends to increase with increasing liquid superficial velocity. This is illustrated in Figure 4-29 below. This confirms that the voltage reading is affected by presence of sand particles. The higher the liquid superficial velocity, the less the sand fraction as mentioned above. The standard deviation of the voltage signal is given in the Appendix A.3.

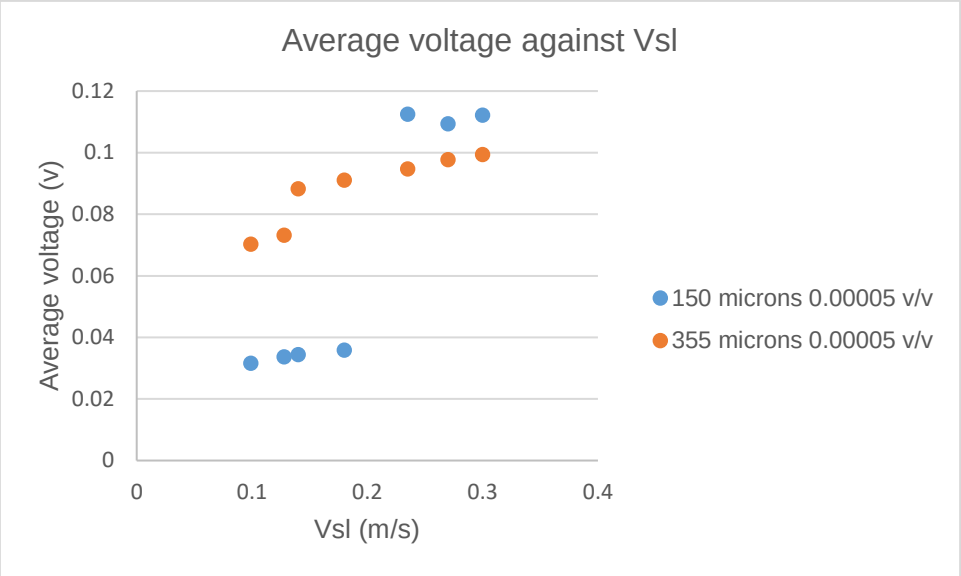

Figure 4-29 average voltage against Vsl for 150 and 350 microns 0.00005 v/v

4.3.1.7 Effect on pressure drop

The experiments have demonstrated that the pressure drop increased with the increase in the liquid superficial velocity. Figure 4-30 give the rise in pressure drop with increase in liquid superficial velocity for 150 microns 0.00005 v/v concentration whilst Figure 4-31 gives the same trend highlighting that pressure drop is much higher for the lighter 0.00005 v/v concentration than the heavier 0.0001 v/v concentration. Similarly Figure 4-32 indicate the trend of higher pressure drop for higher water superficial velocity for 355-micron particle size. It also highlights that the lower concentration of 0.00005 v/v has a slightly higher pressure drop than the higher 0.0001 and 0.0003 v/v concentrations. The comparison of the experimental and theoretical Blasius friction factor are given in Figures 4-33 and 4-34 for 150 and 355 microns respectively.

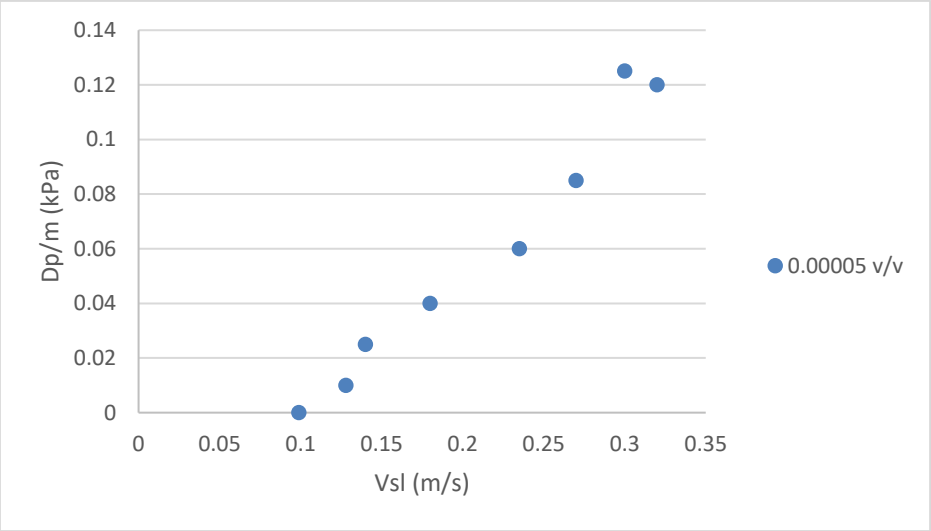

Figure 4-30 DP against Vsl for 150 microns 0.00005 v/v

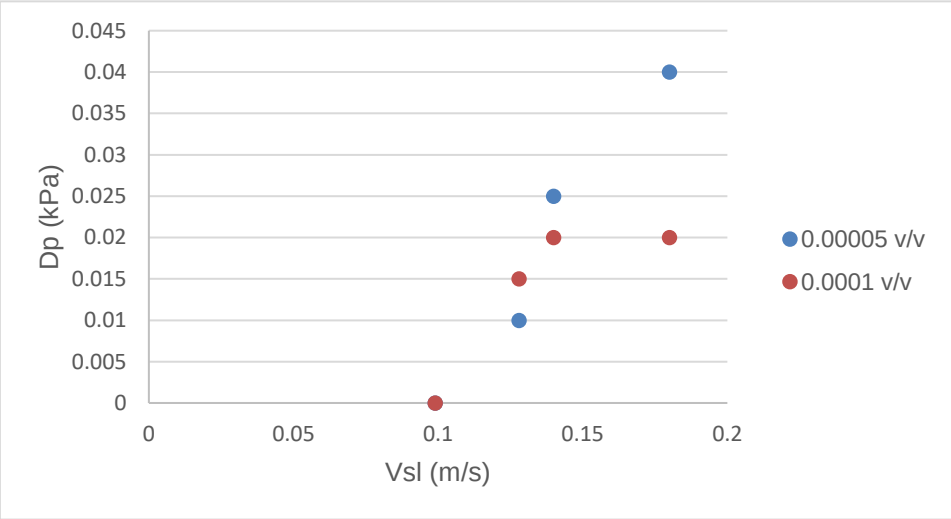

Figure 4-31 experimental pressure drop against Vsl for 150 microns 0.00005 and 0.0001 v/v concentration

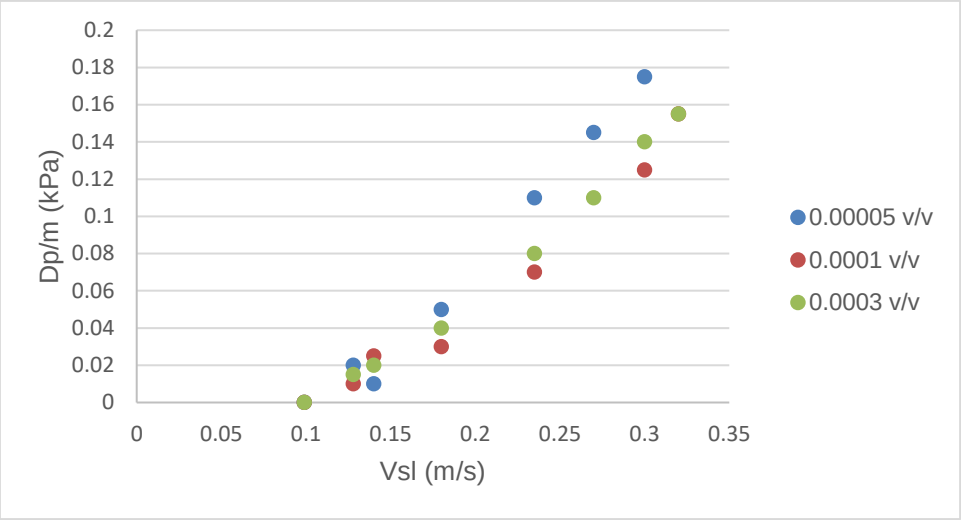

Figure 4-32 experimental pressure drop against Vsl for 355 microns and 0.00005, 0.0001 and 0.0003 v/v concentrations

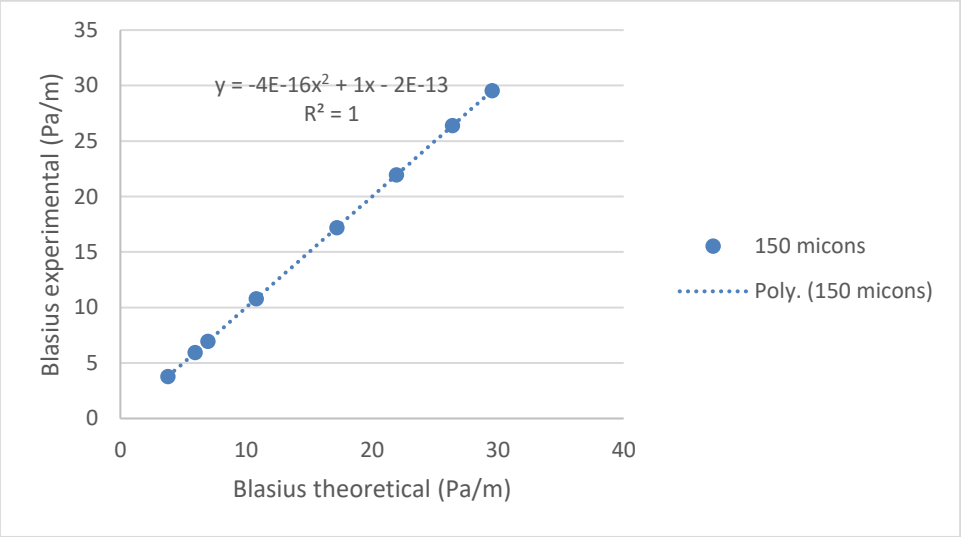

Figure 4-33 Blasius friction factor comparison for 150 microns

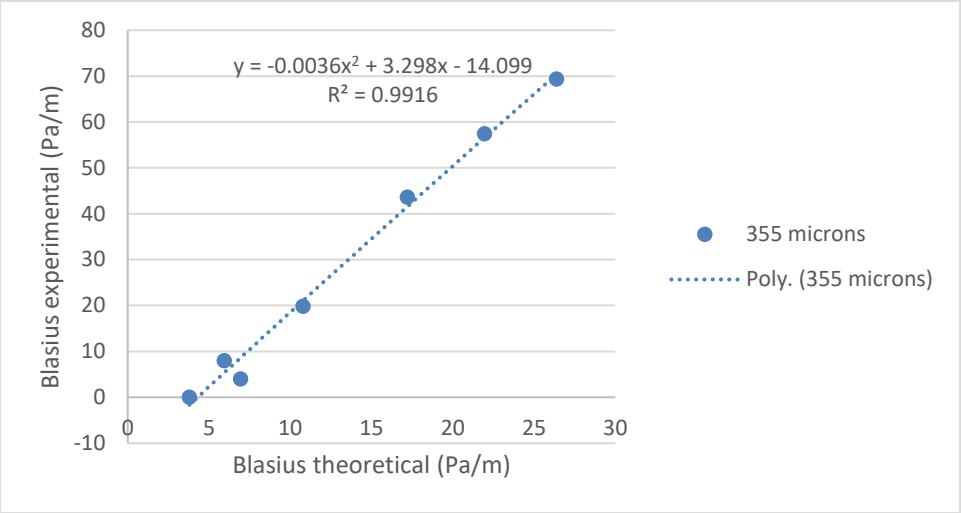

Figure 4-34 Blasius friction factor comparison for 355 microns

4.3.1.8 Sand structural velocity

Structural velocities were obtained from the two sand sensors. The sand structural velocities are given in Table 4-2 below. The coefficient of variation for the cross-correlation data is between 0.015-0.044. The relationship between the sand structural velocity and the liquid superficial velocity is given in Figure 4-35 below and it can be stated that the chaotic nature might be due to the turbulent nature of the sand particle flow.

Table 4-4 sand sensor structural velocity for 150 microns

Vsl	Sv
0.099	0.0018
0.128	0.0023
0.14	0.0139
0.18	0.1034
0.235	0.1037
0.27	0.023
0.3	0.1022

0.32 0.014

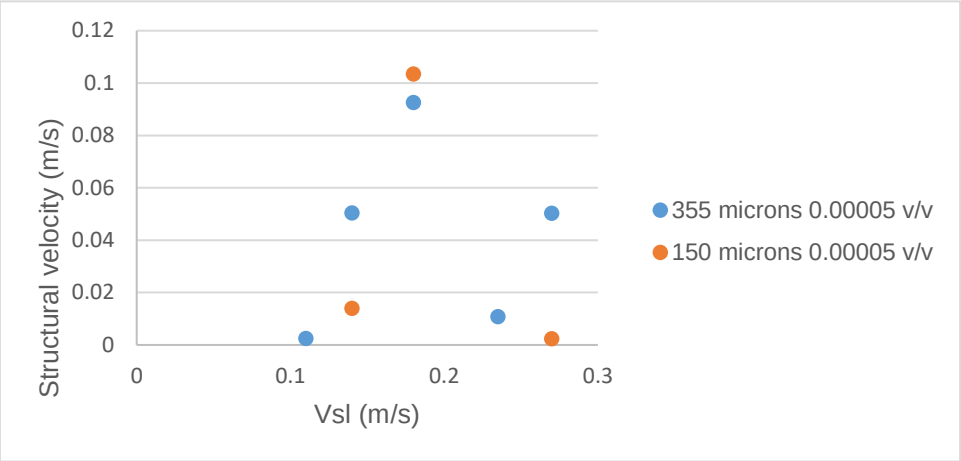

Figure 4-35 sand sensor structural velocity against liquid superficial velocity

4.3.2 Sand in air water pipe flow

There have been some previous studies to investigate liquid-solid and gas such as (Salama, 2000), (Stevenson et al., 2001), (Ladam et al., 2007), (Al-lababidi, Yan and Yeung, 2012) and (Najmi et al., 2015) however this study is the first to investigate the behaviour of dense phase in low concentrations using conductive sensors. Previous work mostly used visual observation. The flow regimes encountered are described in the proceeding section.

Table 4-5 sand in air water pipe experiment conditions

Particle	Nominal diameter (microns)	Density(Kg/m3)	Shape	Sand volume Fraction (v/v)	Vsg range (m/s)	Vsl (m/s)	MTC At Vsg (m/s)
sand	150	2650	irregular	0.00005	3 to 7	0.06	5
				0.0001			
				0.0003			

sand	355	2650		irregular	0.00005	3 to 7	0.06	5
					0.0001			
					0.0003			

4.3.2.1 Moving bed

At Vsl of 0.06m /s and Vsg of 3m /s, a sliding sand bed was observed with sensor response depicted in Figure 4-36 below. The response of the sand sensor indicates a wavy voltage output as the sand fraction undulates due to the height of the sliding sand bed. The pdf of the sand fraction obtained by the sand sensor as in Figure 4-37 highlights the presence of a sand bed that have perturbations as a result of sliding sand dunes, similarly the equivalent sand height varies as result of this behaviour. The frequency domain provides a peak signal at about 0.2Hz with sub peaks at 0.4Hz and 0.5Hz as given in Figure 4-38 below, this indicates that less energy required for flow of the sand particles. This flow regime is different to that of water sand described in the proceeding section in the sense that the presence of air makes the water air interface wavy and the resulting interaction and pressure fluctuations enable the sand particle motion. This happens even with a constant water superficial velocity as the air superficial velocity enable the transport of the sand particles. The bottom and side view of a sliding sand bed is illustrated in Figures 4-39 and 4-40 respectively below.

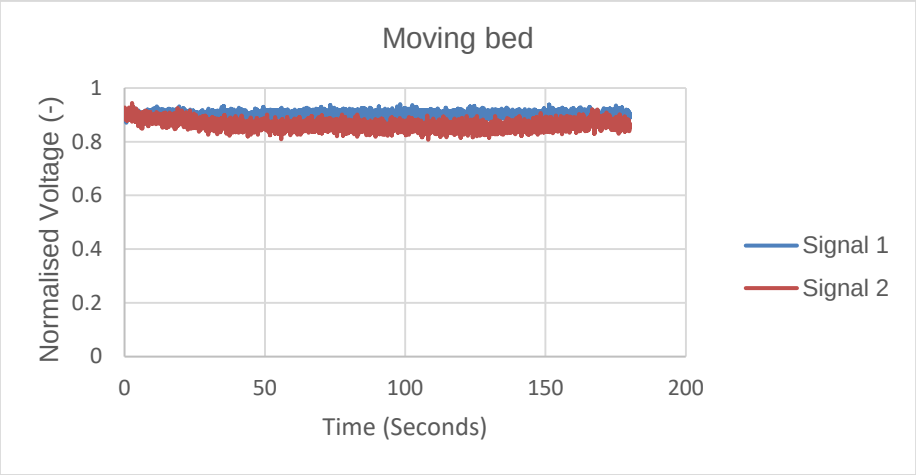

Figure 4-36 normalised voltage and pdf for moving bed at Vsl 0.06m/s Vsg 3m/s 0.00005 v/v

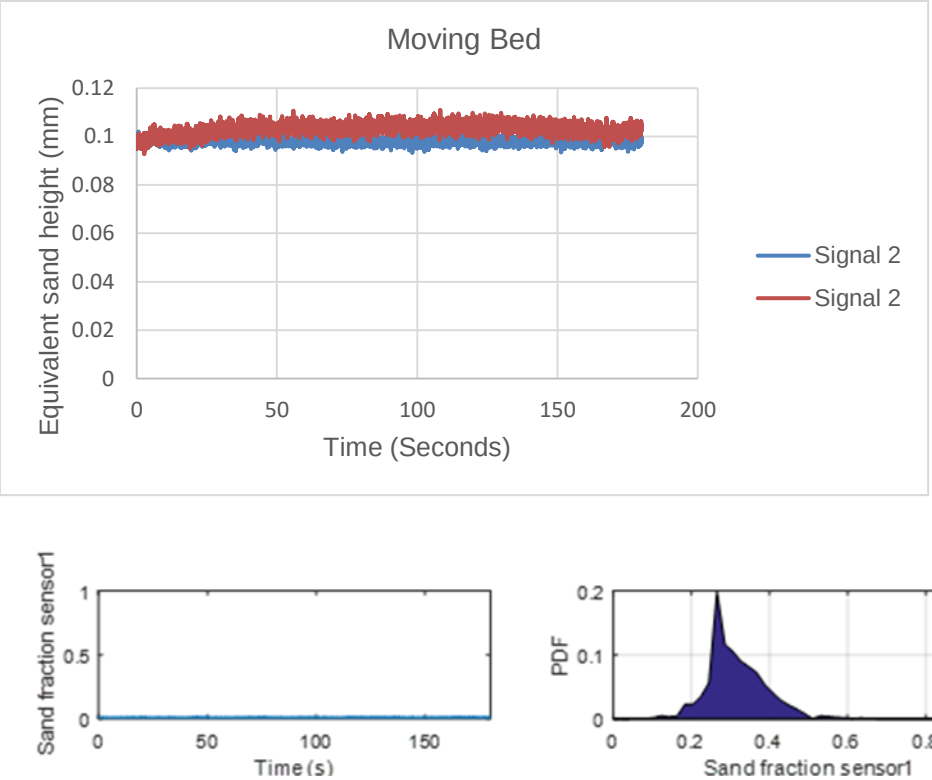

Figure 4-37 equivalent sand height and sand fraction for moving bed at Vsl 0.06m/s Vsg 3m/s 0.00005 v/v

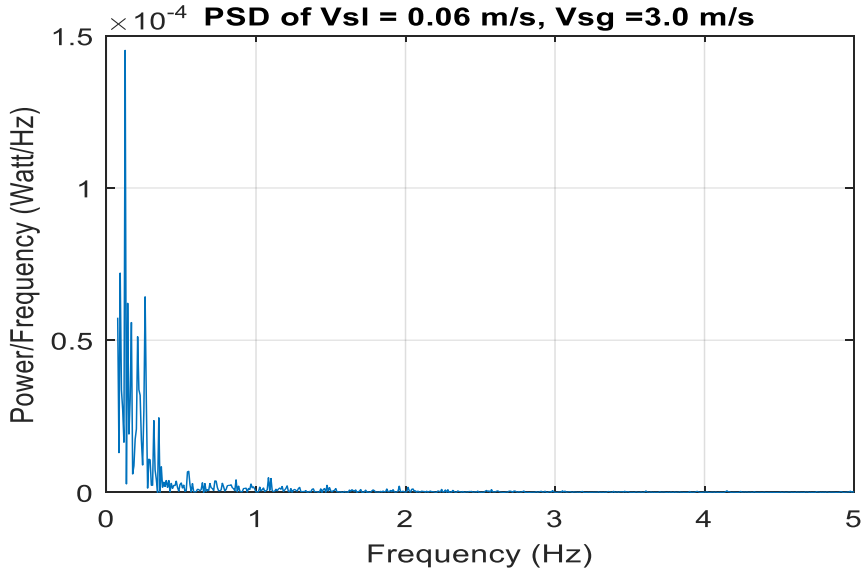

Figure 4-38 PSD for moving bed at Vsl 0.06m/s Vsg 3m/s 0.00005 v/v

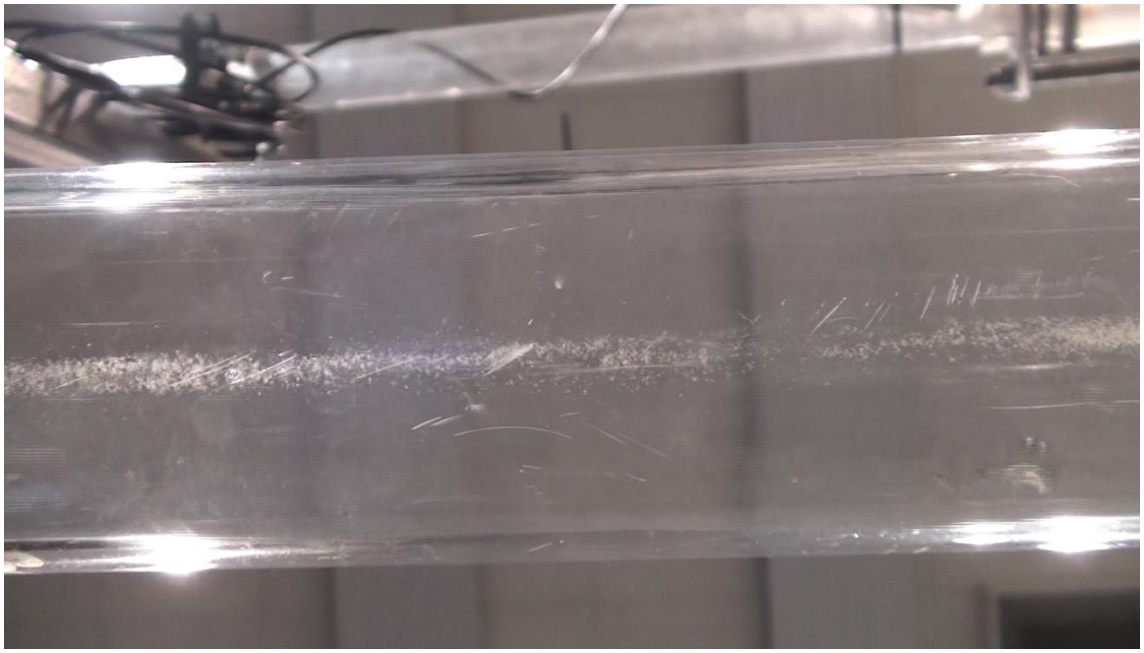

Figure 4-39 moving bed Vsl 0.06m/s Vsg 3m/s 0.00005 v/v

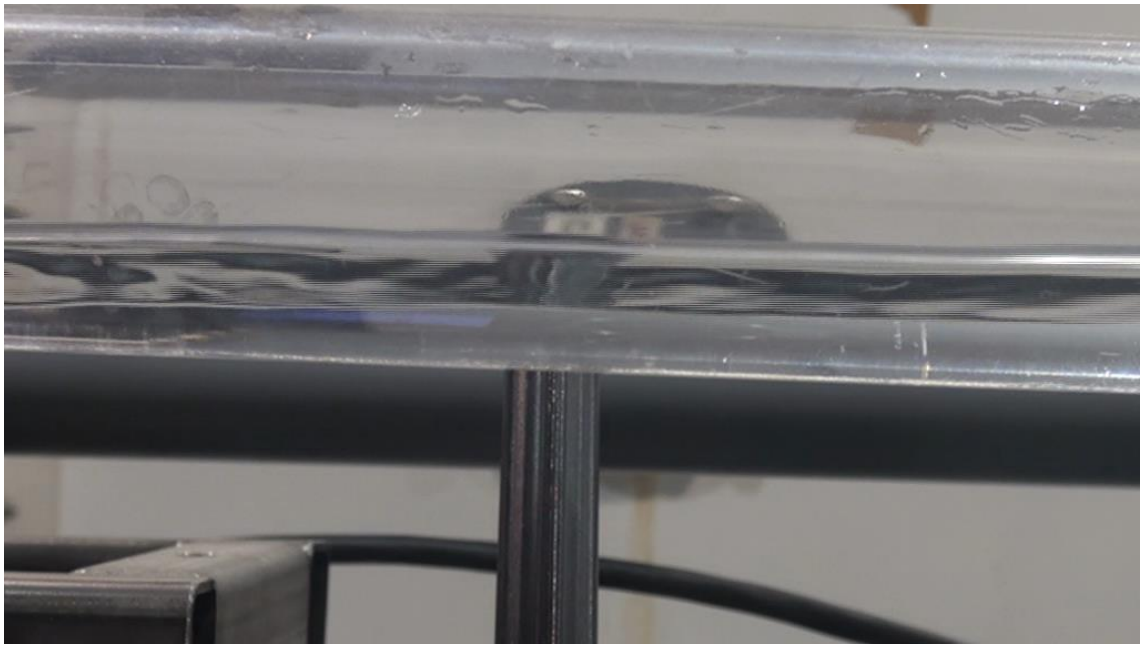

Figure 4-40 side view moving bed Vsl 0.06m/s Vsg 3m/s 0.00005 v/v

4.3.2.2 Saltation

The sand sensor response under the saltation flow regime at Vsl 0.06 m/s and Vsg 4 m/s are given in Figures 4-41 and 4-42 below in the form of normalised voltage, equivalent sand height, sand fraction and pdf. The normalised voltage signal has peak and smaller multiple peaks that could be explained by the moving sand particles covering the sensor and uncovering the sensor as they saltate there is a distinct difference in the sensor response as compared with water sand flow. This could be as a result of increase in the turbulence at the water air interface as the gas superficial velocity is increased. Similarly, from Figure 4-43 the frequency have a peak 0.1Hz and smaller multiple peaks at 0.3Hz and 0.4Hz indicating a slight increase in the energy for the flow in moving the sand particles as compared with a sliding bed. The saltation bottom and side view for sand water-air flow is highlighted in Figures 4-44 and 4-45 respectively below.

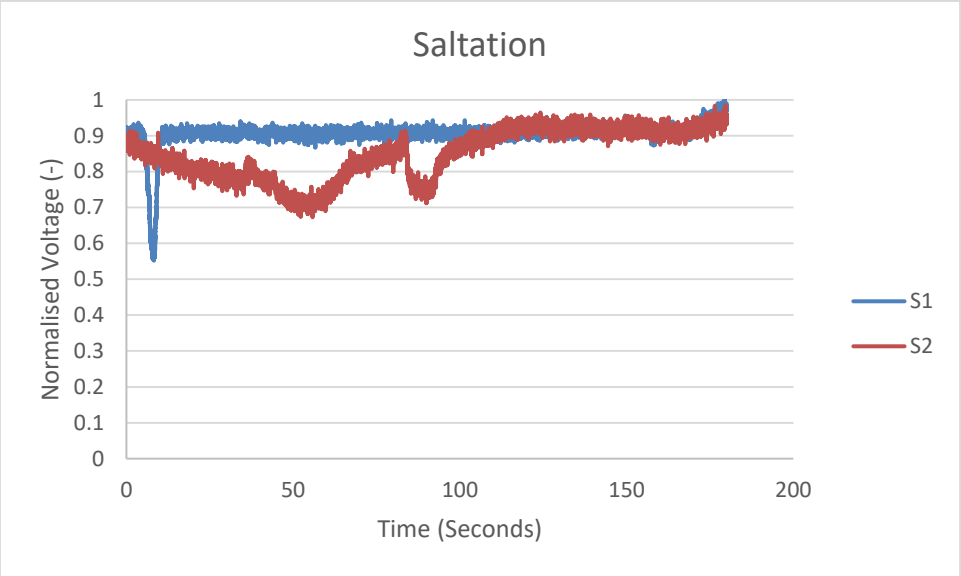

Figure 4-41 normalised voltage for saltation at Vsl 0.06m/s Vsg 4m/s 150 microns 0.00005 v/v

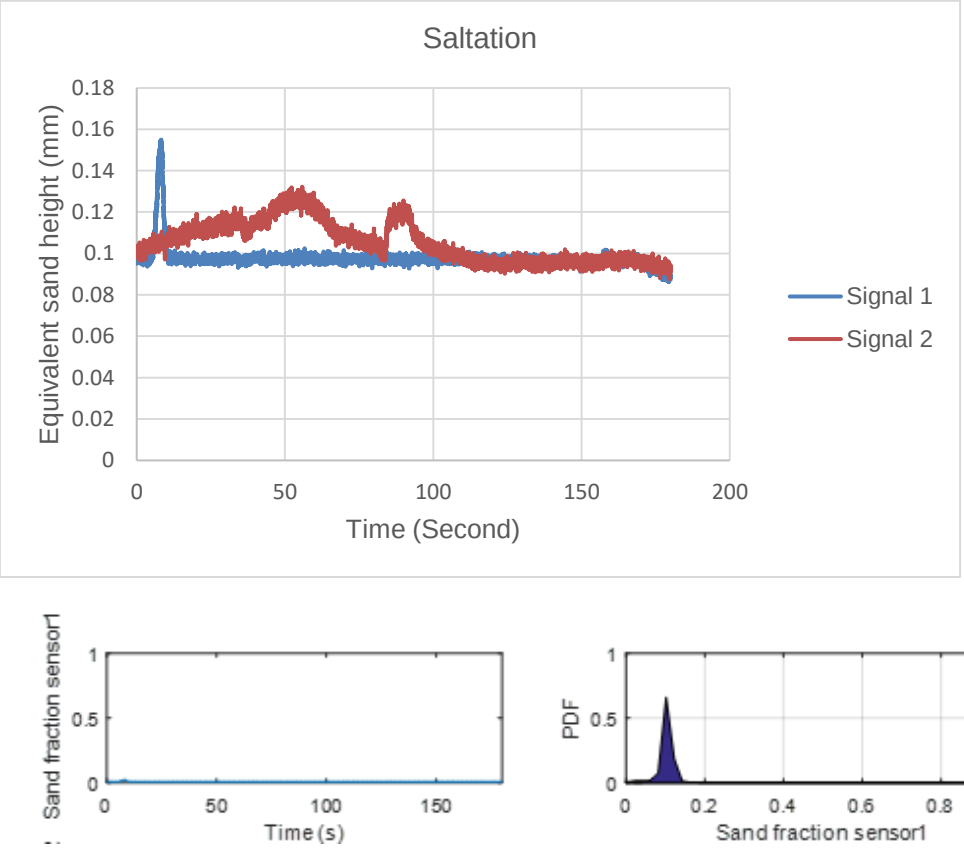

Figure 4-42 equivalent sand height and sand fraction for saltation at Vsl 0.06m/s Vsg 4m/s 150 microns 0.00005 v/v

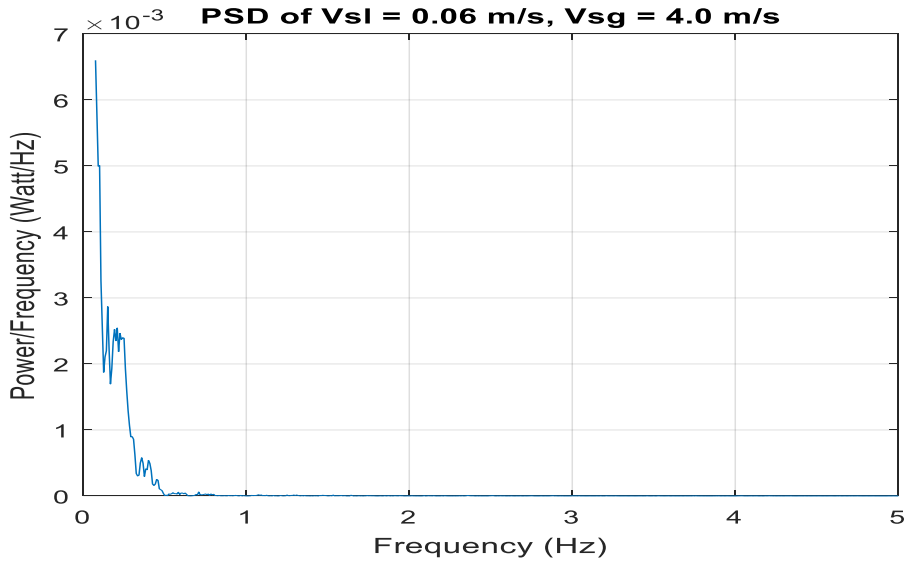

Figure 4-43 PSD for V saltation at Vsl 0.06m/s Vsg 4m/s 150 microns 0.00005 v/v

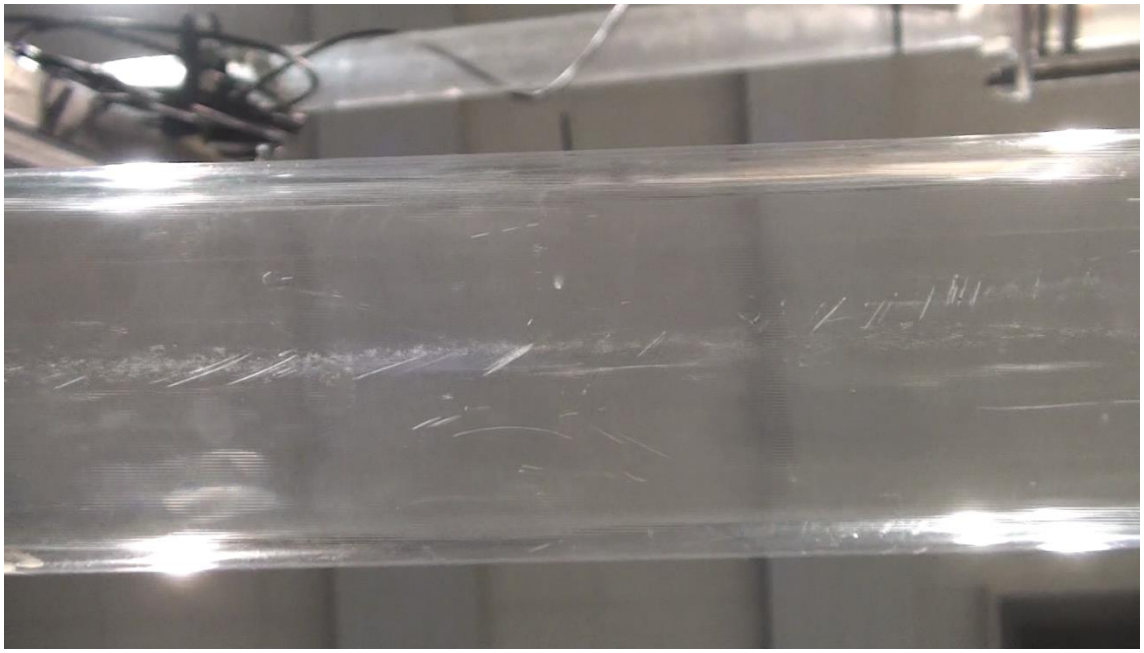

Figure 4-44 bottom view for saltation at Vsl 0.06m/s Vsg 4m/s 150 microns 0.00005 v/v

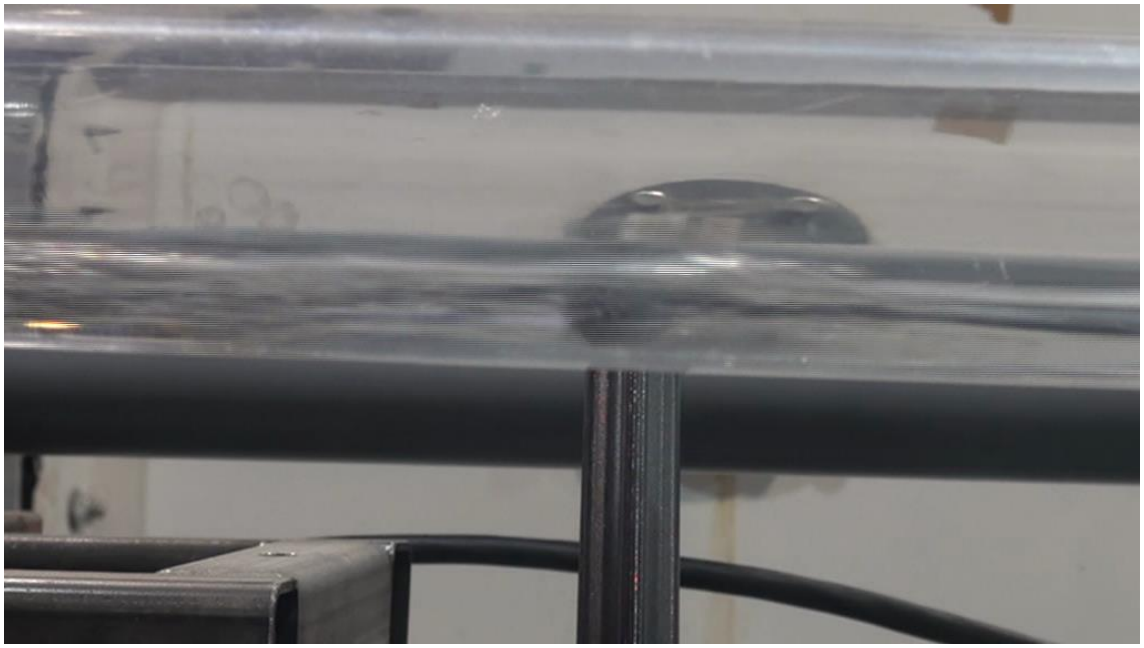

Figure 4-45 side view for saltation at Vsl 0.06m/s Vsg 4m/s 150 microns 0.00005 v/v

4.3.2.3 Streak

The flow regime at Vsl 0.06m/s and Vsg 0.5 m/s which is described as the sand flow mtc is a suspension/streak. The sand sensor response is given in in Figures 4-46 and 4-47 for normalised voltage, equivalent sand height and sand fraction with pdf. The normalised voltage output highlight multiple spike peaks that indicate sudden intermittent covering of the sand sensor by the sand particles. Similarly, the frequency as seen in Figure 4-48 below indicate disturbances peaking at 0.8Hz with sub peaks from 0.2Hz to 3.6Hz implying higher energy required for sand particle flow. Figure 4-49 and 4-50 illustrates the suspension/streak flow regime.

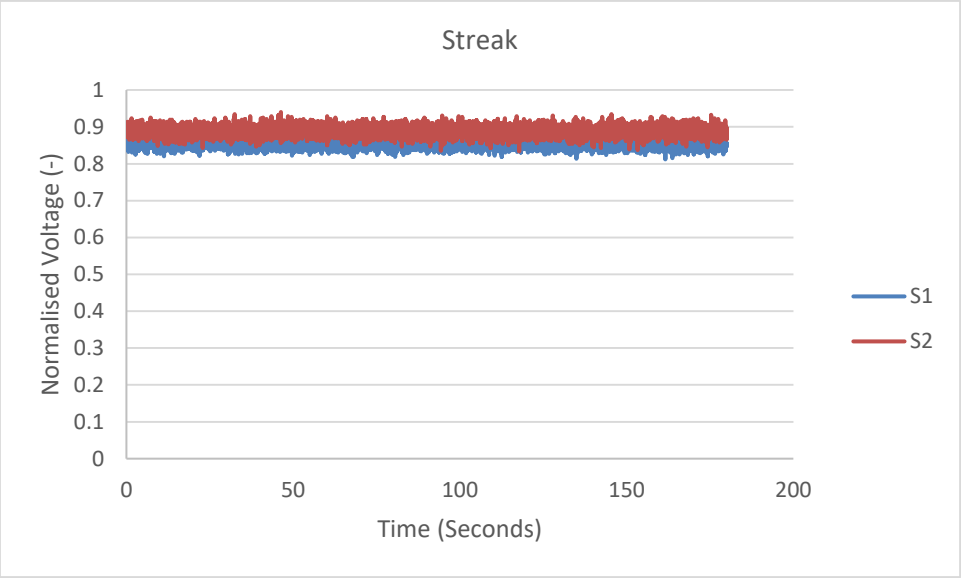

Figure 4-46 normalised voltage for streak at Vsl 0.06m/s Vsg 5m/s 150 microns 0.00005 v/v

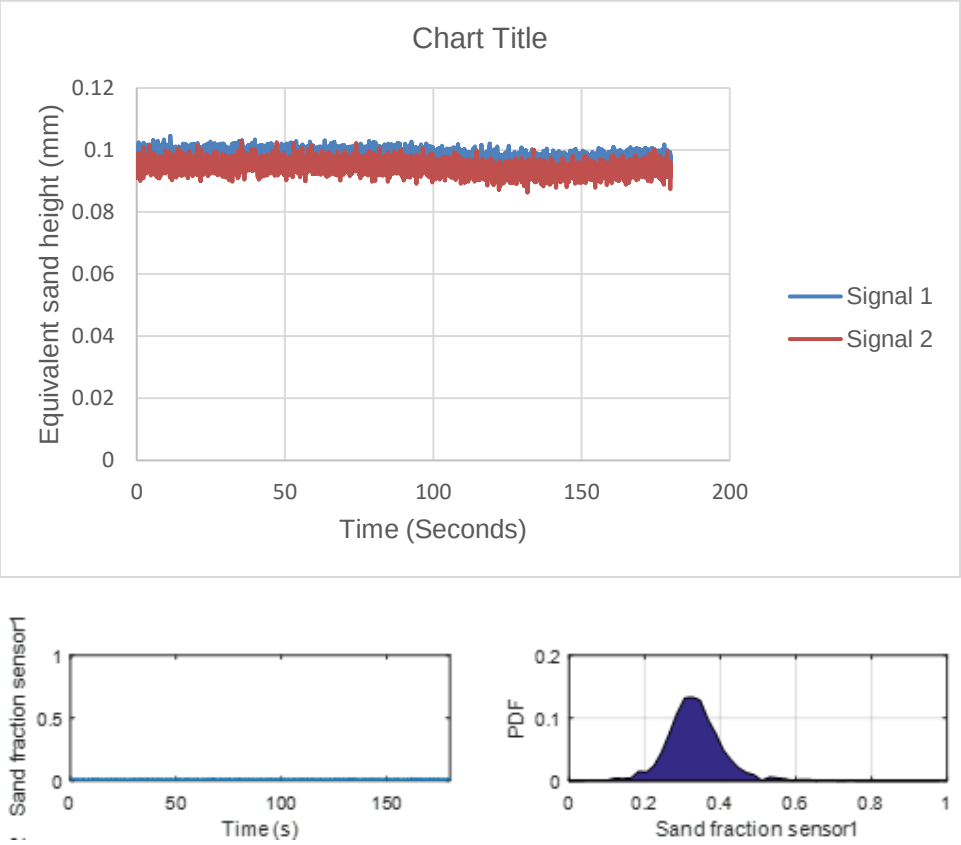

Figure 4-47 equivalent sand height and sand fraction for streak at Vsl 0.06m/s Vsg 5m/s 150 microns 0.00005 v/v

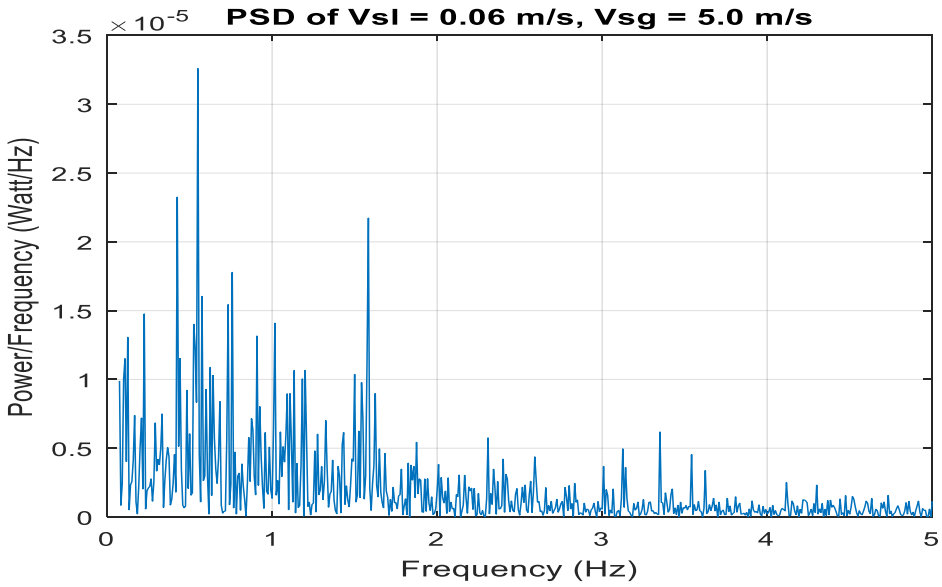

Figure 4-48 PSD and amplitude for streak at Vsl 0.06m/s Vsg 5m/s 150 microns 0.00005 v/v

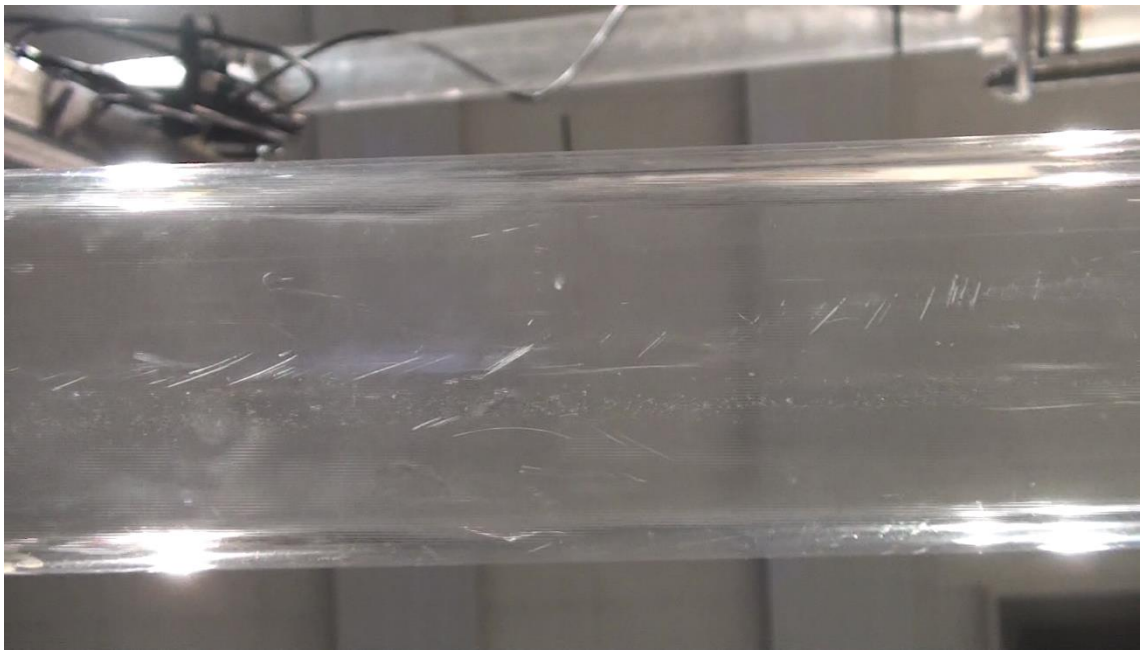

Figure 4-49 bottom view for streak at Vsl 0.06m/s Vsg 5m/s 150 microns 0.00005 v/v

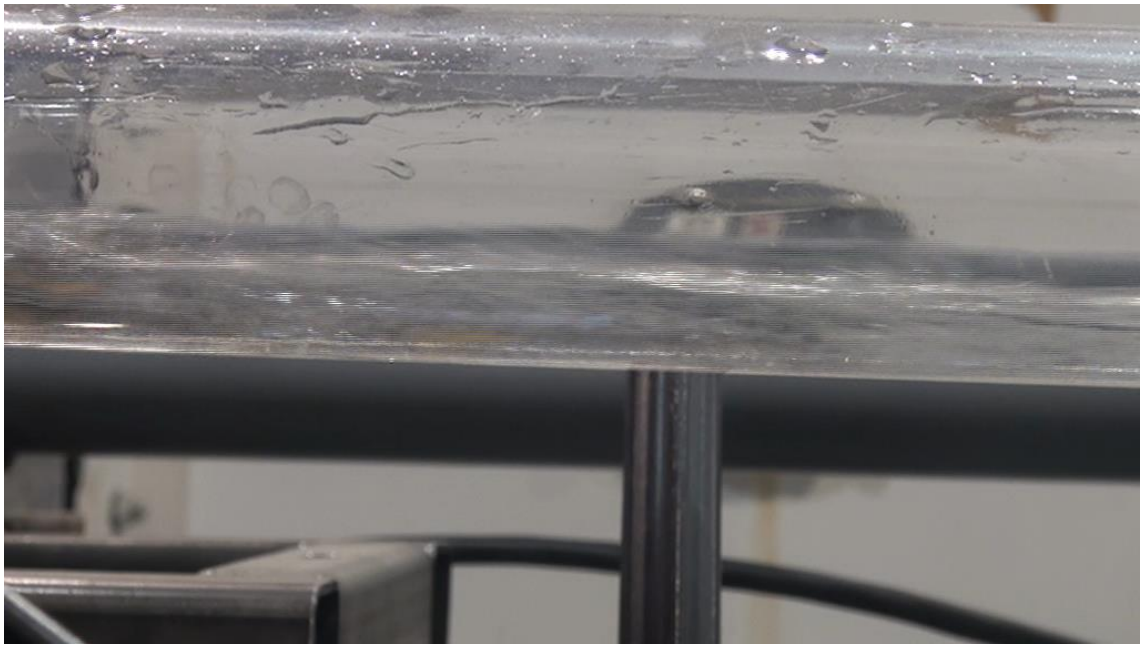

Figure 4-50 side view for streak at Vsl 0.06m/s Vsg 5m/s 150 microns 0.00005 v/v

4.3.2.4 Suspension

The flow regime at Vsl 0.06m/s and Vsg 0.7 m/s can be described as a suspension. This flow regime was identified by the sensor response as highlighted in Figures 4-51 and 4-52 for normalised voltage, equivalent sand height, sand fraction with pdf. The normalised voltage indicate a value close to unity with perturbations that indicate to denote occasional covering of the sand sensor by the sand particles. Similarly, the frequency as seen in Figure 4-53 below indicate multiple peaks between 1Hz and 5Hz peaking at 2Hz implying a higher energy to sustain the sand particles in suspension. Figures 4-54 and 4-55 illustrate the respective bottom and side views of the saltation flow regime.

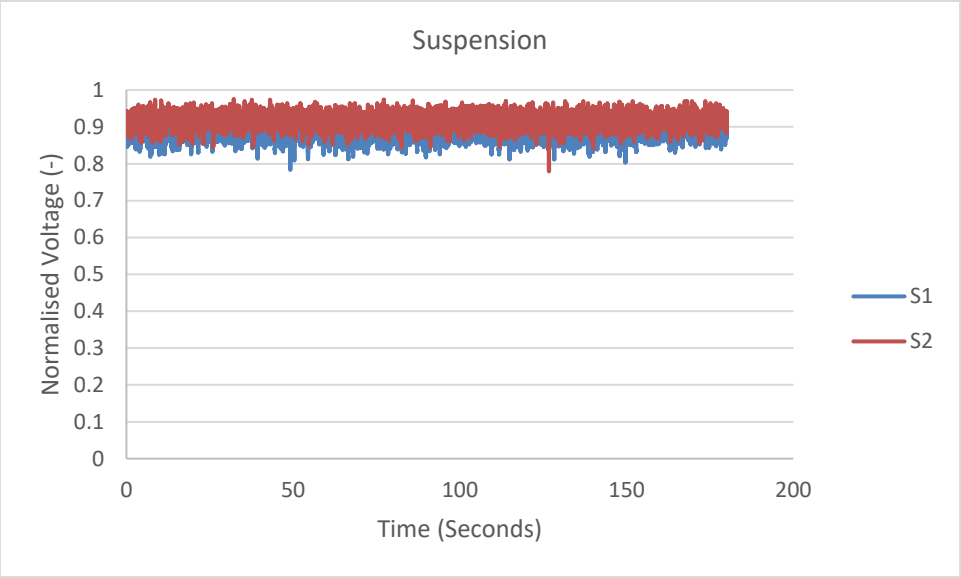

Figure 4-51 normalised voltage for suspension at Vsl 0.06m/s Vsg 7m/s 150 microns 0.00005 v/v

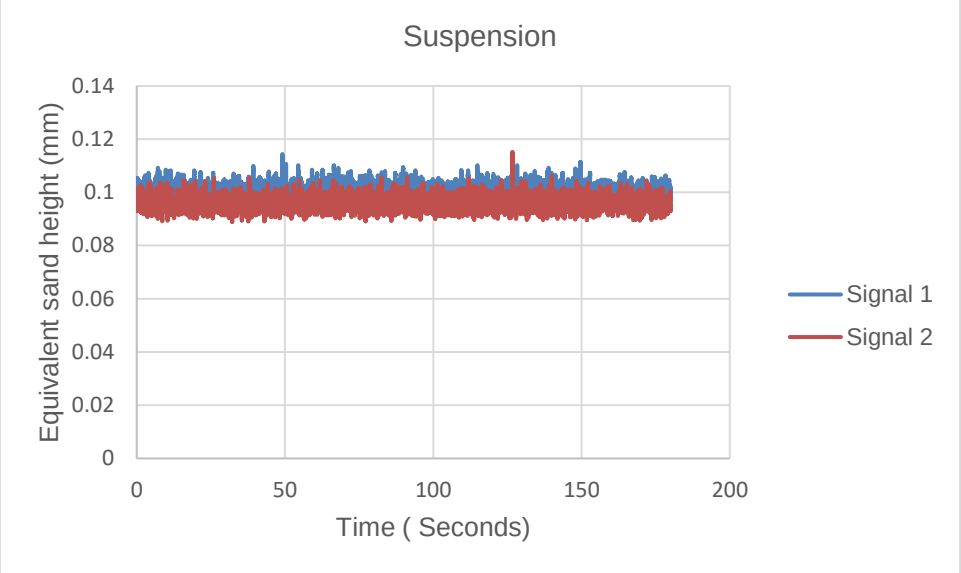

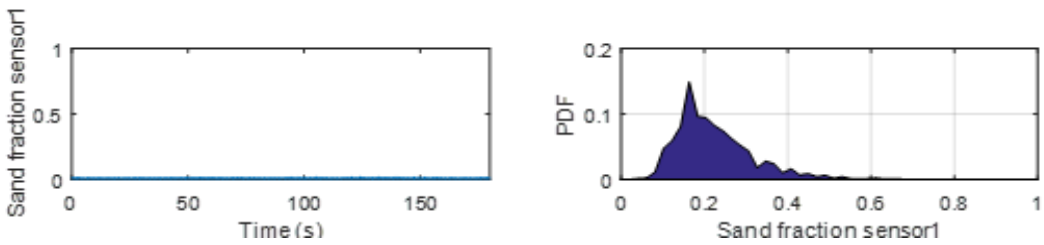

Figure 4-52 equivalent sand height and sand fraction for suspension at Vsl 0.06m/s Vsg 7m/s 150 microns 0.00005 v/v

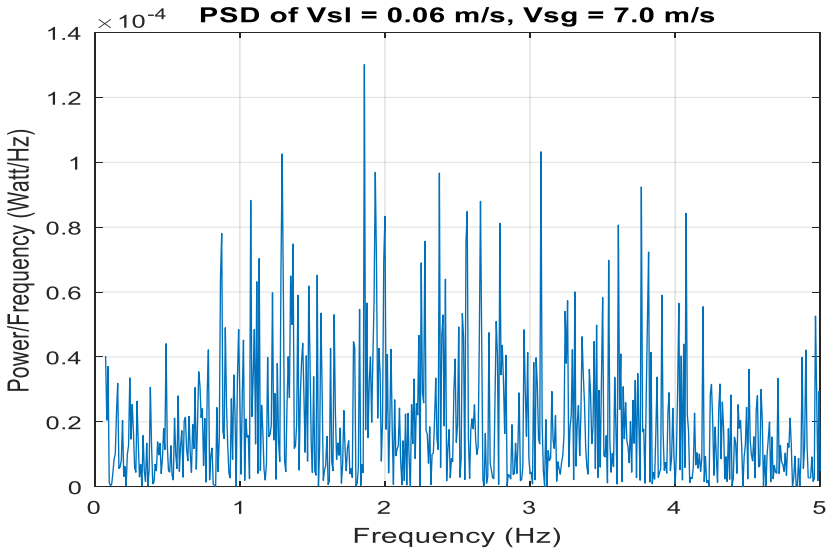

Figure 4-53 PSD for suspension at Vsl 0.06m/s Vsg 7m/s 150 microns 0.00005 v/v

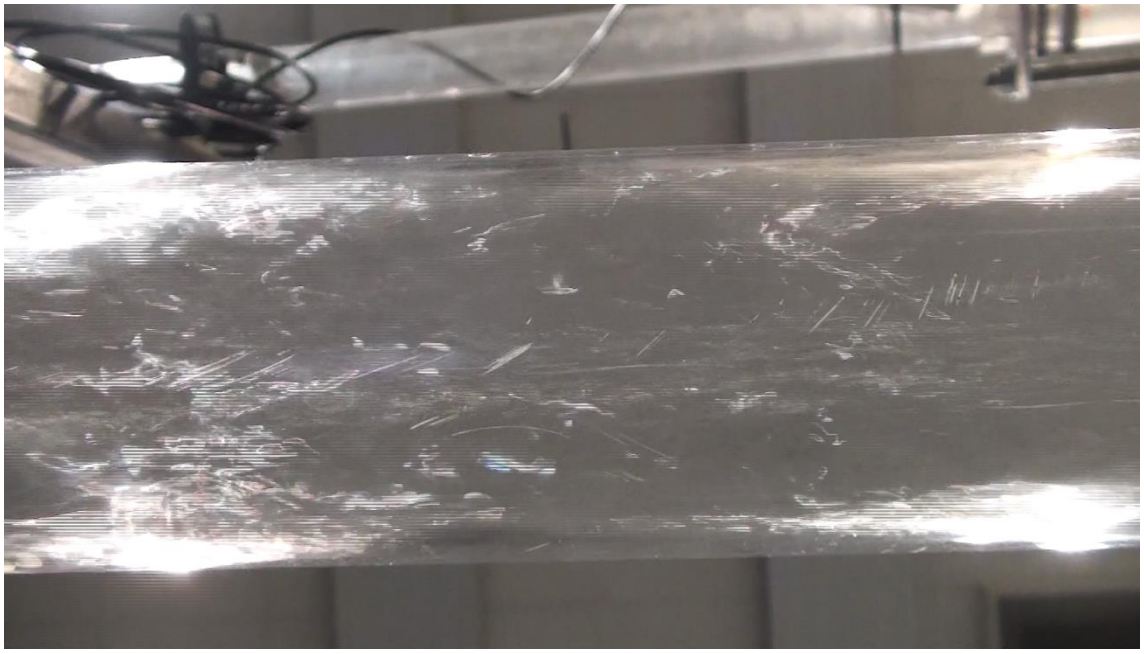

Figure 4-54 bottom view for suspension at Vsl 0.06m/s Vsg 7m/s 150 microns 0.00005 v/v

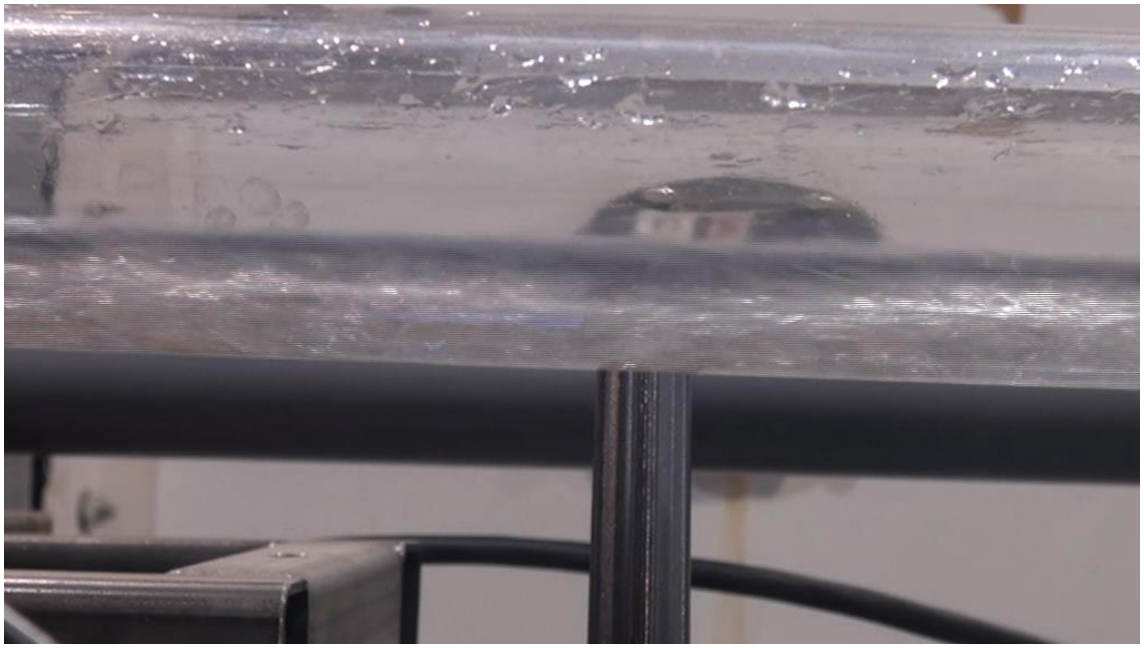

Figure 4-55 side view for suspension at Vsl 0.06m/s Vsg 7m/s 150 microns 0.00005 v/v

4.3.2.5 Comparisons

The Figure 4-56 given below show the current study flow map as compared with the Taitel and Duckler air water flow regime map. It was derived from visual observation and sensor output. The air water boundary transitioned from a stratified smooth at Vsg of 3 m/s to a stratified wavy flow regime from Vsg of 4.4 m/s to 7 m/s. The current study has been conducted mostly within the stratified wavy flow regime boundary. Figure 4-57 compares the study with various predictions by previous studies. It indicates that the current study mtc of Vsg 5 m/s has been over predicted by (Danielson and Co, 2007), Angelson and (Stevenson et al., 2001) though it has been under predicted by the (Salama, 2000) sand water and air flow models.

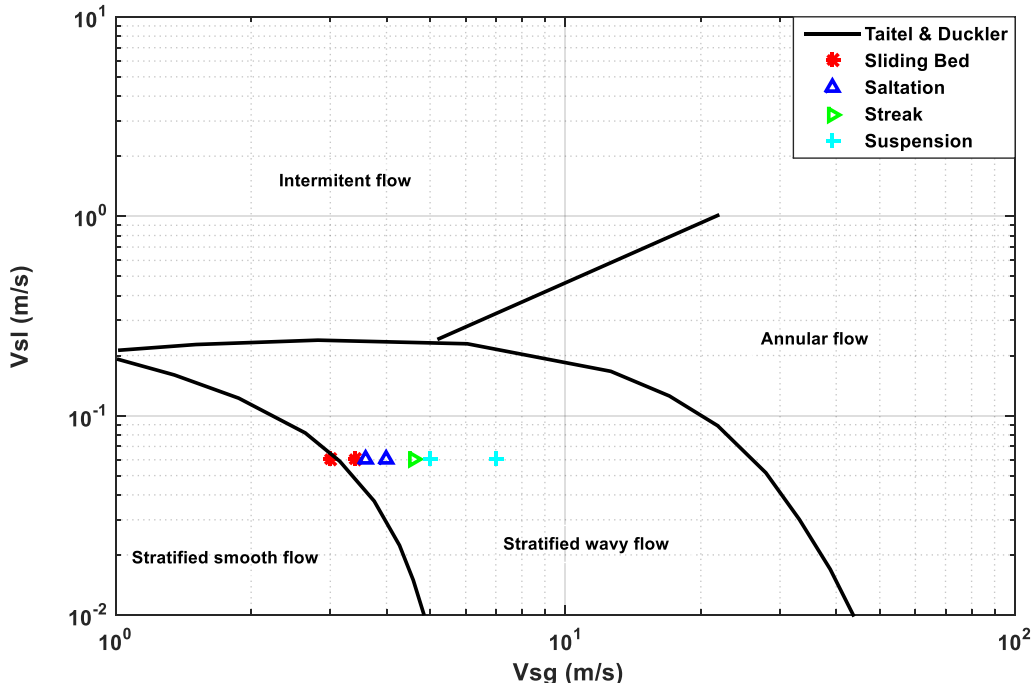

Figure 4-56 sand water air experiment with Taitel and Duckler flow regime map

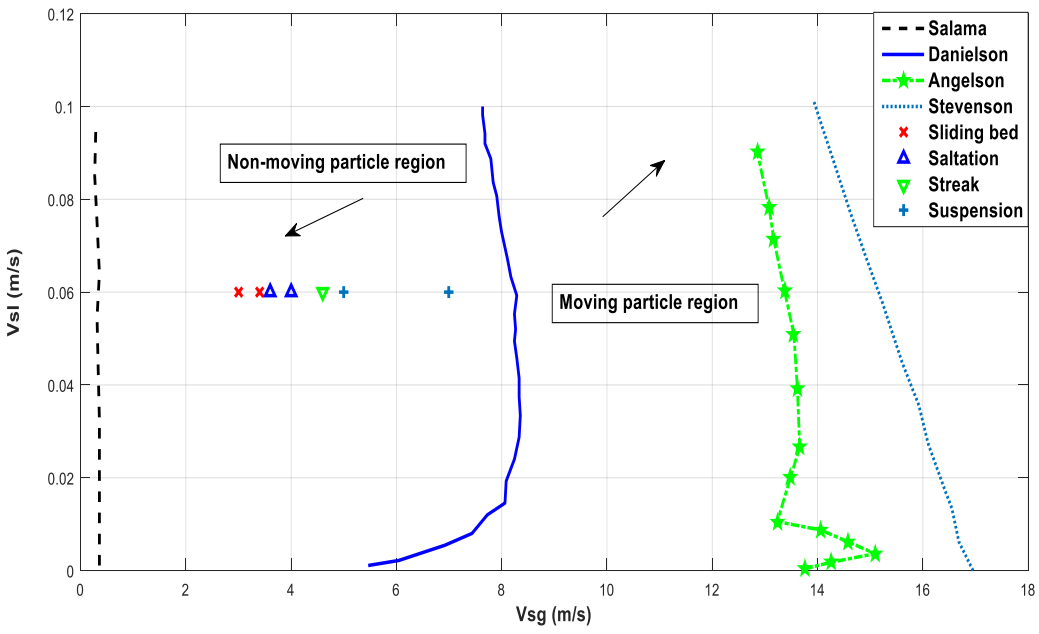

Figure 4-57 current experiment compared with prediction models

The sand fraction obtained from the sand sensor in the sand, air water flow at Vsg of 7 m/s is higher for higher concentration of 0.00001 and 0.0003 v/v than for the lower concentration of 0.00005 v/v as observed in Figure 4-58. This is because of the higher concentrations being more dispersed in the pipe system as compared with low sand concentrations.

The experimental pressure drop also tends to increase with increasing gas superficial velocity which is similar to sand water flow though for sand water and air flow there is much more uncertainty due to turbulence. The Figure 4-59 give the experimental pressure drop against gas superficial velocity for 150 microns 0.00005, 0.0001 and 0.0003 concentrations respectively.

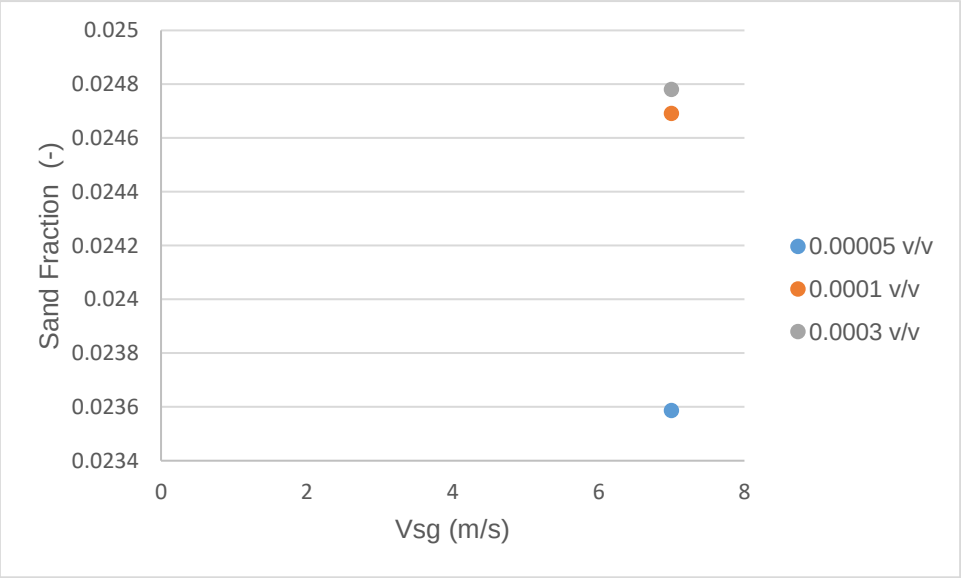

Figure 4-58 sand fraction against Vsg for 150 microns 0.00005, 0.0001 and 0.0003 v/v concentrations

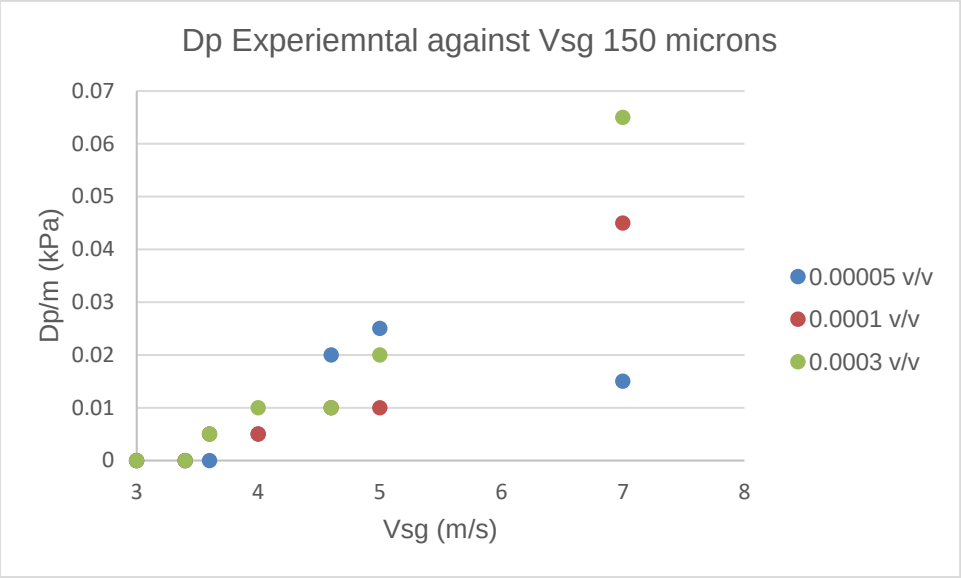

Figure 4-59 experimental DP against Vsg for 150 microns 0.00005, 0.0001 and 0.0003v/v concentrations

Structural velocity

Structural velocities were obtained from the two sand sensors and two conductivity pairs. The sand structural velocities, water translational velocities, holdup from the conductivity ring sensors and calculated actual velocities are given in Table 4-4 below.

Table 4-6 sand water air experiment data

150 microns 0.00005 v/v					
Vsl	Vsg	Sand sensor structural velocity	Water translational velocity	Holdup	Actual water velocity (vsl/holdup)
0.06	3	0.0013	1.3125	0.18	0.333333
0.06	3.4	0.0015	1.2727	0.3	0.2
0.06	3.6	0.0098	1.2353	0.03	2
0.06	3.8	0.0023	1.2353	0.23	0.26087

0.06	4	0.0048	1.2	0.21	0.285714
0.06	4.2	0.0045	1.2727	0.11	0.545455
0.06	4.4	0.0059	1.3125	0.19	0.315789
0.06	4.6	0.0193	1.3548	0.05	1.2
0.06	4.8	0.0047	1.4483	0.04	1.5
0.06	5	0.0249	1.5556	0.02	3
0.06	5.2	0.0509	1.68	0.02	3
0.06	5.4	0.7241	1.75	0.02	3
0.06	6.4	0.7778	1.9091	0.02	3
0.06	6.5	0.7925	1.9091	0.02	3
0.06	7	0.84	2	0.03	2

The structural velocities in form of sand structural velocity and water translational velocity for 150 microns 0.00005 v/v concentration are highlighted in Figure 4-60 below. The trend indicates increase for both the sand structural velocity and water translation velocity with an increase in the gas superficial velocity. There is a slight jump at the mtc of 0.5m/s considered for this study. The figure 4-61 highlight water translational velocity for 355 microns for 0.00005, 0.0001 and 0.0003 v/v concentrations. The trend indicates an increase with increase in gas superficial velocity but there is little difference because of different concentrations.

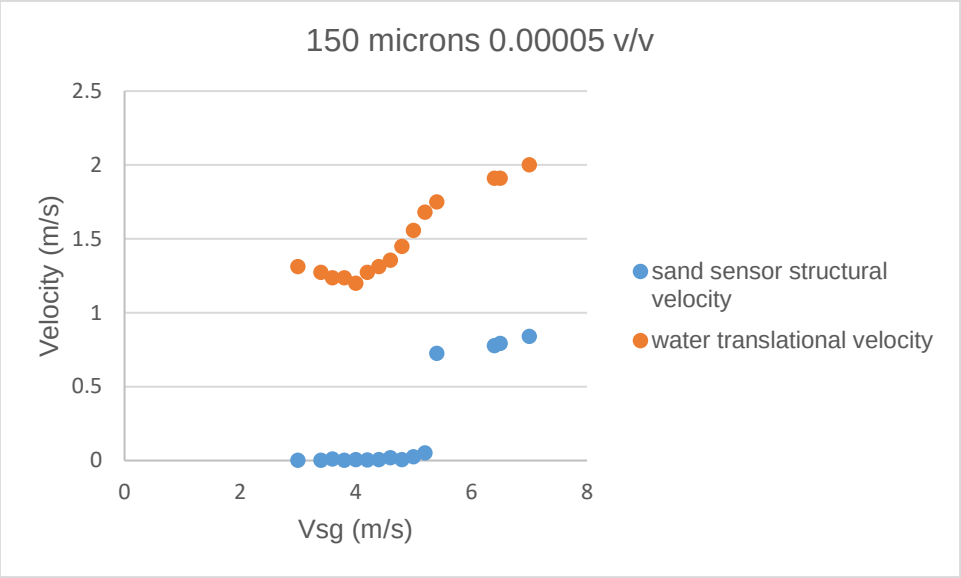

Figure 4-60 sand structural and water translational velocity against Vsg for 150 microns 0.00005 v/v concentration

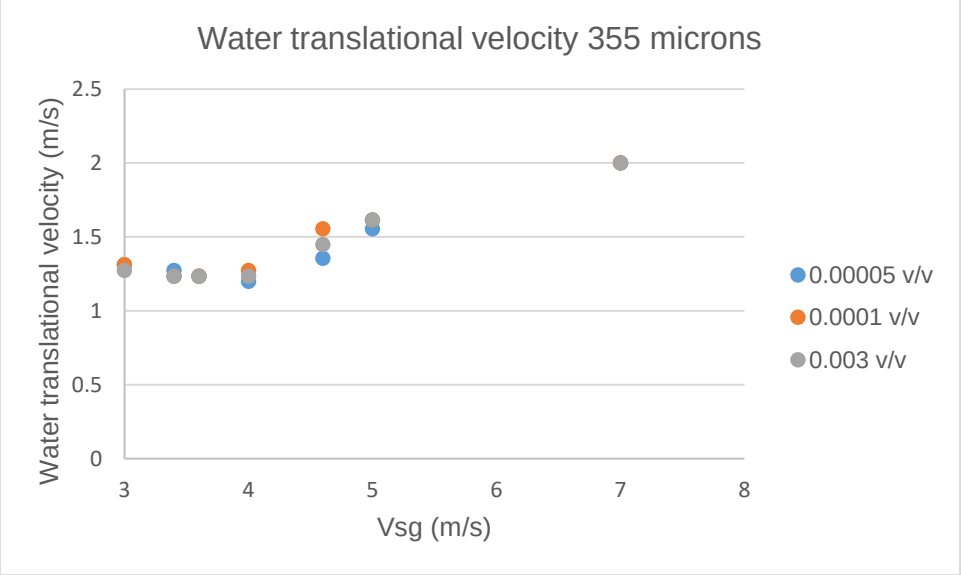

Figure 4-61 water translation velocity 355 microns 0.00005, 0.0001 and 0.0003 v/v concentration

4.4 Conclusion

From this study, it can be concluded that the film thickness sensors are very sensitive to sand presence if there is already water on the film thickness probes surface. From the PSD frequency peaks, there was a distinct increase in the required power from the sand bed, moving dune to the suspension flow regimes. The presence of sand tends to reduce the voltage reading from the water only voltage readings. Thus, these sensors could be used to indicate and estimate the equivalent sand height and sand fraction in air water sand flows as well as in water sand flows. The sensors could also be able to give sand dune velocity if mounted in tandem over a known distance by cross correlation. The conductivity ring also provides water holdup and water translational velocity for water air sand flow by cross-correlation. The measured holdup was also used to get the actual liquid velocity of water in the pipe. The structural velocity and actual liquid velocity tend to increase with increased gas superficial velocity.

5 FLOW BEHAVIOUR NEAR THE BOTTOM OF A V SECTION

5.1 Introduction

This chapter discusses a new set of experiments that were conducted on the two-inch pipe v-section or a dip section to understand the behaviour of dense phase in a bend or undulating pipe. The flow conditions were the same as those conducted on the 2-inch horizontal pipe horizontal described in chapter 3. The experiments aim to observe behaviour and comparisons with horizontal experiments would determine the effects of pipe inclination on heavier phase removal in pipelines.

5.2 Experimental setup

The water and air supply are the same as that of the horizontal two inch rig described in chapter 4. The sand hopper and sand pump are also similarly described in chapter 4. The sketch of the 2" (50.24 mm, ID) dip section is given in Figure 5-1 below and the two inch dip section is highlighted in Figure 5-2 below.

This ±12^{o} dip section consists of a Perspex dip pipeline of 0.8 m high and 7.4 m in length, a horizontal inlet line (2.1m of PVC pipe, 2m of Perspex pipe) and a 2" PVC pipe with the length of 10.5m as the water supply line. A smooth bend with an angle of ±12^{o} connects both sides (downhill and uphill) of the pipelines. Four conductivity sensors were also installed in downhill and uphill pipeline with a differential pressure transducers coupled at each test section (downward and upward section). A flush mounted concentric film thickness sensor was placed at the bottom of the v-section.

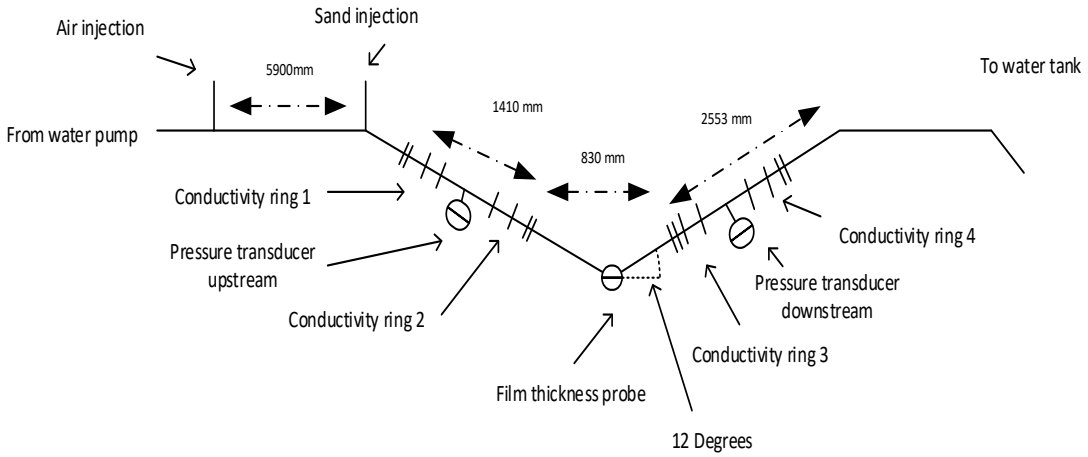

Figure 5-1 sketch of the two inch dip section

Figure 5-2 two inch dip section

5.3 Sand and water flow

For this water superficial velocity the flow conditions are similar to that of the horizontal flow. This aimed at highlighting the flow regime as well as obtaining the sand fraction or equivalent height.

5.3.1 Sand bed

At Vsl of 0.099m /s, a sand bed was observed as depicted in Figure 5-4 and 5-5 below. The response of the sand sensor indicates a high voltage output as well as a higher sand fraction due to the height of the sand bed. The normalised voltage output given in Figure 5-3 is much closer to unity because of the sand particles covering the flush mounted sensor and there little or no undulations due the fact that is a sand bed. The pdf of the sand fraction obtained by the sand sensor as in Figure 5-3 denotes a sand bed because of perturbations as a result of water flow velocity. The frequency domain provides a peak signal at about 0.1Hz as can be observed in Figure 5-3 below, this implies little amount of energy is used thus the sand settling as a bed.

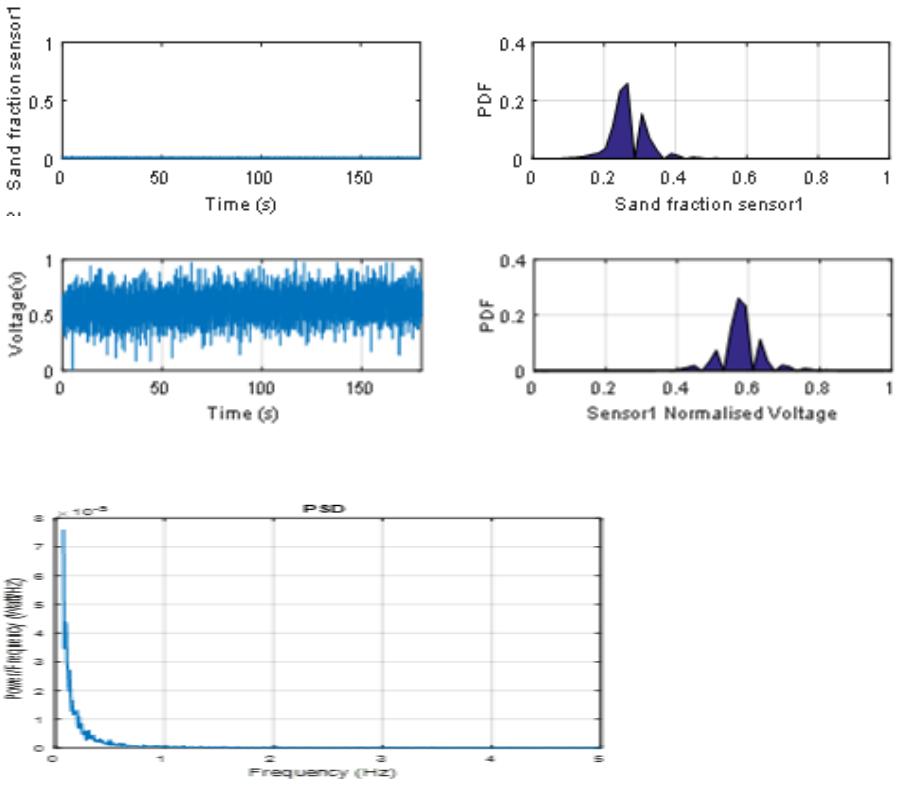

Figure 5-3 sand fraction,normalised voltage, pdf and PSD for Vsl 0.099 m/s 150 microns 0.00005 v/v

Figure 5-4 sand bed at the dip Vsl 0.099 m/s 150 microns 0.00005 v/v concentration

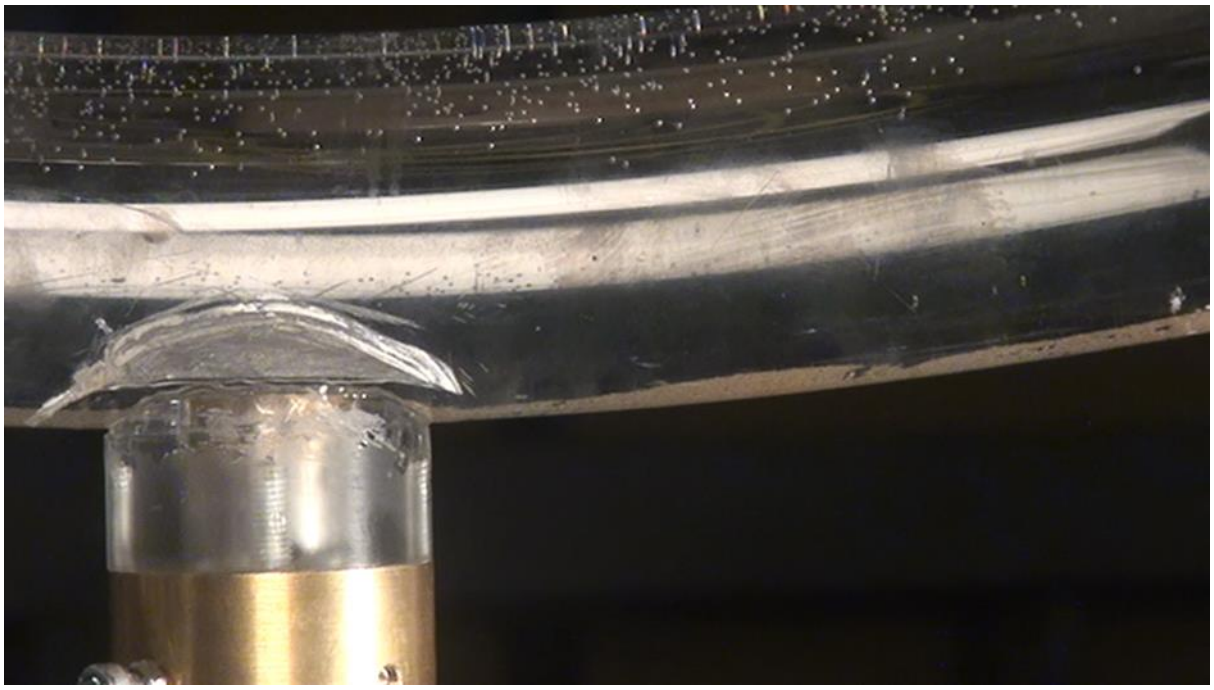

Figure 5-5 side view sand bed at the dip Vsl 0.099 m/s 150 microns 0.00005 v/v concentration

5.3.1.1 Sand dune

For a moving sand bed flow regime, identification can be achieved by using the sand sensor as demonstrated in Figures 5-7 and 5-8 below. From the time series and normalised voltage output the sensors show the passage of a dune. The voltage decreases substantially because of the sand particles covering the sensor resulting higher resistivity of the circuit. This dip in the voltage is recovered as soon as the sand dunes are conveyed further downstream. Water then replaces the sand particles and the voltage returns to that for water. As can be seen in Figure 5-6 the frequency have a single peeks at 0.08Hz indicating the passage of a sand dune. The side view of the dune passage is highlighted in Figure 5-8. The sand sensor sand fraction given in Figure 5-6 indicate the average sand fraction peaking at the passage of the sand dune creast, while the decreasing at the passage of the sand dune trough over the sensors.

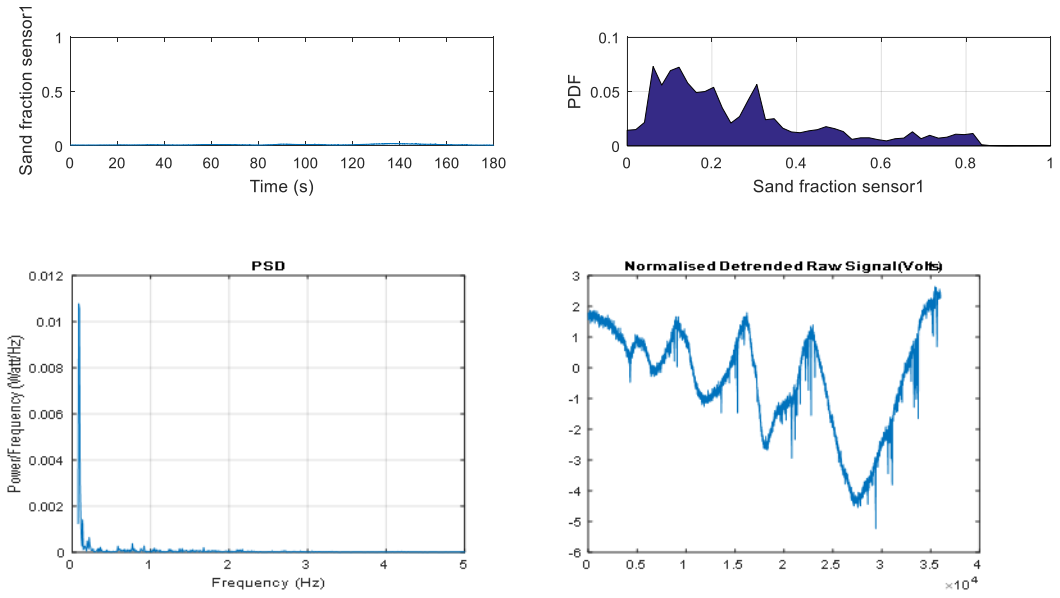

Figure 5-6 sand fraction, pdf, PSD and normalised voltage for Vsl 0.128 m/s 150 microns 0.00005 v/v

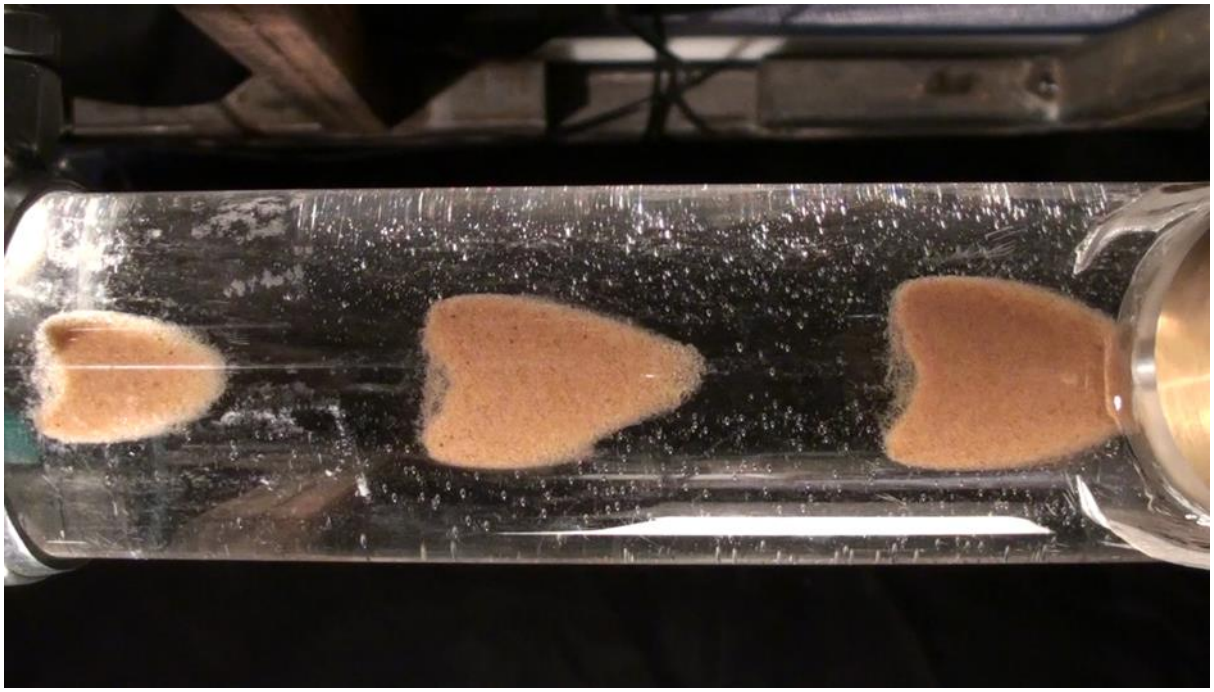

Figure 5-7 moving sand dune at the dip Vsl 0.128 m/s 150 microns 0.00005 v/v concentration

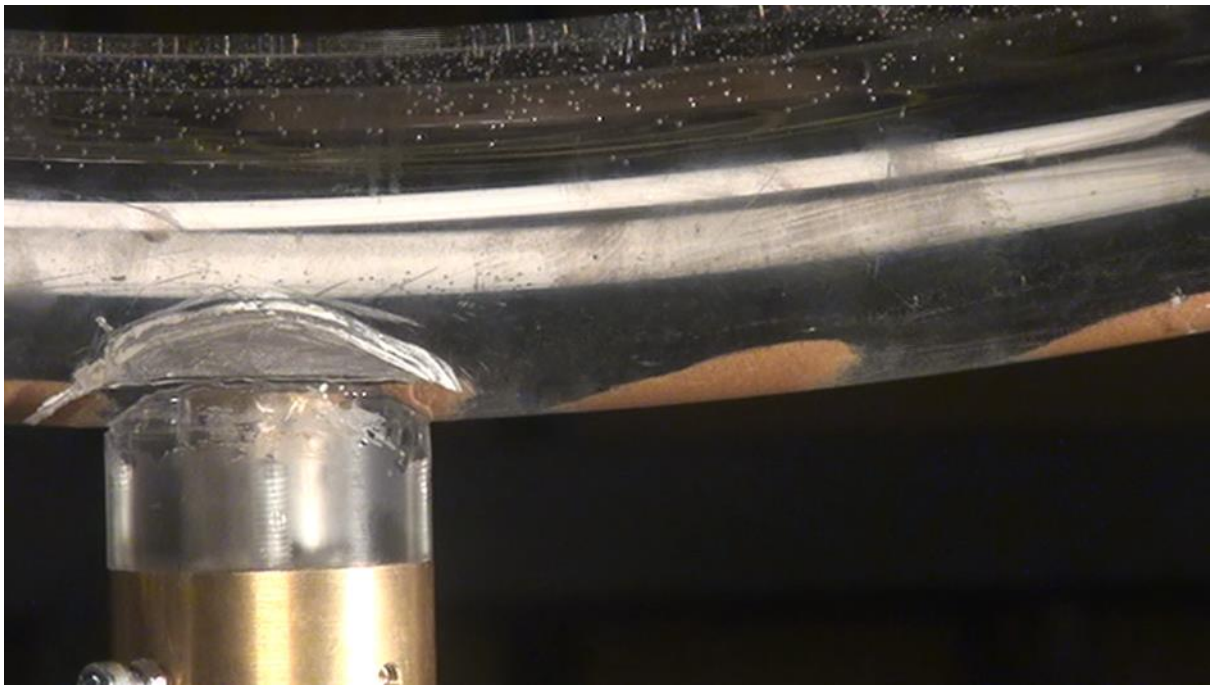

Figure 5-8 side view moving sand dune at the dip Vsl 0.128 m/s 150 microns 0.00005 v/v concentration

5.3.1.2 Saltation

The sand sensor response under the saltation flow regime are given in Figures 5-9 below in the form of sand fraction and normalised voltage and their respective pdf. The voltage signal has multiple peaks that are caused by the moving sand particles covering the sensor and uncovering the sensor as they saltate. Similarly, from Figure 5-9 the frequency have multiple peaks from 0.2 to 0.6Hz indicating the intermittent coverage of the sand sensor by the sand particles, and implying the slight energy increase in moving the sand particles. The sand fraction varies slightly due to the change caused by the Saltating sand particles as depicted in Figure 5-9. The saltation flow is illustrated in Figure 5-10 and 5-11 below.

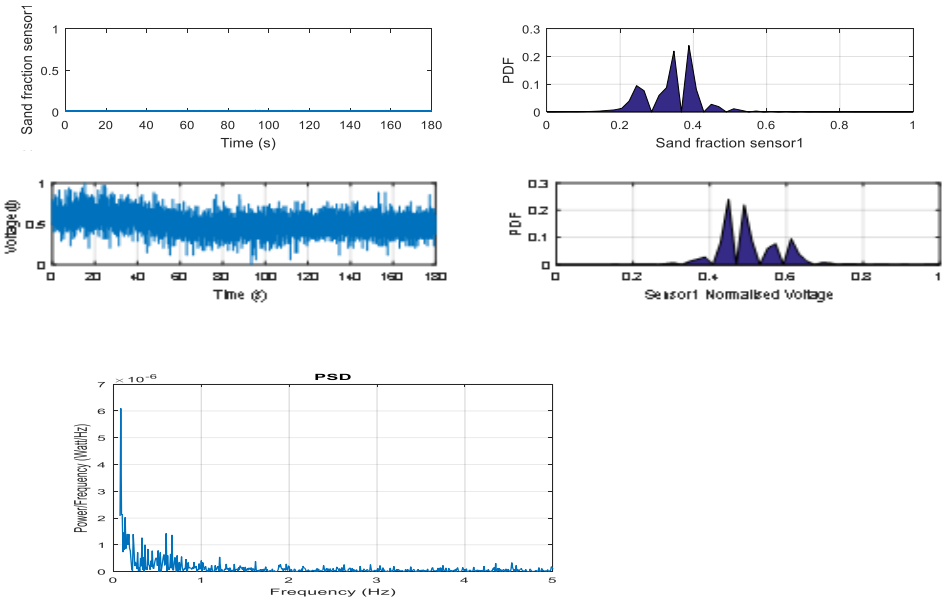

Figure 5-9 sand fraction,normalised voltage, pdf and PSD for Vsl 0.180 m/s 150 microns 0.00005 v/v

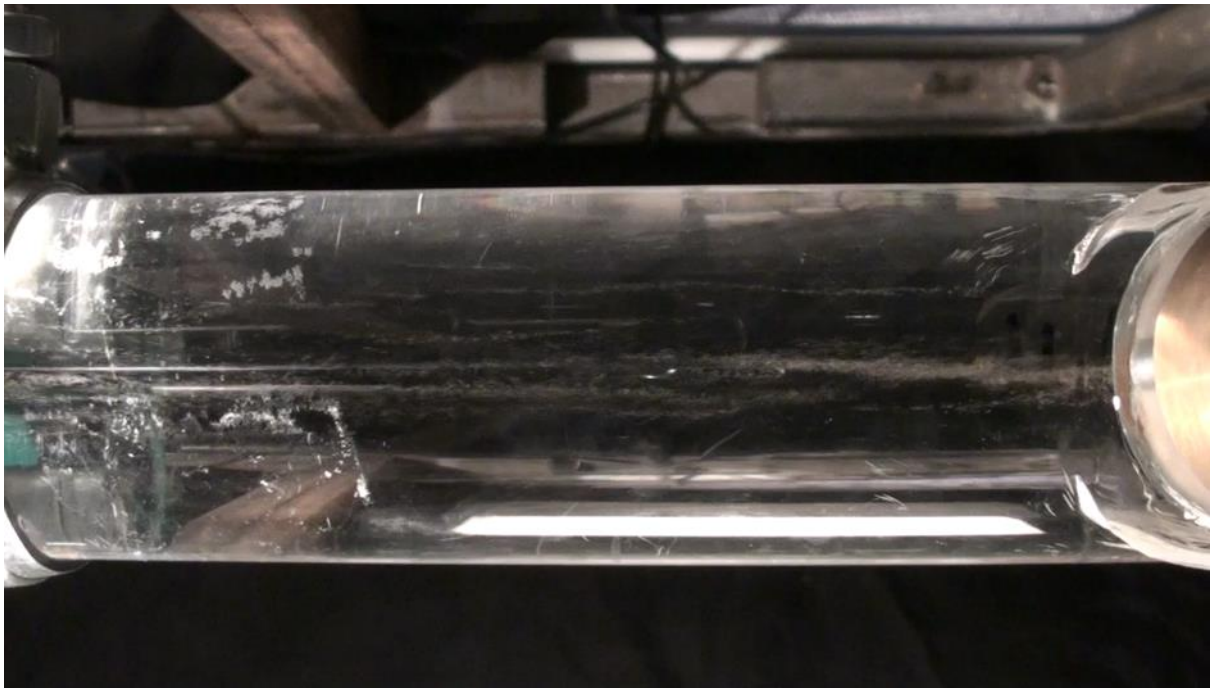

Figure 5-10 saltation at the dip Vsl 0.180 m/s 150 microns 0.00005 v/v concentration

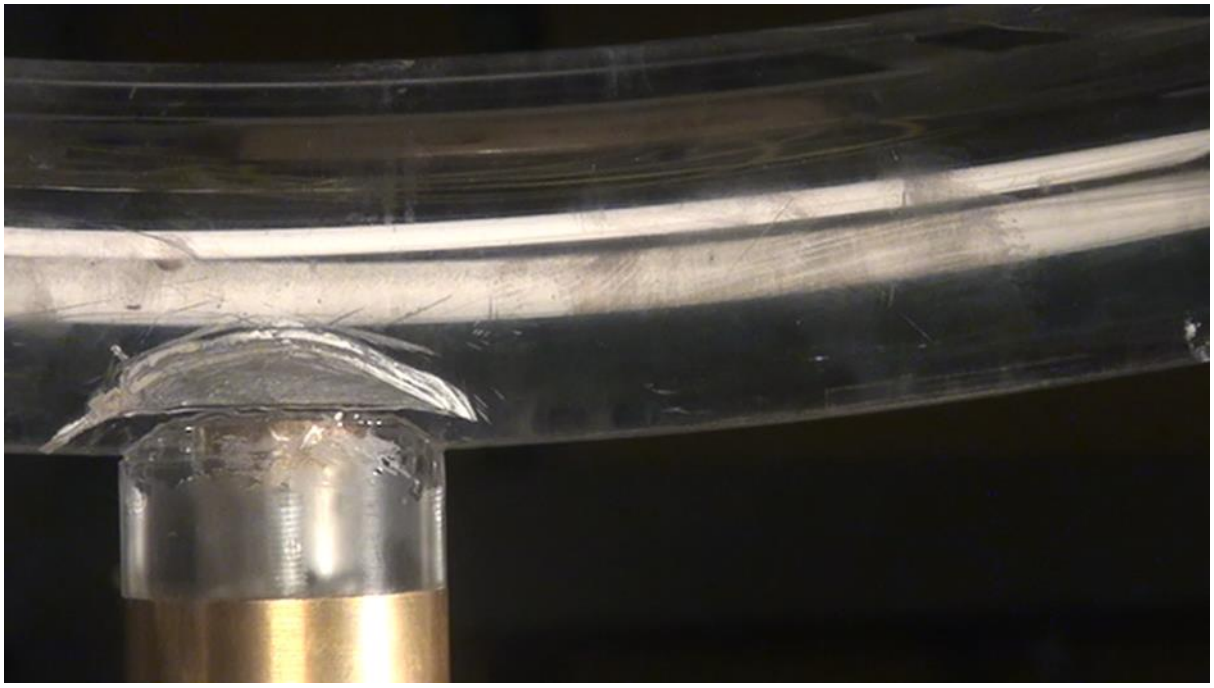

Figure 5-11 side view saltation at the dip Vsl 0.180 m/s 150 microns 0.00005 v/v concentration

5.3.1.3 Streak

The sand sensor response to streak flow regime is given in in Figures 5-12 for sand fraction and normalised voltage output with their respective pdf. Both the voltage and sand sensor pdf highlight multiple spike peaks that indicate sudden intermittent covering of the sand sensor by the sand particles. Similarly the frequency as seen in Figure 5-12 below indicate disturbances peaking between 0.4Hz and 3.9Hz caused by the moving sand streaks, implying greater energy used in moving the sand particles. There is a noticeable drop in sand fraction as given in Figure 5-12. Figure 5-13 and 5-14 demonstrate the streak flow regime.

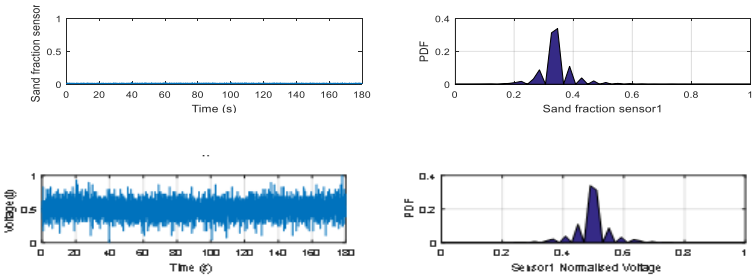

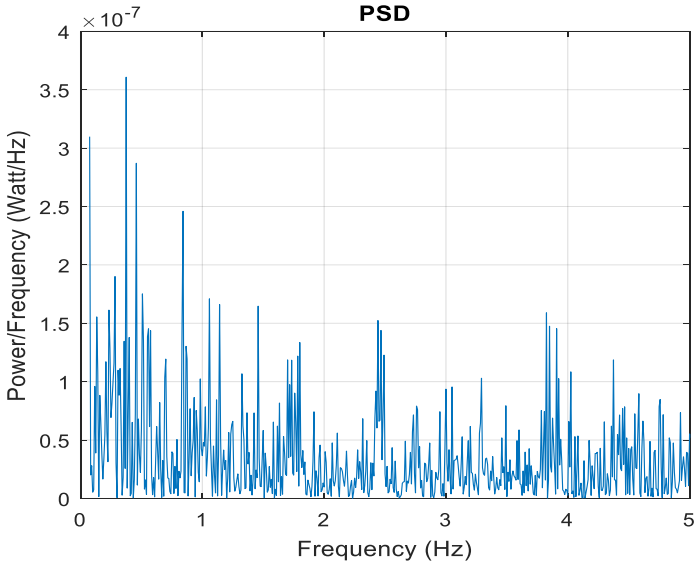

Figure 5-12 sand fraction,normalised voltage, pdf and PSD for Vsl 0.200 m/s 150 microns 0.00005 v/v

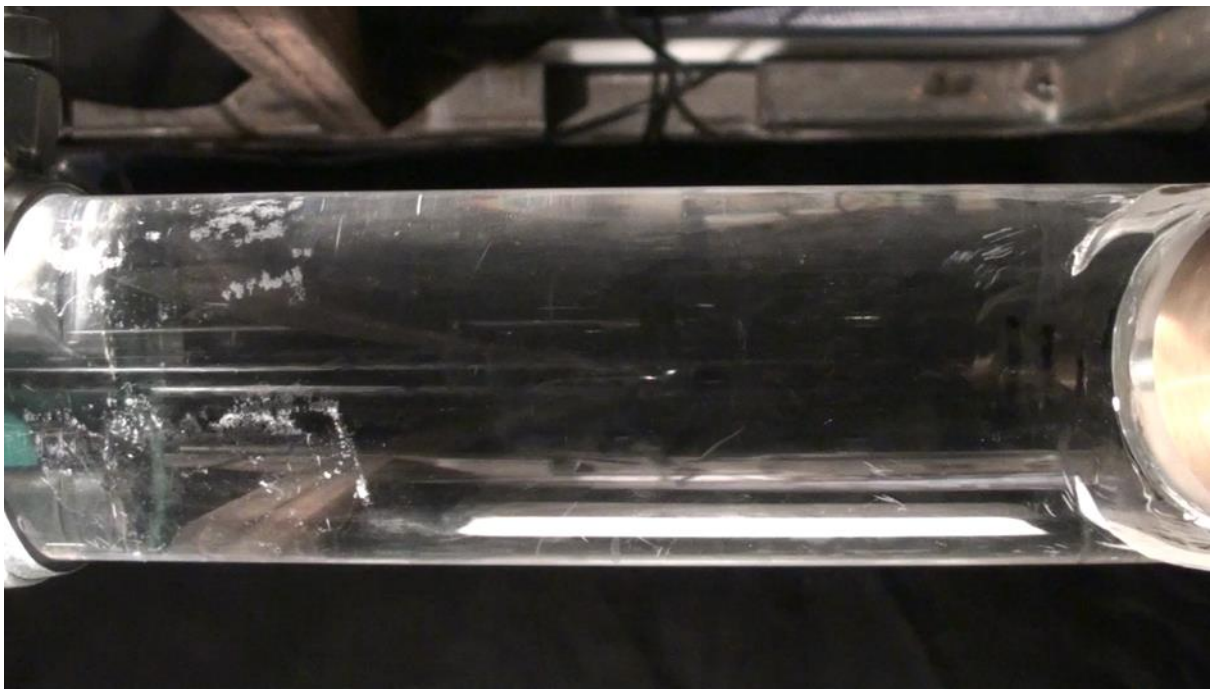

Figure 5-13 streak at the dip Vsl 0.200 m/s 150 microns 0.00005 v/v concentration

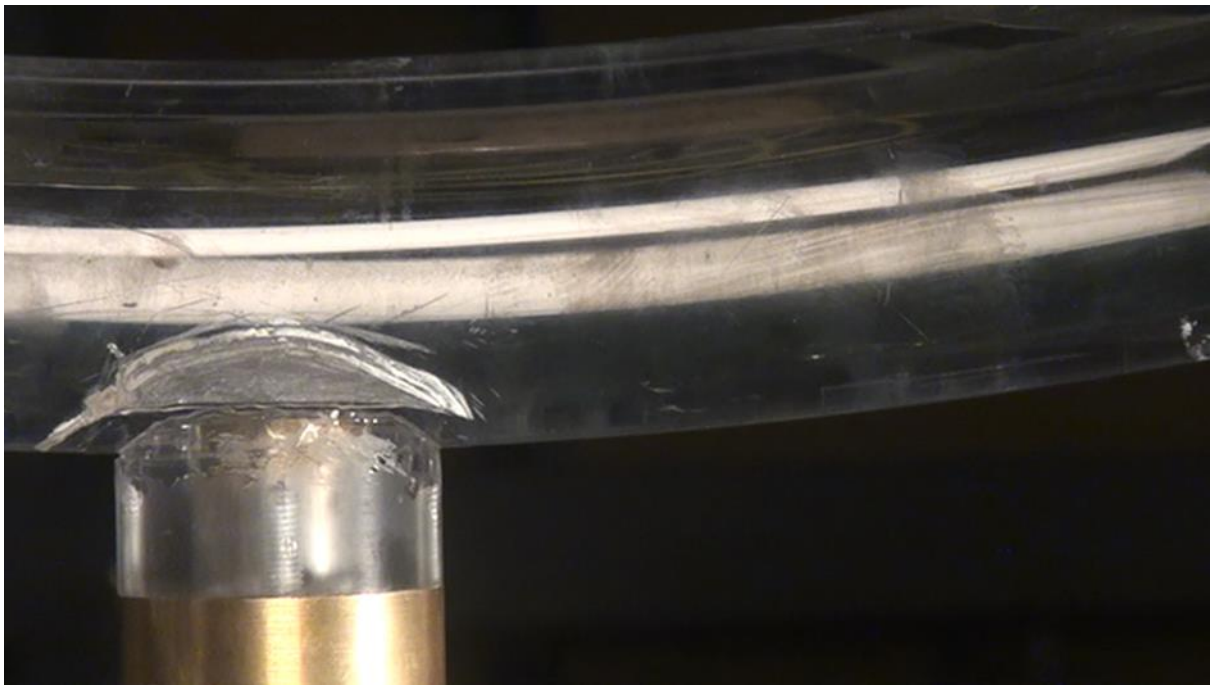

Figure 5-14 side view streak at the dip Vsl 0.200 m/s 150 microns 0.00005 v/v concentration

5.3.1.4 Suspension

This flow regime was identified by the sensor response as highlighted in Figure 5-15 for sand sensor fraction and normalised voltage with their respective pdf. The normalised voltage output is slightly high as the sand particles are suspended in the water flow without impinging on the sensor. Similarly, the frequency as seen in Figure 5-15 below indicate several a peaks between at 0.1Hz and 4.8Hz implying higher energy required to maintain the particles in the flow. Figure 5-16 and 5-17 illustrates the suspension flow regime.

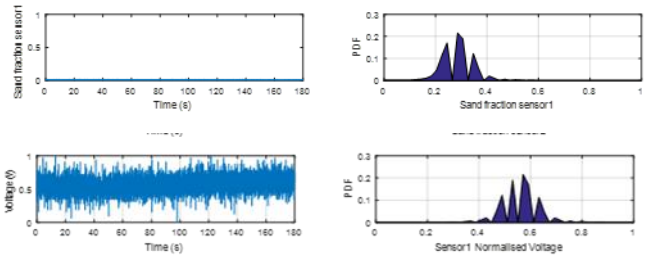

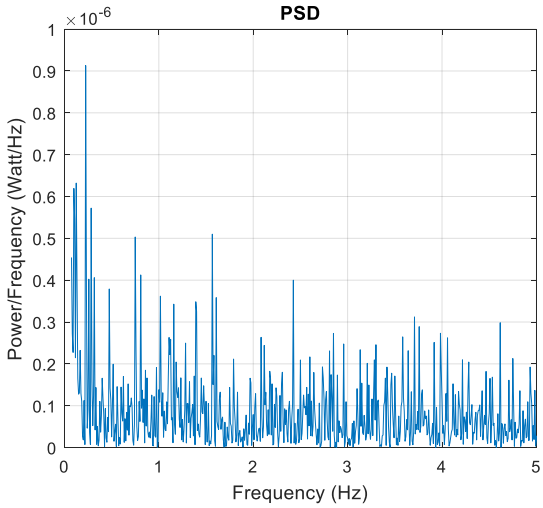

Figure 5-15 sand fraction,normalised voltage, pdf and PSD for Vsl 0.270 m/s 150 microns 0.00005 v/v

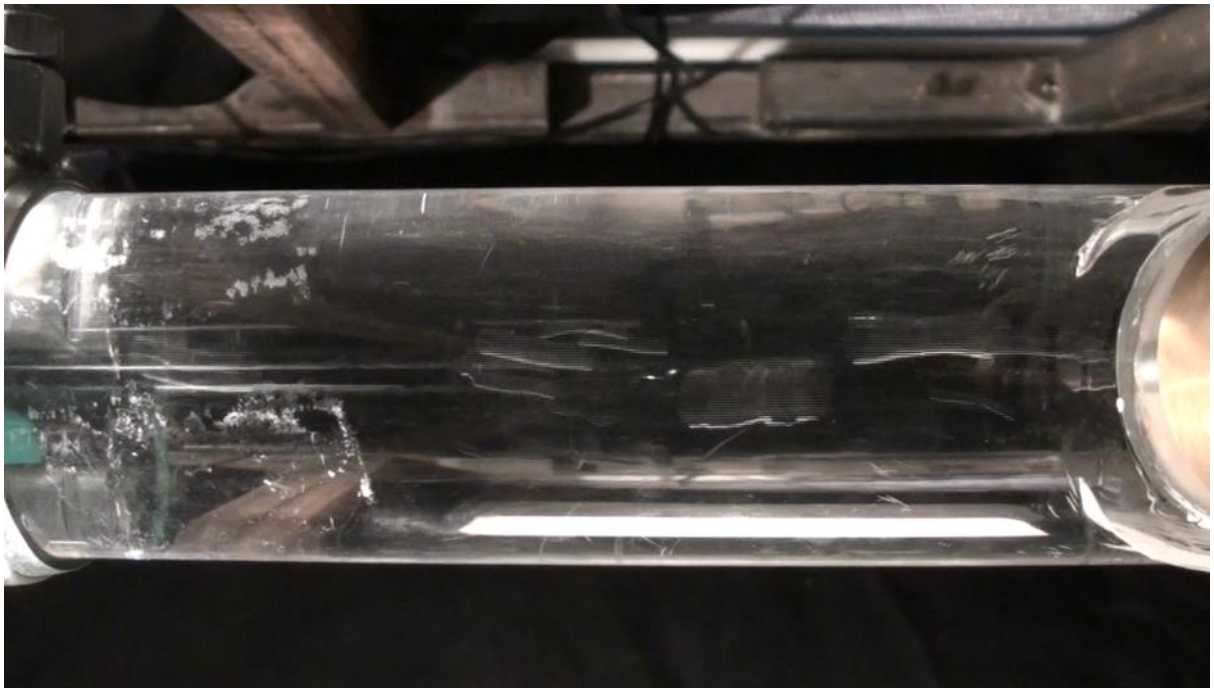

Figure 5-16 suspension at the dip Vsl 0.270 m/s 150 microns 0.00005 v/v concentration

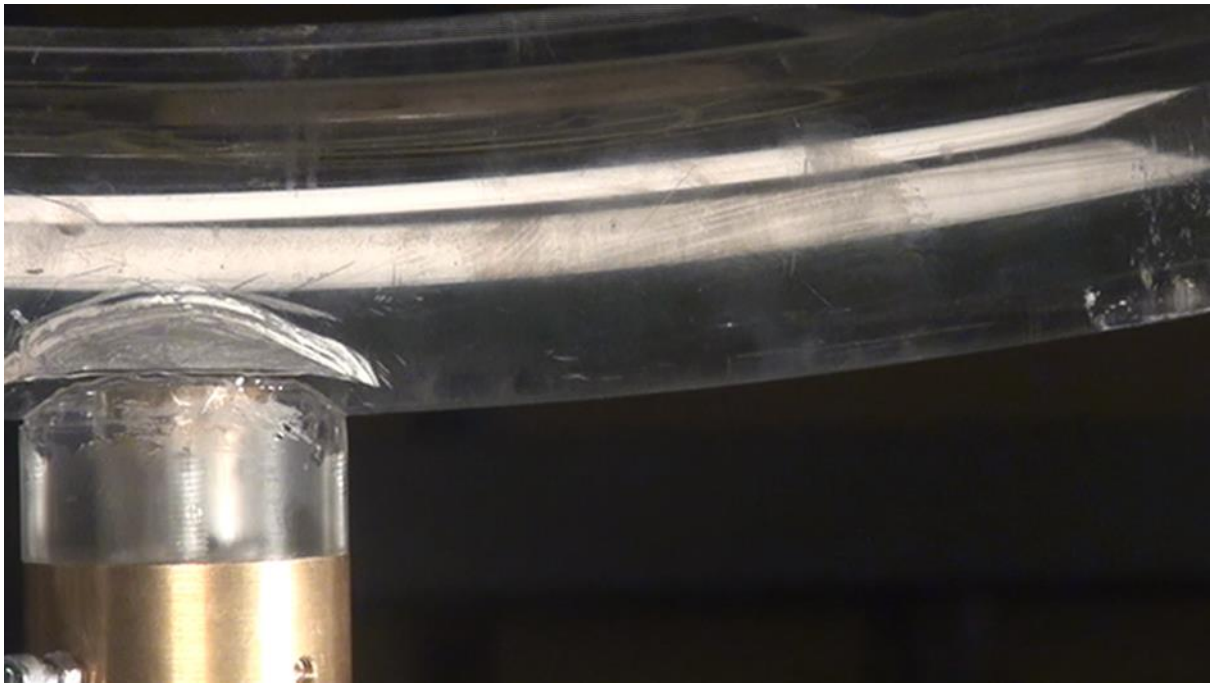

Figure 5-17 side view suspension at the dip Vsl 0.200 m/s 150 microns 0.00005 v/v concentration

5.4 Air water flow

This section describes experiments conducted on the two inch dip section having a low water flow velocity and a high air flow velocity. Figure 5-18 below show a stratified flow with a low gas superficial velocity and low water superficial velocity. The sensor response in Figure 5-19 indicacte intemitent flow of the water and sand particles impinging on the sensor. The condition a the bed is caused by pressure pulsations. There is a peak signal between 0.3 to 1.4Hz indicating some energy needed to maintain the flow.

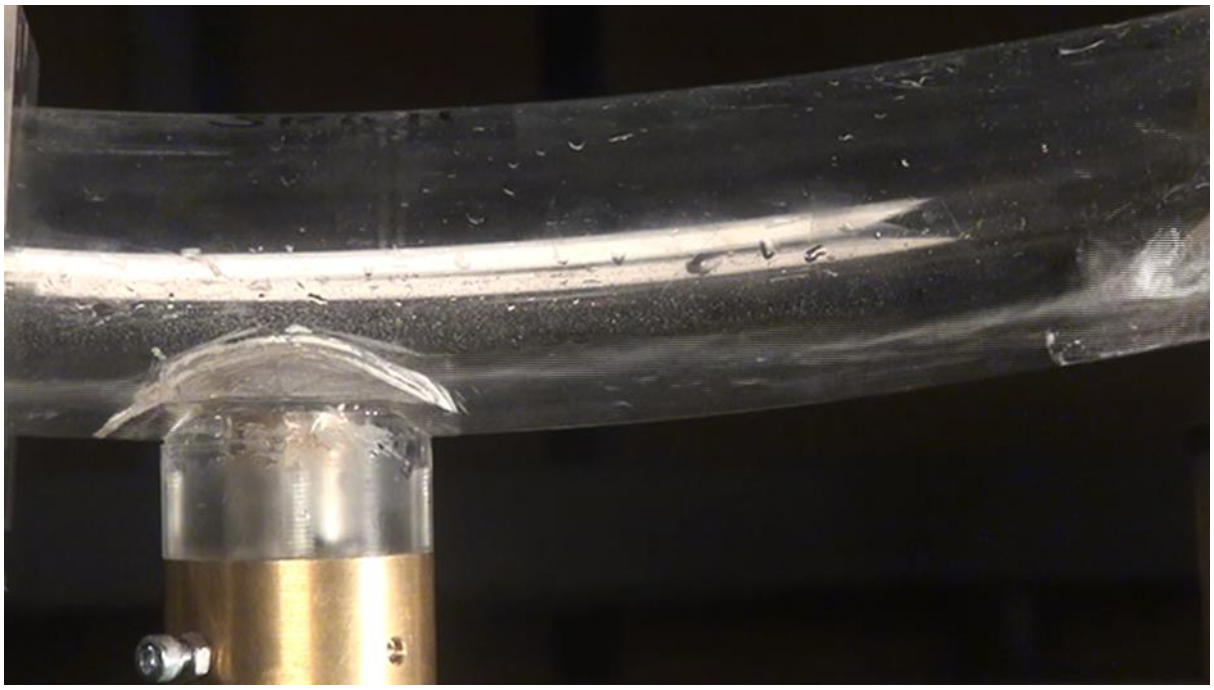

Figure 5-18 water air and sand at Vsl 0.06 m/s Vsg 0.08m/s 355 microns 0.0003 v/v

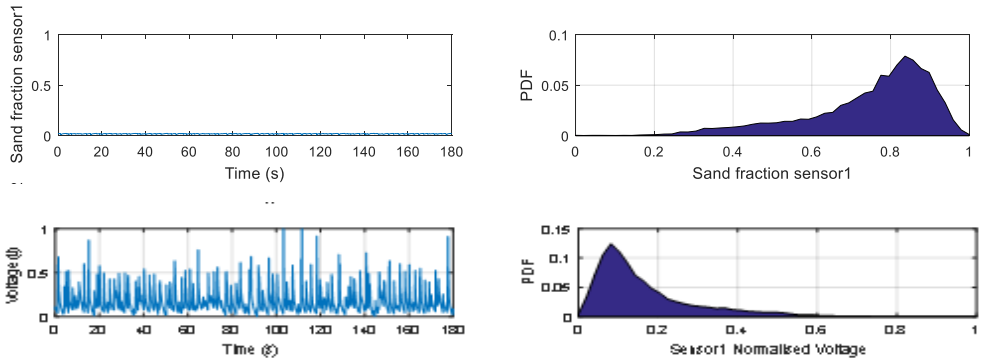

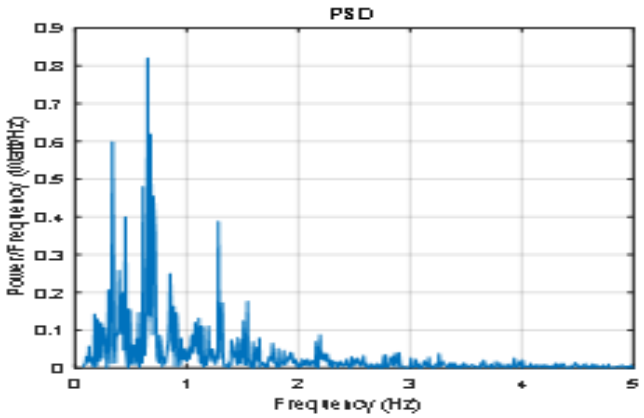

Figure 5-19 sensor response for water air and sand at Vsl 0.06 m/s Vsg 0.5m/s 355 microns 0.0003 v/v

The water flow was kept constant and flow changes gradually with further increase in gas superficial velocity starting with stratified flow at vsg of 0.08 m/s as seen in Figure 5-18 above. This transitions to stratified wavy at 0.5 m/s as given in Figure 5-20 below. The flow transitions to pseudo slug flow at vsg 13 and 17m/s as in Figures 5-21 and 5-22 respectively. Finally the flow tansitions to annular flow at vsg 40m/s illustrated in Figure 5-24 below.

The sand sensor response transitions from in terms of power spectral density from lower peaks decribed earlier for low gas superficial velocity 0.08 m/s to multiple peaks at very gas superficial velocity of 40m/s at given in Figure 5-23 below.

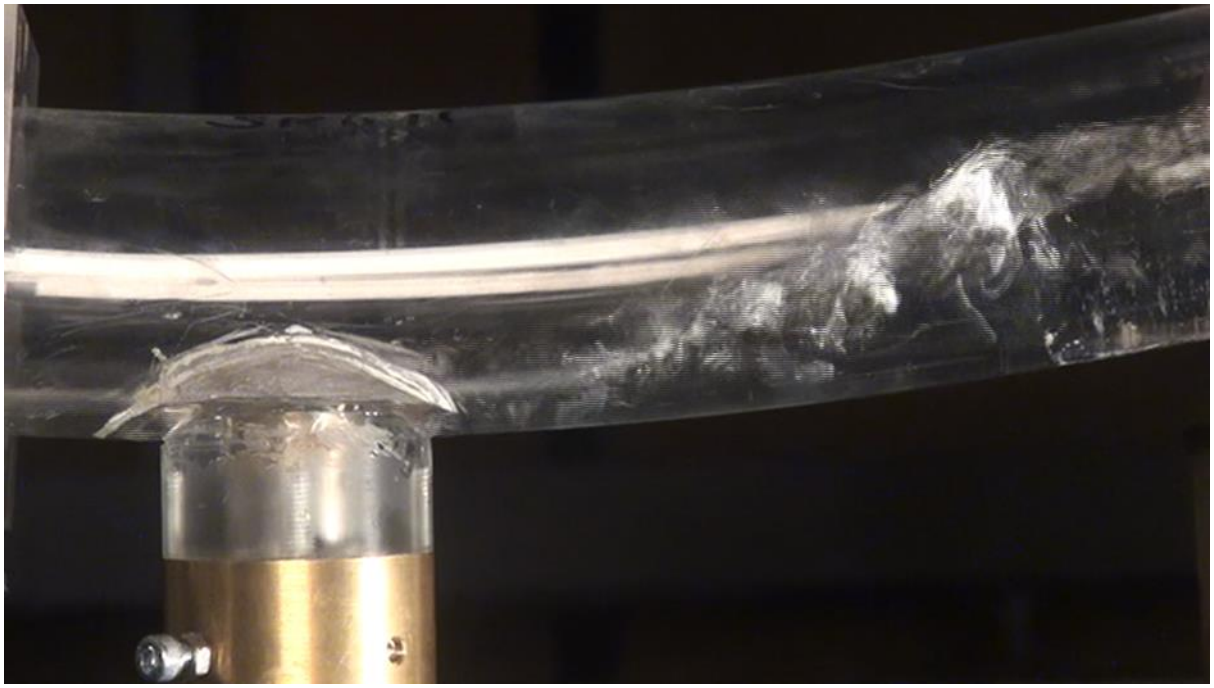

Figure 5-20 water air and sand at Vsl 0.06 m/s Vsg 0.5m/s 355 microns 0.0003 v/v

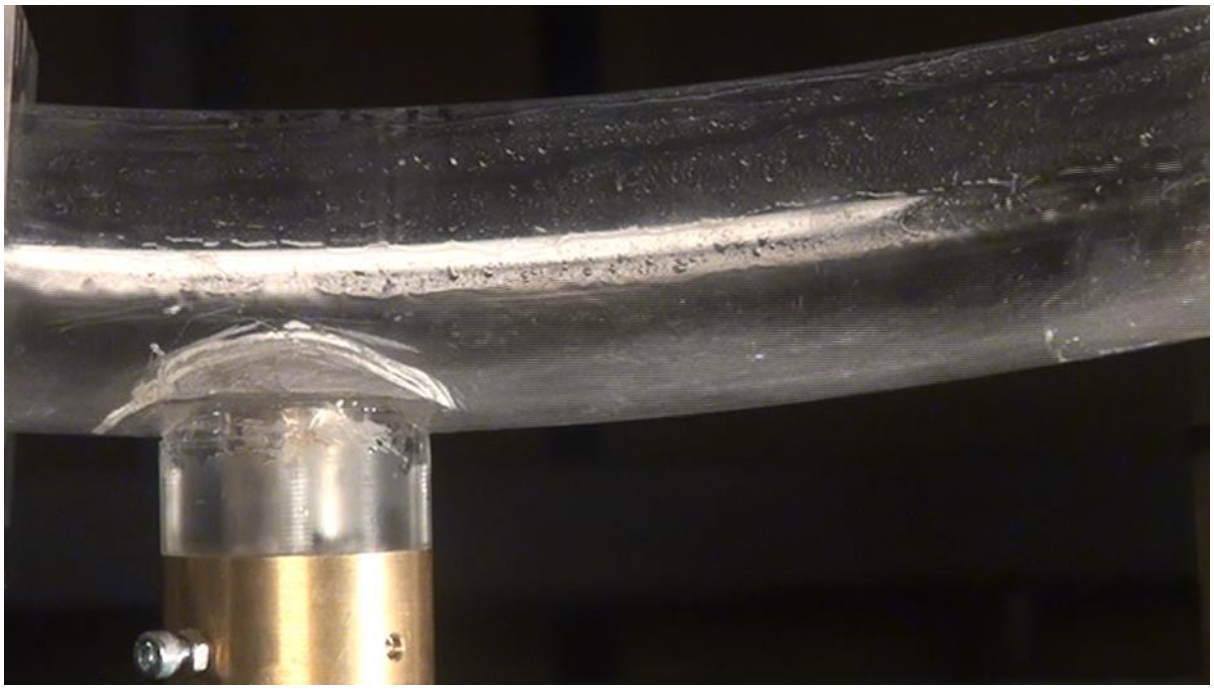

Figure 5-21 water air and sand at Vsl 0.06 m/s Vsg 13 m/s 355 microns 0.0003 v/v

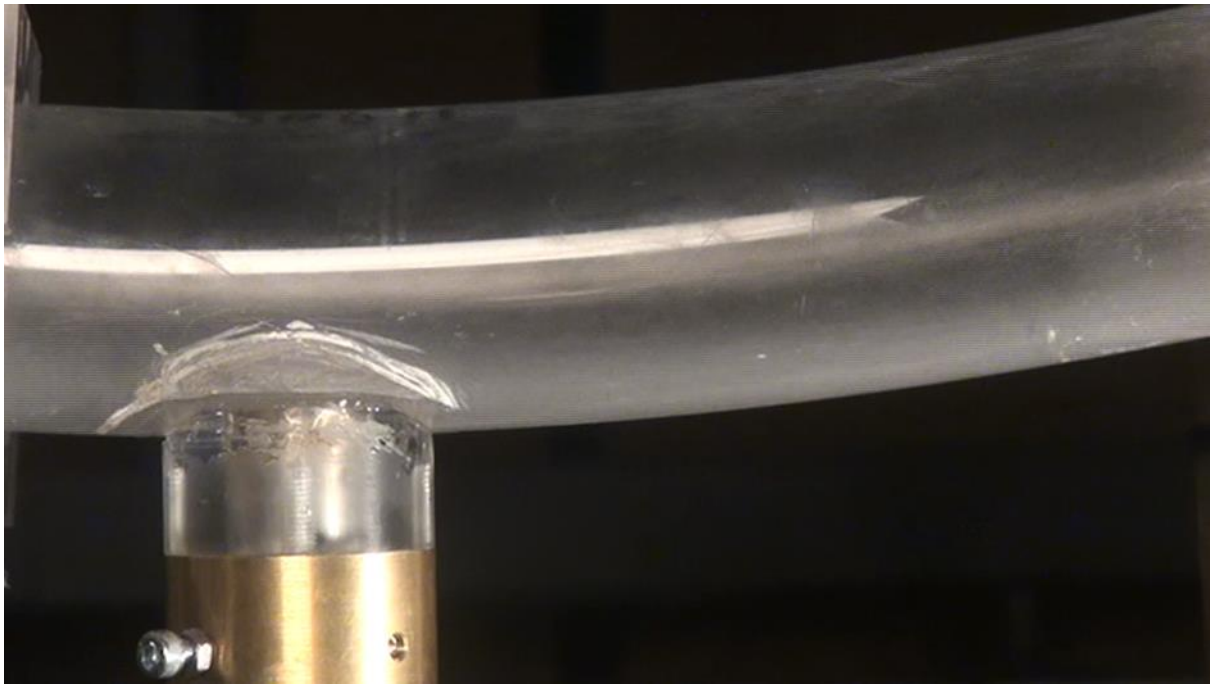

Figure 5-22 water air and sand at Vsl 0.06 m/s Vsg 17 m/s 355 microns 0.0003 v/v

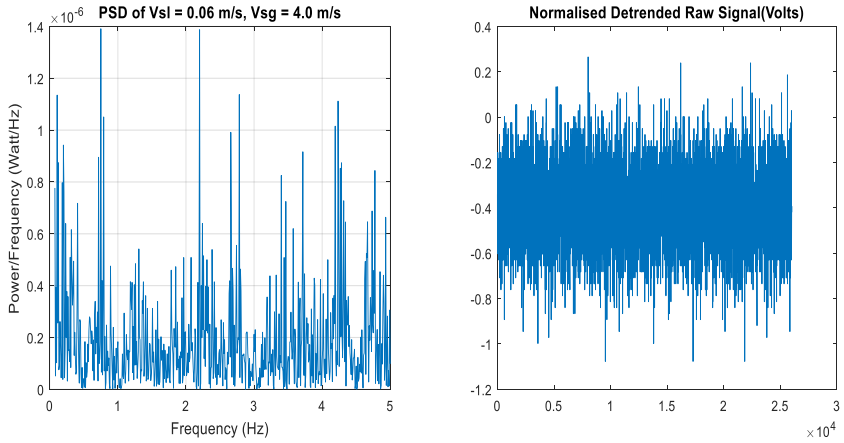

Figure 5-23 sensor response for water air and sand at Vsl 0.06 m/s Vsg 40 m/s 355 microns 0.0003 v/v

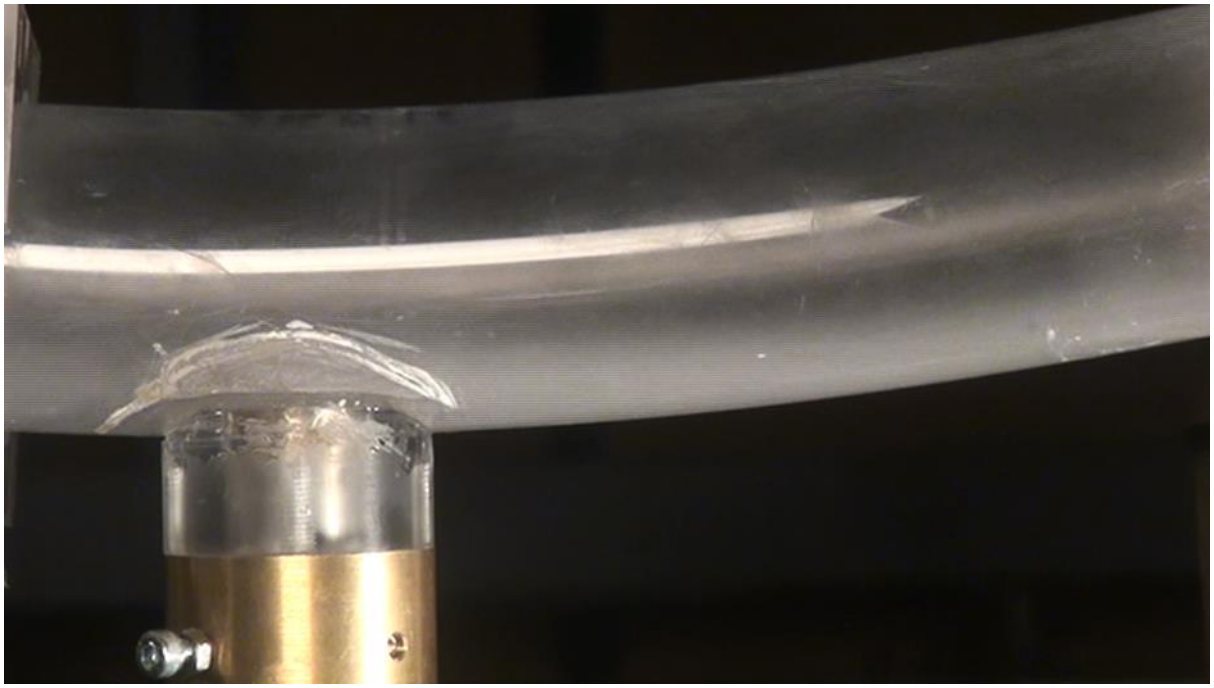

Figure 5-24 water air and sand at Vsl 0.06 m/s Vsg 40 m/s 355 microns 0.0003 v/v

5.5 Conclusion

The observed flow behaviour for water sand flows in the dip section are similar to flows on the horizontal secton for water and sand flows. The flow regimes encountered were at the same velocity. This indicates that the undalations or bends have minimal effect for the flow at low sand concentrations. The sand sensor is also capable of indicating sand presence and fraction at low or bend sectons of a pipe.

For air water sand flows at the dip section the sand sensor can highlight presence of denser water or sand flows in air flow. However, the sand fraction and liquid holdup are affected by the fast response of the senors at high gas flow rates.

6 CONCLUSION AND RECOMMENDATIONS

6.1 Conclusions

The behaviour of low water cut water/ oil flows was observed by conducting a series of experiments. The flow regime and the required velocity to have the water entrained by the less dense oil flow was identified. The flow regimes identified were dispersed , semi dispersed, stratified, transition, and stratified with intermittent globules ocurring at 0.8 to 1 m/s, 0.6 to 0.8 m/s,0.4 to 0.5 m/s,0.3 m/s and 0.1 to 0.2 m/s respectively. Thus, providing a novel flow regime map for low concentration water in oil flow (maximum of 5% water cut).

The parallel plate conductive sensors were used and the related structural velocity obtained through the cross-correlation method. It was observed that the structural velocity tends to change with increase in the flow mixture velocity. The distance of the water injection points have minimal effect on the structural velocity. The average structural velocity tends to increase with increasing mixture velocity up 0.7 m/s before decaying. This shows that the sensor indicates the point of dispersal of the dense water phase.

To establish the conditions and mechanism that dense phase can flow within the lighter phase experimental studies were also carried out . A two fluid model was successfully used to characterise the water film height that was generated from calibration of the conductive sensors. The interface/water film height or hold up increased with increase in water cut. The predictions were in general agreement with experimental data. Thus, the correlation developed by using the two-fluid model could be used to screen the flow conditions which lead to water film formed in the pipe bottom and the estimated film thickness.

The behaviour of low sand content sand/water flows was also studied experimentally. The various flow characteristics of the dense sand was observed in water flow in a horizontal pipe. A novel approach was used in the form of conductive film thickness sensors that could detect the presence of sand in water flow.

To observe the behaviour of small amount sand, air and water as well as small amount of water in air in a horizontal pipe. The observation was made through use of the above mentioned sensors, visual observation and pressure sensors. The pressure drop increased with increasing flow velocity. The sand fraction and sand equivalent height tends to decrease with increase of liquid velocity for water/sand flow, as well as when there is an increase in gas superficial velocity for water/sand air flows. The power spectral density of the sensor output provided a means of identifying the flow regime of the sand/water and sand/water/ air flows especially at suspension or minimum transport conditions. The use of conductivity rings enabled a new contribution of obtaining actual liquid velocity for the water/air and water/sand/air experiments.

The results were similar when compared to previous studies as earlier mentioned in section 4.3.2 such as (Najmi et al., 2015) though the difference is that this sudy provided further insight with a different set of concentrations thus contributing to the scientific society.

The behaviour of settled sand, sand in water and sand in air water in a dip pipeline was used to detect the dense phase by the sensors and this was compared with horizontal pipeline. For the dip or v-section experiments there was not significant change in flow regime as compared with horizontal flows. This was contarary to expections based on previous work at Cranfield University at the earlier stages of this study which indicated that the minimum transport conditions on the dip section were slightly lower than those for a horizontal pipe. The flow regimes were identified in the same manner as horizontal pipe. However for water air flow with increase of gas superficial velocity 0.08, 0.5, 13, 17 and 40 m/s the flow regime was stratified, stratified wavy, pseudo- slug, slug and annular flow respectively.

The conductive sensors are thus suitable for dense phase classification thickness, velocity and holdup measurements in pipelines.

6.2 Recommendations for future work

Air and water prediction model should be developed in conjunction with use of the film thickness sensors. This would involve further experiments using the four inch horizontal pipe using concentric film thickness sensors, this is due to the better suitability as mentioned in (Fossa, 1998b). There results should then be compared with gas liquid models such as that of (Zhang and Sarica, 2011a), (Hamersmat and Hart, 1987), (Ullmann and Brauner, 2006).

Similarly a water sand model for stratified flow should be developed for low loading sand using the film thickness sensor. This would involve comparisions and improvements to (Ibarra et al., 2014), (Najmi et al., 2015) and similar literature.

An investigation should be carried out to ascertain if a water-air-sand model could be developed for low load sand in water flows. Similarly this would involve structured experiments t h Qat would aim at improving available models from literature.

A combined model for phase removal for liquid and solid dense phases in flowing lighter phases could be considered after comparison with available models. This would look into previos sugestions by (Wicks and Fraser, 1975), (Wu, 1995) and (III, 2009)

REFERENCES

Al-lababidi, S. et al. (2012) ‘Sand Transportations and Deposition Characteristics in Multiphase Flows in Pipelines’, *Journal of Energy Resources Technology*, 134(3), p. 34501.

Al-Wahaibi, T. and Angeli, P. (2009) ‘Predictive model of the entrained fraction in horizontal oil–water flows’, *Chemical Engineering Science*, 64(12) Affiliation: Department of Petroleum and Chemical Engineering, Sultan Qaboos University, P.O. Box 33, P.C. 123, Oman; Affiliation: Department of Chemical Engineering, University College London, Torrington Place, London, WC1E 7JE, United Kingdom; Correspon, pp. 2817–2825.

Al-yarubi, Q.S.K. (2012) *A Thesis submitted to the University of Huddersfield in partial fulfilment of the requirements for the degree of Doctor of Philosophy University of Huddersfield*. Huddersfield.

Andreussi, P. et al. (1988) ‘An impedance method for the measurement of liquid hold-up in two-phase flow’, *International Journal of Multiphase Flow*, 14(6), pp. 777–785.

Angeli, P. (2001) ‘Droplet size in two-phase liquid dispersed pipeline flows’, *Chemical Engineering & Technology*, 24(4) Affiliation: Department of Chemical Engineering, University College London, Torrington Place, London, WC1E 7JE, United Kingdom; Correspondence Address: Angeli, P.; Department of Chemical Engineering, University College London, Torrington Place, London, WC, pp. 431–434.

Angeli, P. and Hewitt, G.. (2000a) ‘Flow structure in horizontal oil–water flow’, *International Journal of Multiphase Flow*, 26(7) Affiliation: Department of Chemical Engineering, Imp. Coll. Sci., Technol. Med., P., London, United Kingdom; Correspondence Address: Angeli, P.; Department of Chemical Engineering, University College London, Torrington Place, London WC1E 7JE, United Kingd: Elsevier Science Ltd, pp. 1117–1140.

Angeli, P. and Hewitt, G.F. (2000b) ‘Flow structure in horizontal oil-water flow’,

International Journal of Multiphase Flow, 26(7), pp. 1117–1140.

Anon (n.d.) *ACCURATE BS&W TESTING IMPORTANT FOR CRUDE-OIL CUSTODY TRANSFER - Oil & Gas Journal*. Available at: http://www.ogj.com/articles/print/volume-88/issue-46/in-this-issue/pipeline/accurate-bsw-testing-important-for-crude-oil-custody-transfer.html (Accessed: 6 July 2016a).

Anon (n.d.) *Oil emulsions* -. Available at: http://petrowiki.org/Oil_emulsions (Accessed: 20 August 2016b).

Arirachakaran, S. et al. (1989) 'An Analysis of Oil/Water Flow Phenomena in Horizontal Pipes', *SPE Production Operations Symposium*. Oklahoma City, Oklahoma: Society of Petroleum Engineers, Vol.18836, p. 155.

Beggs, D.H. and Brill, J.P. (1973) 'A Study of Two-Phase Flow in Inclined Pipes', *Journal of Petroleum Technology*, 25(5), pp. 607–617.

Brauner, N. (2001) 'The prediction of dispersed flows boundaries in liquid–liquid and gas–liquid systems', *International Journal of Multiphase Flow*, 27(5), pp. 885–910.

Brauner, N. et al. (1998) 'A two-fluid model for stratified flows with curved interfaces', *International Journal of Multiphase Flow*, 24(6), pp. 975–1004.

Bubar, B.G. (2011) 'Hydrostatic Testing', in *Pipeline Planning and Construction Field Manual*. Boston: Elsevier, pp. 379–404.

Cai, J. et al. (2012) 'Experimental study of water wetting in oil–water two phase flow—Horizontal flow of model oil', *Chemical Engineering Science*, 73(0) Elsevier, pp. 334–344.

Cai, J. et al. (2005) 'Experimental studies of water wetting in large-diameter horizontal oil/water -pipe flows', *SPE Annual Technical Conference and Exhibition (ATCE)*, (1993)

Chu, K.J. and Dukler, A.E. (1974) 'Statistical characteristics of thin, wavy films: Part II. Studies of the substrate and its wave structure', *AIChE Journal*, 20(4), pp.

695–706.

Coney, M.W.E. (1973) ‘The theory and application of conductance probes for the measurement of liquid film thickness in two-phase flow’, *Journal of Physics E: Scientific Instruments*, 6(9), p. 903.

Coordination, A.P.I.M. (1995) ‘*Manual of petroleum measurement standards: section 2--standard practice for automatic sampling of liquid petroleum and petroleum products*’

Danielson, T.J. and Co, C. (2007) ‘Sand Transport Modeling in Multiphase Pipelines’, *Offshore technology conference*

DECC (2012) ‘Guidance Notes for Petroleum Measurement Issue 8’, *Department of Energy and Climate Change*, 1(8), pp. 10–35.

Falcone, G. (2009) 2009_Chapter 4 Key Multiphase Flow Metering Techniques *Developments in Petroleum Science*.

Fossa, M. (1998a) ‘Design and performance of a conductance probe for measuring the liquid fraction in two-phase gas-liquid flows’, *Flow Measurement and Instrumentation*, 9(2) Affiliation: DITEC, Dipto. di Termoenergetica e C., Univ`. degli Studi di Genova, Via all’Opera Pia 15a, 16145 Genoa, Italy; Correspondence Address: Fossa, M.; Universita degli Studi di Genova, Genoa, Italy: Elsevier Sci Ltd, pp. 103–109.

Fossa, M. (1998b) ‘Design and performance of a conductance probe for measuring the liquid fraction in two-phase gas-liquid flows’, *Flow Measurement and Instrumentation*, 9(2), pp. 103–109.

Hamersmat, P.J. and Hart, J. (1987) ‘A pressure drop correlation for gas/liquid pipe flow with a small liquid holdup’, *Chemical Engineering Science*, 42(5), pp. 1187–1196.

Hart, J,Hamersma, P.J, Fortuin, J.M.H. (1989) ‘Correlations predicting frictional pressure drop and liquid holdup during horizontal gas-liquid pipe flow with a small liquid holdup’, *International Conference of Multiphase Flow*, 15(6), pp. 947–964.

Hasson, D. et al. (1970) ‘Annular flow of two immiscible liquids I. Mechanisms’, *The Canadian Journal of Chemical Engineering*, 48(5), pp. 514–520.

Hewitt, G.. and Bouré, J.. (1973) ‘Some recent results and development in gas-liquid flow: a review’, *International Journal of Multiphase Flow*, 1(1) Affiliation: HTFS, AERE, Harwell, Didcot, Berks., England and STT, Centre d’Etudes Nucléaires, Grenoble, France; Correspondence Address: Hewitt, G.F., pp. 139–171.

Hewitt, G.F. (1978) ‘Measurements of two phase flow parameters’, *NASA STI/Recon Technical Report A*, 79 Academic Press Inc, p. 47262.

Hewitt, G.F. (1982) ‘Applications of two-phase flow’, *Chemical Engineering Progress*, 78(7) Correspondence Address: Hewitt, G.F., pp. 38–46.

Hinze, J.O. (1955) ‘Fundamentals of the hydrodynamic mechanism of splitting in dispersion processes’, *AIChE Journal*, 1(3), pp. 289–295.

Hollenberg, J.F. and Oliemans, R.V.A. (1992) ‘*Prediction of flow conditions to minimize corrosion*’

Hutchinson, P. et al. (1971) ‘Deposition of liquid or solid dispersions from turbulent gas streams: a stochastic model’, *Chemical Engineering Science*, 26(3) Affiliation: United Kingdom Atomic Energy Research Establishment, Harwell, England, United Kingdom; Affiliation: Chemical Engineering Department, University of Houston, Houston, TX 77004, United States; Correspondence Address: Hutchinson, P.; United Kingd, pp. 419–439.

Ibarra, R. et al. (2014) ‘Critical Sand Deposition Velocity in Horizontal Stratified Flow’, *SPE International Symposium and Exhibition on Formation Damage Control*, (February), pp. 26–28.

III, J.S.S. (2009) ‘*Flow vewlocity required for solid particle movement in oil and gas pipelines*’, NACE International, pp. 1–15.

Kang, H.C. and Kim, M.H. (1992) ‘The development of a flush-wire probe and calibration method for measuring liquid film thickness’, *International Journal of*

Multiphase Flow, 18(3), pp. 423–437.

King, M.J.S. et al. (2001) 'Solids Transport in Multiphase Flows—Application to High-Viscosity Systems', *Journal of Energy Resources Technology*, 123(3), p. 200.

Koskie, J.E. et al. (1989) 'Parallel-wire probes for measurement of thick liquid films', *International Journal of Multiphase Flow*, 15(4) Affiliation: Boiling and Two-phase Flow Laboratory, School of Mechanical Engineering, Purdue University, West Lafayette, IN 47907, United States, pp. 521–530.

Kostoglou, M. and Karabelas, A.J. (1998) 'On the attainment of steady state in turbulent pipe flow of dilute dispersions', *Chemical Engineering Science*, 53(3), pp. 505–513.

Ladam, Y. et al. (2007) 'Simulation of sand transport in a stratified gas-liquid two-phase pipeflow', *13th International Conference on Multiphase Production Technology*. Affiliation: SINTEF, Norway; Affiliation: ConocoPhillips, United States; Affiliation: TOTAL, Norway; Affiliation: PETROBRAS, Brazil; Correspondence Address: Yang, Z. L.; SINTEFNorway, pp. 327–342.

Li, C. et al. (2006) 'Experimental study on water wetting and CO2 corrosion in oil-water two-phase flow', *CORROSION/2006, paper no. 06595*, (6595) NACE International, pp. 1–26.

Liu, L. et al. (2006) 'Laser-induced fluorescence (LIF) studies of liquid–liquid flows. Part II: Flow pattern transitions at low liquid velocities in downwards flow', *Chemical Engineering Science*, 61(12) Affiliation: Department of Chemical Engineering, Imperial College London, Exhibition Road, London, SW7 2AZ, United Kingdom; Correspondence Address: Hewitt, G.F.; Department of Chemical Engineering, Imperial College London, Exhibition Road, London, SW7 2AZ, pp. 4022–4026.

Lovick, J. and Angeli, P. (2004) 'Experimental studies on the dual continuous flow pattern in oil–water flows', *International Journal of Multiphase Flow*, 30(2) Affiliation: Department of Chemical Engineering, University College London,

London WC1E 7JE, United Kingdom; Correspondence Address: Angeli, P.; Department of Chemical Engineering, University College London, London WC1E 7JE, United Kingdom; email: p.angel, pp. 139–157.

Nädler, M. and Mewes, D. (1995) '*Intermittent Three-Phase Flow of Oil, Water And Gas In Horizontal Pipes*', The International Society of Offshore and Polar Engineers.

Najmi, K. et al. (2015) 'Experimental Study of Low Concentration Sand Transport in Multiphase Viscous Horizontal Pipes', *One Petro*, (4), pp. 17–27.

Paras, S.V. et al. (1994) 'Liquid layer characteristics in stratified—Atomization flow', *International Journal of Multiphase Flow*, 20(5) Affiliation: Chemical Process Engineering Research Institute, Department of Chemical Engineering, Aristotle University of Thessaloniki, University Box 455, 54006 Thessaloniki, Greece, pp. 939–956.

Pharris, T.C. and Kolpa, R.L. (2007) '*Overview of the Design, Construction, and Operation of Interstate Liquid Petroleum Pipelines*', , p. 108.

Pots, B.F.M. et al. (2006) *What are the Real Influences of Flow on Corrosion?*. P.O.Box 1380, Houston, Texas 77251/P.O. Box 38000, 1030 BN Amsterdam, Netherlands: Shell Global Solutions (US) Inc./ Shell Global Solutions International B.V.

Pots, B.F.M. and Kapusta, S.D. (2005) 'Prediction of Corrosion Rates of the Main Corrosion Mechanisms in', *Nace*. NACE International, p. 5550.

Rodriguez, O.M.H. and Oliemans, R.V.A. (2006) 'Experimental study on oil–water flow in horizontal and slightly inclined pipes', *International Journal of Multiphase Flow*, 32(3), pp. 323–343.

Russell, T.W.F. and Charles, M.E. (1959) 'The effect of the less viscous liquid in the laminar flow of two immiscible liquids', *The Canadian Journal of Chemical Engineering*, 37(1), pp. 18–24.

Salama, M. (2000) 'Influence of sand production on design and operations of

piping systems', *Nace Corrosion 2000*, (80) NACE International

Shi, H. et al. (2002) 'Predicting of water film thickness and velocity for corrosion Rate calculation in oil-water flows', *Corrosion 2002*. Denver, Co: NACE International.

Shirley, R. et al. (2012) 'ARTIFICIAL NEURAL NETWORKS IN LIQUID-LIQUID TWO-PHASE FLOW', *Chemical Engineering Communications*, 199(12), pp. 1520–1542.

Snuverink, H. et al. (1987) '*Liquid/liquid oil/water flow in pipes. Entrainment of settled water by flowing oil in pipes*'

Soleimani, A. et al. (1999) 'Spatial Distribution of Oil and Water in Horizontal Pipe Flow', *SPE Annual Technical Conference and Exhibition*. Affiliation: Imperial Coll of Science, Technology and Medicine, London, United Kingdom; Correspondence Address: Soleimani, A.; Imperial Coll of Science, Technology and Medicine, London, United Kingdom: Society of Petroleum Engineers, Vol.5, pp. 1–16.

Stevenson, P. et al. (2001) 'The transport of particles at low loading in near-horizontal pipes by intermittent flow', *Chemical Engineering Science*, 56(6), pp. 2149–2159.

Sunder Raj, T. et al. (2005) 'Liquid-Liquid Stratified Flow through Horizontal Conduits', *Chemical Engineering & Technology*, 28(8), pp. 899–907.

Tang, X. et al. (2007) 'Effect of oil type on phase wetting transition and corrosion in iol-water flow', *NACE corrosion*. NACE International, pp. 1–21.

Trallero.L (1995) *Oil-water flow patterns in horizontal pipes*. University of Tulsa.

Trallero, J.L. et al. (1997) 'A Study of Oil/Water Flow Patterns in Horizontal Pipes', *SPE Production & Facilities*, 12(3), pp. 165–172.

Tsahalis, D.T. (1977) 'Conditions for the entrainment of settled water in crude oil and product pipelines', *83rd National Meeting of the American Institute of Chemical Engineers*

Ullmann, a. and Brauner, N. (2006) ‘Closure relations for two-fluid models for two-phase stratified smooth and stratified wavy flows’, *International Journal of Multiphase Flow*, 32(1), pp. 82–105.

Weber, M. (1978) ‘pseudo homogenous mixtures, part B, from: hydraulic transport in pipes; a practical’, *Hydro transport 5*. Hannover.

Weber, M. (1986) ‘Improved Durand-equation for multiple application’, *International Symposium on Slurry Flows, ASME-VDI*. Anaheim, California USA.

Weber, M. and et al. (1974) *fluid conveying system*. Mainz: Garter head publishing.

Wei, Y. (2010) *Cranfield university*. Cranfield University.

Wicks, M. and Fraser, J.P. (1975) ‘Entrainment of water by flowing oil’, *Materials performance*, 14(5), pp. 9–12.

Wu, Y.-M. (1995) ‘Entrainment method enhanced to account for oil’s water content’, *Oil and Gas Journal*, 93(35)

Xu, G. et al. (2011) ‘Trapped water displacement from low sections of oil pipelines’, *International Journal of Multiphase Flow*, 37(1), pp. 1–11.

Yan, W. et al. (2011) ‘Experimental study on sand transport characteristics in water and air-water flow in dip pipeline’, *15th International Conference on Multiphase Production Technology*. Affiliation: Process and Systems Engineering Group, Cranfield University, United Kingdom; Correspondence Address: Yan, W.; Process and Systems Engineering Group, Cranfield UniversityUnited Kingdom, pp. 51–68.

Zhang, H.-Q. and Sarica, C. (2011a) ‘Low liquid loading gas/liquid pipe flow’, *Journal of Natural Gas Science and Engineering*, 3(2) Elsevier B.V, pp. 413–422.

Zhang, H.-Q. and Sarica, C. (2011b) ‘A Model for Wetted-Wall Fraction and Gravity Center of Liquid Film in Gas/Liquid Pipe Flow’, *SPE Journal*, 16(3), pp. 692–697.

APPENDICES

A.1

Table 6-1 Physical Properties for Liquid-Liquid Horizontal Flow Experiments

Author	Internal diameter (m)	Length & (Inclination)	Material	Viscosity (mPa s) $(\frac{\mu_o}{\mu_w})$	Density (Kg/m^3) $(\frac{\rho_o}{\rho_w})$	Surface tension (mN/m)	Velocity range (water cut)	Observed flow pattern	Other measurements
Russel et al.(1959)	0.203		Cellulose acetate-butyrate	18	834			SM, Do/w Bo	
Brown and Govier (1961)	0.0264		Cellulose acetate-	(0.936 20.1	(0.78 0.851	50.34			Pressure drop, bubble velocity,

Author	Internal diameter (m)	Length & (Inclination)	Material	Viscosity (mPa s) $(\frac{\mu_o}{\mu_w})$	Density (Kg/m^3) $(\frac{\rho_o}{\rho_w})$	Surface tension (mN/m)	Velocity range (water cut)	Observed flow pattern	Other measurements
			Butyrate	150)	0.88)				bubble size distribution
Charles et al.(1961)	26.4mm		Cellulose acetate-butyrate	6.29, 16.8, 65.0.	0.998				
Govier et al. (1961)	0.0264		Cellulose acetate-Butyrate	(0.936 20.1 150)	(0.78 0.851 0.88)	35.3 50.2 49.8			Hold-up, pressure drop

Author	Internal diameter (m)	Length & (Inclination)	Material	Viscosity (mPa s) $(\frac{\mu_o}{\mu_w})$	Density (Kg/m^3) $(\frac{\rho_o}{\rho_w})$	Surface tension (mN/m)	Velocity range (water cut)	Observed flow pattern	Other measurements
Guzhov et al.(1973)	0.039		steel	21.8	896	44.8	0.3 m/s-1.6m/s (30-90%-70-90%)	Sep. Flow With disp. At int. Water or oil/water bottom layer, emulsion of water/oil	Pressure Drop, Visual observation

Author	Internal diameter (m)	Length & (Inclination)	Material	Viscosity (mPa s) $(\frac{\mu_o}{\mu_w})$	Density (Kg/m^3) $(\frac{\rho_o}{\rho_w})$	Surface tension (mN/m)	Velocity range (water cut)	Observed flow pattern	Other measurements
								and oil/water	
Hasson et al.(1973)	12.6mm		Glass hydrophilic (cleaned-d) and hydrophobic (treated)	1	1020				
Malinowsky (1975)	38.4mm		steel	4.6	850	22.3	0.6 m/s- 2 m/s	D o/w and w/o	Visual observation

Author	Internal diameter (m)	Length & (Inclination)	Material	Viscosity (mPa s) $(\frac{\mu_o}{\mu_w})$	Density (Kg/m^3) $(\frac{\rho_o}{\rho_w})$	Surface tension (mN/m)	Velocity range (water cut)	Observed flow pattern	Other measurements
							(55%)		
Laflin and Oglesby (1976)	38.4mm		steel	4.94	828	22.3	0.5 m/s-1.2 m/s (43-64%-58%)	Segregated, Do/w and w/o	Visual observation
Oglesby (1979)	41mm			32	868	30.1	1.4 m/s 74%	Semi-segregated, Semi- mixed	
Cox (1985)	50.8mm	(-15, -30)	Acrylic	1.38	754		0.05-0.54	Stratified bubble	Water hold-up, slip ratio,

Author	Internal diameter (m)	Length & (Inclination)	Material	Viscosity (mPa s) ($\frac{\mu_o}{\mu_w}$)	Density (Kg/m^3) ($\frac{\rho_o}{\rho_w}$)	Surface tension (mN/m)	Velocity range (water cut)	Observed flow pattern	Other measurements
Scott(1985)	50.8mm	(+15, +30)	Acrylic	1.38	754		0.7 m/s-1 m/s (30-76%)	Stratified bubble	Pressure drop Water hold-up, slip ratio, Pressure drop
Zavareh et al. (1988)	0.184		Acrylic	(2.46)	(0.783)			Bubble flow	
Arirachakaran et al. (1989)	41.1mm		steel	84 (and 4.7,58,115)	867 (and 867-898)				

Author	Internal diameter (m)	Length & (Inclination)	Material	Viscosity (mPa s) $(\frac{\mu_o}{\mu_w})$	Density (Kg/m^3) $(\frac{\rho_o}{\rho_w})$	Surface tension (mN/m)	Velocity range (water cut)	Observed flow pattern	Other measurements
Nadler and Mewes (1995)	59mm		Perspex	31	841		0.014-1.44 & 0.009-1.48	SM, D o/w &w, D o/w, D w/o & o/w, D w/o & w	Pressure drop
Trallero (1995)	50.1mm		Acrylic	29.6	850		0.25 m/s->3 m/s (5-95% -50-62%)	ST and MI, D w/o	Visual Observation, Pressure drop, hold-up
Valle and Kvandal	0.037		Glass	(2.55)	(0.792)	37.3		SM, Do/w & w, D w/o & o/w	

Author	Internal diameter (m)	Length & (Inclination)	Material	Viscosity (mPa s) ($\frac{\mu_o}{\mu_w}$)	Density (Kg/m^3) ($\frac{\rho_o}{\rho_w}$)	Surface tension (mN/m)	Velocity range (water cut)	Observed flow pattern	Other measurements
(1995)									
Angeli (1996)	24.3mm		St. steel	1.6	801	17.0	0.3 m/s-1.3 m/s (32-77%-66%)	Stratified wavy/drops, three layer	Mainly visual observation, Impedance probe Pressure drop

Author	Internal diameter (m)	Length & (Inclination)	Material	Viscosity (mPa s)	Density (Kg/m^3)	Surface tension (mN/m)	Velocity range (water cut)	Observed flow pattern	Other measurements
				($\frac{\mu_o}{\mu_w}$)	($\frac{\rho_o}{\rho_w}$)				
Beretta et al.(1997a,b)	0.003		Glass	(61.67 45.49 8.55)	(0.87 0.877 0.874)	0.0315 0.036 0.0374		D, B, intermittent, A pressure drop	
Nadler and Mewes (1997)	0.059		Perspex	31	841		0.014-1.44 &0.009-1.48	SM, Do/w & w, Do/w, D w/o & o/w, D w/o & w	Pressure drop
Valle and Utvik (1997)	77.9mm			1	791	28.5	0-2.33		Water hold-up, slip ratio ,pressure drop

Author	Internal diameter (m)	Length & (Inclination)	Material	Viscosity (mPa s) $(\frac{\mu_o}{\mu_w})$	Density (Kg/m^3) $(\frac{\rho_o}{\rho_w})$	Surface tension (mN/m)	Velocity range (water cut)	Observed flow pattern	Other measurements
Vedapuri et al. (1997)	101.2mm		Plexi-glass	2.0			0.4 m/s-1.4 m/s (20-80%)	Semi-segregated, semi-mixed	Isokinetic probe, Dispersed layer height
Angeli and Hewitt (1998)	24.3mm			1.6	801	17	0.3-3.9		Pressure Drop
Flores et al.(1998)	0.051		Acrylic	(20)	(0.858)	35.5		Do/w, VFD o/w. o/w, CF	hold-up and pressure drop
Hasan and Kabir (1999)	0.0635 and 0.127		Plexi-glass	(1.544)	(0.756)			bubbly flow, pseudo slug flow and churn flow	drift velocity of lighter oil phase

Author	Internal diameter (m)	Length & (Inclination)	Material	Viscosity (mPa s) $(\frac{\mu_o}{\mu_w})$	Density (Kg/m^3) $(\frac{\rho_o}{\rho_w})$	Surface tension (mN/m)	Velocity range (water cut)	Observed flow pattern	Other measurements
Alkaya (2000)	50.8mm	(- ,+ 5 - ,+ 2 - ,+ 1 - ,+ 0.56)		12.9	791	16.7	0.025-1.75		Water hold-up Pressure drop

Author	Internal diameter (m)	Length & (Inclination)	Material	Viscosity (mPa s) $(\frac{\mu_o}{\mu_w})$	Density (Kg/m^3) $(\frac{\rho_o}{\rho_w})$	Surface tension (mN/m)	Velocity range (water cut)	Observed flow pattern	Other measurements
Angeli and Hewitt (2000)	0.0243 and 0.024		Acrylic	1.6	801	0.017	0.3 m/s- 1.6 m/s (33%)	Do/w, D w/o, D o/w & w, D w/o & o, D w/o & o/w	Impedance probe, Phase distribution
Hamad et al.(2000)	0.078		Perspex	(1.6)	(0.803)	17			Drop velocity, size distribution

Author	Internal diameter (m)	Length & (Inclination)	Material	Viscosity (mPa s)	Density (Kg/m^3)	Surface tension (mN/m)	Velocity range (water cut)	Observed flow pattern	Other measurements
				($\frac{\mu_o}{\mu_w}$)	($\frac{\rho_o}{\rho_w}$)				
Elseth (2001)	56.3mm			1.6	790	43	0.3-1.51 &0.1-1.2		Water hold-up slip ratio pressure drop velocity and turbulence
Simmons and Azzopardi (2001)	0.063		PVC	(1.125)	(0.684)	10			Drop size distribution
Angeli et al. (2002)	0.038		Acrylic	(5.25)	(0.828)	0.0447		SW, Do/w, D w/o & o/w, D w/o	

Author	Internal diameter (m)	Length & (Inclination)	Material	Viscosity (mPa s) $(\frac{\mu_o}{\mu_w})$	Density (Kg/m^3) $(\frac{\rho_o}{\rho_w})$	Surface tension (mN/m)	Velocity range (water cut)	Observed flow pattern	Other measurements
Lum et al. (2002)	38mm			5.25	828	40	0.07-2.25		Water hold-up slip ratio Pressure drop
Abduvayt et al. (2004)	106.4mm	(-,+3 -,+0.5 0 90)		1.88	800		0.025-1.502		Water hold-up slip ratio pressure drop
Lovick and Angeli (2004)	38mm			6	828	27.6	0.8-3 (10-90%)		Impedance and conductance

Author	Internal diameter (m)	Length & (Inclination)	Material	Viscosity (mPa s) ($\frac{\mu_o}{\mu_w}$)	Density (Kg/m^3) ($\frac{\rho_o}{\rho_w}$)	Surface tension (mN/m)	Velocity range (water cut)	Observed flow pattern	Other measurements
									probes, phase distribution
Chakrabati et al. (2005)	0.025		PMMA	(1.2)	(0.787)	0.045		SS, SW, P, Do/w w, TL,ID	
Raj et al.(2005)	0.025		PMMA	(1.2)	(0.787)	0.045		SS, SW, P, Do/w w ,TL, ID	

Author	Internal diameter (m)	Length & (Inclination)	Material	Viscosity (mPa s) ($\frac{\mu_o}{\mu_w}$)	Density (Kg/m^3) ($\frac{\rho_o}{\rho_w}$)	Surface tension (mN/m)	Velocity range (water cut)	Observed flow pattern	Other measurements
Jana et al. (2006)	0.025		Perspex	(1.2)	(0.787)	45		B,DB,CT,CA	parallel wire conductivity probe
Lum et al.(2006)	38mm	(-50		5.5	800	40	0.07-2.28		Water hold-up slip ratio pressure drop

Author	Internal diameter (m)	Length & (Inclination)	Material	Viscosity (mPa s)	Density (Kg/m^3)	Surface tension (mN/m)	Velocity range	Observed flow pattern	Other measurements
				($\frac{\mu_o}{\mu_w}$)	($\frac{\rho_o}{\rho_w}$)		(water cut)		
		+10)							
Wegmann and Rohr (2006)	0.0056 And 0.007		Glass	(6.14-5.78)	(0.820-0.822)	0.0622		Stratified, annular, intermittent, dispersed	
Kumara et al. (2010a,b)	56 mm	15 (-5,+5)	Stainless steel	1.64	790		0.25,0.5, 1.0 (50%)		
Mandal et al. (2010)		5		1.2	(0.787)				

A.2

Four inch horizontal rig test spool engineering drawings

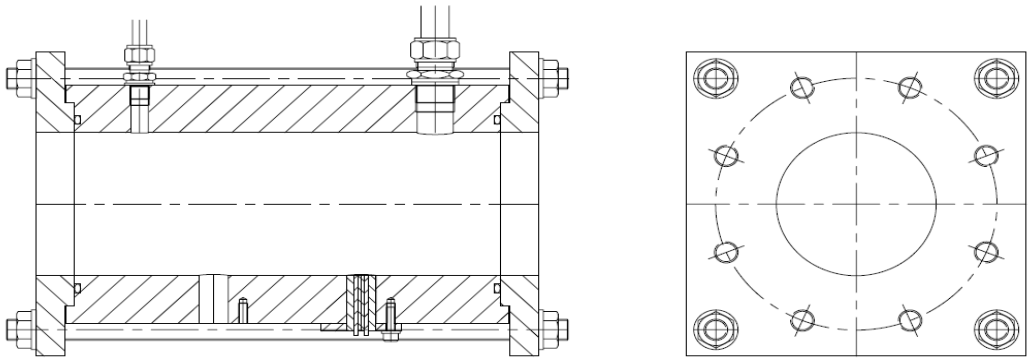

Figure 6-1 test spool side and cross section views

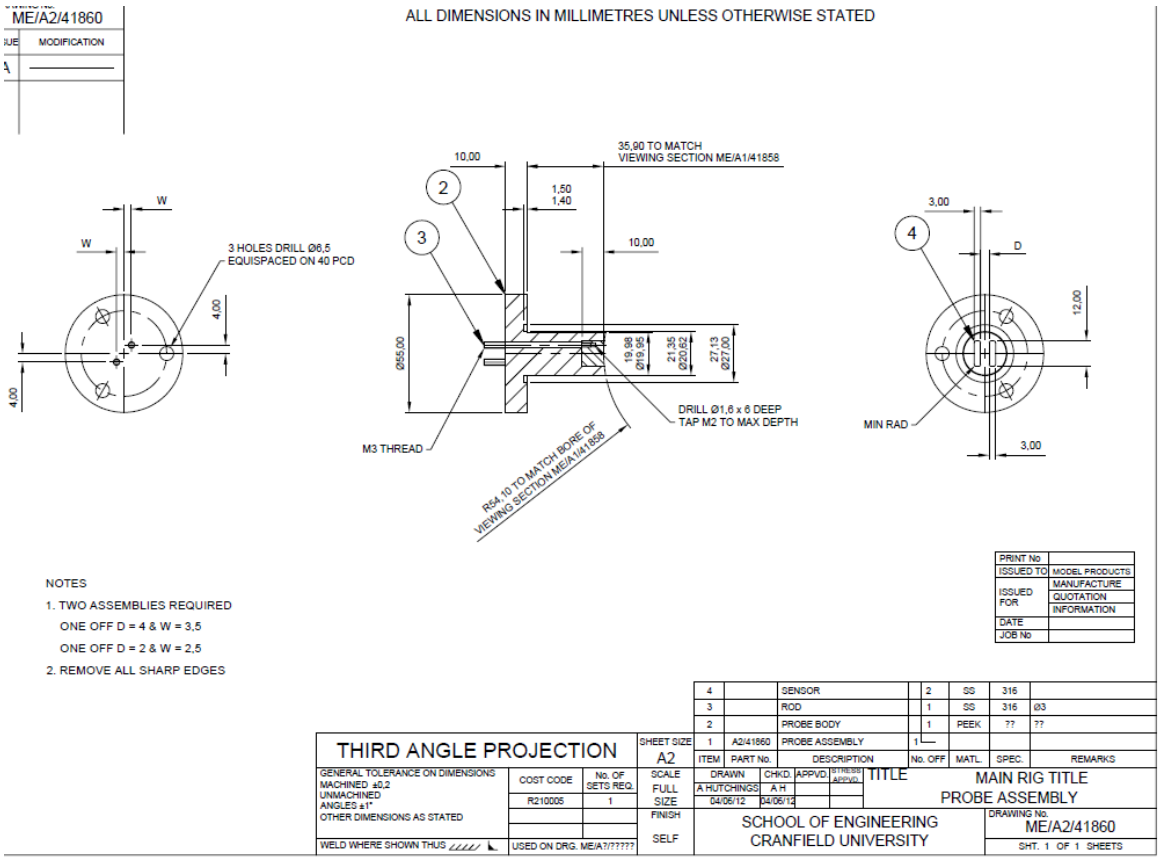

Figure 6-2 Film thickness sensor engineering drawing

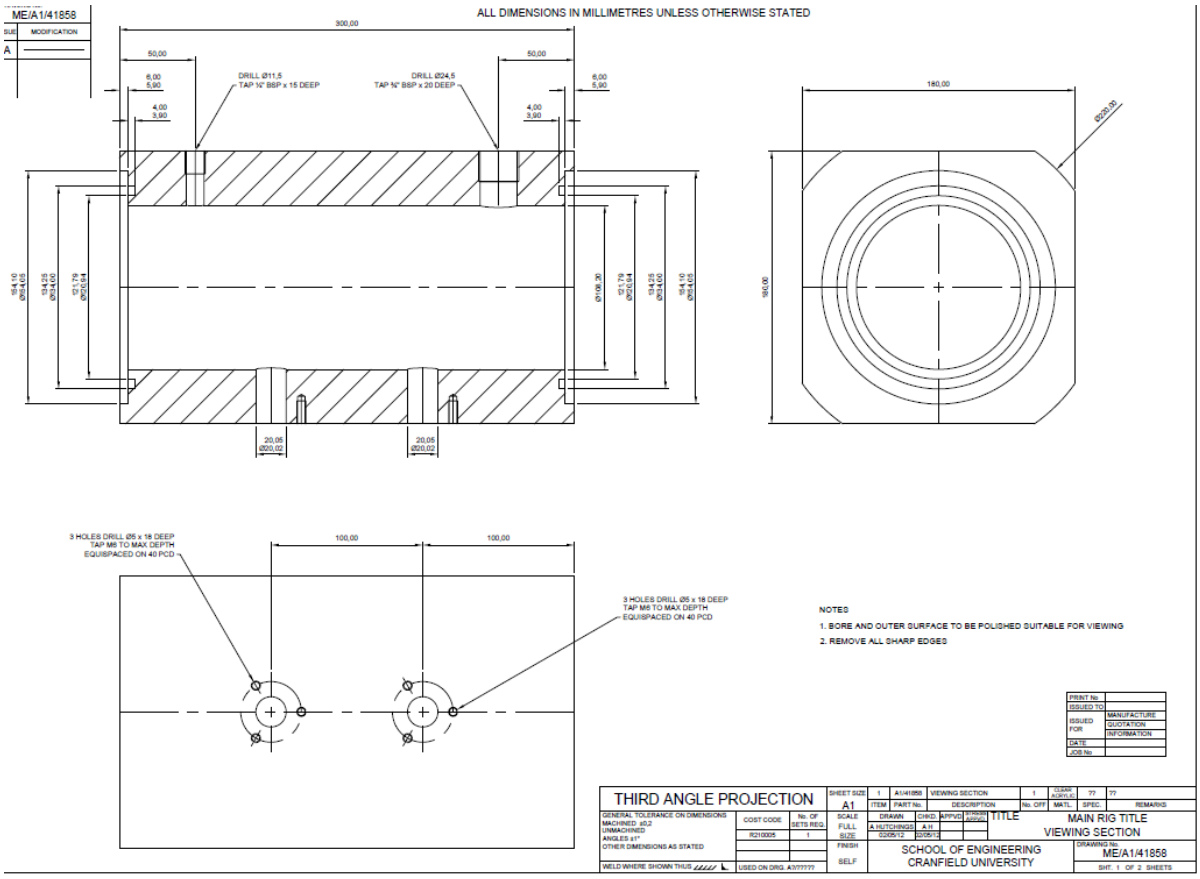

Figure 6-3 film thickness sensor test spool Perspex section engineering drawing

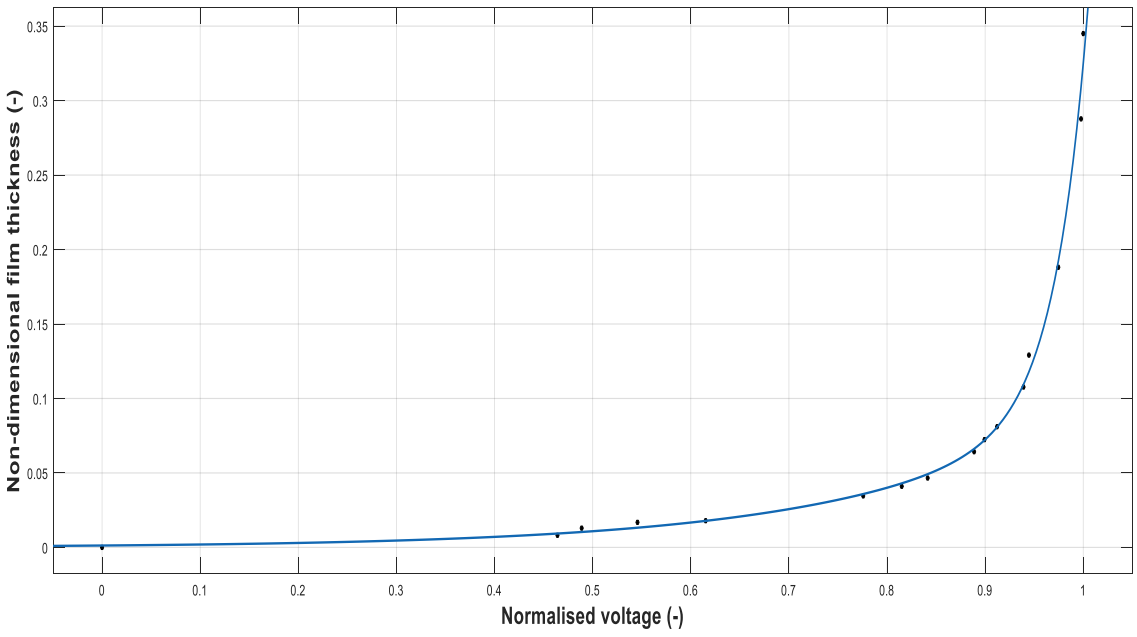

Figure 6-4 film thickness sensor calibration

The curve fit and corresponding coefficient of determination is given in Equation 6-1 below;

$$y = 0.001265 \times \exp\times (4.3x) + 252e^{-14} \times \exp(29.84x) \quad \textbf{(6-1)}$$

$R^2 = 0.9933$

Two-fluid model results

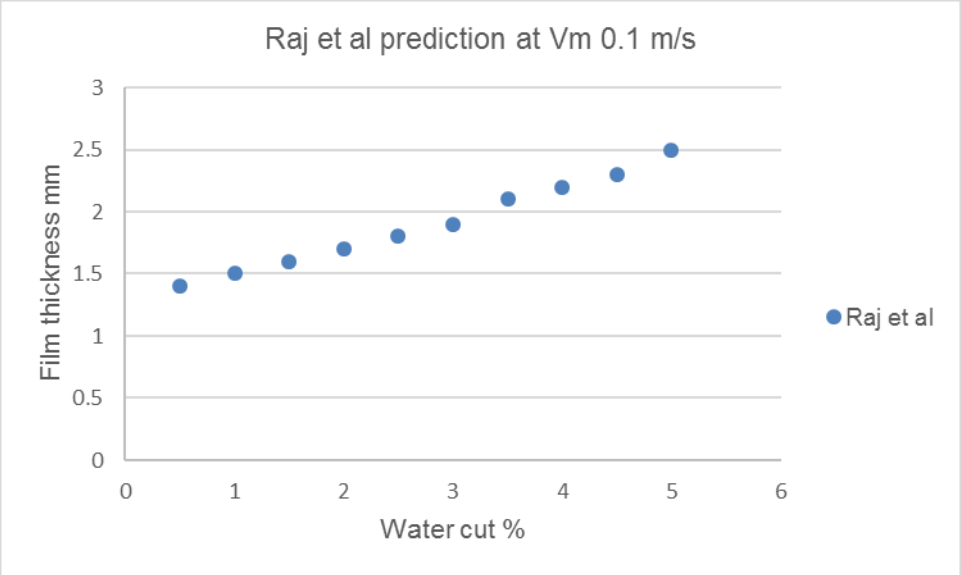

Figure 6-5 film thickness prediction for oil and water mixture velocity of 0.1m/s

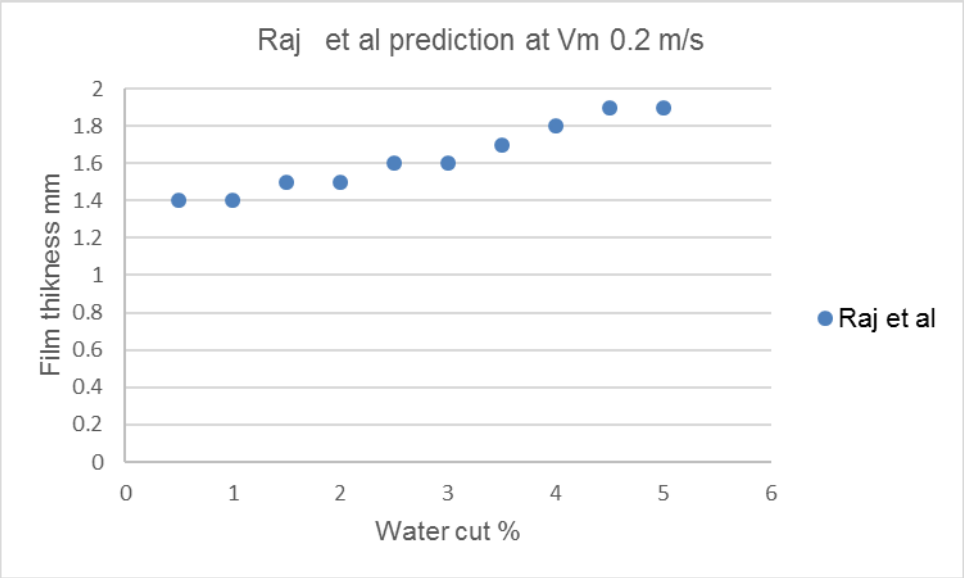

Figure 6-6 film thickness prediction for oil and water mixture velocity of 0.2m/s

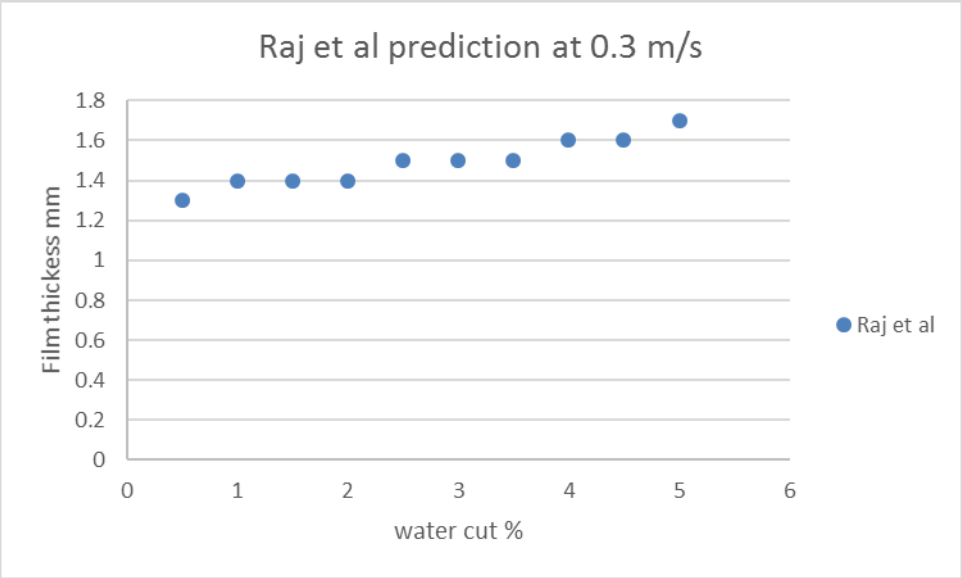

Figure 6-7 film thickness prediction for oil and water mixture velocity of 0.3m/s

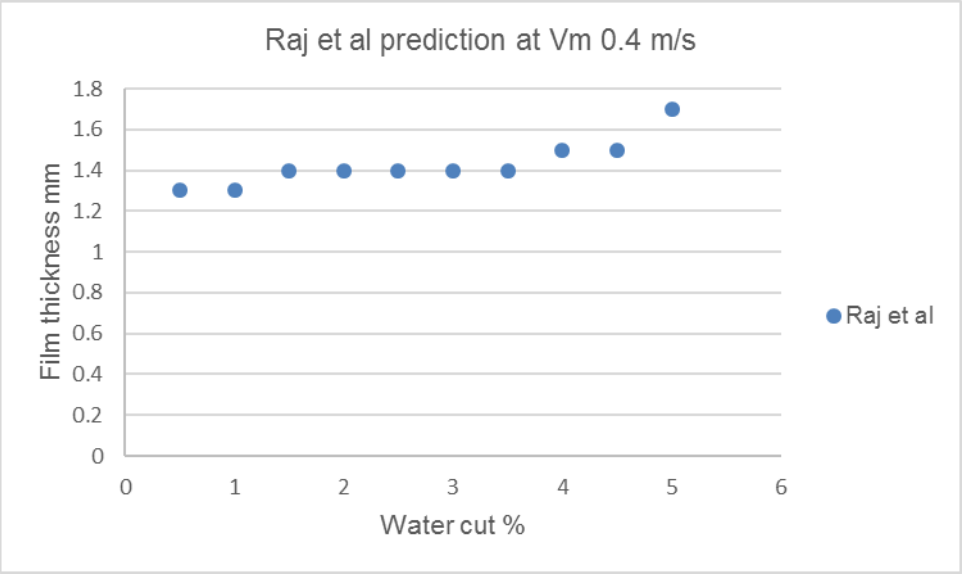

Figure 6-8 film thickness prediction for oil and water mixture velocity of 0.4m/s

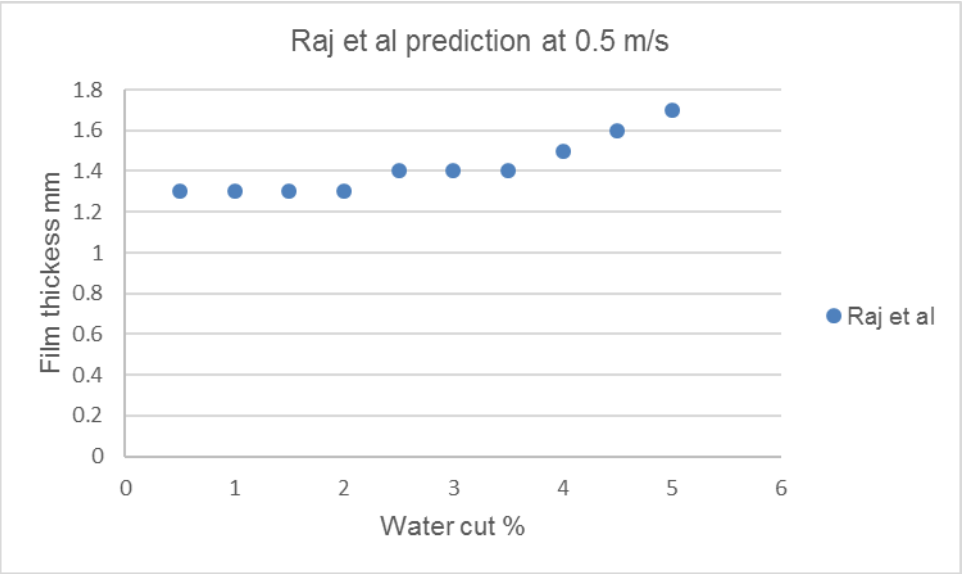

Figure 6-9 film thickness prediction for oil and water mixture velocity of 0.5m/s

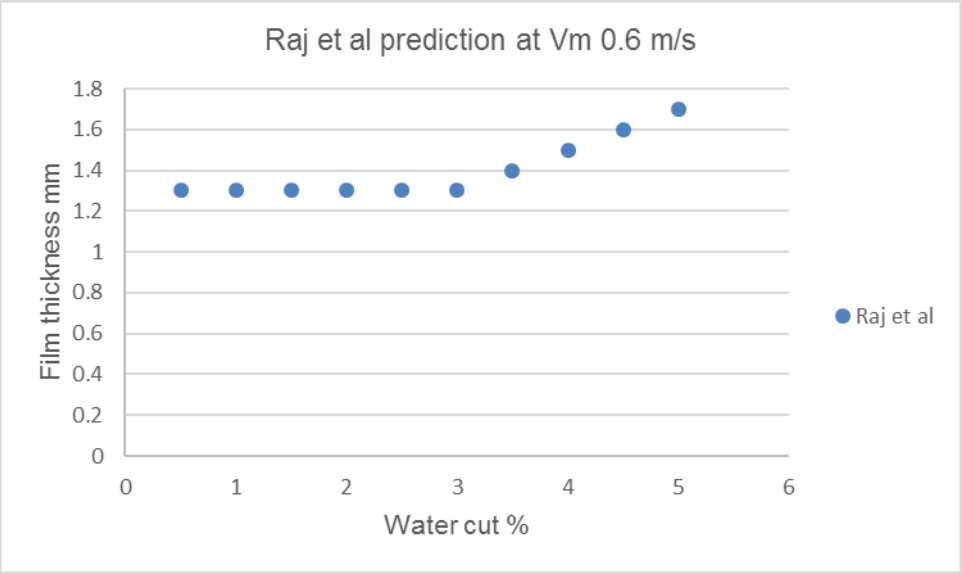

Figure 6-10 film thickness prediction for oil and water mixture velocity of 0.6m/s

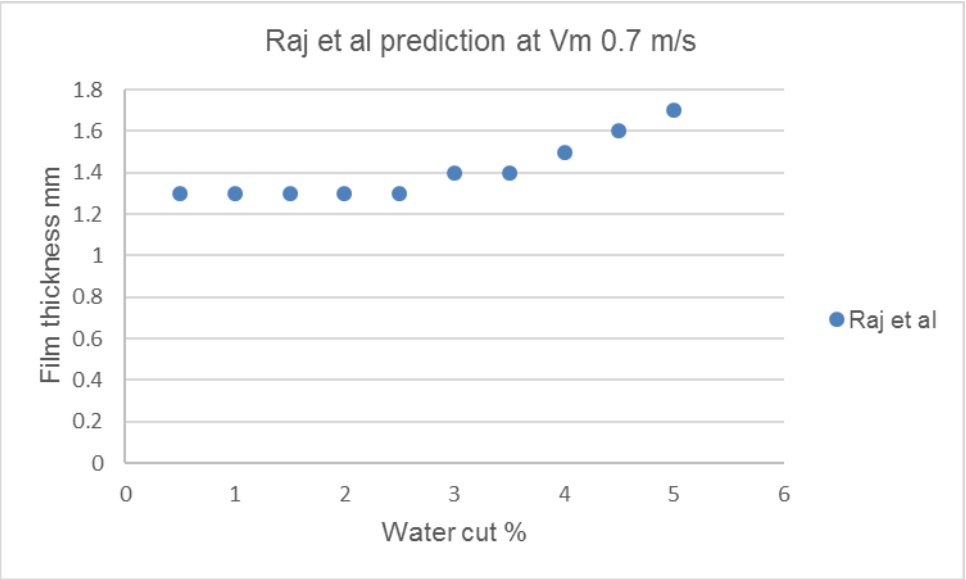

Figure 6-11 film thickness prediction for oil and water mixture velocity of 0.7m/s

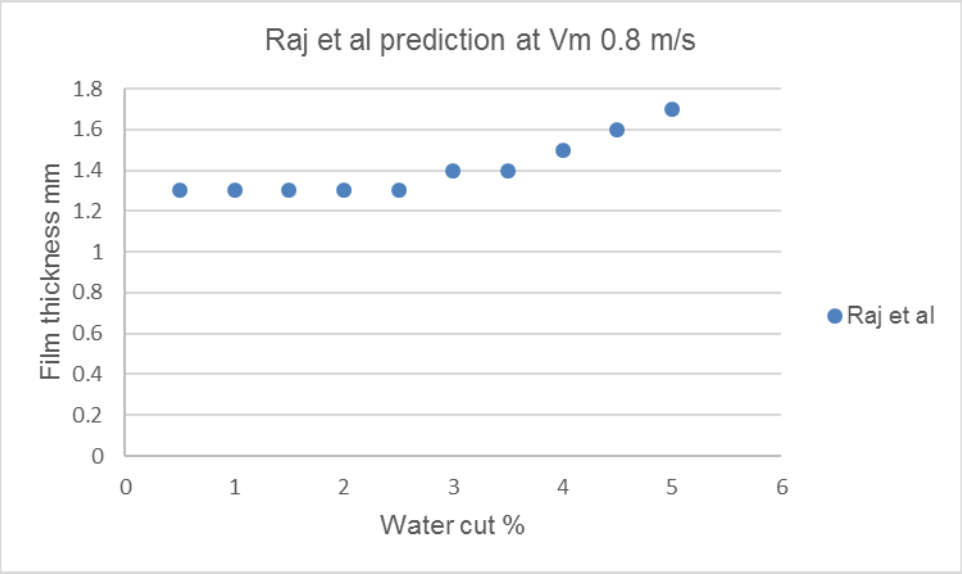

Figure 6-12 film thickness prediction for oil and water mixture velocity of 0.8m/s

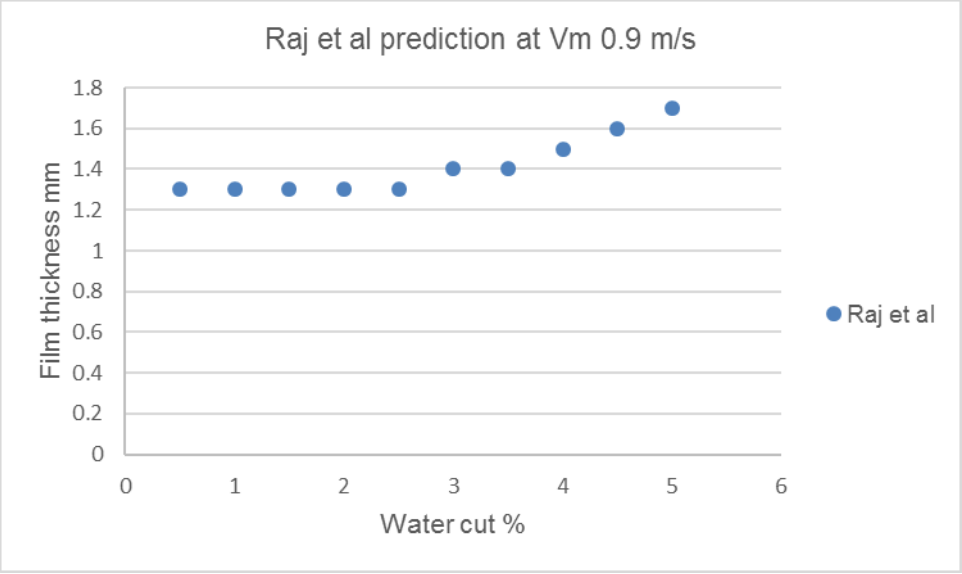

Figure 6-13 film thickness prediction for oil and water mixture velocity of 0.9m/s

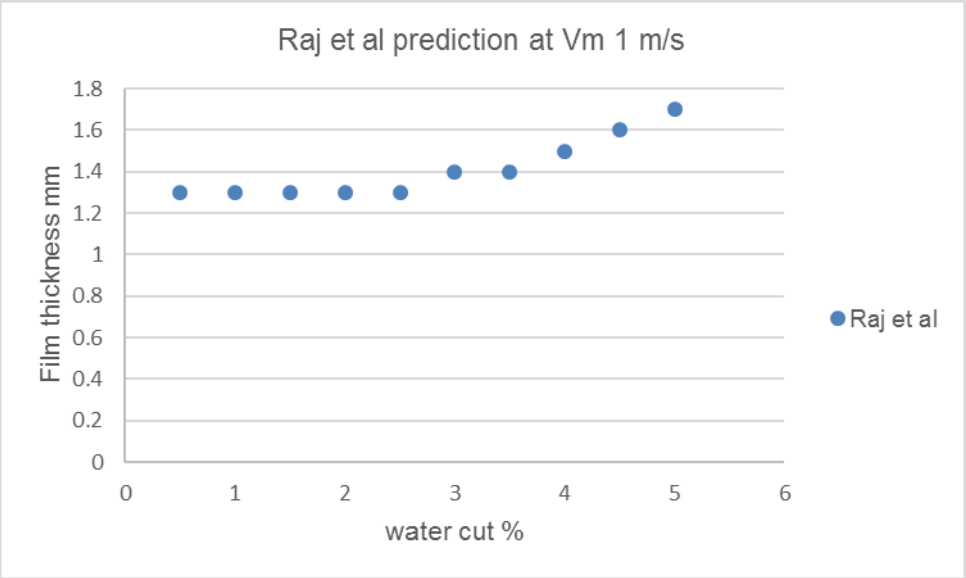

Figure 6-14 film thickness prediction for oil and water mixture velocity of 1m/s

A.3

Pressure transducer calibration

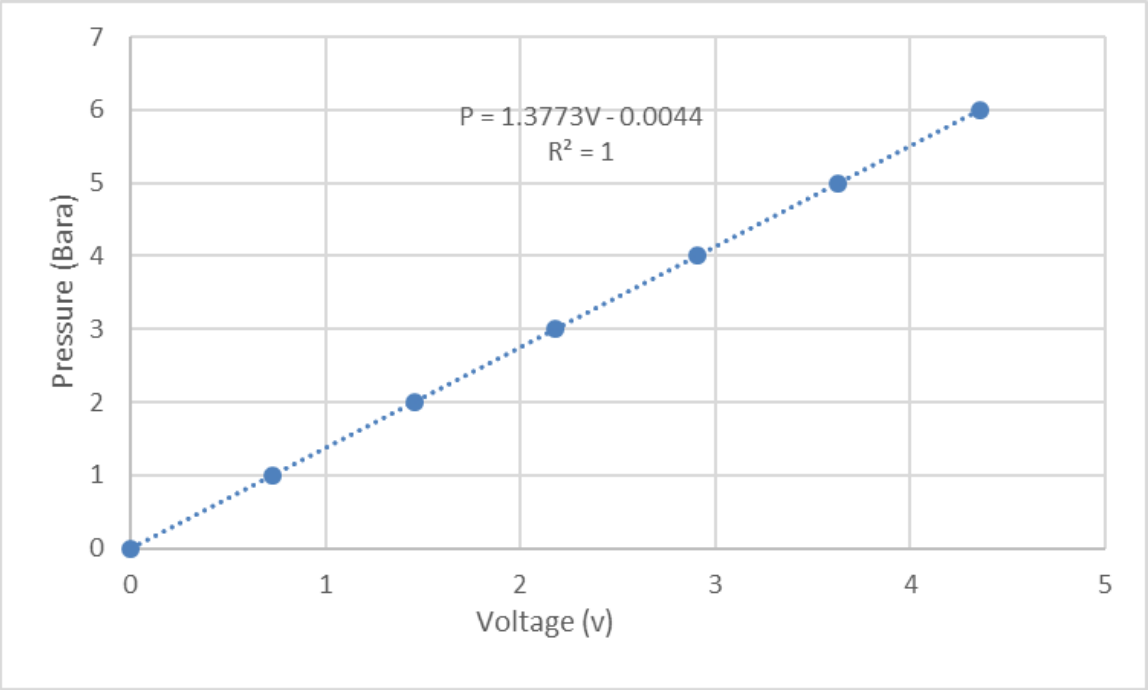

Figure 6-15 calibration curve for pressure transducer upstream

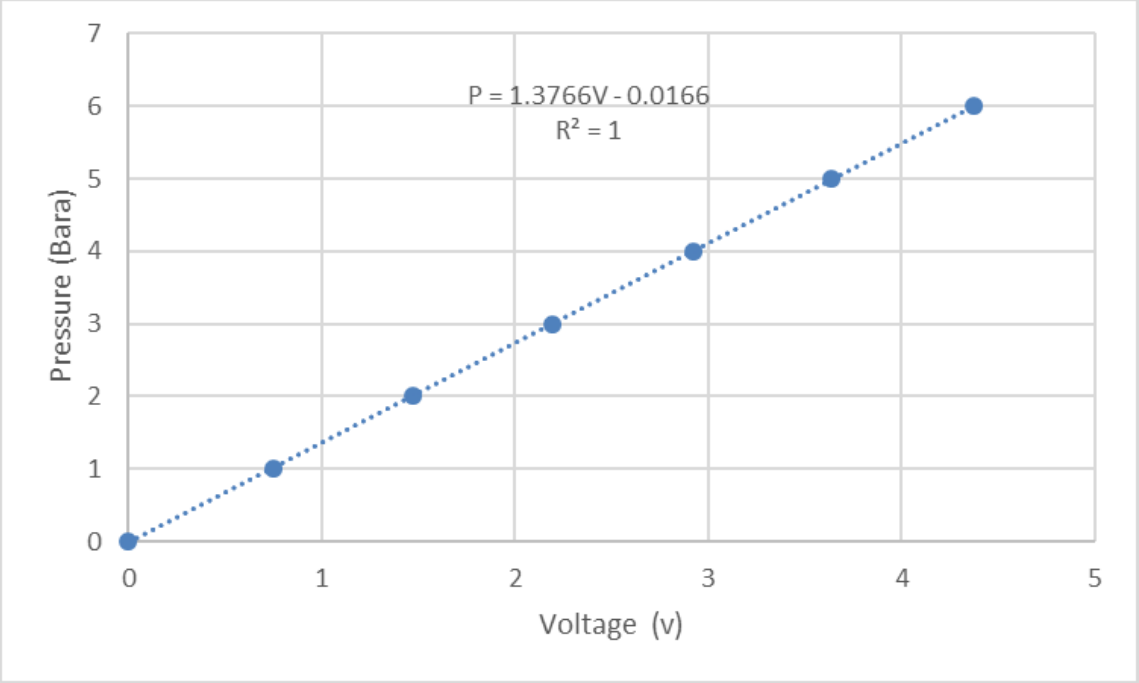

Figure 6-16 calibration curve for pressure transducer downstream

Measurement of sand properties procedure

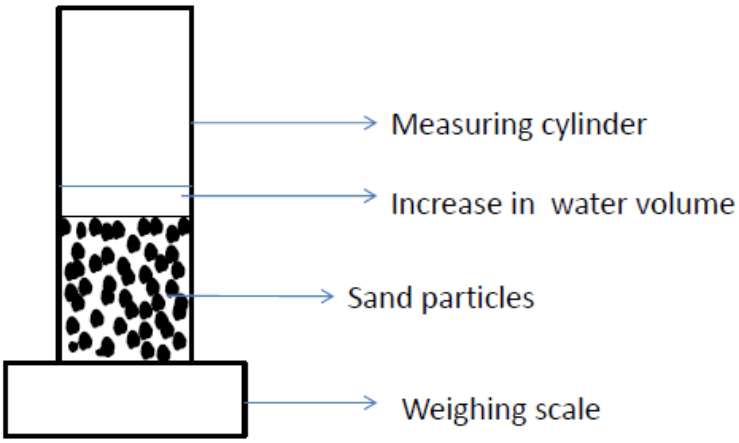

Figure 3-8: Schematic measurement for sand properties

Procedures for sand porosity and density for different particle size

1. Weigh an empty measuring cylinder and record the mass and label it as cylinder A
2. Measure and determine the apparent volume of some known quantity of sand (50g, 100g etc.) in a separate measuring cylinder of the same size and height as the measuring cylinder A, and label it as measuring cylinder B
3. Put about 50ml of water into the measuring cylinder A and determine the weight of the cylinder A and water
4. Add all the sand particles in which the quantity and apparent volume are known from measuring cylinder B to the weighed water and measuring cylinder A and determine the total mass (Sand +Water + Cylinder A)
5. Record the increase in the total volume of the contents in the measuring cylinder when sand is added to the water in the measuring cylinder A
6. Calculate the void volume of the sand and actual volume using equations below:

$$\text{Void volume} = \left[\left(V_{S.app} + V_W\right) - V_m\right]$$

$$V_{S.act} = V_{S.app} - \text{Void volume}$$

Where $V_{S.act}$ is actual volume of sand, V_m is the mixture volume, $V_{S.app}$connotes apparent volume of sand, and V_W is the volume of water

7 Calculate the density and porosity of the sand by using the equations below

Density of sand = $\frac{\boldsymbol{Mass\ of\ the\ sand}}{\boldsymbol{volume\ of\ the\ sand}}$

Porosity =$\left(1 - \frac{Actual\ volume}{Apparent\ volume}\right) * 100\%$

Repeat the above steps for the same sand size particles for two more times, so obtain three measurements of the density and porosity and record.

Table 6-2 water and sand flow pattern results for 150 microns 0.00005 v/v

Flow Regime	Vsl (m/s)	Mean Normalised Voltage	Standard Deviation of Normalised Voltage	Coefficient of variation	Equivalent sand height 1 (mm)	Equivalent sand height 2 (mm)	Equivalent sand height Average (mm)
Moving Bed	0.099	0.9065	0.0009	0.0970	0.1117	0.1383	0.1250
Moving Bed	0.128	0.9188	0.0045	0.4847	0.0933	0.0984	0.0958
Moving Bed	0.14	0.8824	0.0070	0.7945	0.0976	0.1034	0.1005
Saltation	0.18	0.8983	0.0021	0.2342	0.0975	0.0993	0.0984
Streak	0.2	0.9412	0.0026	0.2603	0.0911	0.0950	0.0931
Suspension	0.235	0.9958	0.0015	0.1515	0.0890	0.0849	0.0870
Suspension	0.27	0.9615	0.0019	0.2020	0.0901	0.0910	0.0906
Suspension	0.3	0.9586	0.0024	0.2535	0.0890	0.0929	0.0910
Suspension	0.32	0.9704	0.0021	0.2143	0.0884	0.0907	0.0895

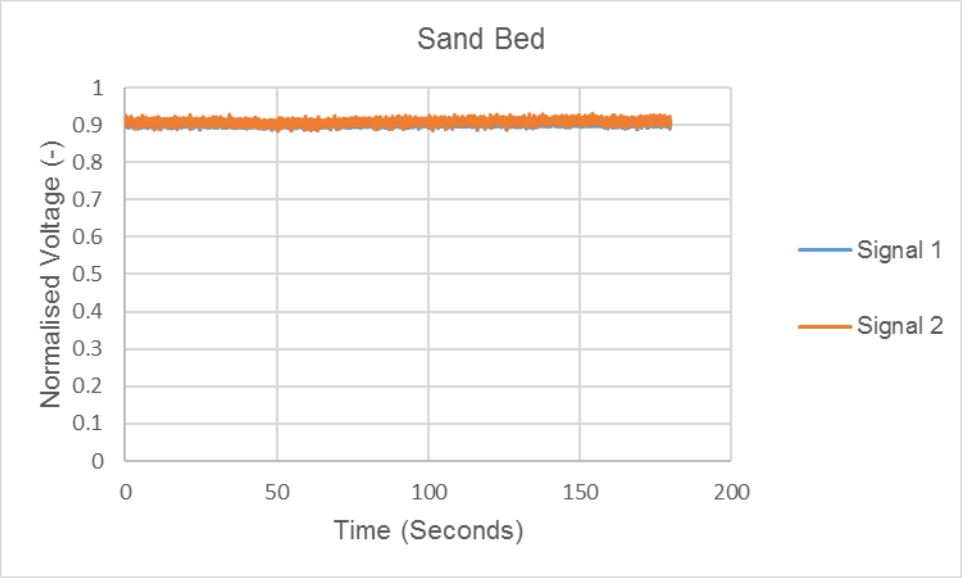

Figure 6-17 normalised voltage for sand bed at 0.099 m/s for 150 microns 0.00005v/v

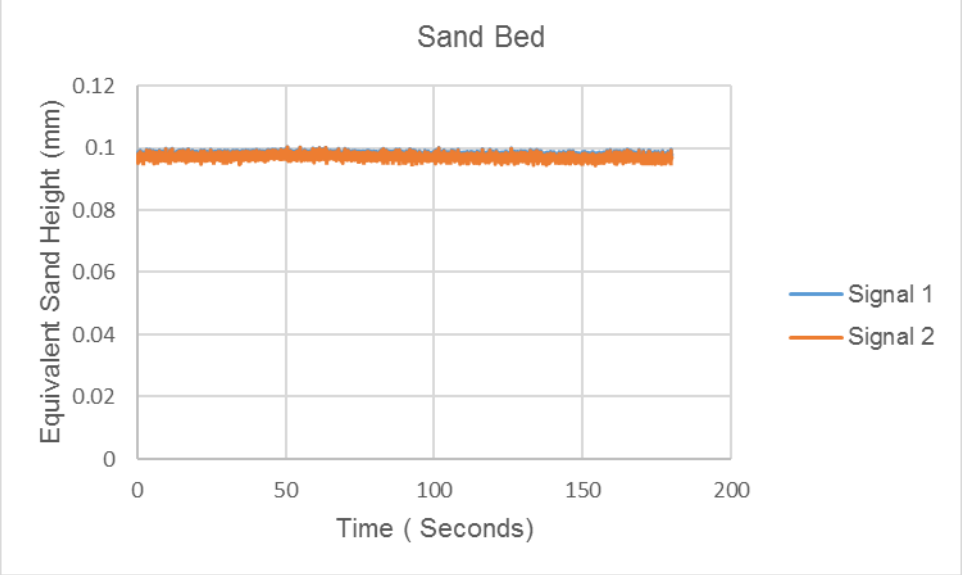

Figure 6-18 equivalent sand height for sand bed at 0.099 m/s for 150 microns 0.00005v/v

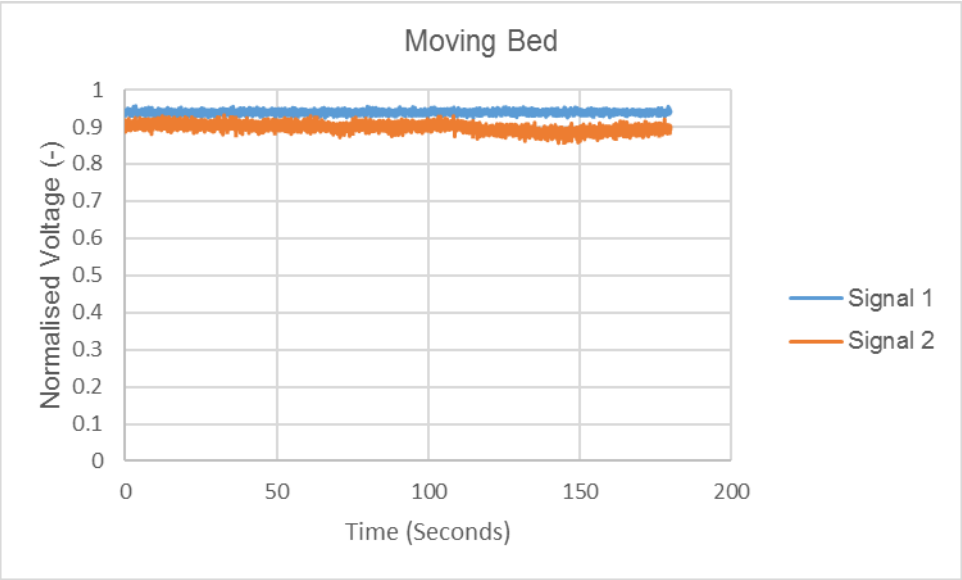

Figure 6-19 normalised voltage for moving bed at 0.128 m/s for 150 microns 0.00005v/v

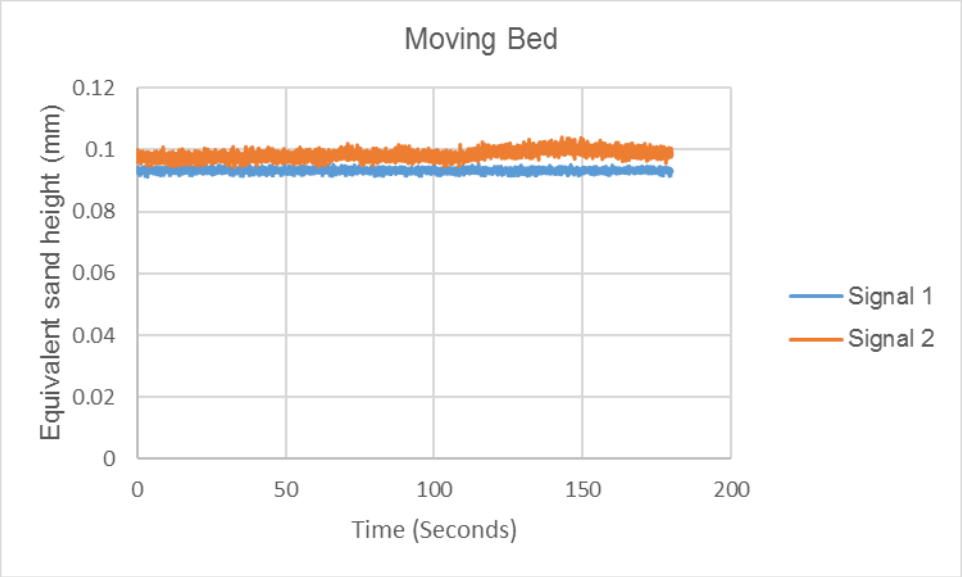

Figure 6-20 equivalent sand height for moving bed at 0.128 m/s for 150 microns 0.00005v/v

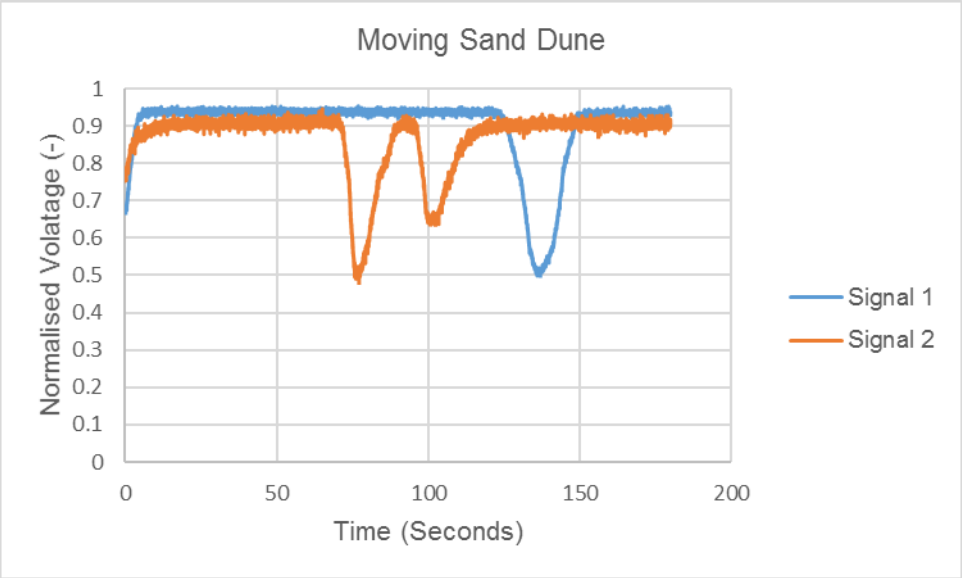

Figure 6-21 normalised voltage for moving sand dune at 0.140 m/s for 150 microns 0.00005v/v

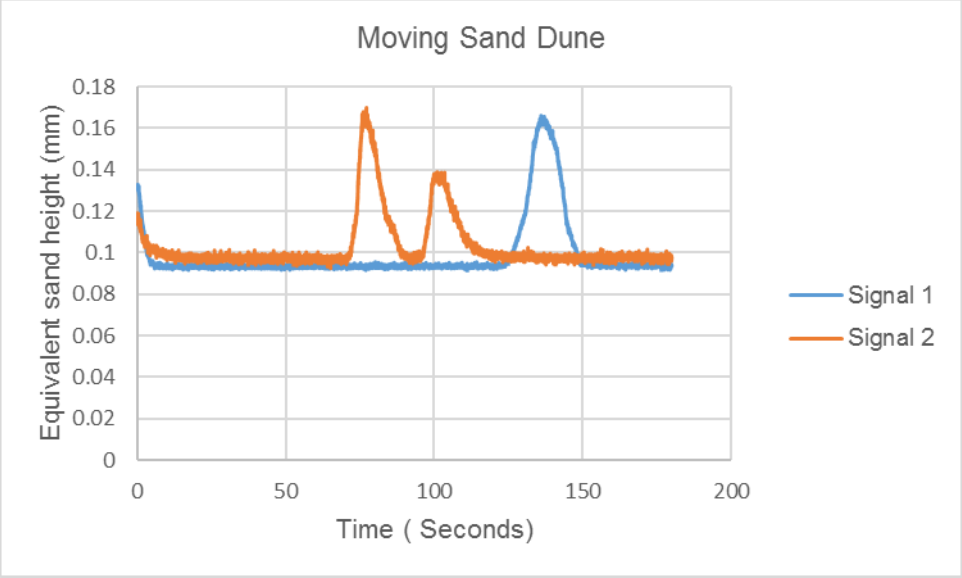

Figure 6-22 equivalent sand height for moving sand dune at 0.140 m/s for 150 microns 0.00005v/v

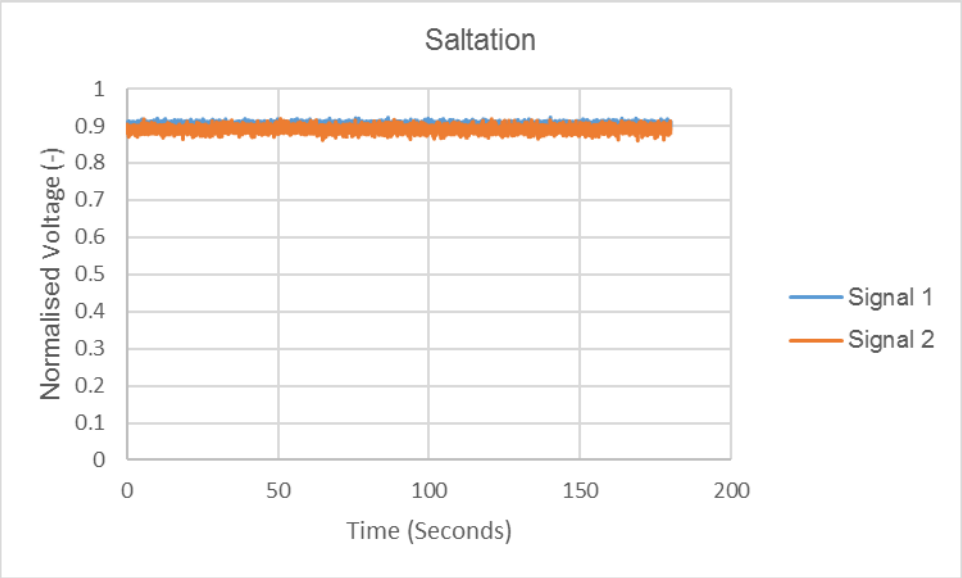

Figure 6-23 normalised voltage for saltation at 0.180 m/s for 150 microns 0.00005v/v

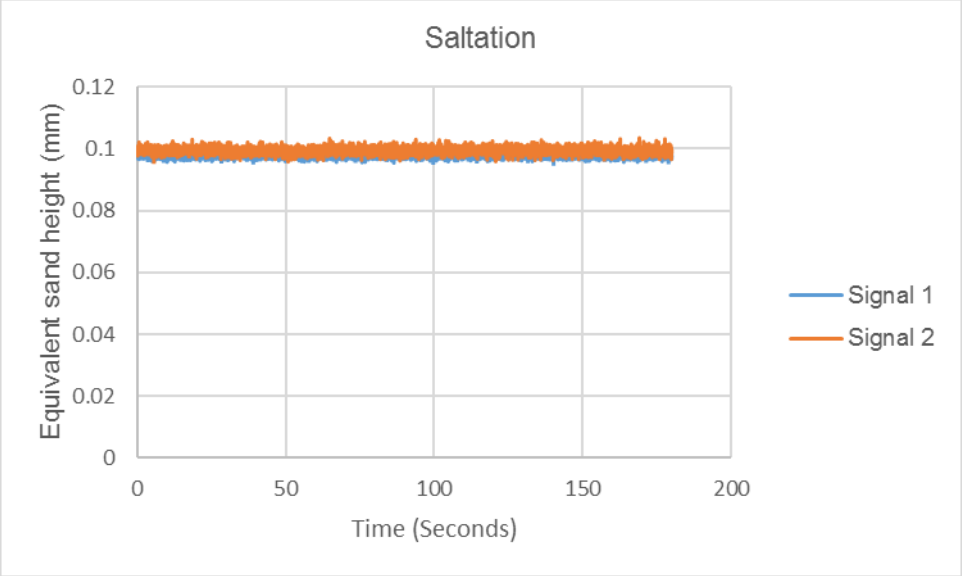

Figure 6-24 equivalent sand height for saltation at 0.180 m/s for 150 microns 0.00005v/v

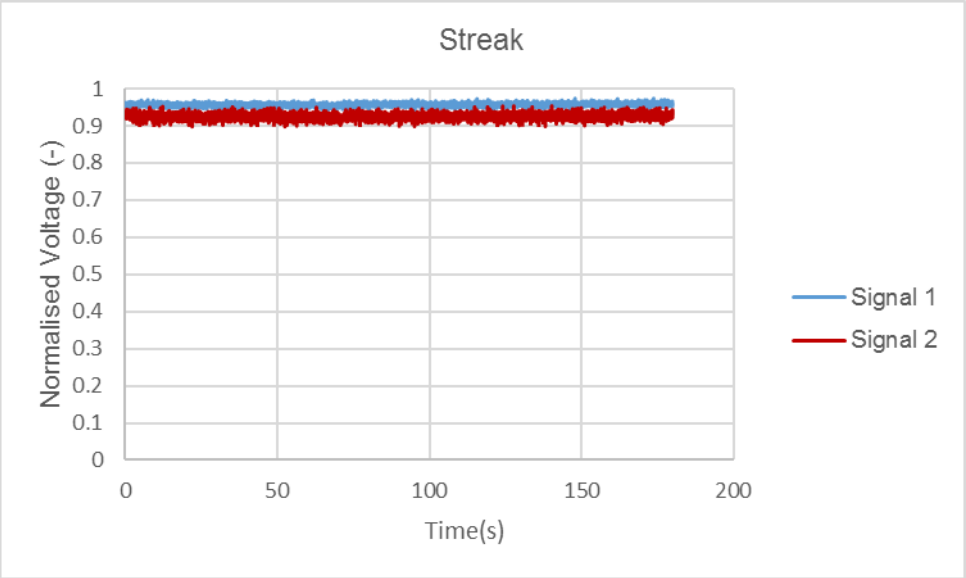

Figure 6-25 normalised voltage for streak at 0.200 m/s for 150 microns 0.00005v/v

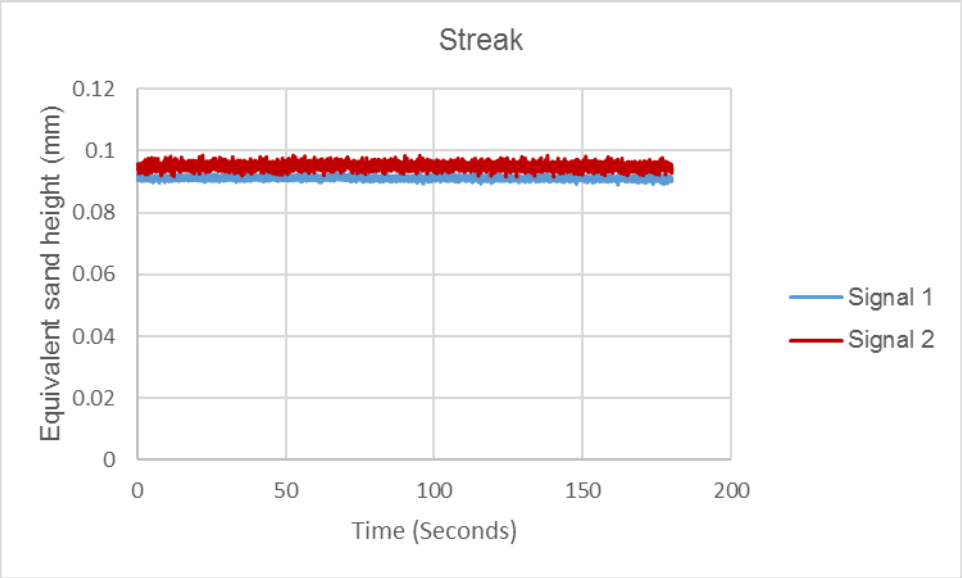

Figure 6-26 equivalent sand height for streak at 0.200 m/s for 150 microns 0.00005v/v

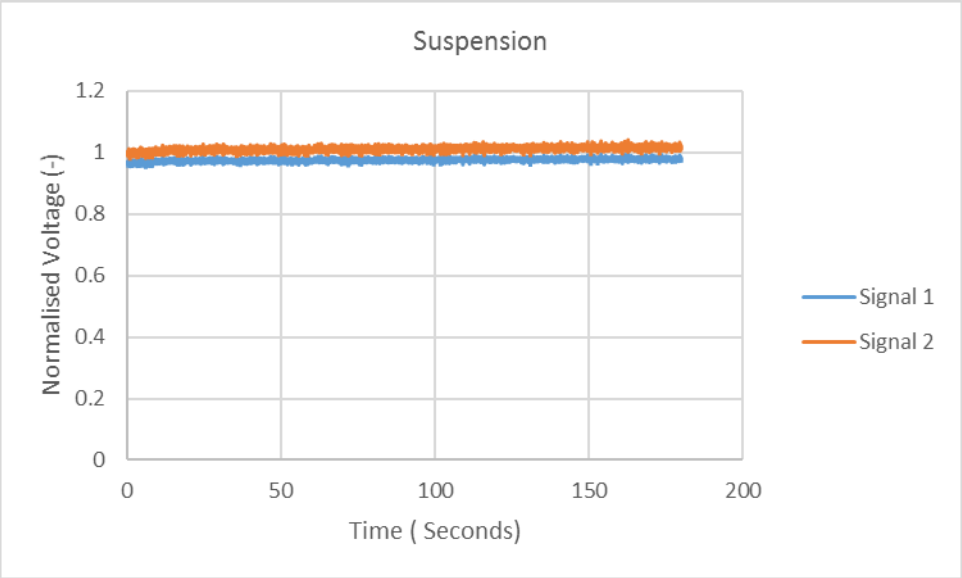

Figure 6-27 normalised voltage for suspension at 0.235 m/s for 150 microns 0.00005v/v

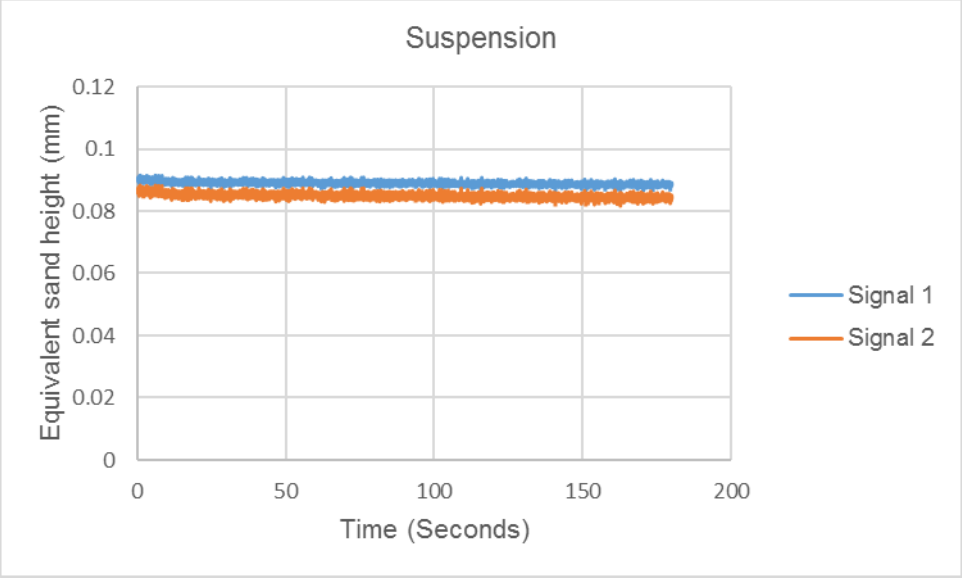

Figure 6-28 equivalent sand height for suspension at 0.235 m/s for 150 microns 0.00005v/v

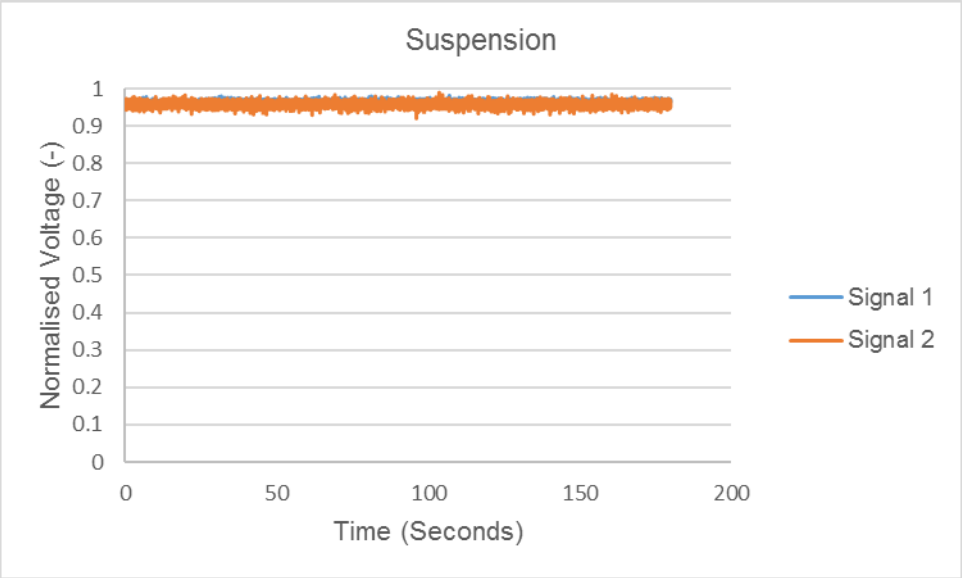

Figure 6-29 normalised voltage for suspension at 0.270 m/s for 150 microns 0.00005v/v

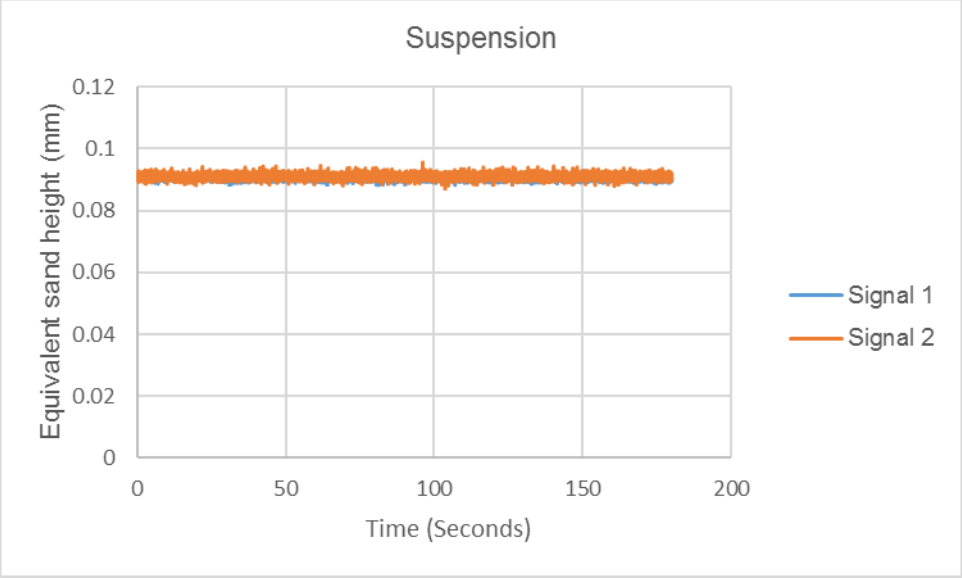

Figure 6-30 equivalent sand height for suspension at 0.270 m/s for 150 microns 0.00005v/v

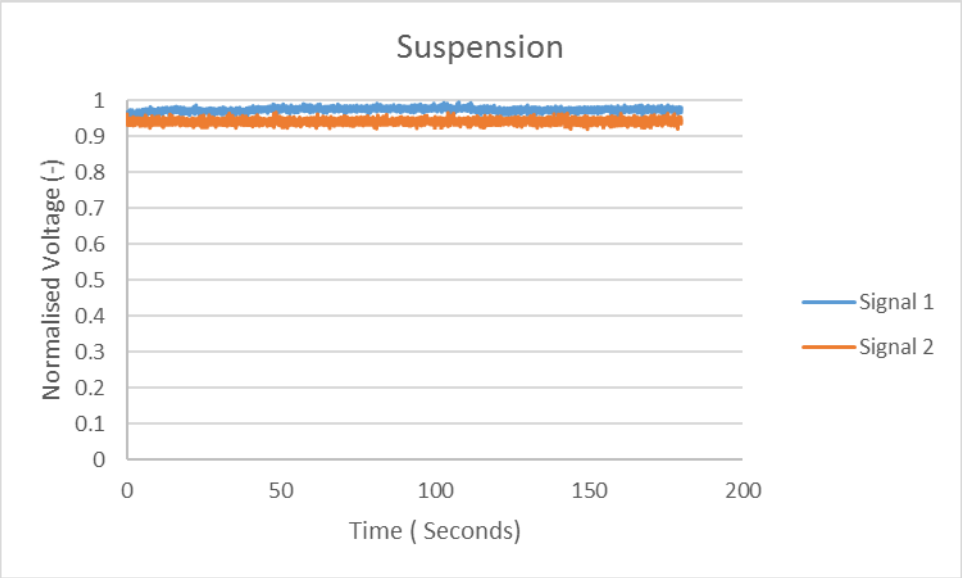

Figure 6-31 normalised voltage for suspension at 0.300 m/s for 150 microns 0.00005v/v

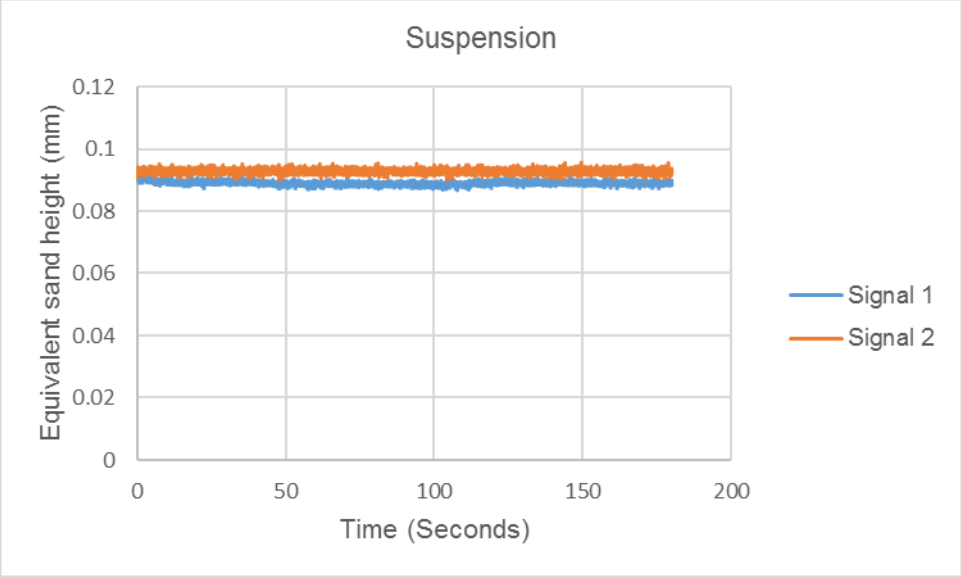

Figure 6-32 equivalent sand height for suspension at 0.300 m/s for 150 microns 0.00005v/v